Analysis of Human Intrinsic Stiffness Modulation and its Use in Variable-Stiffness Robots

Dipl.-Ing. Hannes Höppner

Ph.D. Thesis

Doktorarbeit

TECHNISCHE UNIVERSITÄT MÜNCHEN
Fakultät für Informatik
Lehrstuhl für Echtzeitsysteme und Robotik
Biomimetic Robotics and Machine Learning

Analysis of Human Intrinsic Stiffness Modulation and its Use in Variable-Stiffness Robots

Dipl.-Ing. Hannes Höppner

Vollständiger Abdruck der von der Fakultät für Informatik der Technischen Universität München zur Erlangung des akademischen Grades eines

Doktor-Ingenieurs (Dr.-Ing.)

genehmigten Dissertation.

Vorsitzender:		Univ.-Prof. Dr.-Ing. Alin Albu-Schäffer
Prüfer der Dissertation:	1.	Univ.-Prof. Dr. Patrick van der Smagt
	2.	Univ.-Prof. Dr.-Ing. Veit Senner

Die Dissertation wurde am **23.09.2015** bei der Technischen Universität München eingereicht und durch die Fakultät für Informatik am **08.03.2016** angenommen.

Abstract

Full Abstract — The Thesis ***Analysis of Human Intrinsic Stiffness Modulation and its Use in Variable-Stiffness Robots*** presents a detailed analysis of human intrinsic stiffness modulation capabilities in the upper limb and shows its transfer to variable-stiffness robots. Aiming for service, assistance, and collaborative robotic systems, the focus of robotic research tends towards human-robot interaction, and special attention needs to be paid on saving human and robot. The most up-and-coming approach is the implementation of adaptable compliance techniques, as found in humans, since they allow tuning the impact of external forces. One technique—which is summarized by the terminology *impedance control* and inspired from nature—concerns the integration of force-torque sensors into a feedback loop and *actively* controlling compliance behavior of robots. However, this technique has its limitations, especially regarding the frequency bandwidth of external forces; e.g., it is impossible for the robot to react to highly dynamic impacts. To solve this drawback, the introduction of *passive* mechanical compliance into robotic systems—called variable-stiffness robots (VSAs)—has been researched intensively within the past decade. However, even if an endless amount of different mechanisms for VSAs have been introduced, design criteria regarding their mechanical properties remain unclear.
This Thesis is trying to answer the question by looking into the human locomotor system from the perspective of a mechanical engineer. Special mechanisms for revealing insights into purely mechanic hand and arm compliance behavior and avoiding relevant influences from active response are designed. Since no comparable force–stiffness characteristics—typically used for the specification of VSAs—are available for human, special attention is paid to investigate human capabilities to decouple stiffness from force. Once, during two comparable tasks that require the application of identical forces, and in detail by investigating the strategy of *cocontraction* of antagonistic pairs of muscles. Finally, the transfer of gained insights, i.e. the linear characteristic between force and stiffness, and a biarticular coupling between joints, to robots is analyzed and discussed.

500 characters — This Thesis explores how human are able to modulate intrinsic hand and arm stiffness. The question is increasingly relevant as human and robots start collaborating inside same workspaces and introducing compliance allows tuning forces due to impacts. Mechanisms are developed for measuring purely human mechanical properties, and factors for varying the known force–stiffness coupling are studied. Conclusively, the transfer of gained insights to robots, i.e. the linear relation between force and stiffness, and biarticular joint coupling, is analyzed and discussed.

Zusammenfassung

Vollständige Zusammenfassung — Die Arbeit ***Analyse der Kontrollierbarkeit reiner Steifigkeit des Menschen sowie deren Anwendung für Roboter mit variablen Steifigkeitsantrieben*** präsentiert eine detaillierte Analyse der Fähigkeit des Menschen *reine* Steifigkeit seiner Hände und Arme bewusst einzustellen, sowie die Anwendung der Erkenntnisse auf humanoide Roboter mit variablen Steifigkeitsgelenken. Mit dem Ziel, Roboter zur Unterstützung des Menschen sowie kollaborierende robotische Systeme zu entwickeln, richtet sich der Fokus der Robotik Forschung mehr und mehr auf die sichere Interaktion zwischen Mensch und Maschine, wobei besonders stark auf die Sicherheit vom Menschen, aber auch auf die des Roboters geachtet wird. Der vielversprechendste Ansatz betrifft dabei die Implementierung von einstellbaren Nachgiebigkeitsmechanismen, wie sie auch beim Mensch zu finden sind, da diese die Kontrolle von vorhersehbaren und unvorhersehbaren Kontaktkräften erlauben. Eine Technik — welche unter dem Begriff *Impedanzregelung* zusammengefasst wird — betrifft die Implementierung von Kraft-Momenten-Sensoren in die Regelschleife, um das angestrebte Nachgiebigkeitsverhalten von Robotern aktiv zu regeln. Dieser von der Natur inspirierte Ansatz stößt dabei zunehmend an seine Grenzen, insbesondere, da er die Bandbreite möglicher Kontaktkräfte einschränkt. Beispielsweise ist es dem Roboter unmöglich auf etwaige hochdynamische mechanische Stöße zu reagieren. Um dieses Problem zu lösen, wurden in der jüngeren Vergangenheit *passiv* nachgiebige Mechanismen — sogenannte Variable Steifigkeitsantriebe (VSAs) — in robotische Systeme integriert. Diese bieten weitere Vorteile, zum Beispiel mechanische Energie für die Unterstützung von Bewegungen zwischen zuspeichern. Auch wenn eine schier unendliche Anzahl an möglichen Mechanismen vorgestellt wurde, existieren jedoch bisher keine einheitlichen Auslegungskriterien, insbesondere die mechanischen Eigenschaften betreffend.
Diese Arbeit versucht mit der Analyse des menschlichen Bewegungsapparats aus der Perspektive eines Ingenieurs Hinweise für mögliche Kriterien zu finden. Dafür werden spezielle Manipulanden entwickelt, welche reine mechanische Parameter von Hand und Arm ohne den Einfluss von Reflexen erfassen können. Da in der Literatur keinerlei Hinweise auf vergleichbare Diagramme vom Menschen zu finden sind, wie sie für die Beschreibung von variablen Steifigkeitsantrieben üblich sind, wird insbesondere die Möglichkeit des Menschen zur Entkopplung der Steifigkeit von der Kraft untersucht: einmal in zwei vergleichbaren Aufgabenstellungen, die die Verwendung gleicher Kraft aber nicht zwingend gleicher Steifigkeit erfordern; zum anderen durch sorgfältige Untersuchung des Mechanismus zur Kokontraktion antagonistischer Muskelpaare. Abschließend wird der Transfer der gewonnen Erkenntnisse auf robotische Systeme untersucht und diskutiert, insbesondere der Zusammenhang zwischen Kraft und Steifigkeit und die Implementierung von biartikulären Kopplungen zur Verbesserung der Einstellbarkeit der Nachgiebigkeit.

500 Zeichen — Diese Arbeit untersucht die bewusste Kontrolle *reiner* Steifigkeit des menschlichen Hand-Arm Systems. Die Frage wird zunehmend relevant, da Mensch und Roboter verstärkt in derselben Umgebung arbeiten, wobei der Einsatz robotischer Nachgiebigkeit die Kontaktkraftregelung erlaubt. Die Arbeit beschreibt die Entwicklung von Geräten, fähig reine mechanische Parameter des Menschen zu messen, sowie die Untersuchung der Variierbarkeit der Kraft–Steifigkeitskopplung des Menschen. Abschließend wird der Erkenntnistransfer auf robotische Systeme analysiert und diskutiert.

Acknowledgment

First of all, I want to thank the German Aerospace Center (DLR), since this Thesis was written and its content produced during my employment at the Institute of Robotics and Mechatronics. I am very grateful for the research environment this institution offers. Moreover, I am grateful to Prof. Patrick van der Smagt and Dr. Sc. ETHZ Markus Grebenstein for their supervision. In particular to Patrick van der Smagt for our multiple paper-writing sessions and his patience, his substantiated guidance along the difficulties of scientific research, and his valuable contributions to each single Section. And to Markus Grebenstein for his precious reviews of my mechanical designs, the intensive and enthusiastic discussions, and for always showing confidence in my work. I want to thank the mechanical lab led by Harald Wagner at DLR, since the close contact between mechanical engineers and manufacturers made it possible at all to build highly integrated mechatronic systems. Moreover, I am thankful to Prof. Alin Albu-Schäffer and Prof. Veit Senner, as well, who agreed to join my committee.

Furthermore, special thanks to my colleagues at DLR and the bionics group. In particular, to Rachel Hornung, Georg Stillfried, and Jörn Vogel. Not only since they accepted to review my Thesis. But also for the endless amount of yielding coffee breaks, as their content contributed to several Sections of this Thesis over the past six years. Especially, I want to thank Georg Stillfried, who was always willing to analyze daily challenges of research. Also, it was his initiation which lead to the obtained results on grip stiffness cocontraction. And I want to thank Jörn Vogel and Holger Urbanek for their helpful assistance in configuring experimental setups. It was also Holger Urbanek who took the admirable pictures of the Grip Perturbator. Moreover, I want to thank my students Maximilian Große-Dunker and Wolfgang Wiedmeyer for their helpful contributions.

I am grateful, as well, to all of the EU-projects that I was involved in, and for the opportunities these projects give to researchers, especially to collaborate with their peers. In particular I want to thank Prof. Joseph McIntyre with whom I became acquainted with during the project STIFF, and whose ideas the Grip Perturbator and the measurements within Section 2.3 are based on.

Finally, I want to acknowledge my family. Without their relentless support, such work would never have been possible.

Contents

Abbreviations and Symbols

Abbreviations

ANS Autonomic Nervous System

ATP Adenosine Triphosphate

BAVS Bidirectional Antagonism with Variable Stiffness

CC Contractile Component

CNS Central Nervous System

CSE Coefficient of Standard Error

DoF Degrees of Freedom

E1 Experiment 1: learned; no cuff; weight task first

E2 Experiment 2: learned; no cuff; force task first

E3 Experiment 3: learned; wearing cuff; both, force and weight task first

EMG Electromyography

EPH Equilibrium Point Hypothesis

FAS Flexible Antagonistic Spring

FSJ Floating Spring Joint

FT Force Task

LWR Light-Weight Robot

MVC Maximum Voluntary Contraction

NFL Normalized Force Level

PE Parallel Elastic Element

PNS Peripheral Nervous System

SE Serial Elastic Element

SEM Standard Error of Mean

SoNS Somatic Nervous System

TMC Tendon Muscle Complex

VSA Variable-Stiffness Actuator

WT Weight Task

Muscle Stiffness Glossary—Notations Commonly used in Standard Literature

active stiffness	coming from robotics, where notations like *active impedance control* and *passive stiffness mechanisms* are used; in the author's opinion erroneously used in biomechanics for reflexive stiffness, since the notations *active / passive* refer to the muscular activity (see *passive stiffness*) of a muscle (e.g. see [CCK90])
apparent stiffness	same as *reflexive stiffness* (e.g. see [LZ93])
areflexive stiffness	same as *stiffness* (e.g. see [Str98])
dynamic stiffness	same as *quasi-stiffness*; used to explicitly distinguish between *dynamic* and *static* stiffness (e.g. see [AKP00])
intrinsic stiffness	same as *stiffness* (e.g. see [KSP97])
lumped stiffness	lumped identification of stiffness; inertial and damping parameters highly contribute to the identified stiffness; sometimes includes active responses as well (e.g. see [GM79])
passive stiffness	stiffness of the passive (no attached crossbridges) areflexive muscle caused by muscle tendon, surrounding tissue and ligaments (e.g. see [CCK90])
reflexive stiffness	stiffness of the active reflexive muscle; measured mechanical response is dominated by reflexes (e.g. see [Str99])
short-range stiffness	stiffness dominated by the number of attached crossbridges (e.g. see [HMP11])
static stiffness	same as *stiffness*; measurements are performed around an equilibrium position in isometric conditions, i.e. during posture maintenance; used to explicitly distinguish between *dynamic* and *static* stiffness; sometimes includes active responses as well (e.g. see [AKP00])
stiffness	stiffness of the active, areflexive muscle including passive as well as short-range stiffness (e.g. see [LZ93])
quasi-stiffness	measurements of stiffness are not performed around an equilibrium position (e.g. see [LZ93])

1 Introduction

The engineering of state-of-the-art industrial robots is dominated by one criterion: *making them as stiff as possible*. The criterion arose since it improves accuracy, robustness, and bandwidth of position controlled robots working in precisely known environments. However, accompanied with recent developments the rule falls. Aiming for service, assistance and collaborative robotic systems as well as for increased industrial automation the role of human robot interaction becomes more relevant accompanied with unpredictable environments. Consequently, compliance was introduced into control—known as impedance control [Hog85a]—inspired by a well-known strategy in human motor control, the Equilibrium Point Hypothesis (EPH). This strategy—which is still a hypothesis and could not yet be proven—is based on the assumption that the Central Nervous System (CNS) generates movements by setting equilibrium points along a desired trajectory without precisely covering underlying task dynamics. The goal of the derived impedance control is not to reach a desired Cartesian position with the utmost accuracy, but rather to maintain a certain impedance, i.e. apparent stiffness, in order to be prepared for solving tasks while being in contact with the environment for protecting human *and* robot [HLU+11]. However, this approach has its limitations, as it does not allow for handling high-frequency impacts safely [HASH07, HASEH10], while the increasing dynamic behavior of robotic systems highly demands an answer to that problem. Moreover, common robotic systems are lacking in their energetic efficiency. In order to reduce production times in industry, a large amount of kinetic energy is dissipated by heat in reversal points, especially in cyclic motions which occur reliably during repetitive tasks. To address these issues, biology has recently been mimicked once more by considering spring-like properties of the Tendon Muscle Complex (TMC) and adding nonlinear, pretensionable springs to robotic systems, known as Variable-Stiffness Actuators (VSAs) [GASB+11, VASB+13, WBCt15]. Similar to two antagonistic muscles these mechanisms are able to change their position and *stiffness*. However, even if an endless amount of mechanisms for variable-stiffness techniques have been introduced, defining mechanical meaningful parameters for stiffness in robotics is still heuristically solved, as no general rules of stiffness variation have been devised. Again, nature can give helpful advice by analyzing modulation capabilities of human variable-stiffness mechanisms and answering the following questions: What do the force–stiffness plots commonly used to describe VSAs look like for human actuators? In general, it is known, that force and stiffness are related linearly. Are these parameters rigidly coupled? Or is it possible to considerably decouple the two? If yes, can this mechanism be controlled voluntarily? Or involuntary only, e.g. according to the task? Moreover, by looking

into the human upper limb locomotor system, one can see that the human has six muscles for the actuation of two joints, i.e. elbow and shoulder flexion and extension, while four actuators would be sufficient. Why has nature chosen such a complex variable-stiffness mechanism in which the strongest and most dominating muscles are crossing two joints, i.e. biceps and triceps, while robotics sticks to mono-articular actuation only? And finally, how can reasonable properties of human stiffness modulation mechanisms be transferred to robotics?
In physics and mechanics the notation *stiffness* is a metric easy to understand and to apply—captured by the terms *passivity, resistance*, and *elasticity*. In biomechanics and neuroscience the situation is completely different. Differentiations between joint, intrinsic, passive, areflexive, reflexive, short-range, incremental, lumped, apparent, quasi or even negative stiffness—partly violating the three characteristics mentioned above—can cause serious conflicts among researchers discussing the same topic and making it troublesome for robotic engineers to extract design criteria from standard literature[1]. The most accurate and reliable approach to the *in-vivo* identification of human stiffness is by position perturbation. Moving the limb or fingers over a small distance and measuring the effective force gives, when states are steady, direct information about pure stiffness [MIHB85]. However, existing manipulandi are comparatively slow and/or not very stiff, such that the mechanical response includes active neural effects of spinal reflexes or even from the motor cortex resulting in differentiations in stiffness as mentioned above.

This Thesis is trying to find answers to the questions above by looking into the human upper limb locomotor system, i.e. the hand and arm, from the perspective of a mechanical engineer by focusing on the measurement of purely mechanical responses only. The Thesis will therefore propose new mechanisms—able to perform fast pre-reflexive measurements—that will be used to investigate the raised questions. Focusing primarily on human intrinsic stiffness-modulation capabilities, a one-dimensional perturbation device will be presented. The device reduces the complex mechanism of the pinch grip to a one-dimensional approach, allowing to reveal answers to the questions. The gained knowledge is used to develop a planar manipulandum, which allows for comparable measurements at the human arm.
An essential drawback of the mentioned accurate position perturbation approach is its limitation to discrete measurements only, making it almost impossible to derive stiffness during daily tasks of living, e.g. cutting an onion, cleaning with a sponge or connecting a plug [LBD+15]. Yet, such a method would be highly valuable for teleoperation approaches, since it allows commanding stiffness from human to compliant robotic hands. Thus, this Thesis will further address the development of methods to continuously reveal information about stiffness by measuring muscular activity only.

1.1 Thesis Outline, Contribution, and Sources

Chapter 1 will introduce basic knowledge. Since the TMC is the origin of stiffness that is measured within this Thesis, special attention is paid in Section 1.2 to describe it and its modeling accompanied with an explanation of differentiations in stiffness used in the fields of biomechanics and neuroscience. It is followed by a description of the notation *stiffness*, why it can be used to describe the TMC, its transfer across coordinate frames, modeling, measurement, and possibilities to control it voluntarily. Finally, the Chapter is closed with an introduction to VSAs in general, and the DLR Hand Arm System in particular.

Chapter 2 is about stiffness of the human hand in a pinch grip reduced to a one-dimensional approach. This simplification allows to reveal relevant insights into human biomechanics, espe-

[1] Please have a look into the Muscle Stiffness Glossary at the very beginning of this Thesis.

cially about the mentioned force–stiffness characteristic. Starting with a general overview about related work, the design of a device able to measure areflexive grip stiffness is described. The device is then first validated in a force task showing the linear relation between grip force and stiffness, followed by two experimental setups analyzing the rigidity of this dependency. The first setup investigates the influence of the task on this linear relation, while the second setup investigates human ability to voluntarily decouple grip stiffness from force. The possibility to extract grip stiffness from the measurement of muscular activity is analyzed.

Chapter 3 describes the development of a planar manipulandum—a dedicated orthoglide robot with a focus on a lightweight and stiff design—able to reveal intrinsic mechanical properties of the human arm. A general introduction on background about measuring arm stiffness is given, followed by a description of the device and reasoning of design decisions. Finally, the manipulandum is validated in a force task.

Chapter 4 investigates the transfer of gained knowledge to robotic systems. Based on the mechanism of the *helping antagonism* [FHPH11] used in the forearm rotation of the DLR Hand Arm System, copying the linear characteristic to robotic joints is analyzed. Furthermore, a mechanism with two biarticular couplings and four mono-articular actuators is introduced. It is investigated, what is gained and what is lost by introducing these two additional motors, and reasonable solutions are discussed.

Chapter 5 provides a conclusive review and conclusive remarks on the achievements of the Thesis, in particular by addressing achieved results, limitations, potential applications, and possible future work.

It needs to be mentioned that the research in this Thesis on grip stiffness surmounts research on arm stiffness. This has primarily historical reasons, since the Grip Perturbator introduced in Chapter 2 allowed to quickly gain valuable insights into mentioned force–stiffness characteristics, and—in contrast to arm stiffness—only little literature addressing finger stiffness exists. Beside that, the focus of this work is clearly set to biomechanics, rather than robotics.

1.1.1 Contribution

This work contributes to biomechanic and robotic research as follows:

1. New manipulandi are introduced capable of measuring purely mechanical response, i.e. areflexive stiffness of hand and arm *in-vivo*. To the author's knowledge no manipulandi exist with comparable properties, in particular regarding their *stiffness, power,* and *velocity* (Patent [SHL+11]).

2. Pinch grip stiffness is related linearly to the applied force. However, this relation cannot be regarded as fixed; rather the task plays an important role for the shape of that function; strategies of cocontraction and/or change in kinematics can be used to affect it. Nevertheless, linearity still holds within each task.

3. Humans are able to substantially decouple grip stiffness from force using cocontraction voluntarily with an increasing ability for higher forces. To the author's knowledge, comparable force–stiffness characteristics are neither known in biomechanics nor neuroscience, which might be used as an inspiration for the design of VSAs.

4. The thumb is approximately twice as stiff as the index finger. This is a helpful design criterion for the design of robotic hands with variable stiffness.

5. Solely measuring muscular activity of interossei muscles in the hand allows revealing information on grip stiffness. This method can be used to continuously measure task dependent grip stiffness, or for the teleoperation of soft robotics, be they impedance controlled or passive elastic (Patent pending).

6. Biarticular actuators are able to exceptionally enlarge stiffness modulation capabilities, i.e. by a 70-fold improvement of versatility. A biarticular actuator based on the *helping antagonism* [FHPH11] is proposed, while an under-actuated version with two biarticular couplings and two mono-articular actuators in the base is favored (Patent [HLe13]).

1.1.2 Sources

The work of this Thesis has been established within the context of the European projects STIFF (http://www.stiff-project.org/, grant agreement no. FP7-ICT-231576), VIACTORS (http://www.viactors.org/, grant agreement no. FP7-ICT-231554), THE (http://www.thehandembodied.eu/, grant agreement no. FP7-ICT-248587), and SoMa (http://www.softmanipulation.eu/, grant agreement no. H2020-ICT-645599).

The author of this work is also author and co-author of several publications which are incorporated into this Thesis and of which graphics, text, etc. have been used. Whenever applicable, the publications are cited in the according Sections. This concerns especially—but not exclusively—the following:

- Section 2.2 was published in Hannes Höppner, Dominic Lakatos, Holger Urbanek, Claudio Castellini, and Patrick van der Smagt, *The Grasp Perturbator: Calibrating human grasp stiffness during a graded force task*, In Proceedings of IEEE International Conference on Robotics and Automation (ICRA), pages 3312–3316, 2011,

- Sections 2.3 and 2.4 were published in Hannes Höppner, Joseph McIntyre, and Patrick van der Smagt, *Task dependency of grip stiffness—A study of human grip force and grip stiffness dependency during two different tasks with same grip forces*, PLoS ONE, 8(12):e80889, 12 2013,

- Section 1.7 and 2.5 were submitted as Hannes Höppner, Maximilian Große-Dunker, Georg Stillfried, and Patrick van der Smagt, *Key insights into hand biomechanics: On decoupling grip stiffness from force by cocontraction and stiffness-regression from electromyography* to Frontiers in Neurorobotics and are based on raw data which were acquired during the Master Thesis of Maximilian Große-Dunker [GD13],

- Chapter 3 was published in Hannes Höppner, Markus Grebenstein, and Patrick van der Smagt, *Two-dimensional orthoglide mechanism for revealing intrinsic human arm mechanical properties*, In Proceedings of IEEE/RSJ International Conference on Intelligent Robots and Systems (IROS), pages 1178–1185, September 2015, and

- Section 4.2 and 4.4 were published in Hannes Höppner, Wolfgang Wiedmeyer, and Patrick van der Smagt, *A new biarticular joint mechanism to extend stiffness ranges*, In Proceedings of IEEE International Conference on Robotics and Automation (ICRA), pages 3403–3410, May 2014,

which are subject to copyright protection, published by the author of this Thesis and his co-authors.

1.2 About Biomechanics of the Tendon Muscle Complex

Muscles can be differentiated into skeletal, smooth, and cardiac muscles. Their main functions are movement and motion, posture maintenance, joint stability, shock absorption and heat generation (adapted from [Cli07, MH07]). Cardiac muscles are controlled by the Autonomic Nervous System (ANS) (also referred to by visceral nervous system) and thus are only involuntarily controlled. Smooth and skeletal muscles can be controlled by the ANS as well as the Somatic Nervous System (SoNS) (which together build the Peripheral Nervous System (PNS)) and can be controlled both voluntarily as well as involuntarily. As human limb stiffness is the quantity this Thesis is about, the skeletal Tendon Muscle Complex is of interest only. Skeletal muscles have four functional characteristics [Mut02, MH07]:

- *Contractility*—the ability to produce a tension[2], which is most-likely its most important ability and distinguishes it from other bodily tissue;
- *Excitability or Irritability*—the ability of the tissue to respond to a chemical/thermal/electrical/mechanical stimulus;
- *Extensibility*—the ability to stretch when an external force is applied; and finally
- *Elasticity*—the ability to return to its original length after an external force is released.

In general, the term *Contraction* is misleading, since it suggests in its physical meaning that the muscle needs to change its *length* during activation, which is not the case. Therefore, it is called *concentric contraction* when the muscle shortens during activation depending on the strength of an external load, *eccentric contraction* when the muscle lengthens (e.g. during shock absorption during landing), and *isometric contraction* when the length of a muscle is kept constant during activation (e.g. holding a weight). Concentric contraction describes the action often meant by solely using the terminology *contraction*. Muscles can actively shorten only, which does not contradict the action of eccentric contraction.

The skeletal muscle is a biological system built up similar to a Matryoshka doll (see Fig. 1.1): The muscle is a bundle of fascicles surrounded by connective tissue called epimyosium, while a fascicle is a bundle of muscle fibers (i.e. the muscle cells) surrounded by connective tissue called perimyosium, whereas a muscle fiber is a bundle of muscle fibrils surround by connective tissue called endomyosium. Again, each muscle fibril is a bunch of single force production units—the sarcomeres—connected in series via so-called Z-discs (from the German word *"Zwischenscheiben"*), while each sarcomere is a hexagonal structure of six parallel series of thin and thick filaments—the actin and myosin filaments. Each of the thin actin filaments overlaps two sarcomeres across the Z-disc, while the thick myosin filaments are centered via *elastic* titin in the middle of the sarcomere. The myosin filament consists of two globular heads and a long tail and is able to dissociate Adenosine Triphosphate (ATP), while using the energy of this chemical process to rotate its heads. Since the myosin heads can couple to the thin actin filament, a rotation of the heads causes relative movement of the actin filaments at two Z-discs of approximately 10 to 15 nm. Decoupling and rotating the heads back and repeating the process with 5 Hz for several sarcomeres in series results in noteworthy muscle shortenings/production of tension. This repeating process is usually called *cross-bridge cycle* and refers to the *sliding filament theory*—two filaments sliding past each other while maintaining their length[3]—and was

[2]Note that the term *tension* is used rather than *force* to describe muscle action, since it is used to describe similar three-dimensional repetitive objects and is independent from the cross sectional area of the muscle.

[3]Note that recent research provides evidence that both actin as well as myosin, are not as in-elastically as they have been initially regarded [RMH99].

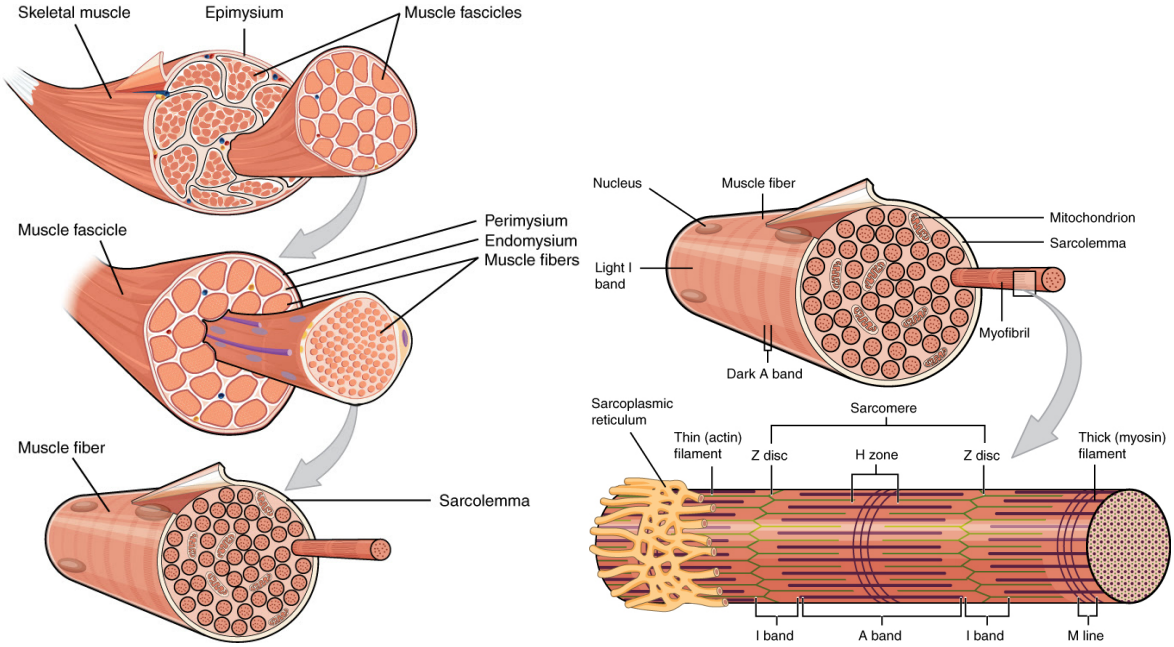

Figure 1.1: The skeletal muscle (reproduced and adapted from [Col13]) — The muscle consists of bundles of muscle fascicles, which consists of bundles of muscle fibers, which consists of bundles of muscle fibrils. The fibril again consists of series of sarcomeres, the force production units.

described first by A.F. Huxley [Hux57a] and H.E. Huxley [Hux57b] independently in 1957[4].
Skeletal muscles can be divided into Type I, *slow twitch* and Type II, *fast twitch* muscle fibers. Slow twitch fibers, also known as tonic skeletal muscle fibers, fire slowly, and can produce less force at slow contraction speeds, but are highly resistant to fatigue. Fast twitch muscle fibers, also known as phasic skeletal muscle fibers, fire rapidly. They can be subdivided into Type II-b fibers, which are strong at fast contraction speeds, but fatigue very rapidly, and Type II-a fibers that are strong and fast, and resistant to fatigue and lie somewhere in-between Type I and Type II-b fibers. Motor units are recruited subsequently from the slowest/weakest to the fastest/strongest, what is commonly called *Henneman's size principle*. This has two main advantages, as a precise control of force over its full range and a minimization of the amount of fatigue, when only using fast-fatigue fibers if high forces are required.
The force–length relationship of an active muscle is dominated by the single sarcomeres and thus by the overlap of actin and myosin filaments (see Fig. 1.2, which is based on the investigation of a frog skeletal muscle [RMH99]). To understand the diagram, some parameters need to be mentioned (adapted from [RMH99]): the actin and myosin filaments are each 0.95 μm and 1.60 μm long, respectively; the Z-disc length is 0.05 μm and in the middle of a myosin filament there is a *dead zone*, which contains no myosin heads. The force which can be produced by the sarcomere is optimal between points (3) and (4): in point (3), the sarcomere length is exactly 2 μm, which is the sum of two Z-discs and two actin filaments. Here, the overlap between actin and myosin heads is optimal. Due to the dead zone the production of force between (3) and (4) from 2 to 2.2 μm sarcomere length is constant, resulting in a force plateau for the optimal length. For a further increase in length and an overstretching of the sarcomere, the number of overlapping myosin heads with actin filament decreases resulting in a linear decrease of possible cross-bridges and hence of active force. For decreasing length from (3) to (2) between 2.0 and 1.7 μm, the two actin filaments start overlapping resulting in an increase of lateral distance

[4] A.F. Huxley explained *"... I am not detectably related to Dr. Hugh Huxley, and it is pure coincidence that, in the same year, he and I independently got onto the idea that muscle contraction takes place by relative sliding motion of two sets of filaments..." [Hux04]*

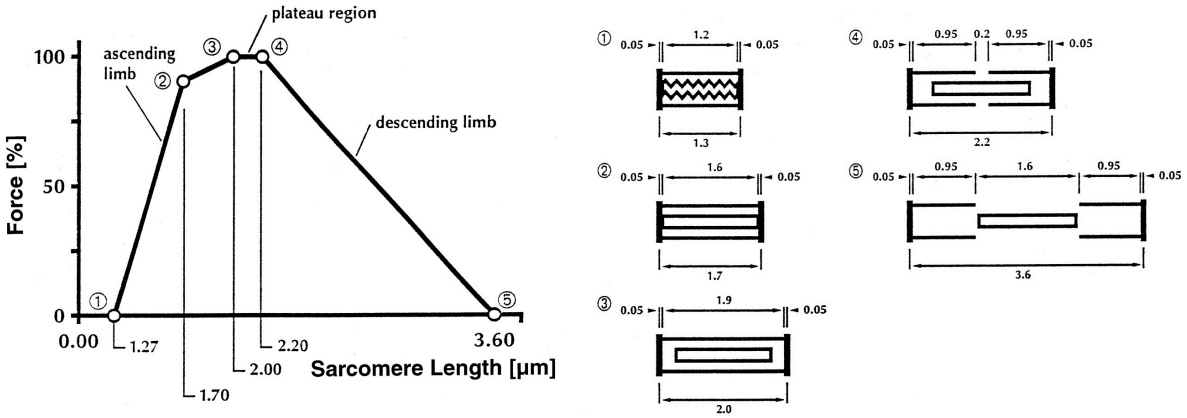

Figure 1.2: Force–length relation of a frog skeletal muscle sarcomere (copied from [RMH99], which is adapted from [GHJ66]) — The force which can be produced by the sarcomere is optimal between points (3) and (4). Here, the overlap between actin and myosin heads is optimal. A further increase in length and an overstretching of the sarcomere causes a linear decrease of possible cross-bridges and hence of active force. For decreasing length from (3) to (2), the two actin filaments start overlapping accompanied with a reduced active force. For further decrease in length below point (2) the sarcomere starts acting against internal forces, resulting in a linear decrease of active force.

between actin and the myosin heads and thus a reduced active force[5]. For further decrease in length below 1.7 μm the sarcomere start acting against internal forces caused by deforming the myosin filament, resulting in a linear decrease of active force. At a length of approximately 1.27 μm no further production of active force is possible.
The active part of the force–length relation of a muscle directly shows the influence of the sarcomeres (see Fig. 1.3). Moreover, the passive characteristic of a muscle is shown, which is dominated by the giant elastic titin filaments [THT05, GKHT97]. As it can be seen, the passive characteristic is designed in a way that it pulls the muscle always back into its optimal length. For the stretched muscle, the developed muscle force is a sum of the stretched passive elastic titin forces and the active cross-bridge forces.

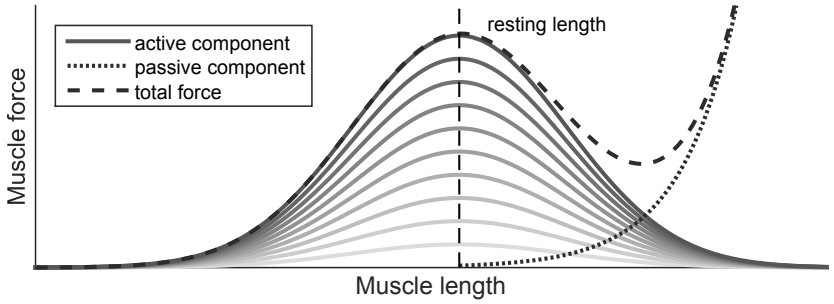

Figure 1.3: Exemplary force–length relation of a skeletal muscle (created using a MATLAB® model distributed by [Yun13]) — The active component (solid lines) is depicted for various muscle activations. The passive component (dotted line) is designed in a way that it pulls the muscle always back into its resting length. The force which can be produced at this optimal length is maximal.

1.2.1 Muscle Modeling—The Hill-Type Muscle Model

The modeling of muscles is mainly affected by a model published by Archibald Vivian Hill, who is a famous researcher dominating the research on muscle biomechanics within the first half of the 20th century. In general, by referring to the *Hill-type muscle model*, a characteristic equation and three-element model is meant describing H.S. Gasser's and A.V. Hill's controversial

[5]Note that the length 1.7 μm is a sum of the lengths of one myosin and two Z-discs.

initial idea [GH24] of muscles having a *viscosity* by relating their force F and velocity v. These researchers found that this viscous friction is not a process actively controlled by the CNS, but rather an intrinsic property of the muscle. They modeled the muscle as a spring-like actuator acting in a viscous medium [WS87]. The aforementioned famous equation was introduced separately by Hill in 1938 [Hil38], when he conducted a set of experiments on isolated frog muscles. He attached a mass to a muscle via a lever arm, which was held at isometric state (e.g. at optimal fiber length) using a catch mechanism[6]. The lever arm was used to minimize the effect of inertia of the load on the performed measurements. He tetanized the muscle so as to exert an optimal amount of force F which is appropriate for a certain length x. After releasing the catch mechanism the muscle switches instantaneously from isometric to isotonic (constant load) state, whereby the attached load is consciously smaller in comparison to the tetanized muscle force in the isometric state. Hill then measured the rate of change in position directly at the onset of a viscous reaction, which he repeated for several weights so as to measure a (a) force-velocity relationship. Within these experiments, Hill also investigated the production of heat in the muscle and found that muscles fibers shorten even during tetanically isometric contractions and (b) liberate a constant amount of energy in forms of heat and mechanical work. Moreover, he found that (c) during concentric contraction the muscle produces an extra amount of heat, which he called the *heat of shortening*, and which relates linearly to the change in length and is independent on the applied force. From these new insights and by appraising the production of heat and mechanical work, Hill found an hyperbolic function between force F and velocity v

$$(F + a) \cdot (v + b) = (F_0 + a) \cdot b = \text{const.}, \tag{1.1}$$

which shows that muscle force is zero for maximum velocities and maximum for the lower ones (a, b, and F_0 are constants). This is somewhat intuitive: A man might lift a light load very rapidly, while a heavier load takes more time [Lie02]. The equation is phenomenological, meaning that it just reflects the measured data set (maximum force, concentric contraction) rather than being revealed from hypothesis mechanisms. Surprisingly, this equation works rather well for describing concentric contractions of muscles for nearly all muscle types examined so far, be they smooth, cardiac or skeletal. Fig. 1.4 graphically depicts the measured relation.

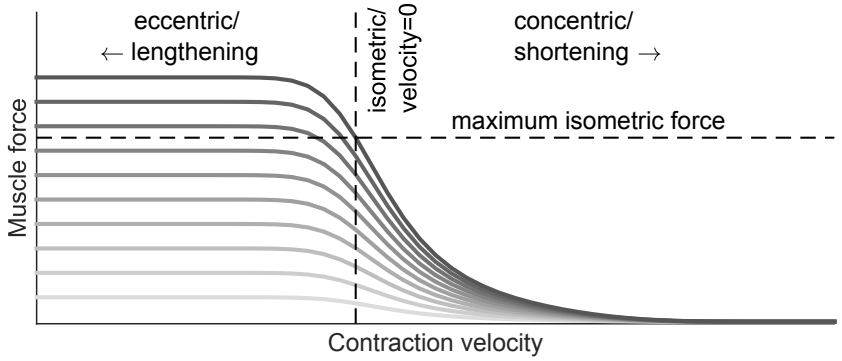

Figure 1.4: Exemplary force–velocity relation of a skeletal muscle for different muscle activations (created using a MATLAB® model distributed by [Yun13]) — The horizontal dashed line depicts the maximum force the muscle is able to produce at isometric state. The muscle force decreases with shortening velocity (concentric contraction), while it saturates with lengthening velocity (eccentric contraction). Keep in mind that the muscle can actively shorten, only.

In contrast, eccentric contraction cannot be described by Hill's Equation (1.1), and to the author's knowledge no mathematically adequate approximation exists, since it differs substantially

[6]Note that Hill received the Nobel-prize in Physiology or Medicine earlier in 1922 *"... for his discovery relating to the production of heat in the muscle..."* [Nob22].

between muscles. In general, it behaves different to concentric contraction, meaning that the exertable forces increase with stretching velocity (see Fig. 1.4 as well), while saturating for the higher velocities up to 1.5 times the isometric force F_0 [BFM13].

More commonly, a three-element model is meant by referring to the *Hill-type muscle model*, rather than Hill's Equation (1.1). In his publication [Hil38], Hill concluded from the performed measurements that *"... the viscoelasticity of contracting muscle is shown to be the property of a two-component system, the one component being undamped and elastic, the other being governed by the characteristic equation..."* acting in series, the Contractile Component (CC) and Serial Elastic Element (SE). The existence of the SE has directly been proven with the performed quick-release experiments: the rapid change in length after a sharp change in force provides evidence for the existence of a solely serial elastic element. Moreover, Hill suggested that the CC consists of a pure force generator, which he called the *active state*, in parallel with a non-linear dashpot which governs the observed viscous damping behavior accompanying a parallel elasticity, the Parallel Elastic Element (PE). Note the analogy: the undamped SE equals the tendon, while the PE corresponds to the soft tissue surrounding the muscle.

The main advantage of the Hill-type muscle model is its striking simplicity: for most of the cases the dynamic behavior of each muscle of the musculoskeletal system can be described with a single differential equation, which makes the model a feasible tool for an adequate modeling of human movement [WS87]. Moreover, it allows researchers to clearly discriminate between slow- and fast-twitch muscle fibers and to estimate peak power from force–power curves. On the other hand, its limitations are (a) that all data on which it relies are obtained at or near optimal fiber length, (b) that it applies only for quick release, (c) that no eccentric contraction is governed (e.g. using a larger load in comparison to the tetanized isometric muscle force before the release), and (d) that the constants a and b in Eq. (1.1) differ from experiment to experiment. Moreover, it performs bad in modeling the property of stiffness measured within this Thesis (see also [HMP11]), which will be discussed in the following.

1.2.2 Muscle Modelling—The Huxley-Type Muscle Model

Beside its striking simplicity, the Hill-type muscle model is lacking on modeling sarcomere stiffness when the muscle is actively producing a force, i.e. modeling a transient change in force due to a small change in length of a sarcomere[7]. However, it is a usual approach to simply take the slope of the force–length characteristic (see Fig. 1.3) to model the stiffness at a certain activation and length [Str99, BL00, IR04] as mentioned by Hu *et al.* [HMP11]. This results in strange problems like (a) a negative stiffness as a result of a negative slope of the force–length relation for the higher activations leading to unstable muscle simulations [MUSD13, BS14], or (b) a constant stiffness with an almost linear increase in force (increase of actomysin-bonds) with length on both sides of the active isometric force–length relation, (c) zero stiffness for optimal sarcomere length, and (d) it suggests similar stiffness if stretched or shortened. Indeed, the force–length curve describes the isometric force a muscle is able to produce when activated at a certain length, but it does not allow drawing conclusions about a fast change in force during rapid displacements [JRW69].

In the 1950's it was still intensively debated whether the cross-bridges are the actuators in generating the force and motion between the two filaments [Wil11]. At the time, most muscle contraction theories were based on the hypothesis of folding of large proteins [ME13]. In order to strengthen the argumentation for the sliding filament hypothesis and based on images of the newly available technology *electron microscopy*, Andrew Fielding Huxley proposed his muscle

[7] Note that for a fully passive muscle, the passive characteristic of the force–length relation does provide a reasonable prediction of muscle stiffness.

model[8]. In contrast to the phenomenological Hill-type muscle model, the Huxley model is a set of mathematical functions, which are directly derived from the hypothesized sliding filament mechanism. In its initial form, the model exists of two defined cross-bridge states: a state where myosin-heads are attached to the actin molecules and another with detached actomyosin bonds. Huxley modeled a bond distribution function $n(x,t)$ at a certain displacement x and time t by

$$\left.\frac{\partial n(x,t)}{\partial t}\right|_{x=\text{const.}} - v(t) \cdot \left.\frac{\partial n(x,t)}{\partial x}\right|_{t=\text{const.}} = [1 - n(x,t)] \cdot f(x,t) - n(x,t) \cdot g(x,t), \tag{1.2}$$

where $f(x,t)/g(x,t)$ are the attachment/detachment rate constants, $v(t)$ the concentric contraction velocity, and x the displacement from an equilibrium position. While $n(x,t)$ represents the number of attached cross-bridges, $[1 - n(x,t)]$ represents the number of detached ones. In its initial representation, the cross-bridge stiffness was assumed to be linear elastic, which it is not [Zah00, HWH$^+$90]. However, *"... the usual assumption of a constant cross-bridge stiffness in two-state models is at best a rough, albeit often a convenient and useful, approximation..."* [Zah00]. The bottlenecks of the equation are the piecewise defined attachment and detachment rates, which defines whether a force can be transmitted by a cross-bridge or not. Huxley adapted these two values by fitting the equation to the empirically observed force–velocity and force–energy relations from A.V. Hill [Hux57a].
By solving the equation for $n(x,t)$—and by assuming a constant contraction velocity, i.e. $(\partial n(x,t)/\partial t)|_{x=\text{const.}} = 0$—the exerted muscle force can directly be derived from the numbers of attached cross-bridges. Furthermore, the equation allows to draw conclusions about the metabolic costs liberated during different contraction speeds, since energy liberated is highly depending on the cross-bridge attachment and detachment. There are several extensions of this model for a better description of phenomena observed in experiments, with up to 18 different states [Pro86], e.g. to account for fast transitions in the order of 1 ms in the cross-bridge cycle[9]. Nevertheless the two-state model allows for a reasonable modeling of the cross-bridge cycle in most of the cases [Zah00].

All in all, it has to be mentioned that the Huxley-type muscle model is computationally time consuming impeding real-time implementations since muscle dynamics are described by a set of multiple differential equations [BLMB04]. Moreover, it only allows for a precise prediction of concentric contractions. Similar to the Hill-type muscle model, eccentric contraction remains an open challenge. Finally, the Huxley Eq. (1.2) is of high relevance for this Thesis, since it allows for drawing conclusions about the sarcomere stiffness, which is similar to the force proportional to the numbers of attached cross-bridges [BFM13].

1.2.3 Reflexive and Areflexive Properties of the TMC

The areflexive *passive* (non-activated) properties of the TMC are dominated by the PE and SE with an essentially stiffer SE. While the SE is dominated by tendons and aponeuroses, the PE mainly consists of the giant protein titin and of three types of soft tissue surrounding the muscle components. The main part of parallel elasticity is caused by the stretch of titin [Jin14], since no cross-bridges are attached in the passive muscle. The tendon is characterized by a so-called *elastic toe* describing its force-displacement relation[10]. The normal working range of a tendon lies within this elastic toe, which is less than 4 % of strain [LZ93]. Beyond the elastic toe, the

[8] Note that in 1963, the Nobel-prize in Physiology or Medicine was awarded jointly to Sir John Carew Eccles, Alan Lloyd Hodgkin and Andrew Fielding Huxley *"... for their discoveries concerning the ionic mechanisms involved in excitation and inhibition in the peripheral and central portions of the nerve cell membrane..."* [Nob63].

[9] For detailed information about this so-called $T_1 - T_2$ phenomenon see [HS71].

[10] Note that the energy dissipation of a tendon is small, meaning that most of the energy stored into it can be regained [LZ93].

force-displacement characteristic is considered to be linear and thus stiffness to be constant. Stiffness of the passive areflexive muscle is 100 times less than tendon stiffness [Arn76]. Within this Thesis, stiffness of the areflexive passive muscle will be referred to as *passive stiffness*.
Stiffness of the areflexive *active* muscle is dominated by the number of attached cross-bridges [BFM13]: Stretching an active muscle causes an increase of force, while stiffness stays constant until the change in length of a single sarcomere unit reaches 15 to 20 nm [BFM13], which is the limit the actomyosin-bond can hold. Thus, the stiffness is a result of the elasticity of the myosin heads. If the sarcomeres are stretched beyond this limit, the actomyosin bonds detach. The stiffness up to this limit is called *short-range stiffness*. This short-range depends on the type of muscle fiber, and no clearly defined limits exist. The length change is distributed among all sarcomeres of a muscle fiber, while the change in force is equal for each sarcomere. Thus, the larger the number of sarcomeres—i.e. the longer the muscle—the lower the stiffness of a muscle fibril [BFM13]. Stiffness of the areflexive, active muscle will be referred to as *intrinsic stiffness* or simply *stiffness* within this Thesis.
Reflex contributions can be subdivided into short- and long-latency components. The short-latency reflex is also known as Hoffmann's reflex (H-reflex) or phasic stretch reflex. It is proportional to a variation in muscle length, i.e. velocity related, connected to the muscle spindles, monosynaptic, and results in rapid and forceful contractions. The abductor pollicis brevis has, for example, a mean onset latency in the order of 30 ms and a duration of 10 ms [DH93]. It reacts more powerful the stronger the intensity/variation of the perturbation is. The long-latency reflex is also known as tonic stretch reflex. It is directly proportional to the displacement, i.e amplitude related and polysynaptic. It causes the muscles to maintain a sustained prolonged contraction, e.g. during slow stretching, with a mean onset latency in the order of 50 ms, and a duration difficult to educe [DH93]. It reacts more powerful the stronger the perturbation is.
Reflex generated stiffness provides a significant fraction to the overall muscle response, while the percentage is highly dependent on muscle force. Albeit differently, both areflexive and reflexive stiffness depend on muscle force and stretching amplitude. For the areflexive muscle stiffness is linearly dependent on muscle force. The reflex response is strong for low forces, while it is lower and converges for high forces [SA92]. This results in a saturating overall reflexive-stiffness response. Conclusively, the reflexive muscle is less force sensitive in comparison to the areflexive one (see Fig.1.5).

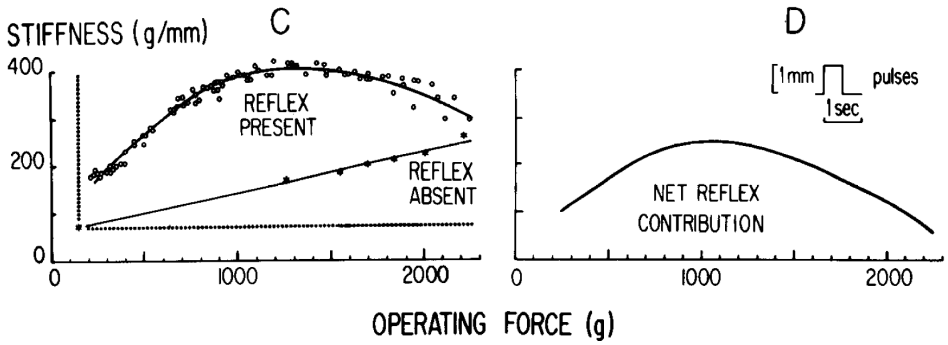

Figure 1.5: Reflexive and areflexive stiffness as it is influenced by muscle force (copied from [HA81]) — Areflexive stiffness of a muscle depends linearly on force. The reflex contribution is strong for low forces, increases for moderate forces, and declines for higher forces again. This results in a saturating overall muscle response for higher forces.

Shadmehr performed analyses, mainly investigating, whether the reflexive muscle can be regarded as an actuator with variable stiffness or an actuator with variable resting length [SA92]. From the performed analyses he revealed that the reflexive muscle *"... resembles a non-linear spring with an adjustable resting length..."* [SA92], supporting Feldman's hypothesis of the EPH, i.e. humans tune the threshold of the tonic stretch reflex. Moreover, he showed that

muscle stiffness cannot be constant, since it will lead to instability of the joint if humans use cocontraction. Rather the stiffness has to be *"... at least linearly dependent on force ..."* under isometric conditions in order to provide joint stability. Similarly to Hogan [Hog84] Shadmehr found that reflexes provide a possibility to maintain joint stability under minimal metabolic costs, since *apparent stiffness* increases faster than linearly with force for the reflexive muscle. Moreover, intrinsic stiffness of the areflexive muscle is highly dependent on changes in the perturbation amplitude—stiffness decreases with displacement [VD98, BFM13]—while reflexive stiffness is less dependent on the perturbation length [NH76]. This means that reflex action introduces linearity in some sense—force increases linearly with displacement, but stiffness remains constant—which is why the authors of [NH76] concluded that stiffness might be the mainly regulated property of the stretch reflex. Moreover, the reflexive response is large for stretching in comparison to the small mechanical response, while the opposite holds for shortening [NH76]. All in all, areflexive stiffness is dominated by the tendon and the number of attached cross-bridges and is linearly related to the operating force. In contrast, reflexive stiffness considerably extends the overall mechanical response with a saturating reflexive stiffness for higher forces.

1.3 Using Impedance and Stiffness to Characterize the TMC

To describe the dynamic and resistive behavior of a muscle, the term of *impedance* is used. Typically, impedance is a notation applied in electronics to describe time dependencies in electronic circuits, but it has been introduced in mechanics, too, e.g. in order to characterize dynamics for robotic joints.
Impedance is the complex ratio of a phasor representing a cyclic varying potential quantity (voltage, force, temperature) to a phasor representing cyclic flow quantity (current, velocity, heat flow)[11]. Admittance is the inverse of impedance. The real part of impedance/admittance, the resistance/conductance, is independent of frequency ω; the imaginary part, the reactance/susceptance, varies with frequency, turning zero at the resonant frequency. The mechanical impedance $\boldsymbol{I}(\omega)$ for a second order spring-damper-mass-system is defined as

$$\boldsymbol{I}(\omega) = \frac{\boldsymbol{F}(\omega)}{\dot{\boldsymbol{x}}(\omega)} = \boldsymbol{B} + j\left(\omega \boldsymbol{M_x} - \frac{\boldsymbol{K}}{\omega}\right); \quad \text{with} \tag{1.3}$$

$$\Re\{\boldsymbol{I}(\omega)\} = \boldsymbol{B} \quad \text{and} \tag{1.4}$$

$$\Im\{\boldsymbol{I}(\omega)\} = \omega \boldsymbol{M_x} - \frac{\boldsymbol{K}}{\omega}, \tag{1.5}$$

where $\boldsymbol{M_x}$ is the inertia, $\boldsymbol{B}$ the viscous damping and $\boldsymbol{K}$ the stiffness. Similar to electronics, the velocity $\dot{\boldsymbol{x}}(\omega)$ lags behind the force $\boldsymbol{F}(\omega)$ at the mass and the force lags behind the velocity at the spring about $\pi/2$. The damping causes no phase-lag between force and velocity.

Metric impedance is able to perfectly represent the mechanical response of a muscle. Nevertheless, due to its applicability and comprehensibility, the notation *stiffness* dominates the representation of muscles mechanical response. Stiffness in its physical meaning describes the deformation of a *passive* object (no metabolic cost is spent to produce the resistance; *passivity*) generating a unidimensional force to *resist* against the presence of an external force. According to Hooke's law an ideal and unidimensional spring is independent from velocity and displacement and can be described by

$$F = -kx. \tag{1.6}$$

[11] Note that there are similar definitions, where velocity denotes the potential and force the flow.

The negative sign is applied to describe its resistive nature against a deformation (*resistance*). Ideally, the resistive force produced by the deformed object is a *conservative* force, which is the most essential property of stiffness. It means that all energy required to deform the object is elastically stored (*elasticity*) and will be regained after releasing the external force, rather than being dissipated. It also implies that stiffness itself can only be *positive*. Moreover, it implies that any negative value of stiffness is unrealistic. It is essential to mention that there are no assumptions regarding linearity nor continuity of the relation between force and displacement [Hog85b].
Stiffness K of a passive object can be revealed by measuring the incremental difference in force F and displacement Δx before and after a deformation around an *equilibrium position*. For the one-dimensional case the simplification

$$\Delta F = -K\Delta x, \quad \text{where} \quad K = K(x,t) = -\frac{\partial F}{\partial x} \tag{1.7}$$

holds, often called *incremental stiffness*. If the measured forces originate from conservative forces only (excluding gravity), the result is pure stiffness. It will be referred to as *areflexive stiffness*, *intrinsic stiffness* or just *stiffness* within this Thesis, and includes effects of passive as well as short-range stiffness.
As results of standard literature in neuroscience and biomechanics on the measurement of stiffness are commonly based on *in-vivo* measurements on human subjects and since it is nearly impossible to perform *in-vivo* measurements on the isolated TMC, the obtained mechanical responses always include effects of the joint mechanisms, as well. Therefore, the notation of *joint stiffness* has been established [LZ93], which also comprises the influence of non-linear muscle moment arms depending on join angles.

Stiffness can be measured by displacement of an object around an equilibrium; this often leads researchers to misuse the term stiffness for interpreting arbitrary changes between force and displacement, which results in unconventional findings such as *negative stiffness* [DPSV91, EB14]. Latash and Zatsiorsky stated: *"... Its* [author's note: stiffness] *usage in many of the studies is likely to make a physicist nervous and the emergence of such expressions as 'negative stiffness' in serious scientific publications may even cause a nervous breakdown ... "* [LZ93]. If the reaction forces are not originating from a purely conservative force field and include reflexive responses as well, they will be referred to by the term *apparent* [LZ93] or *reflexive stiffness*. If the origin of the forces additionally includes wrongly interpreted inertial or damping components but the measurements are still performed around an equilibrium, the term *lumped stiffness* will be used[12]. Finally, if measurements are not performed around an equilibrium, i.e. during movement leading to the interpretation of modeled movement-deviations as stiffness, or recording a torque-angle curve during smooth deflection of a joint, the result will be referred to as *quasi-stiffness* [LZ93].

Conclusively, regarding the TMC as a single unidimensional spring and describing it in terms of one metric *stiffness* is questionable. As mentioned above the muscle state depends on the operating length, its activation, muscle type, and the properties of the externally induced perturbation and is a highly non-linear mechanical system. However, in comparison to *mechanical impedance*, the metric *stiffness* is easy to understand and to imagine, allowing engineers to copy nature by using standard mechanical components. Since the focus of this Thesis lies on design criteria for variable-stiffness robotics, this Thesis obeys with representing the resistive nature of an areflexive muscles at steady states using the notation of stiffness.

[12] To the author's knowledge, initially used by Greene *et al.* in 1979 [GM79], sometimes also including active response.

1.4 Transformation between Muscle, Joint and Cartesian Space

In this Section transformation policies between muscle, joint, and Cartesian space will be introduced, that are required to transfer velocities, forces/torques, and impedances from one space into another. Similarly to Eq. (1.3), that describes the relation between velocity, force and impedance in Cartesian space, Eqs. (1.8) and (1.9) can be conjectured, which does the same for joint and muscle space:

$$\boldsymbol{T}(\omega) = \boldsymbol{Z}(\omega)\,\dot{\boldsymbol{q}}(\omega) \quad \text{and} \tag{1.8}$$
$$\boldsymbol{\Phi}(\omega) = \boldsymbol{\Sigma}(\omega)\,\dot{\boldsymbol{\lambda}}(\omega), \tag{1.9}$$

where $\boldsymbol{T}(\omega)$, $\boldsymbol{Z}(\omega)$, and $\dot{\boldsymbol{q}}(\omega)$ are the joint torque, impedance, and velocity, and $\boldsymbol{\Phi}(\omega)$, $\boldsymbol{\Sigma}(\omega)$, and $\dot{\boldsymbol{\lambda}}(\omega)$ the muscle force, impedance, and velocity, respectively.
The Cartesian and joint velocities are coupled by the Jacobian matrix $\boldsymbol{J}(\boldsymbol{q})$, taking into account bone and segment length; while muscle and joint velocities are coupled by the Jacobian matrix $\boldsymbol{\Pi}(\boldsymbol{q})$, which corresponds to muscles moment arms:

$$\dot{\boldsymbol{x}}(\omega) = \boldsymbol{J}(\boldsymbol{q})\,\dot{\boldsymbol{q}}(\omega) \quad \text{and} \tag{1.10}$$
$$\dot{\boldsymbol{\lambda}}(\omega) = \boldsymbol{\Pi}(\boldsymbol{q})\,\dot{\boldsymbol{q}}(\omega). \tag{1.11}$$

Assuming that the inverse of $\boldsymbol{J}(\boldsymbol{q})$ exists and the Cartesian space has the same dimensionality as the joint space $\dim(\boldsymbol{q}) = \dim(\boldsymbol{x})$ it can be derived that

$$\dot{\boldsymbol{\lambda}}(\omega) = \boldsymbol{J}(\boldsymbol{q})^{-1}\boldsymbol{\Pi}(\boldsymbol{q})\,\dot{\boldsymbol{x}}(\omega). \tag{1.12}$$

Eq. (1.12) couples the Cartesian and muscle velocity with a ratio of the two mentioned Jacobians. The joint torque is coupled to the Cartesian and muscle force similarly to the velocities by the kinematic chain but also by the muscle moment-arms represented by the Jacobian matrices:

$$\boldsymbol{T}(\omega) = \boldsymbol{J}(\boldsymbol{q})^T\boldsymbol{F}(\omega) \quad \text{and} \tag{1.13}$$
$$\boldsymbol{T}(\omega) = \boldsymbol{\Pi}(\boldsymbol{q})^T\boldsymbol{\Phi}(\omega) \tag{1.14}$$

from which can be found that

$$\boldsymbol{F}(\omega) = \boldsymbol{J}(\boldsymbol{q})^{-T}\boldsymbol{\Pi}(\boldsymbol{q})^T\boldsymbol{\Phi}(\omega). \tag{1.15}$$

Again, the endpoint and muscle forces are coupled with a ratio of the two Jacobians. Using these equations and the assumption that the two Jacobians do not change for incremental angular displacements, the relations between the different impedances become

$$\boldsymbol{Z}(\omega) = \boldsymbol{J}(\boldsymbol{q})^T\boldsymbol{I}(\omega)\boldsymbol{J}(\boldsymbol{q}) \quad \text{and} \tag{1.16}$$
$$\boldsymbol{Z}(\omega) = \boldsymbol{\Pi}(\boldsymbol{q})^T\boldsymbol{\Sigma}(\omega)\boldsymbol{\Pi}(\boldsymbol{q}) \tag{1.17}$$

leading to

$$\boldsymbol{I}(\omega) = \boldsymbol{J}(\boldsymbol{q})^{-T}\boldsymbol{\Pi}(\boldsymbol{q})^T\boldsymbol{\Sigma}(\omega)\boldsymbol{\Pi}(\boldsymbol{q})\boldsymbol{J}(\boldsymbol{q})^{-1}. \tag{1.18}$$

1.5 General Model of the Human Limbs and Fingers

In this Thesis apparatuses that measure impedance in Cartesian space will be used only. In order to distinguish between, e.g., influences from inertial properties of the fore- and upper arm and muscle stiffness on the measured impedance, a more general model is required.

A general dynamic model for a system as the fingers and limbs with finite Degrees of Freedom (DoF), namely the generalized linearly independent coordinates $\boldsymbol{q}_i$, can be derived by using the Lagrange formalism. The Lagrange formula is defined by

$$\boldsymbol{L}(\boldsymbol{q},\dot{\boldsymbol{q}}) = \boldsymbol{E}(\boldsymbol{q},\dot{\boldsymbol{q}}) - \boldsymbol{U}(\boldsymbol{q}) \tag{1.19}$$

with the Lagrangian $\boldsymbol{L}(\boldsymbol{q},\dot{\boldsymbol{q}})$ as the difference of kinetic $\boldsymbol{E}(\boldsymbol{q},\dot{\boldsymbol{q}})$ and potential energy $\boldsymbol{U}(\boldsymbol{q})$. If the respective system is conservative and all system forces and torques can be derived out of a potential, the functional derivative of $\boldsymbol{S}(\boldsymbol{q}(t))$

$$\frac{\delta S_i(\boldsymbol{q}(t))}{\delta q_i(t)} = Q_i = \frac{\mathrm{d}}{\mathrm{d}t}\frac{\partial L_i(\boldsymbol{q},\dot{\boldsymbol{q}})}{\partial \dot{q}_i} - \frac{\partial L_i(\boldsymbol{q},\dot{\boldsymbol{q}})}{\partial q_i} \tag{1.20}$$

is zero. The functional $\boldsymbol{S}(\boldsymbol{q}(t))$ is the so called *action* and Eq. (1.20) denotes *Lagrange's equation of the second kind*. If external forces exist, the difference $\boldsymbol{Q}$ is non-zero and denotes the generalized non-conservative system forces. The kinetic energy is a quadratic function of the velocities in generalized coordinates $\dot{\boldsymbol{q}}$ and is defined as

$$\boldsymbol{E}(\boldsymbol{q},\dot{\boldsymbol{q}}) = \frac{1}{2}\dot{\boldsymbol{q}}^{\mathrm{T}}\boldsymbol{M}_{\mathbf{q}}(\boldsymbol{q})\dot{\boldsymbol{q}} \tag{1.21}$$

where $\boldsymbol{M}_{\mathbf{q}}(\boldsymbol{q})$ is a symmetric and positive definite inertia matrix depending on the generalized coordinates $\boldsymbol{q}(t)$. Thus, Eq. (1.20) becomes

$$\boldsymbol{Q}(\boldsymbol{q},\dot{\boldsymbol{q}},\ddot{\boldsymbol{q}}) = \frac{\mathrm{d}}{\mathrm{d}t}\left(\frac{\partial\left(\frac{1}{2}\dot{\boldsymbol{q}}^{\mathrm{T}}\boldsymbol{M}_{\mathbf{q}}(\boldsymbol{q})\dot{\boldsymbol{q}} - \boldsymbol{U}(\boldsymbol{q})\right)}{\partial\dot{\boldsymbol{q}}}\right) - \frac{\partial\left(\frac{1}{2}\dot{\boldsymbol{q}}^{\mathrm{T}}\boldsymbol{M}_{\mathbf{q}}(\boldsymbol{q})\dot{\boldsymbol{q}} - \boldsymbol{U}(\boldsymbol{q})\right)}{\partial\boldsymbol{q}} \tag{1.22}$$

$$= \boldsymbol{M}_{\mathbf{q}}(\boldsymbol{q})\ddot{\boldsymbol{q}} + \underbrace{\dot{\boldsymbol{M}}_{\mathbf{q}}(\boldsymbol{q})\dot{\boldsymbol{q}} - \frac{\partial\left(\frac{1}{2}\dot{\boldsymbol{q}}^{\mathrm{T}}\boldsymbol{M}_{\mathbf{q}}(\boldsymbol{q})\dot{\boldsymbol{q}}\right)}{\partial\boldsymbol{q}}}_{\boldsymbol{C}_{\mathbf{q}}(\boldsymbol{q},\dot{\boldsymbol{q}})\dot{\boldsymbol{q}}} + \underbrace{\frac{\partial\boldsymbol{U}(\boldsymbol{q})}{\partial\boldsymbol{q}}}_{\boldsymbol{g}_{\mathbf{q}}(\boldsymbol{q})} \tag{1.23}$$

finally leading to the equation of motion

$$\boldsymbol{Q}(\boldsymbol{q},\dot{\boldsymbol{q}},\ddot{\boldsymbol{q}}) = \boldsymbol{M}_{\mathbf{q}}(\boldsymbol{q})\ddot{\boldsymbol{q}} + \boldsymbol{C}_{\mathbf{q}}(\boldsymbol{q},\dot{\boldsymbol{q}})\dot{\boldsymbol{q}} + \boldsymbol{g}_{\mathbf{q}}(\boldsymbol{q}), \tag{1.24}$$

where $\boldsymbol{C}_{\mathbf{q}}(\boldsymbol{q},\dot{\boldsymbol{q}})$ is the Coriolis- and centripedal forces matrix and $\boldsymbol{g}_{\mathbf{q}}(\boldsymbol{q})$ the matrix of gravitational forces.
Because external perturbation and internal muscle forces are present, the generalized forces equal the sum of external and internal torques acting at the joints:

$$\boldsymbol{Q}(\boldsymbol{q},\dot{\boldsymbol{q}},\ddot{\boldsymbol{q}}) = -\boldsymbol{T}_{\mathbf{int}} + \boldsymbol{T}_{\mathbf{ext}}. \tag{1.25}$$

The internal forces acting on the joint, namely the muscle forces, are a function of the joint positions, velocities and acceleration and of the muscle activations $\boldsymbol{a}$:

$$\boldsymbol{T}_{\mathbf{int}} = f(\boldsymbol{q},\dot{\boldsymbol{q}},\ddot{\boldsymbol{q}},\boldsymbol{a}). \tag{1.26}$$

From this general formulation a local linearized model with constant parameters can be derived. Using Taylor series expansion and canceling after the first order term an approximation for the internal forces can be formulated:

$$\hat{\boldsymbol{T}}_{\mathbf{int}} = \underbrace{\boldsymbol{T}^{\star}_{\mathbf{int}}\big|_{\boldsymbol{q}_0,\boldsymbol{a}_0}}_{\boldsymbol{T}_0} + \underbrace{\frac{\partial\boldsymbol{T}_{\mathbf{int}}(\boldsymbol{q},\dot{\boldsymbol{q}},\ddot{\boldsymbol{q}},\boldsymbol{a})}{\partial\boldsymbol{q}}\bigg|_{\boldsymbol{q}_0,\boldsymbol{a}_0}}_{\boldsymbol{R}}\Delta\boldsymbol{q} + \underbrace{\frac{\partial\boldsymbol{T}_{\mathbf{int}}(\boldsymbol{q},\dot{\boldsymbol{q}},\ddot{\boldsymbol{q}},\boldsymbol{a})}{\partial\dot{\boldsymbol{q}}}\bigg|_{\boldsymbol{q}_0,\boldsymbol{a}_0}}_{\boldsymbol{D}}\Delta\dot{\boldsymbol{q}} + \ldots \tag{1.27}$$

$$\ldots + \underbrace{\frac{\partial\boldsymbol{T}_{\mathbf{int}}(\boldsymbol{q},\dot{\boldsymbol{q}},\ddot{\boldsymbol{q}},\boldsymbol{a})}{\partial\ddot{\boldsymbol{q}}}\bigg|_{\boldsymbol{q}_0,\boldsymbol{a}_0}}_{\boldsymbol{M}_{\mathbf{j}}}\Delta\ddot{\boldsymbol{q}} + \frac{\partial\boldsymbol{T}_{\mathbf{int}}(\boldsymbol{q},\dot{\boldsymbol{q}},\ddot{\boldsymbol{q}},\boldsymbol{a})}{\partial\boldsymbol{a}}\bigg|_{\boldsymbol{q}_0,\boldsymbol{a}_0}\Delta\boldsymbol{a} + \ldots$$

with $\Delta \boldsymbol{q} = \boldsymbol{q} - \boldsymbol{q_0}$ and $\Delta \boldsymbol{a} = \boldsymbol{a} - \boldsymbol{a_0}$. Assuming $\dot{\boldsymbol{q_0}} = \ddot{\boldsymbol{q_0}} = 0$ and $\Delta \boldsymbol{a} = 0$ (no change in muscular activation during the measurements) Eq. (1.27) reduces to

$$\hat{\boldsymbol{T}}_{\mathbf{int}} = \boldsymbol{T_0} + \boldsymbol{R}\Delta\boldsymbol{q} + \boldsymbol{D}\dot{\boldsymbol{q}} + \boldsymbol{M}_{\mathbf{j}}\ddot{\boldsymbol{q}}, \tag{1.28}$$

where $\boldsymbol{T_0}$ is the equilibrium torques vector, $\boldsymbol{M}_{\mathbf{j}}$ are the inertial parameters of the muscles acting on the joints proportional to joints acceleration $\ddot{\boldsymbol{q}}$, and $\boldsymbol{R}$ and $\boldsymbol{D}$ the symmetric and positive definite local linearized joint stiffness and damping matrices proportional to a displacement $\Delta\boldsymbol{q}$ and to velocity $\dot{\boldsymbol{q}}$, respectively. Combining Eqs. (1.24), (1.25) and (1.28) leads to

$$\boldsymbol{M}_{\mathbf{q}}(\boldsymbol{q})\ddot{\boldsymbol{q}} + \boldsymbol{C}_{\mathbf{q}}(\boldsymbol{q}, \dot{\boldsymbol{q}})\dot{\boldsymbol{q}} + \boldsymbol{g}_{\mathbf{q}}(\boldsymbol{q}) = -\boldsymbol{T_0} - \boldsymbol{R}\Delta\boldsymbol{q} - \boldsymbol{D}\dot{\boldsymbol{q}} - \boldsymbol{M}_{\mathbf{j}}\ddot{\boldsymbol{q}} + \boldsymbol{T}_{\mathbf{ext}} \tag{1.29}$$

and can be simplified to

$$\Delta\boldsymbol{T}_{\mathbf{ext}} = (\boldsymbol{M}_{\mathbf{q}}(\boldsymbol{q}) + \boldsymbol{M}_{\mathbf{j}})\ddot{\boldsymbol{q}} + (\boldsymbol{C}_{\mathbf{q}}(\boldsymbol{q}, \dot{\boldsymbol{q}}) + \boldsymbol{D})\dot{\boldsymbol{q}} + \boldsymbol{g}_{\mathbf{q}}(\boldsymbol{q}) + \boldsymbol{R}\Delta\boldsymbol{q} \tag{1.30}$$

using $\Delta\boldsymbol{T}_{\mathbf{ext}} = \boldsymbol{T}_{\mathbf{ext}} - \boldsymbol{T_0}$. This Eq. (1.24) is the equation of motion in joint space. To get the equation of motion in Cartesian space it is multiplied from the left with $\boldsymbol{J}(\boldsymbol{q})^{-T}$. The following definitions are used:

$$\boldsymbol{M}_{\mathbf{x}}(\boldsymbol{x}) = \boldsymbol{J}(\boldsymbol{q})^{-T}(\boldsymbol{M}_{\mathbf{q}}(\boldsymbol{q}) + \boldsymbol{M}_{\mathbf{j}})\boldsymbol{J}(\boldsymbol{q})^{-1}, \tag{1.31}$$

$$\boldsymbol{B}(\boldsymbol{x}, \dot{\boldsymbol{x}}) = \boldsymbol{J}(\boldsymbol{q})^{-T}(\boldsymbol{M}_{\mathbf{q}}(\boldsymbol{q}) + \boldsymbol{M}_{\mathbf{j}})\dot{\boldsymbol{J}}(\boldsymbol{q})^{-1} + \boldsymbol{J}(\boldsymbol{q})^{-T}(\boldsymbol{C}_{\mathbf{q}}(\boldsymbol{q}, \dot{\boldsymbol{q}}) + \boldsymbol{D}), \tag{1.32}$$

$$\boldsymbol{g}_{\mathbf{x}}(\boldsymbol{x}) = \boldsymbol{J}(\boldsymbol{q})^{-T}\boldsymbol{g}_{\mathbf{q}}(\boldsymbol{q}), \tag{1.33}$$

$$\Delta\boldsymbol{F}_{\mathbf{ext}} = \boldsymbol{J}(\boldsymbol{q})^{-T}\Delta\boldsymbol{T}_{\mathbf{ext}}, \tag{1.34}$$

$$\Delta\boldsymbol{x} = \boldsymbol{J}(\boldsymbol{q})^{-T}\Delta\boldsymbol{q} \quad \text{and} \tag{1.35}$$

$$\ddot{\boldsymbol{q}} = \boldsymbol{J}(\boldsymbol{q})^{-1}\ddot{\boldsymbol{x}} + \dot{\boldsymbol{J}}(\boldsymbol{q})^{-1}\dot{x}. \tag{1.36}$$

The relation $\boldsymbol{x} = f(\boldsymbol{q})$ is incorporated into $\boldsymbol{M}_{\mathbf{x}}(\boldsymbol{x})$, $\boldsymbol{B}(\boldsymbol{x}, \dot{\boldsymbol{x}})$, and $\boldsymbol{g}_{\mathbf{x}}(\boldsymbol{x})$. It follows the equation of motion in Cartesian space

$$\Delta\boldsymbol{F}_{\mathbf{ext}} = \boldsymbol{M}_{\mathbf{x}}(\boldsymbol{x})\ddot{\boldsymbol{x}} + \boldsymbol{B}(\boldsymbol{x}, \dot{\boldsymbol{x}})\dot{\boldsymbol{x}} + \boldsymbol{g}_{\mathbf{x}}(\boldsymbol{x}) + \boldsymbol{K}\Delta\boldsymbol{x}. \tag{1.37}$$

1.6 Measurement of Areflexive Stiffness

This Section explains how to choose a proper perturbation profile and measurement method in order to identify the aforementioned *areflexive stiffness* only.
Ideally, the TMC behavior can be changed by the variation of three variables: neural command, muscle force, and length/velocity (secondary effects, e.g. influence of temperature are neglected). In general, the neural command and one of the latter two are chosen as an input, while the remaining variable is the measured output [Win90]. In order to be able to handle the reflexive muscle as an areflexive system and to identify its mechanical properties only, the neural input needs to be quantified by either measuring or controlling its state. The neural input consists of voluntarily and non-voluntarily controllable effects. While the state of the voluntarily controllable part can easily be fixed by providing subjects a real-time feedback about the measured input states of the muscle, i.e. applied force and neural command, it is much more difficult for the non-voluntarily controllable part, namely reflexes[13]. In literature controlling the reflex state is mainly achieved by muscle deafferentation: (a) either by actively

[13]Please note, within this work it will be refrained from using functional electrical stimulation to control the neural input of the muscle, since it may cause different recruitment of motor units and motor control of the muscles differs considerably to natural stimulation [vdHSdVB02]. Moreover, since type I fibers are stiffer than type II fibers per unit of muscle force the muscle stiffness might be underestimated using electrical stimulations.

re-innervating reflex pathways using electrical stimulation [STAH88, CCK90], or (b) during ischemia [AMV82, SH89], or (c) by using mechanical vibrations [AG80, AMV82]. Each of these methods have their drawbacks and limitations as, e.g. altered motorneuron properties during ischemia or changes of passive elastic properties if using mechanical vibrations [PCK00]. Another approach to account for the state of neural input is to separate areflexive mechanical and reflexive properties by modeling their effects and use parameters from literature or previous experiments [dVvdHSB01, vdHSdVB02]. By using random continuous disturbances, the human behavior is considered to be stationary when asked to minimize the induced displacements and adapting behavior is neglected [vdHSdVB02]. Moreover, the *do-not-voluntarily-intervene* paradigm (the perturbation) is used (see also [MIHB85, OG99, OFK$^+$02, MMIB96, GK97, SMIB93]), in order to reduce the influence of active response. However, this assumption is questionable, since experimental periods lasts around 40 s [vdHSdVB02] each. Yet, for an accurate identification the usage of perturbation bandwidths between 0.06 and 20 Hz is inevitable resulting in mentioned time-window lengths. Burdet *et al.* stated: *"... The inability to readily separate intrinsic and feedback contributions to joint impedance makes it difficult to propose and validate a model structure for feedback... "* [BFM13].

In this Thesis a different approach is used, i.e. finishing measurements before the onset of any kind of neural feedback can influence the response of the mechanical system. The impedance of the remaining mechanical system can be identified by either using *force* or *position perturbations*, where either the force or length/velocity input of the muscle is varied. Usually, the system is perturbed by an external force $\boldsymbol{F}_{\mathbf{ext}}$ and the motion response $\boldsymbol{x}$ over time is measured, leading to an estimate of the instantaneous stiffness $\boldsymbol{K}$. These perturbations can be single steps, ramps, impulses, continuous sinusoidals, white noise, or random pulse oscillations. A step is defined as change in a level that is rapid and an impulse as an input of short time both in relation to the muscle system response [Win90]. Repeating this experiment and using least-squares fit as in [GK97] for arm stiffness yields an overall estimate of stiffness. On the one hand, the frequency bandwidth ω of the perturbation must contain the natural frequencies of the considered system, in order to get a response which quantitatively represents the system [Nel01]. On the other hand, the perturbation profile needs to be chosen such that reflexes do not intervene. If the perturbation does not fulfil these conditions one can obtain physically meaningless impedance parameters [YI03].
This Thesis focuses on areflexive stiffness. Thus, as proposed by [MIHB85], the usage of steps or fast ramps is favored. They can be used for one-DoF, as well as for multi-dimensional approaches. In general, the relation between force and displacement is neither linear nor continuous, but for small displacements during a postural task, Taylor's approximation of Eq. (1.7) holds:

$$\hat{\boldsymbol{K}} = \boldsymbol{K}^{\star} + \left.\frac{\partial \boldsymbol{K}}{\partial \boldsymbol{x}}\right|_{\boldsymbol{x_0}} \Delta \boldsymbol{x} + \left.\frac{\partial \boldsymbol{K}}{\partial t}\right|_{t_0} \Delta t. \tag{1.38}$$

Around an equilibrium position it can be assumed that the time variations in stiffness is caused by changes in muscular activity, actively controlled by the CNS. Since the measurement ends before the onset of relevant neural feedback, the last term of Eq. (1.38) is zero; substituting the second term of the right hand side in Eq. (1.38) with the definition of stiffness in Eq. (1.7), that is $\partial \boldsymbol{K}/\partial \boldsymbol{x} = -\partial^2 \boldsymbol{F}/\partial \boldsymbol{x}^2$, one obtains a second order term for force, which is negligible and leads to a constant approximation of stiffness:

$$\hat{\boldsymbol{K}} = \boldsymbol{K}^{\star}(\boldsymbol{x_0}, t_0) = \text{const.} \tag{1.39}$$

The parameter $\boldsymbol{K}^{\star}$ in Eq. (1.39) directly corresponds to the introduced areflexive stiffness and is a local linearized model of stiffness about the working point $\boldsymbol{x_0}$, when the influence of reflexes can be ignored. This model will be used from now on.

1.7 Voluntary Control of Cartesian Stiffness

The human locomotor system is made up of series of bones providing the stability. They are connected to each other via several skeletal TMCs arranged in an antagonistic manner. The skeletal muscles provide the mechanical resistance of limbs or fingers, i.e. stiffness, measured in this Thesis. Ideally, the stiffness can be influenced voluntarily by two sets of parameters, namely a variation in *cocontraction* of antagonistic muscles, or a change in the kinematic configuration/orientation of the joints. In this Section their influence on the measured stiffness and external force will be analyzed theoretically. A monotonic increase of Cartesian stiffness with the external force is assumed, as found by several studies [VD98, HH97, CCK90, CCG93, GO98, Hog84, HK82]. The mentioned linearity is treated in detail within Section 2.4.
By referring to the terms *cocontraction* or *coactivation* inconsistencies exists among researchers. In general, *cocontraction* is defined as *"... the simultaneous activation of antagonist muscles around a joint ..."* [GMCM03]. However, there are discrepancies whether the process addresses voluntary or involuntary control, i.e. during flexion of agonist, the antagonist (involuntarily) activates as well in order to stabilize the joint. A more critical issue concerns the underlying assumption for force: some researchers assume zero net force [GO98, MYT+13], i.e. no application of force or at least no change in external force by referring to cocontraction. However, the aforementioned definition does not concern force and includes variations of it: by simultaneously and uniformly activating flexor and extensor muscles, a constant overall net force during activation isn't ensured, since flexor and extensor muscles are of different strengths. Therefore, the term *isometric cocontraction* has been established in standard literature to specify that net torque is kept constant. If the joint is in equilibrium state and no force is applied by the joint, an isometric contraction of antagonistic muscles will cause no change in net torque. However, this is true for zero net torque only. If the joint is in contact with the environment, an isometric cocontraction can lead to changes in the applied force even if the muscle lengths are being kept constant. Therefore, the notation *isotonic cocontraction* would be a suitable term ascribing coactivation of antagonistic muscles acting on a joint without changing the overall net torque/ applied external force. Nevertheless, the notations *isometric cocontraction* or just *cocontraction* will be used within this Thesis and will imply no changes in the applied force.

Similar to Eq. (1.18) one can formulate

$$\boldsymbol{K} = \boldsymbol{J}(\boldsymbol{q})^{-T}\boldsymbol{\Pi}(\boldsymbol{q})^{T}\boldsymbol{M}\boldsymbol{\Pi}(\boldsymbol{q})\boldsymbol{J}(\boldsymbol{q})^{-1}, \tag{1.40}$$

showing the dependency between the Cartesian stiffness $\boldsymbol{K}$ measured at the end-effector of the limb or tip or finger and muscular stiffness $\boldsymbol{M}$. Combining Eqs. (1.15) and (1.40) one can conclude that, if $\boldsymbol{F}$ and $\boldsymbol{K}$ are linearly related, then so are $\boldsymbol{\Phi}$ and $\boldsymbol{M}$. In words: if the Cartesian force and Cartesian stiffness are linearly dependent, then this is caused by a linear relationship between the muscle force and muscle stiffness. This corresponds to results of the study [OG99], where the authors showed that the linear relationship between muscle activation and stiffness [SA92, JR69, CZ82] can be generalized to the multi-joint case. From these equations one can derive the influence of the two strategies for changing endpoint stiffness and its effects on the stiffness/force characteristic:

- Cocontraction will increase the force $\boldsymbol{\Phi}$ and stiffness $\boldsymbol{M}$ of agonist and antagonist muscles; forces $\boldsymbol{\Phi}$ of antagonistic pairs of muscles oppose each other, while their stiffness $\boldsymbol{M}$ will summate. Thus, one can maintain the same net force $\boldsymbol{F}$ applied by the limb or finger while increasing its stiffness $\boldsymbol{K}$. Thus, for a given level of cocontraction—i.e. the level of extensor muscular activity—the operating point on the stiffness/force characteristic of each muscle

and each joint will change, but the slope of the stiffness/force characteristic will not be affected. Under the assumption that the kinematic configuration will not be changed due to increased internal forces, cocontraction will lead to an increase in the muscle stiffness $\boldsymbol{M}$ and a proportional increase of the Cartesian stiffness $\boldsymbol{K}$ without a change of Cartesian force $\boldsymbol{F}$. Thus, changing stiffness caused by *cocontraction will affect the offset, but not the slope* of the (linear) Cartesian force–stiffness relation.

- From Eq. (1.40) one can see that a change in the Jacobian by, e.g. changing finger, wrist or elbow orientation will have a non-linear (quadratic) effect on the stiffness/force characteristic and will affect slope and offset. For example by changing the kinematic configuration of the wrist, the lengths of the involved muscles change. Wrist flexion leads to shorter flexor muscles and wrist extension leads to longer flexor muscles.

Note that both strategies will not affect the linear relation between force and stiffness while cocontraction and kinematic orientation remain the same.

1.8 Variable-Stiffness Actuation for Robotics

Typically, industrial robots are built to be as stiff as possible in order to provide high positional accuracy and repeatability for highly dynamic tasks. However, these robots are hazardous for the human and therefore are fenced, immediately stopping when they enter the robot cell. Paving the way towards safe robotic systems for human-robot interaction impedance control [Hog85a] has been introduced into robotics inspired by the EPH found in human. Robotic systems with integrated torque sensors in each of the joints are used, like the DLR Light-Weight Robot (LWR) III [ASHO$^+$07]. By closing the loop between actuator and sensor, these robots can show similar behavior of *apparent stiffness* as human do allowing for safe interaction between human and robot. However, Haddadin *et al.* [HASH07, HASEH10] showed that the peak load during collisions increases so rapidly, that the internal torque sensors are not able to record these, resulting in impedance controlled robots which have to be regarded as stiff during impacts. Inspired by the human locomotor system, VSAs have been introduced in robotics, which allow to adapt the *intrinsic stiffness* of each joint. These actuators address (a) reducing the impact of collisions for the motors and gears [GASB$^+$11], (b) increasing dynamic capabilities by allowing to frequently store elastic energy, and (c) the embodiment of desired behavior [VSB11]. While active compliance control allows to arbitrarily choose the task coordinate frame of desired elastic behavior, VSAs inherently dominate the orientation of favorable compliant directions. By focusing on dominating tasks within the design process of robots, VSAs allow to reduce the control effort and energy consumption by embodying compliant behavior. E.g. during hammering with an oscillating hammer movement, joint elasticity allows to frequently store potential energy in the spring. Wolf [WH08] showed in a throwing task that VSA joints can reach drive speeds at the link side, which are 2.6 times faster than the motor velocity.
Impacts can be classified into known and unknown impacts [Gre14]. For known impacts, like catching a medicine ball, humans guess the amount of impact energy and adapt stiffness of the joints accordingly in order to dissipate the impact energy and avoid reaching joint limits or muscle damage [Gre14]. For unknown impacts, e.g. accidents during skiing, humans use a strategy of maximum cocontraction in order to dissipate as much energy as possible using their muscles and to avoid reaching joint limits [Gre14]. The consequences of considerable muscle damage are hazard knowing that reaching joint limits causes substantially more irreversible injuries. In any case, VSAs allow to actively dissipate the impact energy over a longer period of time [Gre14], since link mass and joint elasticity build a low pass filter mechanically [Pet14].
A broad variety of VSAs exist, e.g. with pneumatic, hydraulic, electromechanical actuation. Within the aforementioned EU project VIACTORS a data sheet was developed allowing to com-

pare these mechanisms [GWG+15]. Moreover, the review of Bram Vanderborght *et al.* developed in the context of the project provides a good overview of state-of-the-art VSAs [VASB+13]. For reasons of simplicity, this work will focus on the VSAs of the *DLR Hand Arm System* only.

The *DLR Hand Arm System* is an anthropomorphic hand and arm system, which intends to reach human size, performance, and dexterity [GASB+11]. It consists of 26 DoF, seven for the arm and 19 for the hand (see Fig. 1.6).

Figure 1.6: The DLR Hand Arm System — 26 joints with variable stiffness, 19 for the hand, and 7 for the arm.

Each of the joints has an adjustable intrinsic compliance mechanism, based on three different mechanical principles. The compliance of the finger-joints of the hand—referred to as the *DLR Awiwi Hand* [Gre14]—is realized by a tendon driven system known as Flexible Antagonistic Spring (FAS) mechanism [FCRG11, Fri11]. Similarly to the human two tendons are coupled via non-linear springs with motors, i.e. an accordant motor movement moves and an inverse movement pretensions the joint. The non-linear elastic elements are realized with linear springs and a non-linear mechanism; if one used solely linear springs the stiffness of the joint would not change by cocontraction. The two wrist joints, as well as the forearm rotation are implemented as a Bidirectional Antagonism with Variable Stiffness (BAVS) mechanism [FHPH11, Höp11], which is also referred to using the term *helping antagonism* and which will be described in detail within Section 4.1. The four joints for elbow and shoulder are realized by a Floating Spring Joint (FSJ) mechanism, for which a small motor changes the stiffness and a large motor realizes joint movements [WEH11, Wol11].

2 Grip Stiffness

2.1 Introduction

Previous research on measuring human stiffness primarily focused on the arm [BOF$^+$00, GK97, MIHB85, PKC01, XHHB91]. Most of these papers refer to Hogan's pioneering work, which summarizes gained knowledge [Hog85b]. Different measurement apparatuses have been developed, mostly planar position perturbation devices[1]; the experience with these manipulandi and the methods used in these works can also be used for the identification of human finger stiffness.
For grip stiffness, the most relevant publication was written by Clayton van Doren in 1998 [VD98]. Van Doren built a table-fixed device with a mass compensation unit based on a parallel mechanism able to compensate most of the mass properties (for the static case only). The device consists of an index/middle finger plate and a thumb plate. It is able to induce a distinct displacement between the two. Van Doren analyzed the influence of initial force, rising time, grip width and perturbation amplitude on his definition of grip stiffness in a *do-not-voluntarily-intervene* paradigm. Grip stiffness was defined as the difference of measurements between an expanding and contracting handle. He found grip stiffness to be decreasing with perturbation amplitude, increasing with rising time and initial force, and changing slightly with grip width. He used rising times between 40 and 250 ms and perturbation amplitudes between ± 2 and ± 10 mm.
Another method and apparatus for measuring the stiffness of the human index finger is described by Milner *et al.* in [MF98]. As the authors measure both finger flexion and extension and in different planar orientations of the index finger, they are able to separate conservative and non-conservative stiffness terms and can also evaluate Cartesian endpoint-stiffness (stiffness ellipses). In order to identify the human finger stiffness the authors apply a method suggested in [MIHB85] for measuring two-dimensional static stiffness of the human arm: by measuring the force before and after the perturbation the method gives—when states are steady—the index finger stiffness. The authors found that—similar as found for the human arm [MIHB85]—the mechanical behavior of the index finger is mainly spring-like. The conservative component of the force field can be modeled by a 2D linear spring. The influence of non-conservative effects is less than 15% of the total force response to static displacements.
In [HH97] Hajian suggested a method and device for the identification of mechanical impedance

[1] To see a more detailed introduction of state-of-the-art planar devices and measurements, please have a look at Chapter 3.

of the human index finger metacarpal joint in extension and abduction. One-dimensional perturbation forces between 2 and 20 N for extension and between 2 and 8 N for abduction are applied, with a maximal duration between 20 and 30 ms in order to avoid reflexes. A pneumatic perturbation system is presented which can displace the index finger around 5 mm. Modeling finger impedance by a second-order translational model the authors are able to identify inertia, damping, and stiffness by using least-squares. The authors found that all measured subjects increase their index finger stiffness and damping when increasing the applied bias force. In further studies, Hajian extended his research on pinch grasp impedance, validating the result that increasing force bias increases damping and stiffness [Haj97]. He found an almost linear relation of bias force to both, damping and stiffness.

In [HC02] Hasser built a measurement device for measuring human grasp impedance when grasping a haptic knob and applying a rotational—rather than translational—perturbation to the pinch grip. Similarly to the research of Hajan, a linear, second-order translational model is applied and impedance is identified by least-squares. Similarly, a roughly linear increase of damping and stiffness with grip strength of the haptic knob is found. Lastly, the authors report about the strong influence of fingerpad impedance, and show that their model fits for light and moderate grip forces, only. For stronger grip forces a higher-order model is required, taking both finger and fingerpad impedance into account.

In [KCJ97] Kao *et al.* suggested a method for identifying a grasp stiffness matrix using a least-squares fit on data obtained during a pinch grip task. The apparatus used consists of two disks connected to a torque motor with two cantilevers. Strain gauges are printed on both cantilevers in order to measure the grasp forces of both, index finger and thumb, separately. The setup can also measure applied tangential forces: the subjects are instructed to grip the disk tightly while their arm and the wrist are blocked, and to move the disk in the proximal/distal and radial/ulnar directions. The main objective of this study was to investigate calibration methods for robotic hands; the authors found that a symmetrical calibration method—that excludes non-conservative components of the stiffness matrices—suffices. Similar to Milner *et al.* [MF98], they claim that the non-conservative components of the stiffness matrices are negligible during human grasping, and that relaxing the arm-blockage induces a smaller stiffness and a higher compliance.

In [AMS83] Akazawa *et al.* investigated changes in stretch-reflex gain and stiffness of the long thumb-flexor muscles in a force task and a constant-load position-control task. They found that cocontraction, defined as the ratio of flexor and extensor forces, increases the stretch-evoked stiffness and reflex responsiveness at a given flexing force with respect to the motor task. Stretch-evoked stiffness as well as reflex responsiveness were larger in the task involving position control than in force control. Thus, higher levels of cocontraction were used to successfully fulfil the position control task. It was found that the reflex responsiveness and stretch-evoked stiffness increase linearly with the defined level of cocontraction. Furthermore, the slope of these linearities increases with force. In the study, however, a reflexive stiffness was measured, which does not allow for differentiating between mechanical and actively controlled properties.

2.1.1 Motivation

All in all, it is clear that intrinsic grip stiffness is linearly related to grip force, but little is known whether this relation is laid down or can be varied, e.g. according to the task. Moreover, it is widely known that the pinch-grip forces of the human hand are linearly related to the weight of the grasped object. Wrist flexion and extension causes stretching and shortening, among others, of the corresponding flexor digitorum superficialis and profundus muscles [BH99], affecting their force/activation relationship as described in the Hill muscle model [Hil38]. This effect can reduce the maximum grip force to 73% of its maximum [OHN+92]. Thus, changes in wrist configuration

should lead to changes in both grip force and grip stiffness. But, even during wrist movements of up to 90°/s, the CNS is able to keep grip force stable [JW84]. In this Chapter, variations to the dependencies between force, stiffness, and grasped weight in different tasks with and without visual feedback will be investigated. Special attention is taken to check whether the mentioned force–stiffness linearity can be violated.

Moreover, little is known about the influence of *cocontraction*. Carter *et al.* showed that for zero net torque at the interphalangeal joint in the human thumb, joint stiffness highly increases with cocontraction. This demonstrates that net torque or force alone does not determine joint stiffness [CCG93]. Nevertheless, to the author's knowledge relevant literature on human grip force focuses on the influence of muscle cocontraction at zero net torque only. Therefore in this Chapter the correlation of force and stiffness for the pinch grip at different levels of cocontraction will be investigated. Apart from gaining biomechanical insight, this issue is particularly relevant for variable-stiffness robotic systems which, can more or less independently control the two parameters. However, no clear design criteria exist for VSA to efficiently exploit them. Moreover, some studies concentrate on the relationship between finger force and Electromyography (EMG), while none compared the regression of force *and* stiffness from EMG. In this Chapter human's ability to decouple grip stiffness from grip force by cocontraction at certain force levels and their linear regression from intra- and inter-subject variability in the electromyogram from relevant groups of muscles will be investigated.

2.1.2 Determination of one-dimensional Grip Stiffness

In this Thesis, intrinsic grip stiffness of the pinch grip will be defined as the relation between force and displacement of the index finger with respect to the thumb. Considering one DoF, displacement is the change in distance from an equilibrium posture Δx between the thumb and index fingertips as a linear motion along a Cartesian axis. The displacement causes a force ΔF in the opposite direction trying to restore the previous state. This model of stiffness $\hat{K}$ is a one-DoF simplification of the multi-joint case described in Eq. (1.39) and will be used in this Chapter. It allows to easily find answers to the questions raised in Subsection 2.1.1. Fig. 2.1 shows an example of a step position perturbation applied with the grip perturbation device used in the experiments described in Section 2.3, where a known change in position is induced (input) and the applied force is measured (output).
It is characterized by two static time intervals T_1 and T_2 at equilibrium, before and after the step. At these states, the velocity and acceleration are almost zero, while one can assume that influences from damping and inertia can be neglected. Thus, the equation of motion in Cartesian space (1.37) simplifies and Cartesian stiffness can be estimated by

$$\hat{K} \;=\; \frac{(E_{\mathrm{T}_2}(F_{\mathrm{ext}}) - E_{\mathrm{T}_1}(F_{\mathrm{ext}}))}{(E_{\mathrm{T}_2}(x) - E_{\mathrm{T}_1}(x))}, \tag{2.1}$$

wherein $E_{\mathrm{T}_{1|2}}(\cdot)$ denotes the average over time intervals $T_{1|2}$. Please note, that within this Thesis influences of gravitational forces $\boldsymbol{g}_{\boldsymbol{x}}(\boldsymbol{x})$ will be neglected, since it can be disregarded for finger dynamics and will be compensated for the measurements of arm dynamics within Chapter 3. In order to measure tendon- and muscle-based influences only, T_2 had to be chosen carefully. For doing so, a time t_{trust} will be defined within which one can ignore effects of fast reflex responses and trust the data to be purely intrinsic.
The mean onset latency of the short-latency reflex is about 30.7 ± 1.7 ms (SD) for the first dorsal interosseus in the hand [TL86]. In [AM84] Allum *et al.* reported a delay of about 20 ms between the onset of the short-latency reflex and first measurable changes in muscle force of stretching triceps surae muscles and releasing tibialis anterior muscles elicited by electrical stimulation.

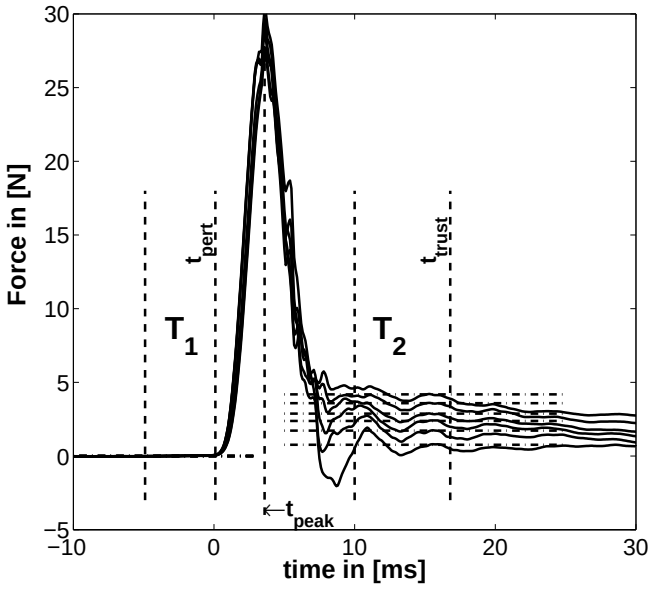

Figure 2.1: Example for typical Perturbation profile (reproduced from [HMvdS13]). — Force profile before, during, and after a perturbation starting at $t = 0$. Additionally, the time windows T_1 and T_2 and the mean of force for six force levels are depicted (mean force $E_{\mathrm{T}_1}(f)$ subtracted).

Thus—assuming that this feedback does not have a measurable influence within 40 ms—t_{trust} will be allowed to vary downward from $t = t_{\mathrm{pert}} + 40\mathrm{ms}$ and the duration T_2 will be allowed to vary between 5 and 20 ms so to minimize an objective function (note: not used for experiments of Section 2.2). One time window T_2 within each experimental study with a fixed start and end will be used, rather than optimizing these windows either subject-wise or force level-wise. This avoids comparing stiffnesses across subjects or force-levels that are affected variously by damping and inertia, even if the influence of dynamics on the obtained results is expected to be small. The objective function is defined by

$$Z = \frac{1}{n_{\mathrm{sub}}} \sum_{i=1}^{n_{\mathrm{sub}}} \left(\frac{1}{n_{\mathrm{level}}} \sum_{j=1}^{n_{\mathrm{level}}} \left(\tilde{e}(k_{ij}) + \frac{1}{n_{\mathrm{trial}}} \sum_{k=1}^{n_{\mathrm{trial}}} \tilde{e}_{\mathrm{T}_2}(f_{ijk}) \right) \right) \tag{2.2}$$

using the whole number of trials n_{trial}, levels n_{level} and subjects n_{sub}. Herein, the Coefficient of Standard Error (CSE) $\tilde{e}(\cdot) \geq 0$ will be used

$$\tilde{e}(\cdot) = \frac{\sigma(\cdot)}{\mu(\cdot)\sqrt{n}}, \tag{2.3}$$

which combines the coefficient of variation and standard error as introduced in [HMvdS13]. Assessing low sample sizes with a higher standard error, the standard error compensates the standard deviation $\sigma(\cdot)$ for sample size n; the coefficient of variation is a normalized measure of the standard deviation and compensates for the sample mean $\mu(\cdot)$. Since the objective function Eq. (2.2) mixes data sets of different size and from different dimensions, the standard deviation $\sigma(\cdot)$ had to be compensated for both. $\tilde{e}_{\mathrm{T}_2}(f)$ denotes the CSE of force for each trial within T_2 and $\tilde{e}(k)$ represents CSE of stiffness values for the different trials. The objective of this optimization is to (a) minimize the oscillations within time interval T_2 and (b) the variation of resulting stiffness values measured under *exactly* the same conditions.
Furthermore, visual inspection of the gradient of the normalized stiffness values within [HMvdS13] showed, that stable results were obtained if the end of the second time window t_{trust} is at least 4 ms higher than the length of T_2. These normalized stiffness values were

calculated according to their dependency on the end and width of the second time window and represent a kind of measure for stability of the achieved results. This corresponds to a second time window not intersecting the first, leaving out the peak of perturbation (see Fig. 2.1). Please have a look into [NH76] for a more detailed analysis of the influence of choosing time windows on the mechanical response.

2.1.3 Device Description

The manipulandum used in this Thesis to reveal information about grip stiffness, and which is called the "Grip Perturbator" is a little hand-held device small enough to be held between index finger and thumb (Fig. 2.5). The device works through position perturbation, i.e. it displaces the relative position of thumb and index by a known distance and measures the reaction force exerted by the fingers. During operation it is held between thumb and index finger in a pinch grip, as defined in standard grasping taxonomies, see, e.g. [Cut89]. Fig. 2.2 shows the first version of the device in detail. A rigid and a moving part are coupled by a linear spring; an electromagnet is mounted on one extremity of the moving part, with the aim of preloading the spring. As the electromagnet is turned off, the spring is released and pushes the two sections apart, until the mechanical stop mounted onto the rigid part is reached by the moving part. The distance between the electromagnet and the mechanical stop, which is the imposed position displacement, is known; an on-board sensor measures the applied force. The stiffness, the initial tension of the spring, and the displacement between the rigid and co-moving part can easily be adjusted before the beginning of the measurement. Comparing to existing measurement devices the device excels with its simplicity.

Figure 2.2: First version of the Grip Perturbator (reproduced from [HLU+11] ©2011 IEEE). — This version is used within section 2.2; from left to right: electromagnet, moving part, rigid part, whole.

Notice that the electromagnet cannot automatically reload the perturbator, which must therefore be preloaded by hand after every measurement (no bidirectional or oscillating perturbation is possible). Furthermore, stiffness only can be measured during flexion tasks.
The dimensions of the first design are 35 mm in diameter and 85 mm in height when the spring is not preloaded and its weight approximates 217 g. The displacement of the position perturbation is approximately 10 mm. The force of the spring of the preloaded device used in the experiments is about 100 N when loaded and 70 N when unloaded; this ensures that the force exerted by the device is always larger than the applied finger force, so that position perturbation is always constrained.
The second version of the Grip Perturbator shown in Fig. 2.3 was used within the experiments of Section 2.3 published in [HMvdS13]. Basically, this version is lighter (weighting 187 g) and smaller with a length expanding from 57 to 64 mm when activated (perturbation length approximately 7 mm). Releasing the spring (gray) causes the device to elongate within a few ms. Additionally, precise grip force measurement is obtained by guiding the grip force through a

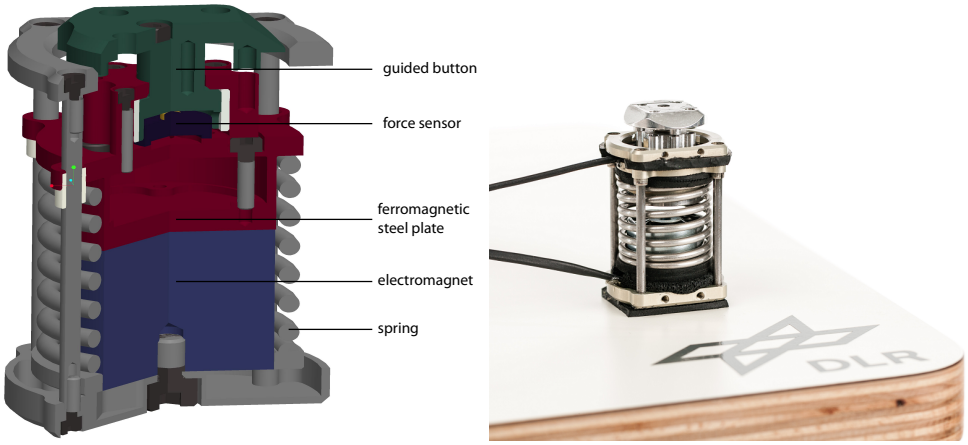

Figure 2.3: Second version of the Grip Perturbator (reproduced from [HMvdS13]). — This version is used within section 2.3.

button (green) to the load cell (black). As noted by van Doren [VD98], grasp span has a small effect on grip stiffness (stiffness changed only 5% for a change of ± 2 cm in grasp span); therefore a fixed Perturbator size was chosen for this version. The spring force was 140 N when loaded and 100 N when unloaded.

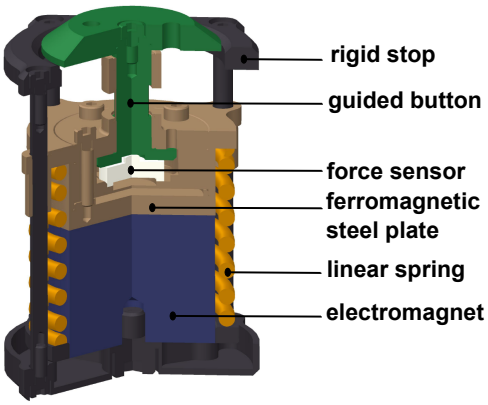

Figure 2.4: Third version of the Grip Perturbator (reproduced from [HGDSvdS16]). — Cross sectional view of the version that is used within Subsection 2.5.

The third and final version of the Grip Perturbator shown in Fig. 2.4 was used within the experiments of Subsection 2.5 and will be published within [HGDSvdS16]. Differences mainly concern the design of the guided button (green) which induces the finger forces into the small load cell and now allows a smaller perturbator grip length. Additionally, three markers for optical tracking and two small fans are attached in order to reduce the heating caused by the electromagnet. The perturbator is again a bit lighter and smaller, weighting 165 g and its length varies between 54 and 61.5 mm, resulting in a perturbation length of approximately 7.5 mm.

2.2 First Experiments—Results of a Force Task

In this Section first experiments with the Grip Perturbator will be reported that were published within [HLU+11]. In this work, human finger stiffness is investigated in a simple force task, in order to validate the demonstrated device of Subsection 2.1.3. An underlying assumption of that work is that finger stiffness is directly correlated to exerted finger force and can be reconstructed from that signal. For the analysis of data time window length of 10 ms each were used (see 2.1).

Furthermore, t_{trust} was set to 25 ms from visual inspection of the respective force perturbation profiles, leading to a length of the second time window of 15 ms.

2.2.1 Experiments

Five healthy male subjects, four right- and one left- handed (subject C), age 26–39 years, joined an experiment designed to measure their finger stiffness while pinch-gripping the Grip Perturbator. They had no knowledge about the experiment itself.

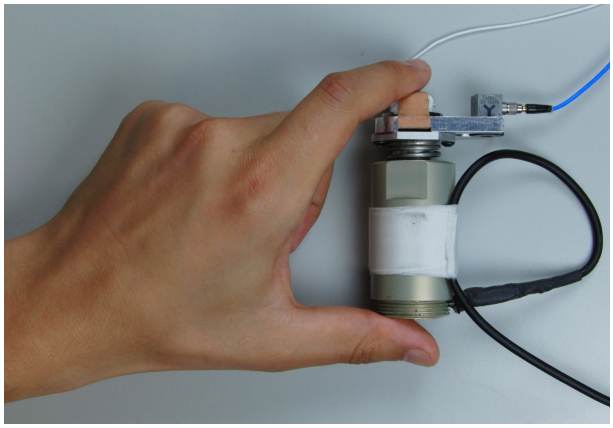

Figure 2.5: First version of the Grip Perturbator held by a human subject in a pinch grip (reproduced from [HLU+11] ©2011 IEEE).

The Grip Perturbator (see Fig. 2.5) was put on a table without any fixations. The subject was asked to sit comfortably in front of the table, relax and let the dominant arm lie on the table in order to be able to grasp the device with the thumb and index finger. Middle, ring and little finger have to lie bent and relaxed below the palm. It was stressed that the subject should relax as much as possible also while grasping, in order to minimize disturbances to the finger stiffness induced by the hand/arm/body muscle tension.
Initially, the subject was instructed to hold the device in pinch grip and apply Maximum Voluntary Contraction (MVC), i.e. to hold the manipulandum as firmly as possible for 10 seconds, while its maximum gripping force was estimated (resulting in values between 25 and 40 N). Subsequently, subjects were shown a live visualization of the force applied to the device, as well as two lines representing 1.15 and 0.85 times a required amount of force; they were then instructed to reach that level with the aid of the bands, and keep it until the perturbation was felt. The perturbation was issued at a time chosen randomly between 2 and 4 seconds after the reaching of the required force. The amount of force (Normalized Force Level (NFL)) was either $10, 20, 30, 40, 50$ or 60% of the maximum gripping force measured beforehand and will be referred as NFL1 . . . 6.
This stimulus/response cycle was repeated 10 times per level (total 60 times per subject) in a randomized order. In-between cycles, the experimenter pre-loaded the spring, reset the force sensor and checked once again the muscular relaxation of the subject. If the subject reported fatigue, it was allowed to rest as much as needed. The experiment lasted on average 18 minutes and no subject reported uneasiness.
The measurement setup consisted of a host running Windows, and a real-time target machine running QNX where a Matlab/Simulink model to control the device was running at 10 kHz sample frequency. The sensor signals were amplified and measured with an analogue digital converter and the electromagnetic field was switched using a relay card; the cards were directly connected to the real-time machine. The acceleration signals were additionally filtered with an analogue 3 kHz low-pass filter. The acceleration sensor can measure translational accelerations

in all three dimensions with a sensitivity of $1.02\,\mathrm{mV}/\frac{\mathrm{m}}{\mathrm{s}^2}$ and a measurement range of $\pm 4905\,\frac{\mathrm{m}}{\mathrm{s}^2}$ peak. Its bandwidth along the z-axis is 2 Hz to 10 kHz. The nominal sensitivity of the force sensor is 1 mV/V, the nominal range 1 kN.

2.2.2 Results

The mean and Standard Error of Mean (SEM) stiffness values are listed in Table 2.1, for each NFL and subject; each point and error bar is evaluated over the related 10 stimulus/response cycles.

Table 2.1: Experimental Results of the force task (reproduced from [HLU+11]).

	NFL1	NFL2	NFL3	NFL4	NFL5	NFL6
A	76±6	126±7	183±10	224±13	262±16	340±20
B	250±14	310±19	406±12	469±14	502±29	554±21
C	201±10	230±10	295±9	330±13	369±19	444±17
D	47±9	96±18	156±16	178±32	264±37	262±20
E	198±10	237±15	302±26	367±13	419±28	454±42

Mean ± SEM stiffness values (N/m) for each subject (rows) and NFL (columns). Each point is evaluated over 10 stimulus/response cycles.

Fig. 2.6 depicts these data graphically. Also, for each subject a least-squares linear fit, the related R^2 coefficient (values of R^2 close to 1 denote a perfect linear regression) and the linear regression slope, α are shown.

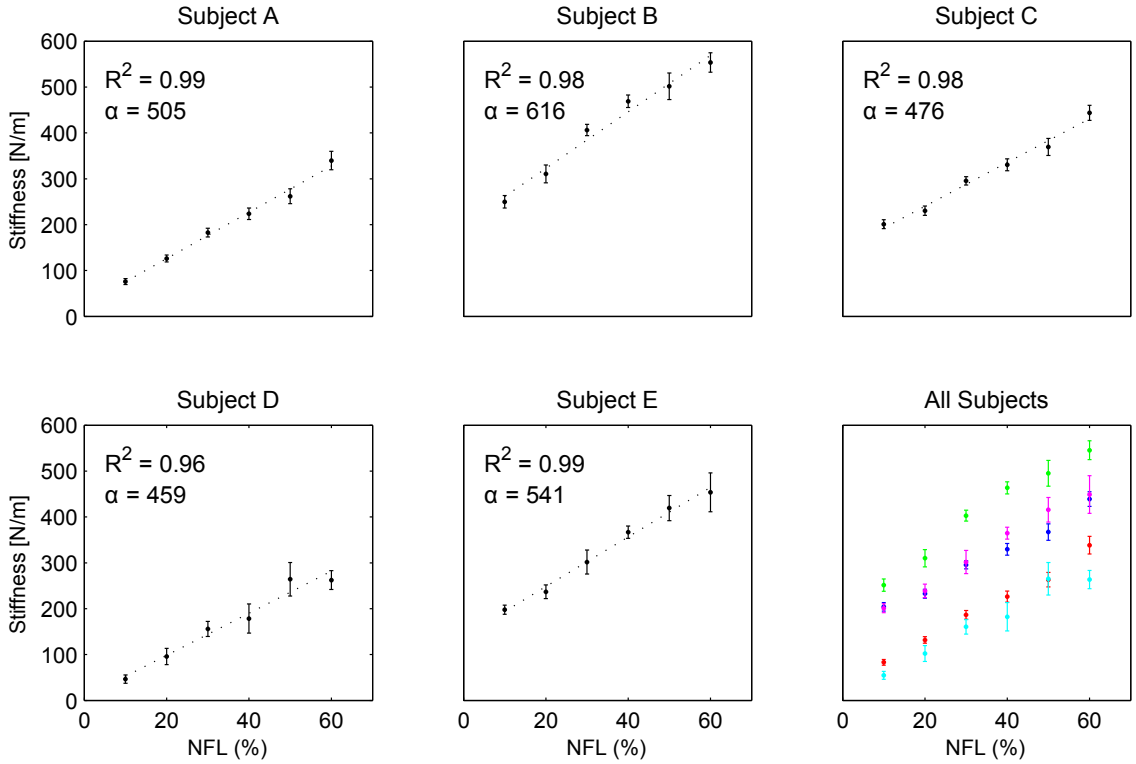

Figure 2.6: Experimental results of the force task (reproduced from [HLU+11] ©2011 IEEE). — Graphical representation of the estimated stiffness per each subject and Normalized Force Level NFL.

As it can be seen, the relationship between stiffness and the required force level is essentially linear ($R^2 \geq 0.96$) and the order of magnitude of the regression slopes is the same for all subjects.

2.2.3 Conclusion

In this Section a novel hand-held device was demonstrated in a simple force task. Assuming that grasping stiffness is correlated to finger force [HH97], the device was validated by showing that human subjects produce a linear increase in finger stiffness as they grip the device with linearly increasing force. Stiffness was measured according to existing literature; linearity was found to be very strong and uniform across subjects, be they right- or left-handed ($R^2 \geq 0.96$). The whole measurement time for estimating the stiffness was less than 25 ms (t_{trust}), thus no influences of voluntary interactions nor reflexes distorted the result. In the performed experiments the intrinsic stiffness of the grasp due to tissue properties was measured only.
The measured linear relationship between stiffness and force

$$K = K(x,t) = -\frac{\partial F}{\partial x} = c_1 \cdot F(x) + c_2, \tag{2.4}$$

leads in solving the differential equation to

$$F(x) = k_1 \cdot \exp(k_2 \cdot x) + k_3, \tag{2.5}$$

where c_1, c_2 and k_1, k_2, k_3 are constants. This result implies that there is a non-linear intrinsic exponential relationship between force and displacement. Thus these measurements confirm to a model of the pinching hand in which the muscles are represented by (non-linear) exponential elements [Gla74]. This representation is relevant in the design of variable-impedance robotic hands, where such linearity may influence the mechanical design of the actuators (see Section 4.2).

2.3 Task Dependencies of Grip Stiffness

A vast body of literature is devoted to the regulation of grip force. Indeed, the force necessary to stably hold an object in our hand is continuously regulated by the CNS [EWJ92, JW84] in a process known as "grip-force / load-force coupling". Already in children at the age of 2, this grip force is regulated depending on an object's weight [FEK+91]. Furthermore, the CNS is capable of modulating grip force to account for load forces acting on the hand-held object, such as the inertial forces induced by movement of the arm [FW93, FW95], or whole body movement during running [KKIT96] and jumping [FT94].
It has been shown that forces of an uncompensated grip decrease for contracting and increase for expanding objects [ZGL06], which evokes the concept of grip *stiffness* (i.e. the change in grip force versus a change in grip aperture) and may play an important role in maintaining grip stability. Additionally, a linear relation between grip force and stiffness measured in a force task was presented in the previous Section 2.2.
But how do load force, grip force and grip stiffness relate to each other? Can grip stiffness be modulated independently of grip force and if so, would such modulation have functional significance? Or are these three parameters rigidly coupled? Furthermore, the way in which the subjects were required to apply different grip forces in the previous Section 2.2 (i.e. through visual feedback) was not very natural. What would the stiffnesses be like if a subject would lift an object in a weight task without any feedback about the applied force? Would the stiffnesses measured in the two tasks be comparable? Or would subjects be able to regulate force and stiffness independently?
Two possibilities to decouple grip stiffness and force are acknowledged: either by isometric cocontraction of antagonistic pairs of muscles or by changing the finger/wrist configuration (see Section 1.7).

Does the neuromuscular system allow for an active use of these effects on grip stiffness and an independent control of both, force and stiffness? White *et al.* showed that the CNS is able to decouple grip and load force in anticipation of a collision, with a rise in grip force before the expected impact and a peak in grip force around 65 ms after the impact [WTW+11]. They hypothesized that the CNS increases the net grip force in order to regulate grip stiffness and damping, with the goal of optimizing stability in object manipulation. They did not, however, directly measure grip stiffness. Furthermore, not only might one wish to modulate the grip force on an object to keep it stable in the face of predictable events like a self-generated collision, one might also wish to regulate the stiffness of the grip in anticipation of unexpected perturbations depending on the constraints of a specific task.
In this Section grip stiffness modulation as a function of the natural tendency to increase grip force when lifting increasingly heavy objects [EWJ92, JW84] will be investigated. Human participants will be asked to perform the visually-guided force-control task (Force Task (FT)) described above and a task in which they lifted objects of different weight (Weight Task (WT)), without any specific instructions or visual feedback about the forces applied to the object in the pinch grip. Given the previous conjecture for the force task:

$$K_{\mathrm{FT}} = -\left.\frac{dF_{\mathrm{FT}}}{dx}\right|_{a=\mathrm{const.}} = m_{\mathrm{FT}} F_{\mathrm{FT}} + n_{\mathrm{FT}} \tag{2.6}$$

where f is the exerted force, k the stiffness of the pinch grip, x the pinch grip aperture, a the muscle activation and m and n are slope [1/m] and offset [N/m],

$$K_{\mathrm{WT}} = m_{\mathrm{WT}} F_{\mathrm{WT}} + n_{\mathrm{WT}} \tag{2.7}$$

can be similarly conjectured for the weight task. To compare grip force–stiffness coupling between these two tasks, the following two specific hypothesis will be tested:

- $\mathbf{H_{0_1}}$: The measured stiffness in both tasks are equal for same grip force, i.e. $K_{\mathrm{FT}}(f) = K_{\mathrm{WT}}(f)$;
- $\mathbf{H_{0_2}}$: The relationship between grip stiffness and grip force are equal for the two tasks, i.e. $m_{\mathrm{FT}} = m_{\mathrm{WT}}$ and $n_{\mathrm{FT}} = n_{\mathrm{WT}}$.

Following the analysis of Section 1.7 about the influence of cocontraction and a change in kinematics on the measured force stiffness characteristics, the following assumptions can be taken required for the experiments of this Section: A change of the slope between the two tasks will indicate an influence caused by a change of the Jacobian rather than by cocontraction. A change of the offset, however, can be caused by either or both. Furthermore, a change in the kinematic configuration possibly predominates effects of cocontraction on the force–stiffness characteristics.

2.3.1 Experimental Procedure and Setup

A total of 15 healthy right-handed male subjects, age 22–45 years, performed the two experimental protocols, WT and FT, as described below. No subject had a history of neither neurological disorder nor neuromuscular injury affecting the CNS or the muscles. All subjects gave written consent to the procedures which were conducted partially in accordance with the principles of the Helsinki agreement[2]. The collection of subject data was approved by the institutional board for protection of data privacy and by the work council of the German Aerospace Center.

[2]Non-conformity concerns the point B-16 of the 59th World Medical Association Declaration of Helsinki, Seoul, October 2008: no physician has supervised the experiment.

Subjects stood throughout the experiment, except for a 10-minute break between FT and WT. Standing and lifting weights with respect to the WT was found to be intuitively more natural than sitting. In difference to the measurements performed within Section 2.2 with the Grip Perturbator lying on a desk, all subjects within this Section had previous experience working with the Perturbator and were able to stably hold the device, even after the perturbation. Fully naive subjects would often drop the device during perturbation, leading to useless data because of a missing second static force level.
Ten subjects performed the main experiment in which the arm and wrist were free to move, although subjects were instructed to hold the forearm steady in a horizontal posture. These ten subjects were divided into two groups, counter-balanced as to whether FT or WT was done first (Experiment 1: learned; no cuff; weight task first (E1) and Experiment 2: learned; no cuff; force task first (E2), respectively). To investigate whether changes in the wrist configuration might have an influence on grip stiffness an additional group of 6 subjects (Experiment 3: learned; wearing cuff; both, force and weight task first (E3)) performed the two protocols with the wrist held at a constant orientation with respect to the forearm and with the relaxed arm and wrist supported by a table. Fixation was favored over controlling wrist position using optical tracking in order to keep the task natural and to avoid providing visual feedback in the WT. Half of the subjects in E3 (subjects S11, S12, S13) did WT first, the rest FT first. Note that one subject took part in two experiments, and is referred to as S6-1 in E2 and S6-2 in E3. The whole experiment lasted about 90 minutes per subject. No subject reported discomfort during FT, some reported fatigue during WT.
For the measurements in this Section the second version of the Grip Perturbator was used (see Fig. 2.3). The measurement setup consisted of a host running Windows and a real-time target machine running QNX. The real-time machine ran a Matlab/Simulink model to control the electromagnet and read out the force sensor at 10 kHz. After pressing a release button, the perturbation was applied after a random delay 4 to 7 s. The load cell consisted of a KM10 force sensor and a measurement amplifier GSV-11H (both from ME-Messsysteme GmbH) with a nominal force of 100 N and an overall accuracy of the force signal of 0.1 N. It was verified that perturbations caused no significant phantom force changes in the device by testing it with known springs. The offset of the measured force signal was calibrated before each trial.

2.3.2 Data Processing

The force signals were first filtered using a 21-point moving average filter. The time when the electromagnet was released and the time $t_{\text{pert}} = 0$ at which the perturbation started (see Fig. 2.1) varied considerably because the breakdown of the electromagnetic field depends highly on the applied grip forces. Therefore, t_{pert} was defined as the end of the period T_1, where T_1 was defined as the last 10 ms time interval before t_{peak} having a standard deviation below $5 \cdot 10^{-4}$ N. These numbers were empirically determined and led to stable results. The rise time between start of the perturbation and t_{peak} was on average 3.6 ± 0.62 ms (SD) and showed no significant correlation with force or weight levels.
As explained within Section 2.1, T_2 was varied so as to optimize the objective function

$$Z = \frac{1}{n_{\text{sub}}} \sum_{i=1}^{n_{\text{sub}}} \left(\frac{1}{n_{\text{level}}} \sum_{j=1}^{n_{\text{level}}} \left(\tilde{e}(K_{\text{WT}_{ij}}) + \tilde{e}(K_{\text{FT}_{ij}}) + \frac{1}{n_{\text{trial}}} \sum_{k=1}^{n_{\text{trial}}} \left(\tilde{e}_{\text{T}_2}(f_{\text{WT}_{ijk}}) + \tilde{e}_{\text{T}_2}(f_{\text{FT}_{ijk}}) \right) \right) \right) \tag{2.8}$$

using the whole number of trials n_{trial}, levels n_{level} and subjects n_{sub} [3]. The length of the second time interval T_2 and its end t_{trust} were found to be optimal under named constraints at 6.8 and

[3] Please note, that Eq. 2.8 is an adapted version of the optimization function Eq. 2.2 introduced within Section 2.1 for the experiments performed in this Section.

16.7 ms, respectively.

Weight Task

In the WT, six different weights ranging from 0.2, 0.4, ..., 1.2 kg were attached to the Perturbator, and for 10 trials each of the subjects had to lift the device off of the table (Fig. 2.7). The lower arm was requested to be held at approximately a 90 degree angle with the body. There was no visual feedback w.r.t. the grip force to the subject. Once the grasp was stable, the experimenter pressed the button to apply the perturbation between 4 and 7 s later (randomly chosen by the control computer).

Figure 2.7: Second version of the Grip Perturbator held in a pinch grasp with attached weights (reproduced from [HMvdS13]).

Force Task

The procedure of the FT is almost the same to the force task of Section 2.2, except that subjects lifted and held the Perturbator above the table (as in WT, but with no additional weight attached). The subject received visual feedback about the actual force applied to the Perturbator and was asked to maintain a visually instructed predefined force. Once this force level was reached, the release button was pressed by the experimenter, unknown to the subject, and the perturbation was performed between 4 and 7 s later. Six instructed force levels were randomly presented to each subject, for a total of 10 times per force level.

Since applied grip forces for lifting the weights differed considerably across subjects, the natural grip force when holding the device with different weights was measured—thus leading to different grip forces—and 6 different grip force levels were chosen to subsequently use for FT. If subjects were instructed to do the FT first, they were asked to lift the Perturbator once with each weight attached before the FT without applying any perturbations. If the WT had to be done first, the information of the WT was used to estimate the required force levels for the FT.
For both tasks, experimenter release was preferred over automated release because previous experiments revealed increased participant fatigue in the latter case—holding the force level

steady for a while, especially at high levels is increasingly difficult and troublesome. Note that the non-rigid coupling between the Perturbator and the additional weight in the WT meant that the inertia of the Perturbator was effectively constant, so that this effect did not have to be accounted for in the data analysis (see Fig. 2.7).

2.3.3 Results

Fig. 2.8, Fig. 2.9, and Fig. 2.10 show the results of the experiments for each subject. Each graph depicts the measured stiffness for FT in red and WT in black and their linear regressions as dashed lines. For each force and weight level, the mean values and their SEM in force and stiffness and the mean in force and stiffness used for testing $\mathbf{H_{0_1}}$ are plotted as circles. Additionally, the related R^2 coefficient (values of R^2 close to 1 denote a near-perfect linear regression) for a linear assumption of FT and WT, and the two normalized mean inter-subject ratios of stiffness $\Delta K^* = (K_{\mathrm{FT}} - K_{\mathrm{WT}})/(K_{\mathrm{FT}} + K_{\mathrm{WT}})$ and linear regression slopes $\Delta m^* = (m_{\mathrm{FT}} - m_{\mathrm{WT}})/(m_{\mathrm{FT}} + m_{\mathrm{WT}})$ are depicted. Furthermore, Tables 2.3 and 2.5 list the results of the measured stiffnesses and the linear regressions between force and stiffness for each subject in both tasks. Based on these data and regression fits statistical tests were performed of the previously conjectured two hypotheses. For testing these, a fixed level of significance was chosen to $\alpha = 0.05$ for all tests.

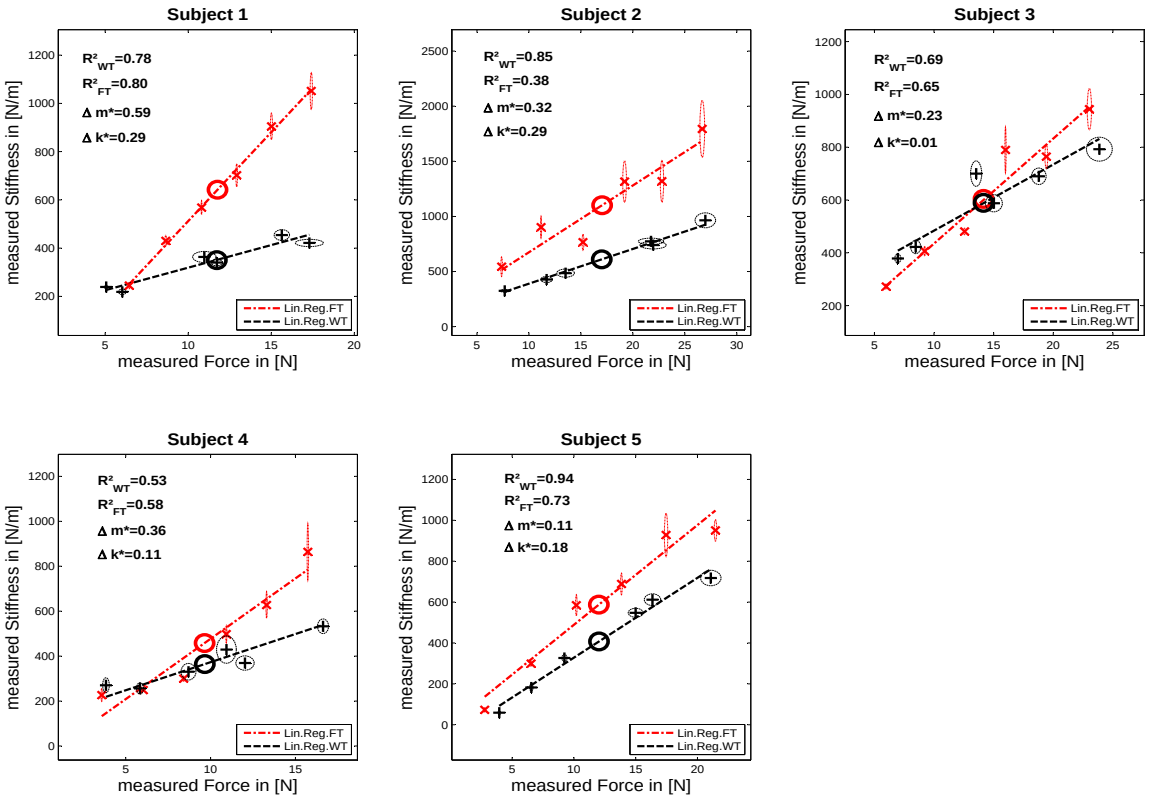

Figure 2.8: Results Experiment 1 (reproduced from [HMvdS13]). — Subjects doing the WT first without a cuff.

Results Main Experiment—Groups E1 and E2

The subjects of groups E1 and E2 were asked to do either FT or WT first with an unconstrained wrist.

H_{0_1}: Equal stiffness for equal grip force ($\mathbf{K_{WT}(f) = K_{FT}(f)}$)— For each subject it was tested whether the same stiffness was generated in each task, on average across all grip forces. Since the ranges of grip force differed considerably between the two tasks—especially for subjects doing the FT first (see, e.g. subject S9 in Fig. 2.9)—the datasets were algorithmically adjusted on a subject-by-subject basis by discarding trials with the highest or lowest grip-force values so as to align the mean grip forces before perturbation in WT vs. FT. Table 2.3 summarizes the results for each subject in detail for comparing the average stiffness levels[4]; the mean values in force and stiffness are additionally depicted in Figs. 2.8 and 2.9. It was then tested whether grip stiffness differed for the two tasks by testing if their difference was significantly different from zero, on average across subjects, by performing Student's dependent paired t-test on mean inter-subject stiffness ΔK^*, normalized by the sum of K_{WT} and K_{FT} for each subject, for groups E1 and E2. These results (Table 2.2) indicate that mean stiffness differed significantly ($p < 0.05$) with higher stiffness measured in FT, regardless of which task was performed first by each subject (see Figs. 2.8 and 2.9). Furthermore, Table 2.3 includes results of an F-test for testing if the variances in intra-subject stiffness of both tasks were equal. The results provide evidence that, for all subjects of groups E1 and E2 excluding subject S6-1 and S7, it can be rejected that the variances in intra-subject stiffness were equal (Table 2.3), even if the tested standard variation was calculated across all data.

Table 2.2: Testing $\mathbf{H_{0_1}}$ (reproduced from [HMvdS13]).

$\frac{\mathbf{K_{FT}-K_{WT}}}{\mathbf{K_{FT}+K_{WT}}}$	**E1**	**E2**	**E1+E2**
$\bar{\mathbf{x}}$	0.18	0.13	0.16
$\sigma^{\mathbf{2}}(\mathbf{x})$	0.12	0.069	0.095
p (2-tailed)	2.9%[1]	1.3%[1]	0.058%[1]

[1] $\mathbf{H_0}$ is rejected for probability values less than 5% (paired t-test).

Testing H_{0_1}, whereby the two stiffnesses in Eqs. (2.6) and (2.7) are equal $K_{\mathrm{FT}}(f) = K_{\mathrm{WT}}(f)$ across subjects. The mean normalized difference of the two stiffnesses ΔK^* and its standard deviation are listed (inter-subject variability). Data were discarded such that mean in force of both data sets align.

H_{0_2}: Equal force–stiffness slopes ($\mathbf{m_{WT} = m_{FT}}$) and offsets ($\mathbf{n_{WT} = n_{FT}}$)— For each subject and task a linear regression between force and stiffness was made and the slope and offset of the resulting regression were calculated (see Table 2.5 for details). It was then tested whether the parameters of the force–stiffness regressions differed between the two tasks, on average across subjects via a dependent paired t-test using the normalized difference of the slopes Δm^* and the mean of the offsets (see Table 2.4). The results provide evidence that, in general, the slopes in FT differed significantly from WT ($p < 0.05$) with higher slopes in FT, regardless of which task was performed first by each subject. Furthermore, it cannot be rejected that the mean offsets in group E1 or group E2 were equal; conversely, this can be rejected when data from the two groups were combined (E1+E2).

What can be concluded from the above? When holding the weight in the hand, higher muscle activation was required for WT in order to counteract the vertical load. Furthermore, to stabilize the wrist against this vertical load, antagonistic pairs of muscles will have been activated. One might expect a higher measured stiffness in comparison to FT, in which no additional

[4]These data were only discarded for testing $\mathbf{H_{0_1}}$. Note that this data adaptation had no qualitative effect on the results; even without this normalization, the mean FT stiffness was always higher than the mean WT stiffness.

Table 2.3: Testing $H_{0_1} : K_{WT}(f) = K_{FT}(f)$ (reproduced from [HMvdS13]).

group	subj.	$\overline{K_{WT}}$ [N/m]	$\overline{K_{FT}}$ [N/m]	ΔK^*	$\overline{F_{WT}}$ [N]	$\overline{F_{FT}}$ [N]	No. WT	No. FT	F-test [%]
E1	**S1**	350 ± 99	642 ± 302	0.29	11.7 ± 4.5	11.8 ± 3.7	10%	0%	9.4 E-12[1]
E1	**S2**	611 ± 249	1101± 648	0.29	17.0 ± 7.3	17.0 ± 6.6	0%	0%	6.0 E-10[1]
E1	**S3**	589 ± 160	604 ± 285	0.013	14.2 ± 5.0	14.2 ± 5.6	15%	3.3%	6.0 E-3[1]
E1	**S4**	365 ± 151	458 ± 293	0.11	9.7 ± 4.4	9.6 ± 4.2	0%	0%	8.2 E-5[1]
E1	**S5**	408 ± 250	588 ± 363	0.18	12.0 ± 6.2	12.0 ± 6.3	0%	0%	0.45[1]
E2	**S6-1**	1309± 622	1565± 789	0.089	15.2 ± 5.4	15.2 ± 5.2	0%	0%	6.8
E2	**S7**	451 ± 197	495 ± 191	0.047	12.7 ± 3.8	12.7 ± 5.1	5.1%	20%	82
E2	**S8**	362 ± 121	473 ± 189	0.13	10.8 ± 3.3	10.8 ± 4.5	18%	11%	0.20[1]
E2	**S9**	354 ± 163	557 ± 478	0.22	6.5 ± 2.6	6.5 ± 3.5	0%	48%	2.5 E-10[1]
E2	**S10**	649 ± 388	927 ± 693	0.18	14.1 ± 8.0	14.1 ± 6.7	0%	0%	1.4 E-3[1]
E3	**S11**	1075± 654	1034± 625	−0.019	14.1 ± 6.8	14.2 ± 6.8	1.6%	0%	73
E3	**S12**	329 ± 163	381 ± 172	0.074	9.9 ± 4.7	10.0 ± 4.5	0%	0%	69
E3	**S13**	495 ± 204	479 ± 211	−0.016	9.6 ± 3.9	9.6 ± 4.0	3.4%	0%	81
E3	**S6-2**	715 ± 276	785 ± 393	0.047	11.9 ± 3.5	11.9 ± 4.8	0%	6.6%	0.80[1]
E3	**S14**	408 ± 168	502 ± 197	0.10	8.7 ± 3.0	8.7 ± 3.5	18%	43%	31
E3	**S15**	394 ± 184	473 ± 184	0.090	10.6 ± 4.7	10.6 ± 4.7	8.3%	11%	99

[1] $\mathbf{H_0}$ of the F-test (Variances are equal) is rejected for probability values less than 5%.

The mean and standard deviation of stiffness of both tasks, their normalized difference ΔK^*, the percentage of data discarded for these tests and the result of the F-test are listed. Data were discarded such that mean in force of both data sets align.

weight must be supported. But the opposite was measured: by increasing the load, the stiffness decreased at constant grip force.

One could argue that the higher stiffness in the FT was required to accurately hold a certain force level using cocontraction, while for the WT it was not, because there no visual feedback of force was presented. As discussed in Section 1.7, using cocontraction will affect the offset of the force–stiffness relation. Because the results of testing $\mathbf{H_{0_2}}$ provide evidence that the regressed offsets of the two tasks were different, it was interesting to know if each of them differed from zero. It was found that it can be rejected for the WT across both groups E1 and E2 that the

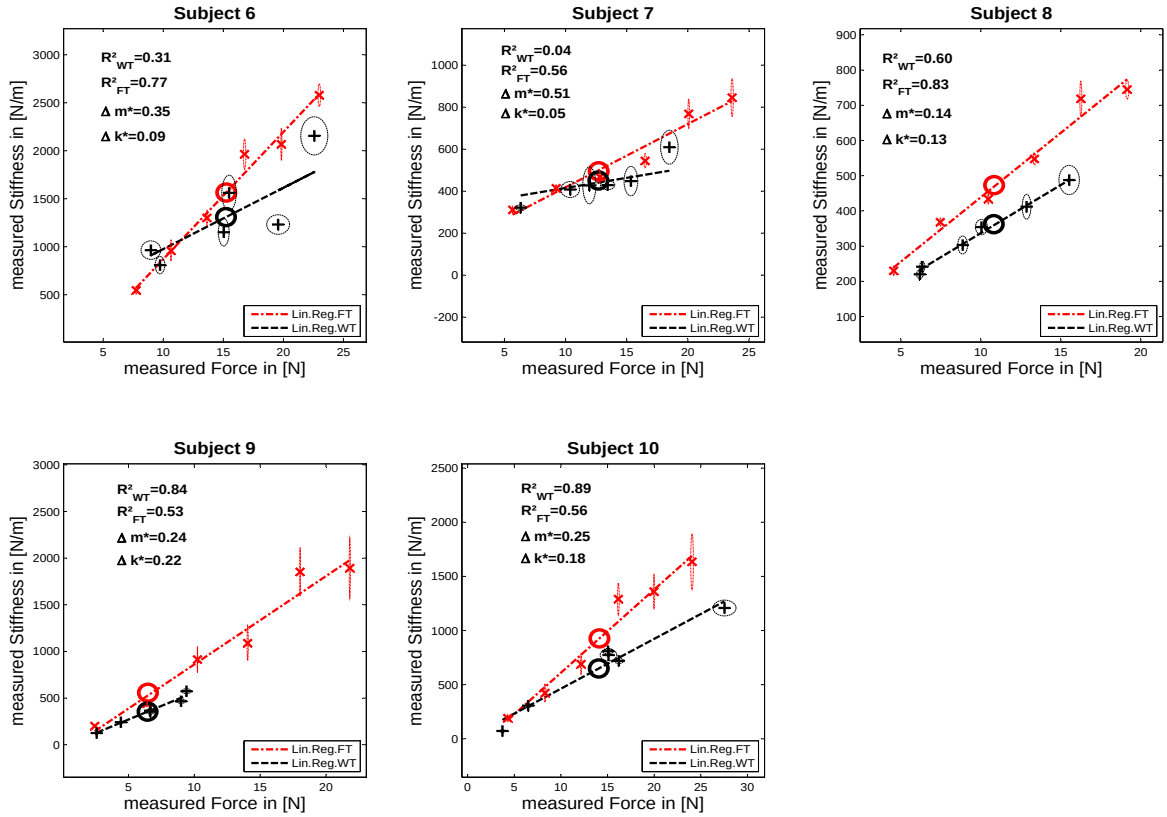

Figure 2.9: Results Experiment 2 (reproduced from [HMvdS13]). — Subjects doing the FT first without a cuff.

Table 2.4: Testing H_{0_2} (reproduced from [HMvdS13]).

$\frac{m_{FT}-m_{WT}}{m_{FT}+m_{WT}}$	E1	E2	E1+E2
$\bar{x}$	0.32	0.30	0.31
$\sigma^2(x)$	0.18	0.14	0.15
p (2-tailed)	1.6%[1]	0.88%[1]	0.012%[1]

$n_{FT} - n_{WT}$	E1	E2	E1+E2
$\bar{x}$	-136	-242	-186
$\sigma^2(x)$	167	319	247
p (2-tailed)	14%	17%	3.9%[1]

[1] H_0 is rejected for probability values less than 5% (paired t-test).

Testing H_{0_2}, whereby the two slopes and offsets in Eqs. (2.6) and (2.7) are equal $m_{\mathrm{FT}} = m_{\mathrm{WT}}$ and $n_{\mathrm{FT}} = n_{\mathrm{WT}}$ across subjects (inter-subject variability). Left table: The mean normalized difference of the two slopes Δm^* and its standard deviation. Right table: The mean difference of the two offsets and its standard deviation. No data were discarded.

offset listed in Table 2.5 is equal to the origin (two-tailed t-test; $p < 0.025$), but not for the FT.

Furthermore, it was looked at the correlation between slope and mean intra-subject stiffness across all subjects (no data were discarded; see Table 2.6). The results indicate that there is a significant correlation between mean stiffness and slope for the FT, which further argues for a force–stiffness relation going through the origin for the FT. As a corollary, the results are consistent with the finding that the force–stiffness curve of a single muscle most likely goes through the origin [SA92][5].

[5]Note that the offset of measured force–stiffness characteristic of the antagonistic system at zero net force is not precisely zero because of the *passive* stiffness of surrounding tissues and ligaments in the arm and hand.

Table 2.5: Linear regression and Mandels test for linearity (reproduced from [HMvdS13]).

grp.	subj.	m_{WT}	m_{FT}	Δm^*	n_{WT}	n_{FT}	R_{WT}^2	R_{FT}^2	M-test WT	M-test FT
E1	**S1**	19	74	0.59	132	-224	78	80	20	97
E1	**S2**	31	61	0.32	75	69	85	38	73	24
E1	**S3**	25	40	0.23	233	37	69	65	40	67
E1	**S4**	25	54	0.36	123	-60	53	58	7.8	0.61[1]
E1	**S5**	39	49	0.11	-62	1.6	94	73	0.015[1]	1.6[1]
E2	**S6-1**	64	133	0.35	337	-457	31	77	24	50
E2	**S7**	10	30	0.51	318	117	4.4	56	14	34
E2	**S8**	27	37	0.14	64	73	60	83	30	65
E2	**S9**	58	95	0.24	-22	-85	84	53	25	93
E2	**S10**	46	77	0.25	3.1	-158	89	56	0.16[1]	62
E3	**S11**	76	75	−0.009	-21	-34	68	66	12	15
E3	**S12**	31	37	0.08	18	15	80	92	1.7[1]	14
E3	**S13**	45	38	−0.09	63	117	79	52	13	26
E3	**S6-2**	55	67	0.10	67	-19	47	76	7.9	1.4[1]
E3	**S14**	48	50	0.02	-17	65	86	94	77	11
E3	**S15**	25	38	0.20	109	69	58	93	5.7E-10[1]	1.8[1]

[1] For probability values less than 5% it is rejected that a linear relation is as good as a quadratic.

Slope $m_{WT/FT}$ [1/m], their normalized values Δm^*, offset $n_{WT/FT}$ [N/m], the related R^2 [%] coefficient for a linear model and the results of the Mandel test in [%] are listed.

Table 2.6: Correlation $r_{WT/FT}$ between slope and mean intra-subject stiffness and its probability $p_{WT/FT}$ in % for groups E1 and E2 (reproduced from [HMvdS13]).

$\bar{K} \sim m$	E1	E2	E1+E2
r_{WT}	24%	57%	59%
r_{FT}	28%	99%	88%
p_{WT}	69%	31%	7.5%
p_{FT}	65%	0.16%[1]	0.089%[1]

[1] The correlation is significant.

For probability values less than 5% the correlation is significant. No data were discarded.

Results Experiments with Fixed Wrist—Group E3

Given that it was found both higher grip stiffness and a higher force–stiffness slope for FT together with an offset in the FT not different from zero and an offset significantly larger than zero for the WT, the results argue strongly for a change in the kinematics as the predominantly underlying mechanism rather than a change of cocontraction (see Section 1.7). To further test this hypothesis, subjects in group E3 performed the two tasks with the wrist held in a constant position by a rigid cuff in order to minimize the influence of a change in the kinematics. The cuff used here was made of a thermoplast with a steel plate parallel to the arm axis in order to maximize its stiffness; but still the wrist could be bent within small ranges. In order to prevent subjects from moving their wrist, the arm and hand were additionally rested on a table.

Table 2.7 shows the results of comparing the average stiffness across all grip-force levels, the slope of the force–stiffness relationship and their correlation. One can see that force–stiffness relationship, i.e. the slopes and the offsets, differed much less between the two tasks when the

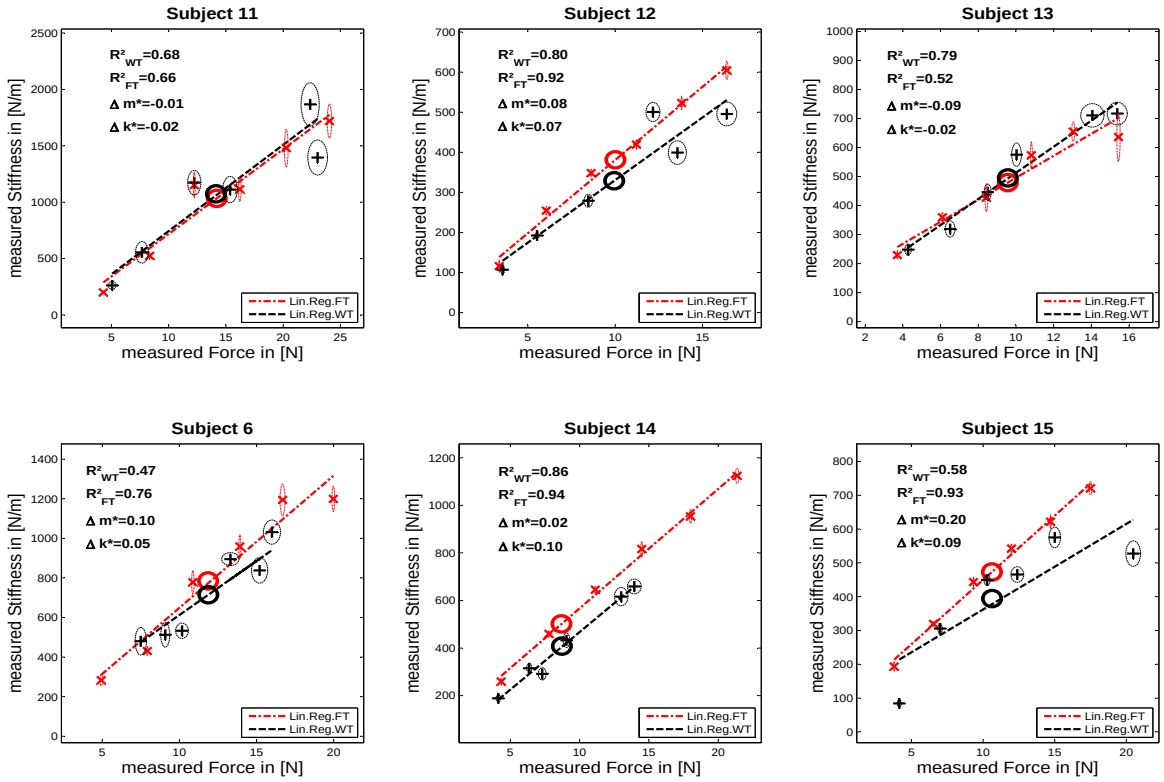

Figure 2.10: Results Experiment 3 (reproduced from [HMvdS13]). — Subjects who performed the experiment with the wrist cuff (WT first: top row, FT first: bottom row).

wrist was stabilized. Nevertheless grip stiffness was still higher for FT versus WT. Furthermore, there was a highly significant correlation between mean intra-subject stiffness and the slope of the force–stiffness curve for the WT ($p < 0.01$) and FT ($p < 0.001$). It cannot be rejected for either task that the mean offset across subjects was equal to zero. Further, the results on testing equal variances in intra-subject stiffness using the F-test provide evidence that, for all subjects of group E3 except S6-2, it cannot be rejected that these variances were equal.

Table 2.7: Testing $\mathbf{H_{0_2}}$ for group E3 when the wrist was held in a constant posture by a cuff (reproduced from [HMvdS13]).

E3	$\frac{\mathbf{K_{FT}-K_{WT}}}{\mathbf{K_{FT}+K_{WT}}}$	$\frac{\mathbf{m_{FT}-m_{WT}}}{\mathbf{m_{FT}+m_{WT}}}$	$\mathbf{n_{FT} - n_{WT}}$
$\bar{\mathbf{x}}$	0.046	0.051	-0.91
$\sigma^2(\mathbf{x})$	0.053	0.099	61
p (2-tailed)	8.6%	27%	97%

E3	$\tilde{\mathbf{K}} \sim \mathbf{m}$
$\mathbf{r_{WT}}$	92%
$\mathbf{r_{FT}}$	98%
$\mathbf{p_{WT}}$	$0.92\%^2$
$\mathbf{p_{FT}}$	$0.091\%^2$

[1] $\mathbf{H_0}$ that $K_{\mathrm{FT}} = K_{\mathrm{WT}}$, $m_{\mathrm{FT}} = m_{\mathrm{WT}}$ and $n_{\mathrm{FT}} = n_{\mathrm{WT}}$ is rejected for probability values less than 5% (paired t-test), respectively.

[2] For probability values less than 5% the correlation is significant.

Left table: dependent paired t-test of greater inter-subject grip stiffness, force–stiffness slope and offset for FT versus WT. Right table: Correlation between slope and mean intra-subject stiffness and its probability in %. No data were discarded.

2.3.4 Discussion and Conclusions

The main result of these experiments is that grip stiffness is regulated independently from grip force, at least to some extent. The conventional assumption that stiffness increases linearly with applied force did hold in all of the experimental conditions, but the parameters of that linear relationship varied according to the task. Mean grip stiffness was considerably higher in FT than in WT, for all subjects of the groups E1 and E2, without any significant differences between early and late trials of single subjects, in much the same way that average grip force varied between static and dynamic grasping of different weights [ZGL05], regardless of which task was performed first by each subject. But the slope of the grip force–stiffness relationship was also higher for FT. Furthermore, WT stiffness was higher for lower grip forces (compare subjects S1, S3, S4, S6-1, S7 and S10). This is confirmed by the finding that over all subjects of both groups the offsets were significantly higher in the WT ($p < 0.025$; one-tailed dependent paired t-test; find the corresponding mean and standard deviation in Table 2.4). Additionally, the WT offsets were significantly higher than zero, while the FT offsets were not. Together with a strong correlation between slope and mean intra-subject stiffness for the FT, these results portend to a change of finger/wrist configuration as the predominant mechanism underlying this change in the force–stiffness relationship, as opposed to a change in the level of cocontraction of antagonistic muscles of the fingers. This hypothesis was tested with a new set of subjects having their wrist fixed by a cuff and rested on a pedestal so as to maintain the same posture at the wrist. It was found that both curves matched in terms of stiffness, slope, and offset and for both tasks a strong correlation between mean intra-subject stiffness and slope was observed. Furthermore, it was found that variances in intra-subject stiffness matched as well, which also argues in favor of data coming from the same population and thus for similar experimental conditions in both tasks. However, even if not for subjects S11 and S13, the measured mean stiffnesses in the FT were still somewhat higher for the group (see Table 2.7).

The limitations of the experimental conditions in E3 had to be mentioned as well: fixating the wrist and resting it on a pedestal in order to prevent the wrist from bending reduced activation in WT, possibly leading to lower WT stiffnesses. As initially explained in Section 1.7, a change in kinematics possibly predominates effects of cocontraction on the force–stiffness characteristics. Thus, from measurements done within E3 it cannot be excluded, that the difference found in E1 and E2 is a combination of a change in kinematics *and* cocontraction, with subjects using both strategies in the WT simultaneously.

Comparing the slopes and the mean stiffness between subjects, one can see that they differed considerably. Some of these large differences in inter-subject stiffness could be explained by a difference in grip force, but certainly not everything. Furthermore, for groups E1 and E2, some of the inter-subject variability can be explained by different wrist positions of the subjects. But even within group E3, where the wrist was fixed in one position, the stiffnesses differed considerably between subjects. Measuring planar human arm stiffness, Mussa-Ivaldi [MIHB85] reported that qualitative measures such as *shape* and *orientation* of a stiffness ellipse measured at the endpoint are similar over different subjects for different postures, but the quantitative measure *size* is not, and even varies considerably for identical subjects measured on different days.

The force ranges differed considerably between the two tasks, especially for subjects doing FT first. Since one aim was to exclude the influence of which task is done first, the subjects of this group were allowed to lift each weight only once before the FT in order to avoid learning. This leads to a data set of 6 different force levels, while for subjects doing WT first a data set of 60 data points was used to calculate the force levels. Thus, the force ranges between both tasks differed more for the group doing FT first, leading to a larger force range of FT. However, the influence of this difference is expected to be small. Remember that for testing $\mathbf{H_{0_1}}$ data within

equal force ranges was compared only by discarding extreme values (6.6%) of the data set.
A number of studies have already demonstrated how the finger [MF98] and wrist [OHN+92] can affect fingertip forces and stiffness in the human hand and the idea that one might adjust the configuration of a redundant multi-joint linkage to optimize impedance with respect to the task or to the environment [Hog85b, RH01] has also been proposed. The question which remains to be clarified here is: Are the found differences between the two tasks actively controlled by the CNS? And if yes, why should subjects minimize the influence of the wrist in an FT where they get a visually-presented feedback about variations of the actual grip force?
To maximize the efficacy of the visually-guided control loop, one could reasonably strive to minimize the latency between commanded changes in muscle activations and the actual changes of grip force applied at the fingertips. As muscles are constrained by activation dynamics, there is a theoretical limit to the rate of change of muscle force F with respect to time, dF/dt, that a given muscle can produce. The rate of change of force measured at the fingertip would be modulated by the same Jacobian that governs the relationship between muscle force and finger force, and between muscle stiffness and finger stiffness, i.e. $df/dt = \boldsymbol{J}(\boldsymbol{q})^{-T}\boldsymbol{\Pi}(\boldsymbol{q})^{T}dF/dt$. Thus, by maximizing the norm of $\boldsymbol{J}(\boldsymbol{q})^{-T}\boldsymbol{\Pi}(\boldsymbol{q})^{T}$, one maximizes the ability to rapidly effectuate a change in grip force in response to a visually presented force error. From this point of view, the modulation of grip stiffness observed in this experiments is simply a corollary of the real optimization, that of maximizing responsivity to a visual command, rather than an optimization of grip impedance *per se*, to the differences in mechanical constraints between FT and WT. On the other hand, the signal-dependent noise of the corresponding sensors (viz. the Golgi tendon organs) increases with their activation, and will therefore increase its effect on fingertip force. Conclusively, it can only be clarified to some extent and not with significance if the found difference is actively optimized or just passively caused by a bent wrist.
All in all, of course static grip stiffness is linearly related to grip force, caused by the exponential stiffness of tendon tissue. But by changing the kinematics of our grip—and thus just changing the force transfer function from muscle to finger—one can actively change the increase of stiffness with force by flexing our wrist and thus change the stability of the grip. In that it is highly relevant that, in this experiments, low stiffness values were obtained when holding objects of different weights rather than exerting a predefined force—a natural task, which human likely have learned to solve at minimal cost.

2.4 About Linearity between Force and Stiffness

As mentioned within Sections 2.2 and 2.3, a strong linear correlation between grip force and stiffness exists and could be revealed during a force task. It is of further interest whether linearity was indeed obtained or, e.g. violated according to the task. Based on the measurements of Section 2.3, Mandel's technique will be used to test whether a linear or a quadratic model provides a significantly better fit for the investigation of the force–stiffness relation [Man84, p. 165ff][6]. The test compares the standard deviations of the residuals

$$W = \frac{(n-2){s_1}^2 - (n-3){s_2}^2}{{s_2}^2}, \tag{2.9}$$

where s_1 and s_2 are the residual standard deviations of a linear and quadratic fit and n the sample size. s_1 and s_2 are computed as

$$s_1 = \sqrt{\frac{1}{n-2}\sum_{i=1}^{n}(y_i - \hat{y}_{1_i})^2}; \quad s_2 = \sqrt{\frac{1}{n-3}\sum_{i=1}^{n}(y_i - \hat{y}_{2_i})^2}, \tag{2.10}$$

[6]Please note that the results of this Section were reported within [HMvdS13].

where y_i are the measured and y_{1_i}, y_{2_i} the fitted values. If the linear model is a correct assumption, the numerator and denominator in Eq. 2.9 will tend to be alike and W will be close to 1; if the quadratic model is a better assumption, the numerator will tend to be larger than the denominator. The Mandel-test uses again the F-distribution to test for significance: If W is less than or equal to the value of the F-distribution $F(f_1 = 1; f_2 = n - 3; \alpha = 0.05)$, it can be rejected that a quadratic model provides a considerably better fit to the measured values; if it is higher, than a quadratic fit is significantly better (f_1 is the number of degrees of freedom of the numerator; f_2 of the denominator).
The results of the Mandel-test listed in Table 2.5[7] provide evidence that a linear relationship captures the underlying relationship to a reasonable degree for most of the subjects and tasks, consistent with the findings in [HLU+11] and Section 2.2. Contrary, the authors of [OG99] reported about a joint stiffness saturation with increasing muscular activity. However, this might be related to the fact that measurements in this study were mostly influenced by reflexive rather than areflexive stiffness [SA92].
Moreover, please note the difference between R^2 and the Mandel-test for linearity. R^2 indicates the percentage of the variance which can be explained by a (cq.) linear model. Thus, by implication R^2 of a quadratic model is never worse than that of a linear one. The Mandel-test compares the difference of both model residuals by taking also the statistical degrees of freedom into account and indicates whether the difference is significant. E.g., the amount of data that can be explained by a linear model for the WT of subject S5 is not bad (93.7%) and indicates a linear relation, but using a quadratic model is significantly better (95.1%).

2.5 Grip Stiffness and its Dependency on Cocontraction

The capabilities of modern robotic systems to mechanically change their elasticity [VASB+13, GASB+11] by the use of non-linear springs is a concept copied from flexibility found in biological limbs. Through *cocontraction* we can increase the stiffness and damping characteristics of our limbs, thus influencing the energy exchange characteristics with our environment. But how can these extra degrees of freedom be exploited, and what stiffness ranges are useful? What relationships between torque and stiffness are useful?
In Section 2.2 it was shown, that grip force is linearly related to areflexive stiffness under identical experimental conditions. In the following Section 2.3 it was shown, that this coupling is not rigid; rather, the task plays a prominent role in the force-to-stiffness ratio. Two possibilities to decouple intrinsic grip stiffness and force were acknowledged: either by cocontraction of antagonistic pairs of muscles, or by kinematically changing the wrist configuration (see Section 1.7 as well). Using a control group it was shown, that a change in the kinematics accounts for most of the differences.
Having laid down the cause of the found variabilities, several questions arise mainly concerning the role of cocontraction: Why didn't subjects go for the strategy of cocontraction to stably *hold the force level* in the force task? For reasoning the role of cocontraction, Selen *et al.* investigated in a simulation study its role in reducing kinematic variability that arises from internal sensorimotor noise [SBD05]. Since force fluctuations and joint impedance both increase linearly with muscular activation, they analyzed the role of impedance in this paradoxical situation: Does cocontraction lead to more joint stability or larger fluctuations caused by an increase of motor noise? They concluded *"... that the strategy of the neural system to control the effects of force variability on kinematic variability strongly depends on neural noise levels and sources, muscular architecture and skeletal properties..."* [SBD05].

[7] Note that the data were also corrected for non-normality (see [dV02, p. 78ff.] for details), because the F-test is very sensitive to non-normally distributed data. Since the results of the Mandel-test are identical (rejection or not), it will be refrained from a detailed explanation for correction of non-normality.

Furthermore, human can vary reflexive stiffness by changing reflex gains. If so, when do we use cocontraction to change intrinsic stiffness? In [Hog84] Hogan analyzed the role of cocontraction of an antagonistic setup for *maintaining position* (no external torque) in a simulation study in comparison to using active control. He revealed that controlling apparent stiffness using reflexive feedback is energetically efficient, but necessarily limited due to transmission delays of the feedback loop, sensory delay, and by muscle activation dynamics. On the other hand, cocontraction of an antagonistic pair of muscles to vary passive stiffness is highly effective in order to maintain stability, but incurs large metabolic energy costs.

From the above we can conclude that cocontraction is a successful strategy to maintain a position for the higher frequencies, while not for holding a force level. That's reasoning, why the found differences of Section 2.3 cannot be attributed to a change in cocontraction. But for multi-joint systems, another effective and efficient strategy to increase Cartesian stiffness is to move the serial chain in the null-space [AGTB13, ATL$^+$14]; the strategy of changing kinematic configurations requires low metabolic costs with a possibly similar result on position stability. If we have both abilities affecting passive (by kinematics) as well as active (by reflex gains) stiffness, what do we need cocontraction for? Various studies focused also on the change of arm stiffness when using cocontraction: In [OFK$^+$02], Osu *et al.* investigated short- and long-term changes in cocontraction when interacting in known and unknown environments. They found that their defined index of muscular cocontraction around the joint (IMCJ) increased linearly with arm joint stiffness. Using the IMCJ, the authors revealed in a set of motor tasks that viscoelasticity contributes more when the internal models are incorrect, while the internal models contribute more after periods of learning. In another study [GMCM03] Gribble *et al.* found an inverse relationship between cocontraction and the target size in a pointing task. The researchers found the trajectory variability decreasing and endpoint accuracy improving with an increase of cocontraction. They concluded that the CNS may use cocontraction to facilitate movement accuracy. Thus, cocontraction is a successful strategy to stably hold a static position for the higher frequencies and to meet (position) accuracy demands during predictive arm movements.

But the investigation of the mechanism *cocontraction* is rather limited, all named studies investigated the usage of cocontraction at zero net torque only. Contrary, in general the production of forces is highly relevant for interacting with environmental constraints and the manipulation of objects and possibly the ability to alter stiffness at this force, too. Is the ability of decoupling force and stiffness using cocontraction limited to the lower force ranges, e.g. to zero net force, since intrinsic stiffness increases with force anyway [HLU$^+$11]? Or are we able to considerably decouple the two by cocontraction also for the higher forces?

Two ways of forcing subjects to cocontract are acknowledged, either by (a) the application of unstable force fields [AMS83] or by (b) presenting a visual feedback about the applied muscular activity from relevant muscle groups [OFK$^+$02]. Using unstable force fields seems to force subjects to increase cocontraction in a natural way but is probably limited to the production of zero net torque, which means that no forces where applied by the finger or limb. On the other side, forcing subjects to produce cocontraction based on measured EMG is an unnatural task, but allows commanding different combinations of contraction and cocontraction. However, other studies investigated different levels of cocontraction at zero net torque only.

In this Section the possibility of subjects to decouple areflexive grip stiffness from grip force by using cocontraction only will be investigated. The position of arm and fingers are continuously monitored through optical tracking and corrected where necessary, so as to ensure identical experimental conditions. Rather than using EMG feedback as a measure of muscular activation, as practiced in [SKK09, OG99, OFK$^+$02], a different approach (c) will be used by presenting visual feedback of the applied force and stiffness of each prior trial to a participant. EMG will be used to investigate the role of relevant intrinsic and extrinsic muscle groups and their relationship to measured stiffness and force for single subjects (intra-subject variability) as well

as between subjects (inter-subject variability) will be evaluated.
The experiments were performed within the Master Thesis of Maximilian Große-Dunker and the results of this Section are based on the obtained raw data [GD13].

2.5.1 Expected Influence of Cocontraction on Stiffness, Force and Muscular Activity

Before starting, an investigation of the expected role of cocontraction on the Cartesian stiffness and net force as well as on the measured muscular activity of a joint with multiple muscles acting on it will be presented, which will help to interpret the results. See, e.g., Fig. 2.11 as an example for a finger joint: it depicts the force–stiffness curve of an antagonistic setup consisting of two flexor and two extensor muscles.

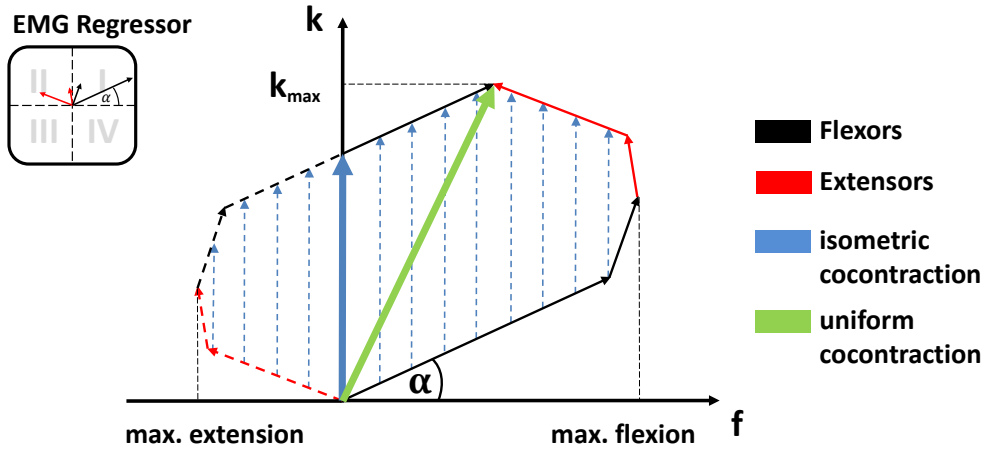

Figure 2.11: The expected influence of cocontraction on the Cartesian net force f and stiffness k (reproduced from [HGDSvdS16]). — The theoretically achievable force stiffness range of a joint consisting of two flexor and two extensor muscles (assumption: linear dependence between force and stiffness of a single muscle; independently voluntarily controllable). The field is defined by the vector-sum of the single muscle curves. Uniform cocontraction leads to an increase in force and stiffness along a line pointing in the direction of maximum stiffness *(green)*, isometric cocontraction leads to an increase in stiffness, but not in Cartesian net force *(blue)*. The EMG regressors achieved from a multiple linear regression between $\sqrt{\text{EMG}}$ and force and stiffness can be depicted as a multitude of arrows *(Top left)*. If muscular activity is ideally linear related to force and stiffness, these arrows will point in exactly the same direction as the force stiffness relations (assumption: muscular activity independently measurable).

The red and black arrows in Fig. 2.11 denote the force–stiffness relations of the single muscles with their tips pointing to muscles maximum force and the respective stiffness. While an activation in both flexor (black arrows) and extensor (red arrows) muscles will contribute to stiffness in a positive way, the flexor muscle activation will increase and extensor muscle activation decrease the applied force. If force and areflexive stiffness of a single muscle are linearly related [SA92, Zaj89] the reachable force–stiffness range of an antagonistic setup is defined by the vector-sum of the single force–stiffness relations of the single antagonistic muscles (see Fig. 2.11, similar to the quadrilateral region of two antagonist muscles defined in [KH90]). If human would be able to activate all muscles independently, they would be able to reach the entire area by cocontraction. However, it is well known, that due to neural and mechanical constraints they are by far not [MCLF95].
Exemplary, the aforementioned *isometric cocontraction* is depicted as a blue arrow (see Section 1.7), keeping the overall applied force constant while increasing joint stiffness. Moreover, a uniform cocontraction of antagonistic muscles is depicted (green arrow), leading to an increase in stiffness as well as a variation in the applied force.
Furthermore, Fig. 2.11 reveals another information: if muscle force and stiffness are linearly

scaled by the muscle activation as it is measurable with EMG, the two scaling factors (activation–force and activation–stiffness) can be depicted as an arrow in a force–stiffness plot pointing in the same direction as the muscle force–stiffness characteristic (see Fig. 2.11). This means that if the activation measured with EMG reflects the activation of all muscle fibers, which are simultaneously activated and if the muscular activity measured by EMG of multiple muscles in an antagonistic setup can be measured independently (no crosstalk), the EMG regressor of a multiple linear regression between stiffness/force and EMG can be depicted as such a multitude of arrows revealing the theoretically achievable force–stiffness range at the end-effector.

2.5.2 Measurement Setup

The measurement setup consists of a host computer running Linux, a real-time target computer running QNX, and a Windows computer. The real-time computer runs a Matlab/Simulink model to control the electromagnet, to read out the force sensor at 10 kHz and the EMG sensors. The surface EMG sensors *Delsys Trigno Wireless System* have an internal amplification of 1 kV/V and provide an analog signal at 4 kHz with a constant delay of 48 ms. Additionally, for capturing the kinematics an optical *Vicon Motion Capture System* consisting of 8 *MX3+* cameras and a *MX Ultranet* controller is used. This optical tracking system is controlled by the Windows computer. The cameras are arranged at a distance between 0.5 and 1 m around the forearm position (for all subjects the same). The cameras have an optimal resolution of 659 (horizontal) x 494 (vertical) pixels at 242 frames per second. In this study, a higher frequency of 400 Hz is used, which reduces the field of view. The marker positions are transferred from the Windows computer to the Linux host using the DLR communication protocol *arDNet* [BH08]. A triggered recording of the Vicon data is started 250 ms before each perturbation and lasts 1 s. The idea of the optical tracking system is to give the subject and the experimenter a feedback about variations in kinematics during the experiment in order to constrain it and correct when necessary, rather than using the measured optical tracking data to identify influences and their significance. It was decided to use optical tracking rather than different cuffs to constrain the kinematics since it offers more possibilities to control it in a subject specific posture and avoids occupying suitable EMG positions. Furthermore, there is no risk that the subjects apply wrist torque against the cuff, the influence of which on the EMG signal would not be possible to quantify.
After pressing a release button, the perturbation is applied a random interval between 0.5 and 2.5 s later. A force sensor KM10 (ME-Messsysteme GmbH) with a nominal sensitivity of 1 mV/V and a nominal range of 100 N was used. The accuracy of the analog signal provided by the measurement amplifier GSV-11H (ME-Messsysteme GmbH) is 0.1 N. Measured force signals are calibrated—no application of force—before each trial since the output of the force sensor is marginally influenced by the heating of the electromagnet.
For the experiments conducted within this Section the third version of the Grip Perturbator is used (see Fig. 2.4 of Section 2.1).

2.5.3 Prestudies

Within earlier prestudies, which were conducted without any tests for significance and thus not published, the influence of index finger stiffness on the measured grip stiffness was analyzed. The Grip Perturbator was fixed on a table, and the subject was asked to apply forces using index finger only while grasping a handle with the other four fingers. Comparably stiffnesses and force–stiffness relations as measured in a pinch grip with the same subject were found. Since the index finger was found to predominate the measured grip stiffness, it was concluded that the thumb had to be much stiffer than the index finger. Thus, within this Section it will be refrained from measuring EMG of corresponding muscles of the thumb (M. flexor pollicis longus, M. extensor pollicis brevis, M. extensor pollicis longus). Furthermore, it was tested to measure

the M. adductor pollicis. Due to strong sweating and large movement of the underlying skin for the pinch grip the electrodes took off very rapidly what makes it impossible to measure this muscle.

2.5.4 Experimental Procedure of the Main Study

A total of 10 healthy fully naive subjects, nine male and one female (S3), seven right and three left-handed (S5, S7, S9), age 22–27 years, perform the two experimental protocols, with and without isometric cocontraction (see Section 1.7), as described below. The whole procedure lasted between 90 and 120 minutes per participant. Subjects had neither history of neurological disorder nor neuromuscular injury affecting the CNS or the muscles. All subjects participated voluntarily and gave written consent to the procedures which were conducted in partial accordance with the principles of the Helsinki agreement (Non-conformity concerns the point B-16 of the 59th World Medical Association Declaration of Helsinki, Seoul, October 2008: no physician supervised the experiments). Approval was received from the works council of the German Aerospace Center, as well as its institutional board for data privacy ASDA; the collection and processing of experimental data was approved by both committees. The used recording equipment measuring muscular activity complies with the requirements put forth by the Medical Device Directive 93/42/EEC, and it is complied with its intended use.
For all subjects and experiments the right hand is used, be they right- or left-handed, which is restricted by the new design of the perturbator with its fans and optical markers. The EMG electrodes are attached in accordance with the recommendations of the SENIAM project [HFDKR00]. Before the experiment the subjects are asked to wash their arm with water; no soap is used. For an optimal EMG signal the respective part of the skin is again moistened with water. Keeping in mind a possible application in telerobotics, it will be sticked to non-invasive surface electrodes rather than invasive needle electrodes. As a result of earlier prestudies a total of six muscles is chosen to be relevant for the experimental procedure: two extrinsic index flexor muscles (FDP and FDS), two extrinsic index extensor muscles (EIP and ED), and two interossei muscles in the hand (MID1 and MID2; see Table 2.8).

Table 2.8: Investigated muscles and their function [SSS05] (reproduced from [HGDSvdS16]).

muscle	abbreviation	function
M. flexor digitorum superficialis	FDS	wrist flexion; flexion of the metacarpophalangeal and the proximal interphalangeal joints of index, middle, ring and little finger
M. flexor digitorum profundus	FDP	wrist flexion; flexion of the metacarpophalangeal, the proximal interphalangeal and the distal interphalangeal joints of index, middle, ring and little finger
M. extensor digitorum	ED	extension of the metacarpophalangeal, the proximal interphalangeal and the distal interphalangeal joints of index, middle, ring and little finger
M. extensor indicis proprius	EIP	extension of the metacarpophalangeal, proximal interphalangeal and distal interphalangeal joints of the index finger
Mm. interossei dorsales I/II	MID1/MID2	flexion of the metacarpophalangeal joints of the index and middle finger; extension and abduction of the proximal and the distal interphalangeal joints of the index and middle finger

The electrodes are placed close to the six corresponding muscles (see Fig. 2.12) by the subjects

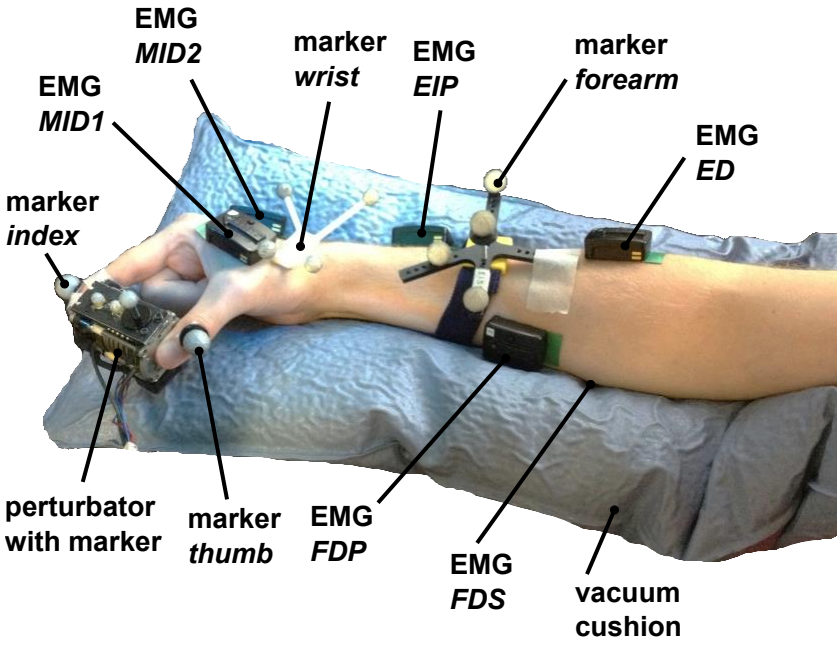

Figure 2.12: Measurement Setup (reproduced from [HGDSvdS16]). — The forearm is placed in a vacuum cushion to assist subjects holding their wrist and arm position stable. The position of index finger, thumb, perturbator, wrist and forearm and the orientation of perturbator, wrist and forearm are tracked with an optical tracking system. 6 EMG electrodes are placed to corresponding flexor and extensor muscles on the hand (MID1, MID2) and forearm (FDP, FDS, EIP, ED). The perturbator is held by the subject between index finger and thumb, while middle finger, ring finger and pinky had to be flexed. Two small fans on its back side reduce the heating caused by the electromagnet.

using palpation and visual feedback of the EMG signal. After positioning the EMG sensors, markers for tracking the position and orientation of wrist and forearm and single markers to track the position of the distal phalanx of index finger and thumb are positioned (see Fig. 2.12). The optical tracking system is calibrated using the orientation of the table. In order to assist the subjects holding their wrist and arm orientation stable during the measurements, a vacuum cushion is used which is adjusted to each subject. Subjects are sitting for all experimental conditions.

Additionally, subjects see a graphical representation of the measured data on a screen (see Fig. 2.13). Directly after each perturbation the measured stiffness and force is visually presented to the subject as a dot in a force–stiffness graph. This procedure allows commanding a combination of a certain force and stiffness. Furthermore, the following kinematic information is presented to the subjects: the planar positions of forearm, wrist, perturbator, thumb and index finger; the orientation of the longitudinal perturbator axis (roll axis) in reference to the table plane; the angular distances of wrist and forearm in reference to their initial orientations. The subjects are asked to keep the positions of perturbator, wrist and forearm within tolerance ranges, depicted as circles with a radius of 15 mm around the initial captured positions, for all experimental conditions. They are furthermore asked to keep the orientations of the wrist and forearm (displayed as angular distances in Fig. 2.13) close to the initially detected ones and the roll axis of the perturbator parallel to the table plane. Note that for a successful perturbation the force is controlled automatically to be kept within a certain force range; despite that, the positions are just visually inspected by the experimenter and not constrained in order to avoid fast fatigue of the subjects.

At first subjects are asked to lay their arm relaxed on the table in order to measure the EMG base noise for 5 s. Furthermore, the initial pose of wrist, forearm and perturbator and the position of index finger and thumb are measured in this relaxed pose. Secondly, subjects are asked to fulfil

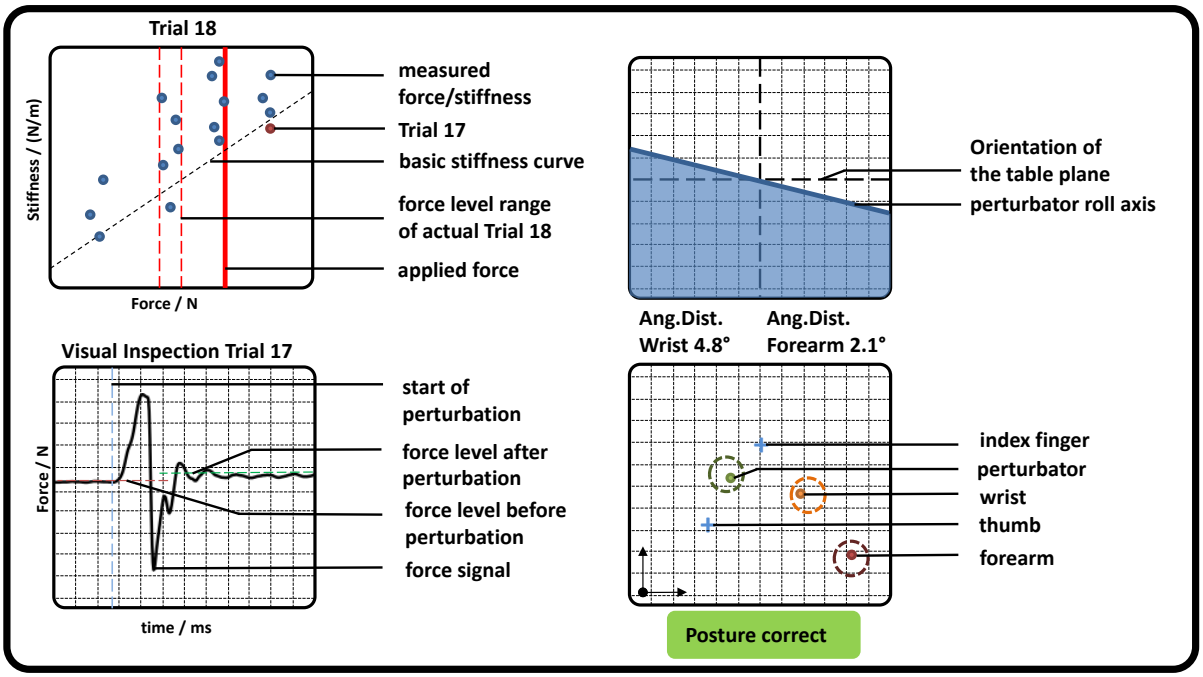

Figure 2.13: Graphical representation of measured pose and force data (representative; reproduced from [HGDSvdS16]). — *(Top left)* Applied force (red solid line) and actual force level (red dashed lines). All previous measured perturbations are depicted as blue dots showing the applied force and stiffness, while the very last is highlighted in red. The estimation of the basic stiffness curve achieved in *task 1* is depicted as a diagonal black dashed line. *(Bottom left)* The last perturbation is depicted for visual inspection for artifacts. Furthermore, the detected mean forces before and after perturbation as well as its beginning are shown. *(Top right)* The roll axis of the perturbator and its radial deflection in reference to the table plane (similar to an attitude indicator in an airplane). *(Bottom right)* The position of perturbator, index, thumb, wrist and forearm depicted as dots in a plane planar to the table. Additionally, a circle with an radius of 15 mm is plotted which indicates a tolerance around each initial measured position. If all dots are inside each circle a text "Posture correct" is shown in green; otherwise a comment "CAUTION!! Correct posture!" is shown in red.

MVC, i.e., to grip as strong as they are able to, three times for 5 s each, and the maximum grip force and corresponding EMG are measured. The MVC is used to set the prescribed force levels in the following two main tasks.

Task 1—Force Task without Voluntary Cocontraction

In *task 1*, subjects are asked to stably hold six different visually presented force levels (15, 25, 35, 45, 55 and 65 % of MVC) within a range of ±5 % of MVC without using any kind of voluntary cocontraction. The force levels are given to them in a randomized order four times each, leading to a total of 24 perturbations. This procedure is similar to the one of the previous sections 2.2 and 2.3, except that wrist and finger positions are measured and constrained, and EMG is measured. This force task is considered to deliver information about the subject's basic stiffness and its dependency on force.
A linear fit between force and stiffness is calculated from the measured perturbations and plotted as the basic stiffness curve in the force/stiffness graph (Fig. 2.13 top left).

Task 2—Force Task with Isometric Cocontraction

In *task 2*, subjects are asked to produce a certain force and decouple the stiffness from the force by using isometric cocontraction (for its definition see Section 1.7). Before the actual task, subjects have the possibility to learn how to voluntarily increase grip stiffness by cocontraction using 10 to 20 trials that are not recorded. After this learning procedure, subjects are asked to reach 5 different force levels (15, 25, 35, 45, and 55 % of MVC) within a range of ±5 % of MVC 15 times each and use cocontraction to produce higher stiffness at a similar force than in *task 1*, leading to 75 perturbations. After each set of 25 perturbations, the subjects are asked to pause for 5 minutes. During these breaks, again the EMG base noise is recorded for 5 s in order to detect strong deviations. After all perturbations, the subjects are asked to produce three times the MVC level for 5 s again. Note that this method does not allow commanding one cocontraction level twice.

2.5.5 Data processing

Determination of Force and Stiffness

The methods to define the two time windows T_1 before and T_2 after the perturbation were introduced in Section 2.1, and are performed offline. The force signals f are first filtered using a 21-point moving average filter. The beginning of the perturbation t_{pert} was defined as the end of the first period T_1, where T_1 was defined as the last 10 ms time interval before t_{peak} (the peak after the perturbation / maximum of the force signal) having a standard deviation below $5 \cdot 10^{-4}$ N. These numbers are empirically determined and lead to stable results. The force before the perturbation was calculated using T_1.
As explained within Section 2.1, T_2 was varied so as to optimize an objective function

$$Z = \frac{1}{n_{\text{sub}}} \sum_{i=1}^{n_{\text{sub}}} \left(\frac{1}{n_{\text{level}}} \sum_{j=1}^{n_{\text{level}}} \left(\tilde{e}(k_{\text{task1}_{ij}}) + \frac{1}{n_{\text{trial}}} \sum_{k=1}^{n_{\text{trial}}} \left(\tilde{e}_{T_2}(f_{\text{task1}_{ijk}}) + \tilde{e}_{T_2}(f_{\text{task2}_{ijk}}) \right) \right) \right) \tag{2.11}$$

using all trials n_{trial}, levels n_{level} and subjects n_{sub} [8]. The minima of this cost function minimizes the variation of resulting stiffness values k measured under *exactly* the same conditions (which is true for *task 1* only) and the oscillations in force within time interval T_2 of both tasks. Since

[8] Please note, that Eq. 2.11 is an adapted version of the optimization function Eq. 2.2 introduced within Section 2.1 for the experiments performed in this Section.

subjects cannot produce the exact same cocontraction level twice and thus the experimental conditions between perturbations in *task 2* cannot be trusted to be identical, the part of the objective function which accounts for variations in measured stiffness consider *task 1* only. The length of the second time interval T_2 and its end t_{trust} are found to be optimal under named constraints at 18.3 and 33.3 ms, respectively.

For investigating intra- and inter-subject variability force and stiffness are normalized subject-wise by their maximum values and divided by their standard deviations for the correlation and regression analysis. Since it is difficult to ask subjects to reach a cocontraction twice, repeatable experimental conditions exists for *task 1* only, but not for *task 2*.

Evaluation of Optical Tracking Data

Since the optical tracking data is influenced by artifact occasionally, the beginning of the perturbation within this data is detected manually for each trial. For determining finger and thumb displacement caused by the perturbation, the same time windows were applied as for estimating stiffness from force. Furthermore, as already said, the measurements of the single markers at the index finger and thumb are not stable and sometimes flip. Thus, a procedure was implemented which allocates these two markers with respect to their distance from the perturbator.
Additionally, these two marker positions sometimes switch for a few ms to unreasonably high values or to zero. These values were detected automatically (within two samples the position of the fingers cannot change more than 10 mm) and replaced by NaN values (not a number), which avoids that building the mean over the time windows T_1 and T_2 of kinematic data will be influenced by unreasonable large values. For all kinematic data, if the detected position or orientation inside the time windows T_1 and T_2 are exactly zero (see Fig. 2.1), this data point was discarded due to missing information. For evaluating the kinematics two main metrics were used, the standard deviation of the distance to describe the variation in position and, if available the standard deviation in angular distance to describe the variation in orientation. While the distance is calculated using the Euclidean norm, the angular distance between two rotation matrices R_1 and R_2 is calculated according to [SHSvdS14]:

$$\text{angdist} := \arccos\left(\frac{\text{trace}(\mathrm{R}_2 \cdot {\mathrm{R}_1}^{-1}) - 1}{2}\right). \tag{2.12}$$

Since the kinematic position is controlled to be kept stable and not commanded *per se*, it will be refrained from analyzing the influence of kinematics on stiffness and from drawing wrong conclusions. Thus, its still remaining influence will be part of the measured statistics.

Evaluation of the EMG Data

The oversampled EMG signal (analog card sampling inside the real-time target computer rate 10 kHz; sampling rate of the EMG signal provided by the Delsys Trigno Wireless EMG system 4 kHz) is filtered offline using a delay-free second-order Butterworth bandpass filter between 25 and 450 Hz. The produced muscular activity is evaluated using the average rectified value (ARV) over a time frame of 200 ms before the perturbation. From the relaxation task a steady time window of about 500 ms is chosen manually (identical for all electrodes within a task) in order to identify EMG base noise. In the relaxing task a mean base noise ARV of $5.8 \pm 1.7\,\mu$V over all subjects and electrodes is measured, which is consistent with literature [Kon05]. The base noise of each electrode is subtracted from the EMG data subject-wise. Again all EMG data are normalized by their maximum values and divided by their standard deviations for each electrode and each subject.

Evaluation of Intra- and Inter-Subject Variability

Intra- and *inter*-subject variability in force and stiffness will be analyzed with respect to its linear regression from EMG. All normalized EMG as well as force and stiffness data of each subject will be divided by their standard deviations, since they are expected to vary considerably between subjects. The regressed models are cross-validated; for intra-subject regression each value will be predicted subject wise by building a model regressed from all other (leave-one-trial-out), while for inter-subject regression all values of one subject will be predicted with a model regressed from all other subjects (leave-one-subject-out). Since a non-linear dependency between measured EMG and force is expected, it will be tested if taking the square root [Hog84] or square [SKK09] of all EMG data improve the quality of the linear fits in force and stiffness (note that the method of depicting the EMG regressor as explained in Subsection 2.5.1 also works for this non-linear dependency). The average cross-validated coefficient of determination R^2 will be used to judge goodness of all fits.

Methods for Testing Statistical Significance

For testing significance of a correlation a standard implemented function in MATLAB will be used which provides a p-value based on results of an F-test testing differences in variances. Similar to that, an F-test will be used when performing a test for differences in sample variances. For all other statistical tests which are performed in this Section the assumption of underlying normal distribution within each sample is first tested using a Shapiro-Wilk test for sample sizes $n \leq 50$ and a single-sample Kolmogorov-Smirnov test for sample sizes $n > 50$. If the assumption of normal distribution holds, a parametric paired t-test for dependent samples will be used (unknown variance of the population), and a two-sample t-test with pooled or unpooled variance estimate (equal or unequal variances of the two populations). Equality of variance is therefore tested in advance using a two-sample F-test. If normality can be rejected for one of the tested samples, it will be tried first to transform the tested distribution to normality according to its skewness [dV02, p. 78ff.]. Note, that for a two-sample test both samples are transformed with the same transformation. If normality can still be rejected, a non-parametric Kolmogorov-Smirnov two-sample Z-test will be used (see [dV02, p. 77ff.]) for independent test statistics and a non-parametric Wilcoxon signed rank test for dependent test statistics. For all statistical tests performed within this Section a statistical significance level of $\alpha = 0.05$ is applied. For each p-value the performed test statistics is denoted (parametric/non-parametric).

2.5.6 Results

The results of measurements are depicted as force–stiffness plots in Fig. 2.14. The result of *task 1*—force task without cocontraction—is depicted as crosses and ellipses in black denoting the mean values and their standard error of mean in force and stiffness, while results of *task 2*—force task with cocontraction—is depicted as red dots denoting the single perturbations.
For *task 1*, a linear regression between force and stiffness over all values and a corresponding coefficient of determination R^2_{Task1} as a measure of linearity is shown. Since experimental conditions within *task 1* are repeatable a linear fit using all data points captures its underlying variabilities (see Section 2.4), while not for *task 2*. Thus, a linear fit for the maximum stiffness values at each force level is shown for *task 2*. Furthermore, the intra-subject EMG regressors to regress force and stiffness are depicted as arrows in the upper left corner for each subject as well as the inter-subject regressor for all subjects. The used representation of the EMG regressor is explained in Subsection 2.5.1. Additionally, Figs. 2.15 and 2.16 depict the normalized force and stiffness in their representation to normalized $\sqrt{\text{EMG}}$, respectively, for each of the six electrodes.

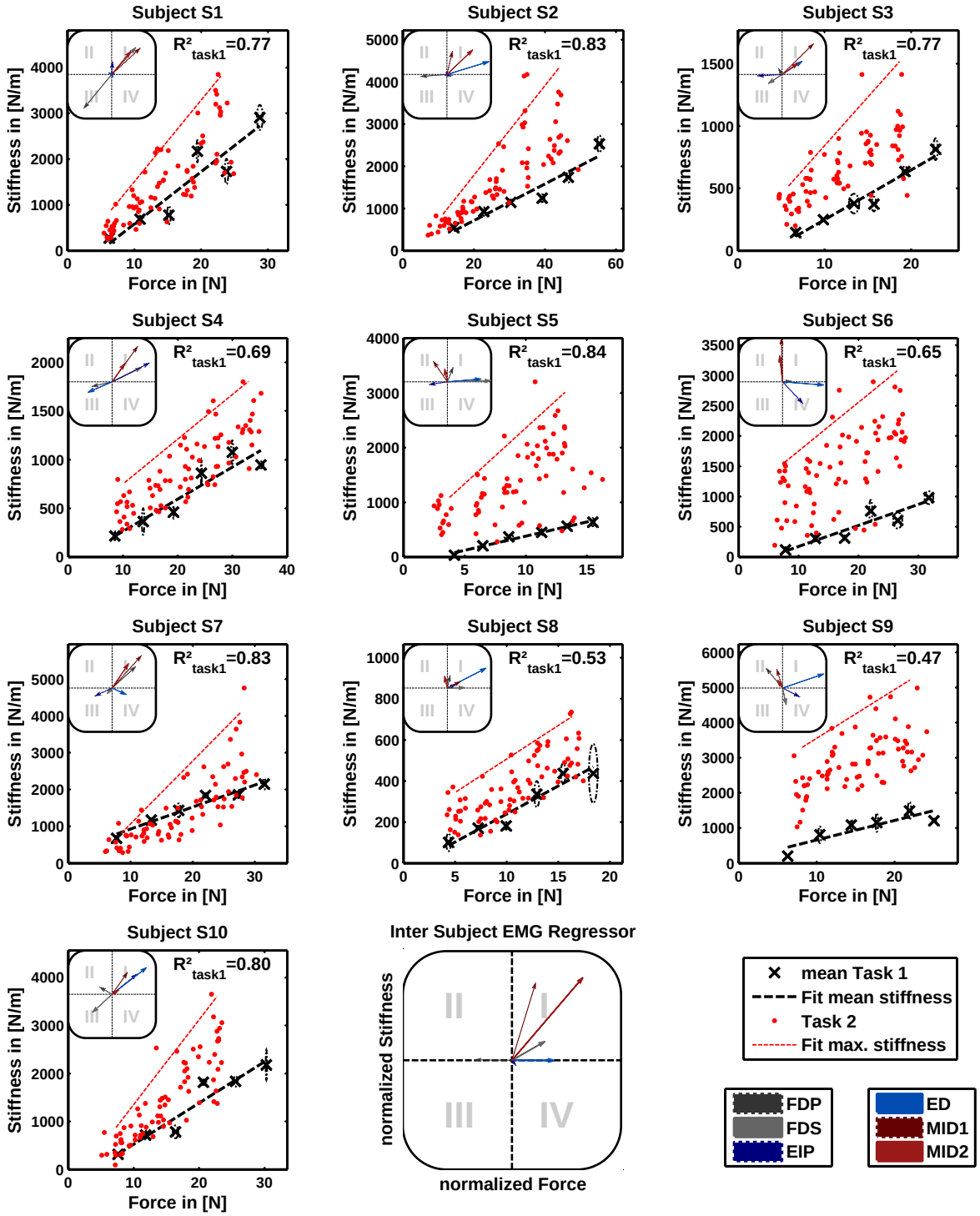

Figure 2.14: Measured grip stiffness and its dependency on grip force and their Regressors to $\sqrt{\text{EMG}}$ (reproduced from [HGDSvdS16]). — For *task 1*—force task without cocontraction—depicted as crosses and ellipses in black denoting the mean values and their standard error of mean in force and stiffness, while results of *task 2*—force task with cocontraction—are depicted as red dots denoting the single perturbations. For *task 1*, a linear regression between force and stiffness and for *task 2* a linear regression between maximum stiffness for each level of force and force is shown. Furthermore, the two regression coefficients for each of the six EMG electrodes to force and stiffness are depicted as arrows for each subject and for all (the length of quadrant are normalized by the maximum values of force and stiffness).

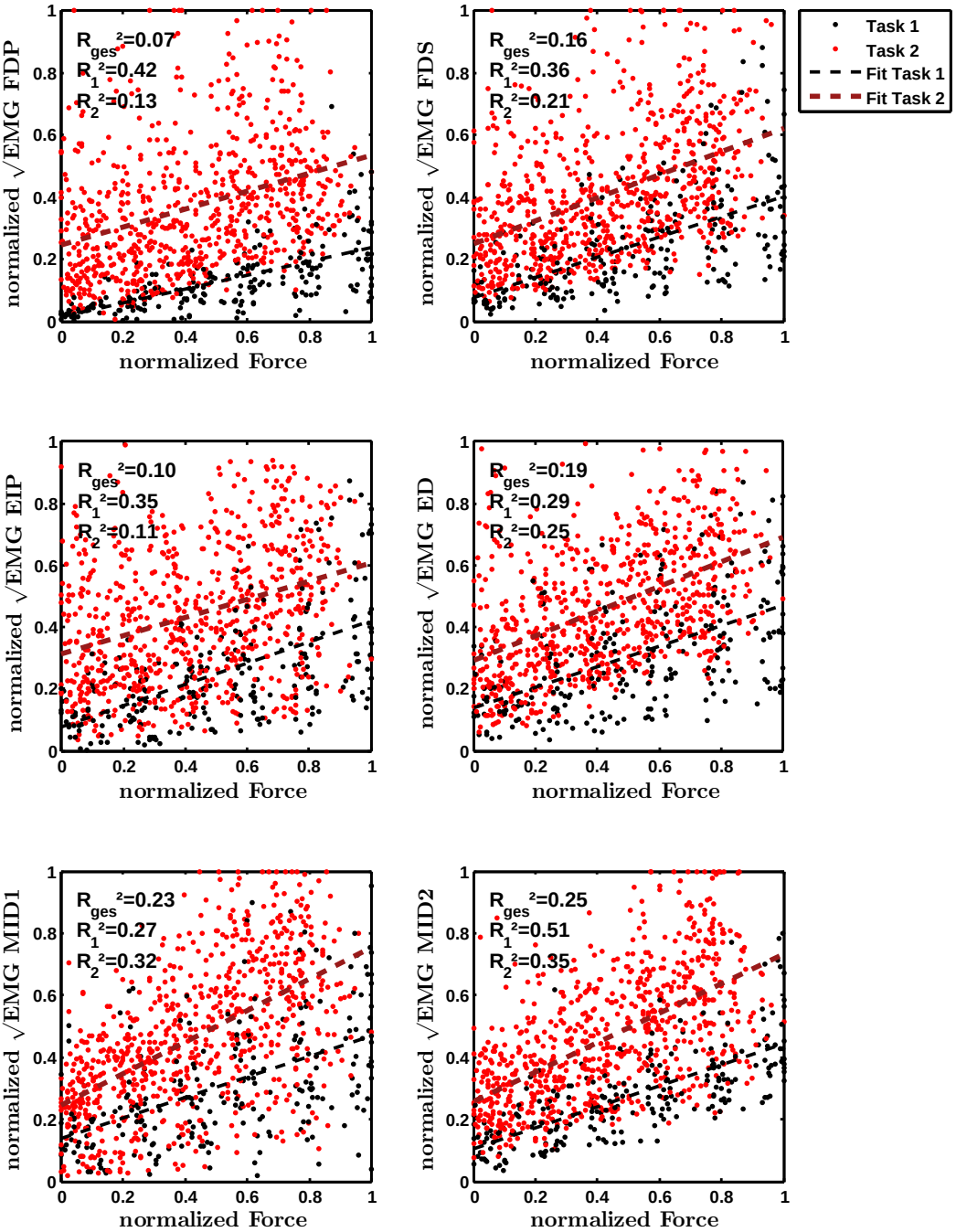

Figure 2.15: Normalized force depending on normalized √EMG of all 10 subjects for the 6 different EMG electrodes (reproduced from [HGDSvdS16]). — The black dots denote the results of *task 1*, the red the results of *task 2*. Additionally, a linear regression is depicted for both. The coefficient of determination is given for a linear fit of each single task and both together.

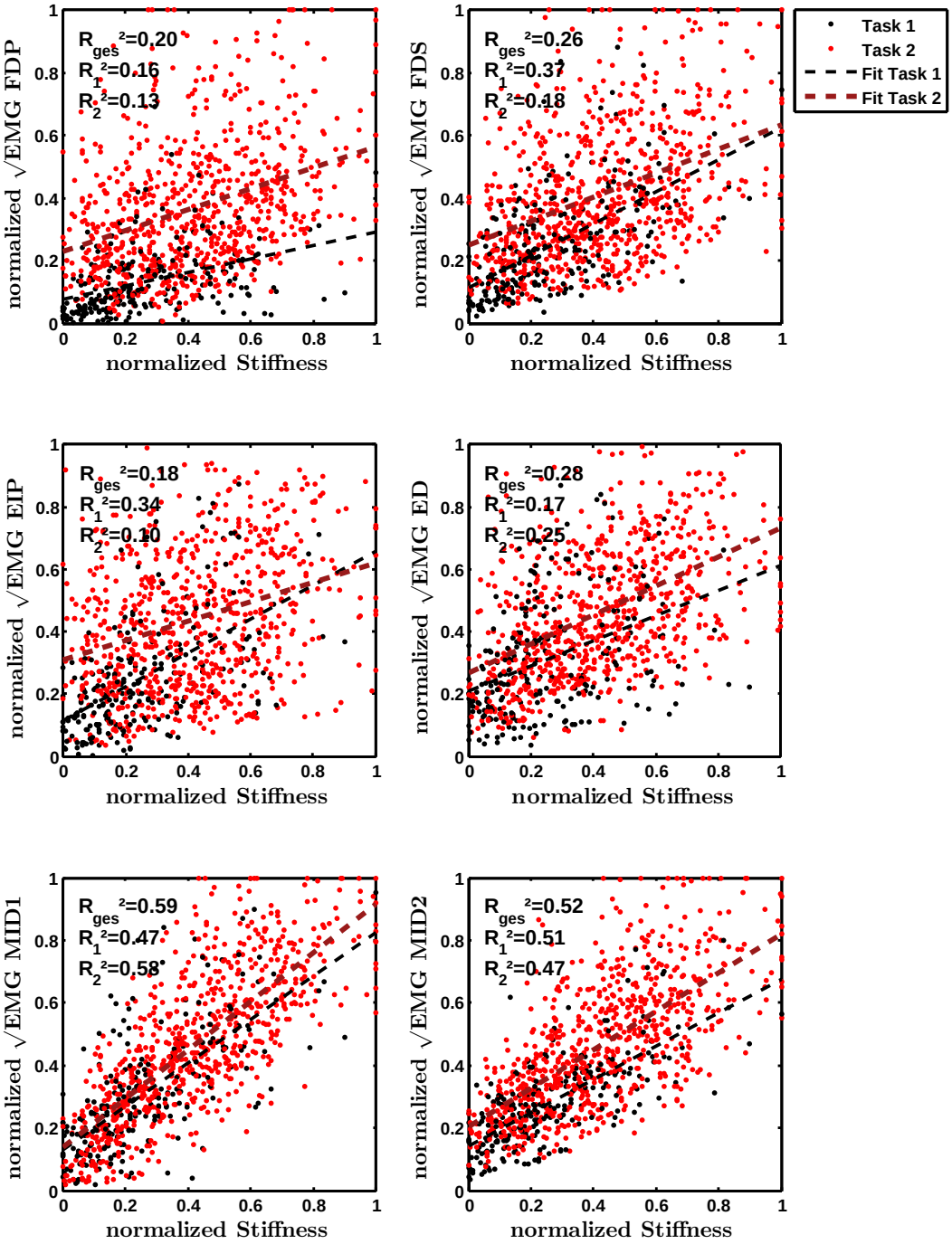

Figure 2.16: Normalized stiffness depending on normalized √EMG of all 10 subjects for the 6 different EMG electrodes (reproduced from [HGDSvdS16]). — The black dots denote the results of *task 1*, the red the results of *task 2*. Additionally, a linear regression is depicted for both. The coefficient of determination is given for a linear fit of each single task and both together.

Table 2.9: Mean difference in normalized stiffness of the two tasks for the single force levels (reproduced from [HGDSvdS16]).

	NF1	**NF2**	**NF3**	**NF4**	**NF5**
$\langle \mathbf{k^*_{task1_i}} \rangle$	8.7 %	18 %	22 %	35 %	40 %
$\langle \mathbf{k^*_{task2_i}} \rangle$	23 %	32 %	42 %	56 %	66 %
$\langle \mathbf{k^*_{task2_i}} - \mathbf{k^*_{task1_i}} \rangle$	15 %	14 %	21 %	21 %	26 %
$\langle \mathbf{k^*_{task2_i}} \,/\, \mathbf{k^*_{task1_i}} \rangle$	5.3	2.2	2.2	1.9	1.9
$\sigma^2(\langle \mathbf{k^*_{task1_i}} \rangle)$	±5.7 %	±7.7 %	±8.7 %	±16 %	±15 %
$\sigma^2(\langle \mathbf{k^*_{task2_i}} \rangle)$	±12 %	±14 %	±16 %	±17 %	±16 %
p (one-tailed)	0 %[1]	1.4E-12 %[1]	0 %[1]	1.2E-9 %[1]	0 %[1]
t -value	−10.7	−8.7	−11	−7.1	−9.5
degrees-of-freedom	139	111	117	188	187

[1] For probability values less than 5 % it can be rejected that the stiffness in *task 1* is higher.

Mean difference in normalized stiffness$\langle k^*_{task2_i} - k^*_{task1_i} \rangle$ and their ratio $\langle k^*_{task2_i} \,/\, k^*_{task1_i} \rangle$ for all force levels NF over all subjects. If $p \leq 0.05$ it can be accepted, that the stiffness in *task 2* is higher (one-tailed two-sampled t-Test with pooled or unpooled variance estimate; t-values and degrees-of-freedom of the test statistics are listed). Note that the index i denotes the mean over subjects.

No significant correlation between trial number to both, force and stiffness was found for the experimental condition of *task 1*. There was a significant positive correlation for subject S6 between trial number and stiffness and a significant negative correlation for subject S5 between trial number and force for the experimental condition of *task 2* (representing effects of learning and fatigue).

Ability of Cocontraction

The central question of this Chapter is how much subjects are able to increase grip stiffness at a certain force using cocontraction. In Table 2.9 different measures for this ability are given at different force levels over the pooled trials of all subjects.
The stiffness values are normalized per subject by their maximum value. The baseline stiffness at each force level is given in the first row as the mean of stiffness in *task 1*, $\langle k^*_{task1_i} \rangle$, in which subjects are asked to produce simply force without cocontraction. In the second row, the mean stiffness of *task 2*, $\langle k^*_{task2_i} \rangle$, is given, in which the subjects try to increase stiffness by cocontraction. Thus, the difference $\langle k^*_{task2_i} - k^*_{task1_i} \rangle$ in the third row describes the average voluntary-increase in stiffness using cocontraction, while the fourth row show their ratio $\langle k^*_{task2_i} \,/\, k^*_{task1_i} \rangle$. Furthermore, the standard deviations $\sigma^2(\langle k^*_{task1_i} \rangle)$, $\sigma^2(\langle k^*_{task2_i} \rangle)$ of the mean stiffness are given, as well as the p-values for testing with the null hypothesis that the stiffness in *task 1* is larger than in *task 2* (*independent two-sample one-tailed parametric test statistics*). The table shows that the mean in stiffness of *task 2* is always significantly higher than the measured stiffness of *task 1* ($p < 0.001$). Subjects are able to significantly increase stiffness by 20% on average over all force levels using cocontraction, with an increasing ability for the higher levels. The higher the force the higher the difference in stiffness $\langle k^*_{task2_i} - k^*_{task1_i} \rangle$ between the two tasks.

Kinematics

Beside the variation in kinematic orientation and position during the experiments, it is of interest how the total perturbation length of 7.5 mm is distributed between thumb and index finger, because this gives an indication of the relative stiffnesses of the two digits.

Table 2.10: Perturbation-Displacement of index finger and thumb (reproduced from [HGDSvdS16]).

Subjects	**S1**	**S2**	**S3**	**S4**	**S5**	**S6**	**S7**	**S8**	**S9**	**S10**	$\overline{(\cdot)}$
Index [%]	67	63	65	85	67	56	82	63	77	71	**69**
σ [%]	±7.7	±8.5	±22	±13	±7.4	±10	±8.7	±14	±13	±13	±**15**
Thumb [%]	31	33	35	28	24	38	23	29	31	28	**30**
σ [%]	±4.3	±8.9	±5.8	±8.0	±4.0	±8.3	±6.3	±11	±15	±7.3	±**9.7**
Total [%]	98	96	100	112	91	94	104	93	108	98	**100**
σ [%]	±9.9	±4.9	±21	±10	±5.3	±13	±10	±6.6	±23	±12	±**15**

Mean displacement $\overline{x_{T_{1|2}}}$ before and after perturbation and its standard deviation σ for intra-subject displacement of index finger and thumb and their inter-subject correspondents in [%]. The displacements are divided by the total perturbator displacement of 7.5 mm. 2.5 % of the data set was deleted.

Table 2.11: Standard deviation in distance between all tracked markers (reproduced from [HGDSvdS16]).

σ [mm]	**Thumb**	**Index**	**Pert.**	**Wrist**	**Forearm**	**World**
Thumb	—	±0.72	±0.72	±1.7	±3.8	±3.9
Index	±0.72	—	±1.2	±1.4	±2.9	±2.8
Pert.	±0.72	±1.2	—	±2.3	±3.4	±3.4
Wrist	±1.7	±1.4	±2.3	—	±2.3	±2.7
Forearm	±3.8	±2.9	±3.4	±2.3	—	±2.2
World	±3.9	±2.8	±3.4	±2.7	±2.2	—

Standard deviations in distance over all subjects for the single tracked markers index finger, thumb, perturbator, wrist and forearm inside T_1 in [mm] in reference to each other and to the world coordinate system. 0.7 % of the data set was deleted.

Table 2.10 provides the results of the finger and thumb perturbation displacements for all subjects with respect to the wrist frame, their average values and standard deviations in [%]; all displacements are divided by the total perturbator displacement of 7.5 mm (2.5 % of the data is zero and thus deleted; see Subsection 2.5.5). The displacement of the index finger is found to be slightly decreasing (*test statistics for correlation* r= −0.17; p ≤ 0.001) and the displacement of the thumb slightly increasing (*test statistics for correlation* r= 0.20; p ≤ 0.001) with force over all subjects, while there is no significant correlation to stiffness. Furthermore, there is a slight increase of index finger and thumb displacement (*test statistics for correlation* r= 0.16 and r= 0.077; p ≤ 0.025) with the number of perturbations (duration of the experiment). Note that the thumb and index finger position before and after perturbation are related to the wrist frame rather than to the world coordinate frame in order to get rid of forearm movements interpreted as grip displacements; anyway, both lead to similar results (world coordinate frame related data not listed here).

Additionally, Table 2.11 lists the variation in distance of all markers over all subjects in reference to the world coordinate frame and in reference to each other (0.7 % of the optical tracking data is zero and thus deleted). Table 2.12 does the same for the orientation of perturbator, wrist and forearm (0.6 % of the optical tracking data is zero and thus deleted). The marker position and orientation of the forearm of subject S8 was controlled during the experiment but not recorded for some unknown reason. The standard deviation of the horizontal orientation of the perturbator is found to be ±2.95° (see Fig. 2.13).

Table 2.12: Standard deviations in angular distance between all tracked markers (reproduced from [HGDSvdS16]).

σ [°]	Pert.	Wrist	Forearm	World
Pert.	—	±3.5	±3.0	±3.3
Wrist	±3.5	—	±3.2	±3.2
Forearm	±3.0	±3.3	—	±1.4
World	±3.3	±3.2	±1.4	—

Standard deviation in angular distance over all subjects for the single tracked markers perturbator, wrist and forearm inside T_1 in [°] in reference to each other and to the world coordinate system. 0.6 % of the data set was deleted.

Models for Regressing Force and Stiffness from EMG

It is tested whether taking the square root or square of EMG data improves the quality of the linear fits in force and stiffness (see Fig. 2.17).
The tests show that it can be rejected for all groups of muscles and for variabilities in both force and stiffness that taking the square of the muscular activation provides a significantly higher correlation than the linear case or taking the square root (testing mean of correlation coefficients; *dependent one-tailed parametric test statistics* $p < 0.005$); and it can be rejected for all groups of muscles and for both force and stiffness that the linear case provides a significantly better correlation than taking the square root of the muscular activation (*dependent one-tailed parametric test statistics* $p < 0.05$). Thus, the following analysis focusing on regression of stiffness and force from EMG uses its square root only.

Correlation of Force and Stiffness to $\sqrt{\text{EMG}}$

In Fig. 2.18 the mean and standard deviation of the correlation coefficients between force and stiffness to $\sqrt{\text{EMG}}$ over all subjects are depicted for the muscle groups flexor (FDP and FDS), extensor (EIP and ED), and interossei (MID1 and MID2) in each experimental condition.
It also includes results of statistical testing depicted as significance brackets. All measured muscular activations had a positive correlation to stiffness and force (*one-sample one-tailed parametric test statistics* $p < 0.005$). The correlation between force and $\sqrt{\text{EMG}}$ drops significantly for all 3 muscle groups from *task 1* to *task 2* (*dependent one-tailed, 1 non-parametric/ 2 parametric, test statistics* $p < 0.001$). On the other side, the correlation between stiffness and $\sqrt{\text{EMG}}$ drops significantly for the extrinsic muscles from *task 1* to *task 2* (*dependent one-tailed parametric test statistics* $p < 0.01$), while this difference is not found to be significant for the intrinsic muscles in the hand (*dependent one-tailed parametric test statistics*).
Furthermore, even if there seems to be a considerable difference in the correlation coefficients of force to $\sqrt{\text{EMG}}$ of extrinsic (flexor and extensor) and intrinsic (interossei) muscles in *task 2*, this difference is not found to be significant for any of the experimental conditions, which means similar correlations between force and $\sqrt{\text{EMG}}$ are found for all muscle groups. On the other side, the correlation between Mm. interosseus and Mm. flexor as well as extensor activation to stiffness was found to significantly differ for *task 2* (*dependent two-tailed parametric test statistics* $p < 0.01$), while not for *task 1*. Furthermore, the difference in the correlation of $\sqrt{\text{EMG}}$ to force and stiffness between flexor and extensor muscles is not significant for any experimental condition (*dependent two-tailed, 2 non-parametric/ 2 parametric, test statistics*). The difference in the variances (see error bars in Fig. 2.18) is found to be significant between intrinsic and extrinsic muscle groups for all experimental conditions (*F-test* $p < 0.05$), but not between flexor and extensor in all experimental conditions for both force and stiffness. Furthermore, the difference in the correlation of $\sqrt{\text{EMG}}$ to stiffness is found to be significantly higher than to force for the

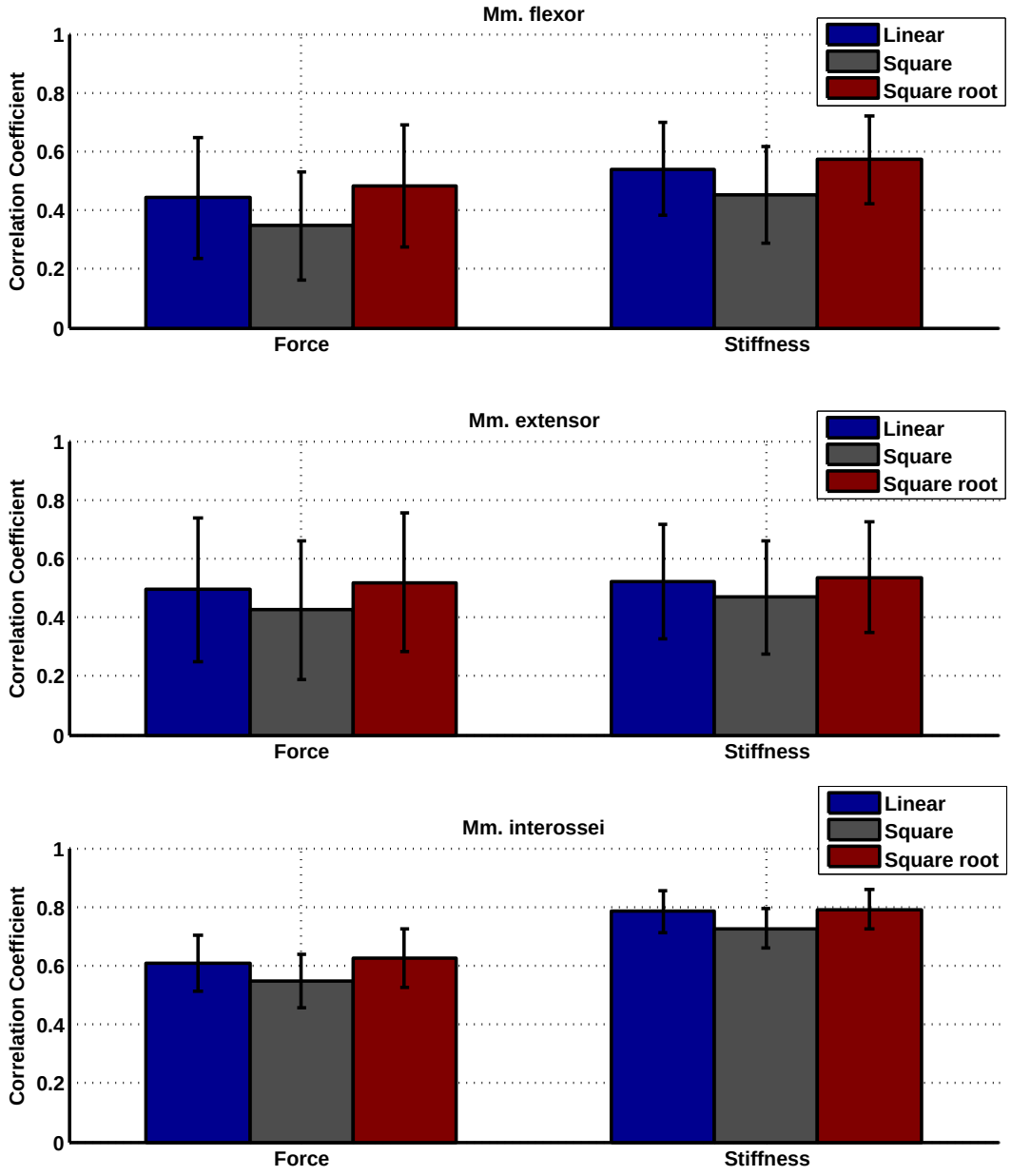

Figure 2.17: Models for regressing force and stiffness from EMG (reproduced from [HGDSvdS16]). — It can be rejected for all groups of muscles, that using the square provides a significantly better fit. Moreover, it can be rejected, that the linear case provides a significantly better fit in comparison to taking the square root.

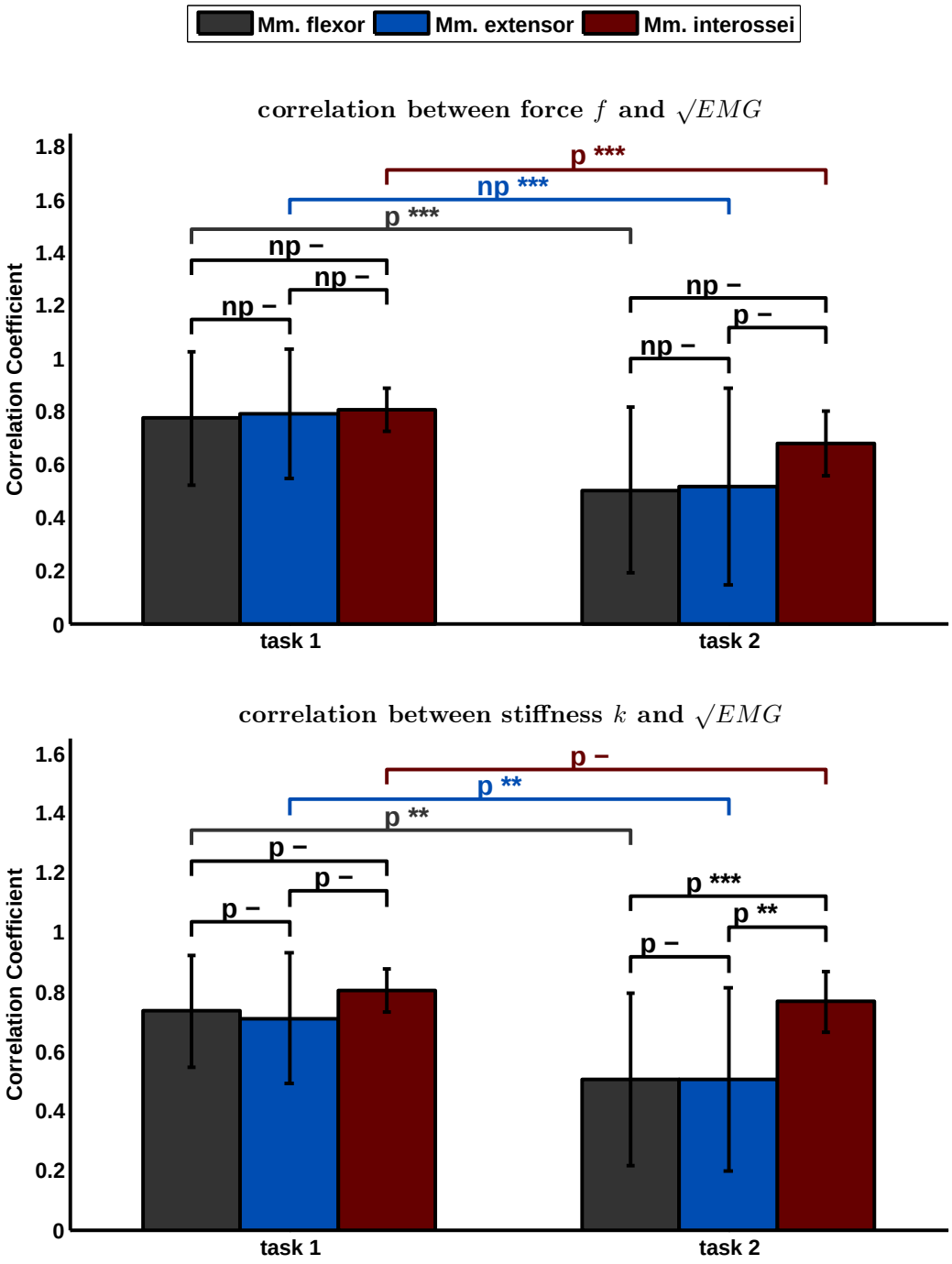

Figure 2.18: Mean correlation coefficients of muscle activation $\sqrt{}$EMG to stiffness and force and their standard deviation for the three muscle groups in the two tasks (reproduced from [HGDSvdS16]). — The diagram on the top denotes results of correlation between force and $\sqrt{}$EMG, the one below between stiffness and $\sqrt{}$EMG for both tasks. The standard deviations over ten subjects and two electrodes are depicted as error bars. The brackets show the performed statistical testing and their results (p:parametric; np:non-parametric; *:$p < 0.05$; **:$p < 0.01$;***:$p < 0.001$; -:no significance).

flexor muscles in *task 1* and the interossei in *task 2* (*dependent two-tailed 3 parametric / 3 non parametric test statistics* $p < 0.01$).

Intra- and Inter-Subject Regression

An important result of this Chapter is how well force and stiffness can be determined from the $\sqrt{}$EMG measurements. Furthermore, it is tested how the results change if only the signals of specific muscle groups are used. These are the extrinsic flexors, extrinsic extensors, and intrinsic interossei, with two electrodes in each group. The results of a linear regression on intra- and inter-subject variability of stiffness and force from the square root of $\sqrt{}$EMG (and force) are plotted in Fig. 2.20. As a measure of each model fitness the cross-validated coefficient of determination R^2 is used. For the intra-subject R^2 values as many models as perturbations per subject (leave-one-trial-out) and for the inter-subject R^2 values as many models as subjects (leave-one-subject-out) are used.
Furthermore, Fig. 2.19 depicts the results of the intra-subject regression of stiffness $k(f, \sqrt{}\text{EMG})$ and force $f(\sqrt{}\text{EMG})$ in comparison to their measured values for the two tasks. Significance brackets show the results of performed statistical tests and their significance.

Regressing Stiffness from $\sqrt{}$EMG

See Fig. 2.20, top plot. The results show that stiffness can be significantly better regressed using $\sqrt{}$EMG of the interossei in comparison to using $\sqrt{}$EMG of any of the extrinsic muscle groups in the forearm for both intra- as well as inter-subject regression (*dependent two-tailed parametric test statistics* $p < 0.005$).
While regressing stiffness from all six muscles works significantly better than just using the interossei for intra-subject regression (*dependent two-tailed parametric test statistics* $p < 0.01$), this difference is not found to be significant for inter-subject regression. Intra-subject regression works significantly better than inter-subject regression when using all muscles (*dependent two-tailed parametric test statistics* $p < 0.025$).

Regressing Stiffness from Force and $\sqrt{}$EMG

See Fig. 2.20, center plot. Using force and $\sqrt{}$EMG of the single muscle groups to regress stiffness works significantly better than just using force for intra-subject regression (*dependent two-tailed parametric test statistics* $p < 0.025$). Regressing stiffness from $\sqrt{}$EMG of the interossei and force works significantly better than using $\sqrt{}$EMG of the extrinsic muscles and force for intra- as well as inter-subject regression (*dependent two-tailed parametric test statistics* $p < 0.025$). While it works significantly better to use the $\sqrt{}$EMG of all muscles and force in comparison using just the $\sqrt{}$EMG of the interossei and force for intra-subject regression (*dependent two-tailed parametric test statistics* $p < 0.05$), the difference is not found to be significant for inter-subject regression. Again, intra-subject regression works significantly better than inter-subject regression using the $\sqrt{}$EMG of all muscles and force (*dependent two-tailed parametric test statistics* $p < 0.025$). Regressing stiffness using force and $\sqrt{}$EMG in comparison to just $\sqrt{}$EMG significantly improves the intra-subject regression (*dependent two-tailed parametric test statistics* $p < 0.025$), while not the inter-subject regression for all three muscle groups. In contrast, there is no significant difference using $\sqrt{}$EMG of all electrodes and force in comparison to just $\sqrt{}$EMG for both, intra- as well as inter-subject regression.

Regressing Force from $\sqrt{}$EMG

See Fig. 2.20, bottom plot. There is no significant difference in the regression of force from $\sqrt{}$EMG using the different muscle groups for intra- as well as inter-subject regression. Using all

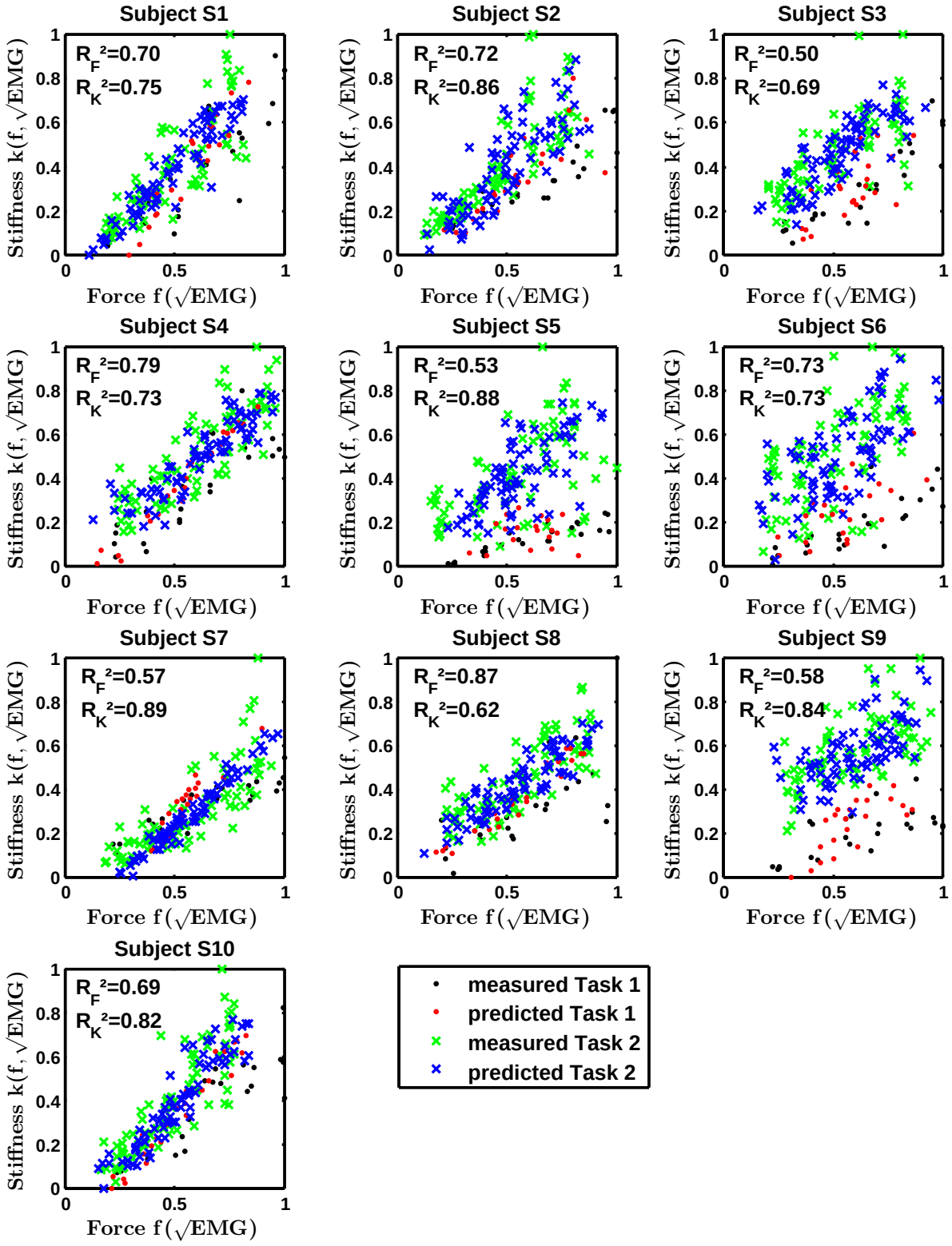

Figure 2.19: Independence of predicted data of intra-subject regression (reproduced from [HGDSvdS16]). — Results of multiple linear regression of stiffness $k(f, \sqrt{\text{EMG}})$ and force $f(\sqrt{\text{EMG}})$ and their coefficients of determination R^2 in comparison to the measured values for both tasks. If the predicted values are located more or less on a line, the two regression models are most likely not linear independent and the content of information of the respective EMG signals reduces to one.

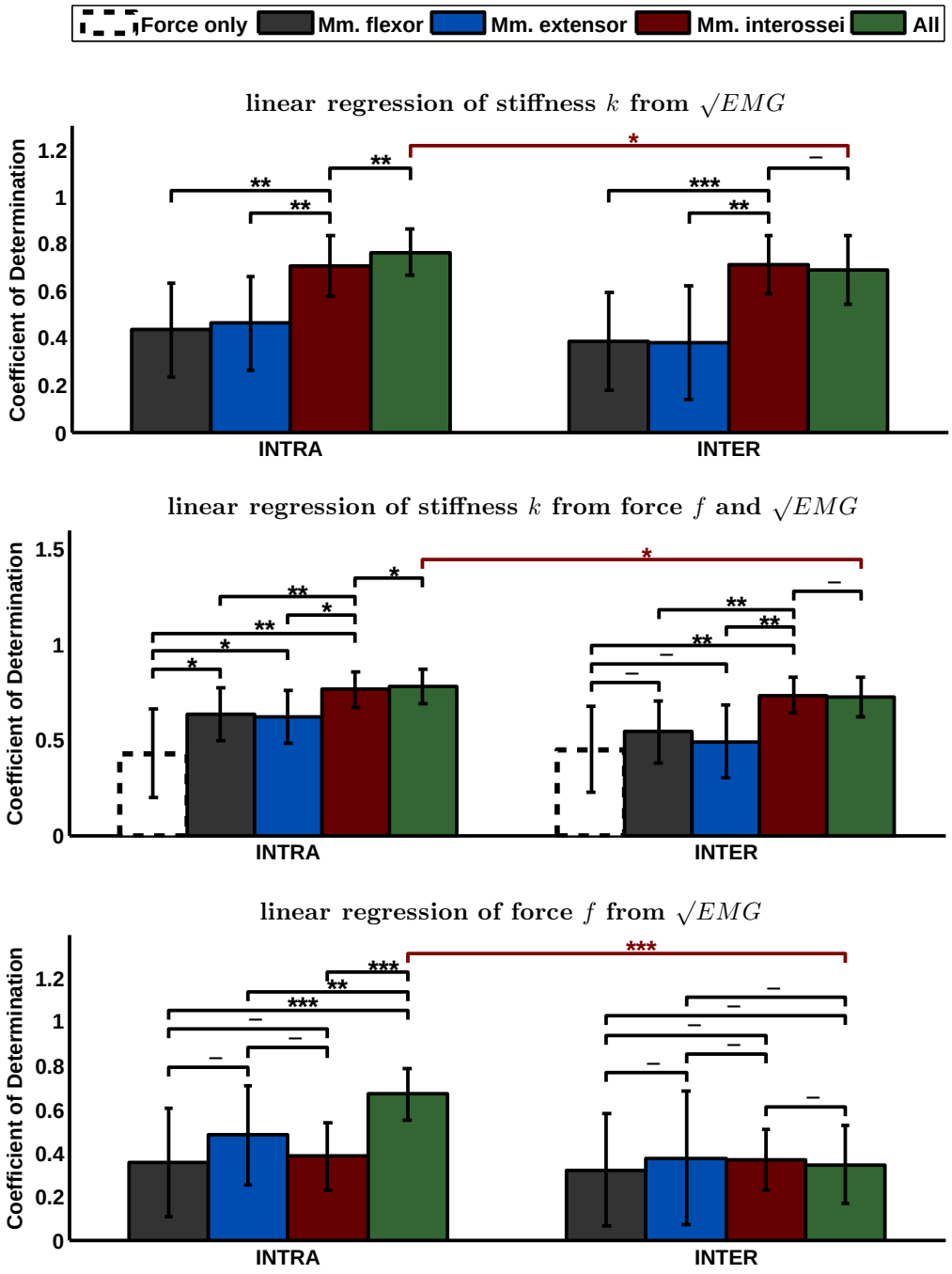

Figure 2.20: Mean of intra- and inter-subject coefficients of determination R^2 for different linear models between stiffness, force and $\sqrt{}$EMG and results of performed statistical testing (reproduced from [HGDSvdS16]). — Mean leave-one-out cross-validated coefficient of determination R^2 for intra- (left; leave one trial out) and inter-subject (right; leave one subject out) stiffness and force over all subjects for regressing stiffness from $\sqrt{}$EMG or force, from $\sqrt{}$EMG and force and for regressing force from $\sqrt{}$EMG using different muscle groups. The standard deviations over ten subjects are depicted as error bars. The brackets show the performed statistical testing and their results (dependent two-tailed parametric test statistics— *:p $<$ 0.05; **:p $<$ 0.01;***:p $<$ 0.001; -:no significance).

six muscles works significantly better for intra-subject regression (*dependent two-tailed parametric test statistics* $p < 0.01$), while there is no significant difference for inter-subject regression in comparison to just using the $\sqrt{\text{EMG}}$ of a single muscle group. Intra-subject regression works significantly better than inter-subject regression using all six muscles (*dependent two-tailed parametric test statistics* $p < 0.001$).
Fig. 2.19 shows plots of measured and predicted stiffness and force data using intra-subject regression for both tasks. These plots—often called independency plots—show how force and stiffness can be extracted from the EMG signals. If the predicted force–stiffness points cover the same area as the measured force–stiffness points, their independence is completely retained after the prediction from EMG. If the predicted points lie on a line, their independence is completely lost and the information content of the EMG signal is reduced to one.

2.5.7 Discussion

In this Section, raw data based on measurements performed by Große-Dunker in his Master Thesis [GD13] was analyzed. In order to measure influences from cocontraction only, effects of variabilities in kinematics were minimized by providing subjects a visual feedback of the current hand and arm posture. In a first task subjects were asked to apply a set of force levels several times without the use of cocontraction in order to achieve a basic force–stiffness relation. In a second task, subjects were then asked to decouple force and stiffness with the aid of cocontraction when holding a specific force level. Finally, the measured EMG was analyzed to investigate effects of intra- as well as inter-subject variability and to analyze the role of respective muscle groups.

Ability of Cocontraction

The results show that subjects are able to vary normalized grip stiffness at a certain force level between 15 and 26 % of maximum stiffness (see Table 2.9). Milner and Franklin reported in [BFM13] based on results of [MCLF95] a 5-fold range in modulation of wrist stiffness at zero net joint torque, what corresponds to the first force level the measurements (see $\langle k^*_{task2_i} \rangle / \langle k^*_{task1_i} \rangle$ in Table 2.9). Subjects are able to vary stiffness $\langle k^*_{task2_i} \rangle / \langle k^*_{task1_i} \rangle$ with cocontraction on average by a 2.7 ± 2.2-fold range over all subjects and force levels (maximum at 1st force level of subject S5 with an 22-fold and minimum at 2nd force level of subject S7 with an 0.8-fold modulation in stiffness). Furthermore, the data show a significant increase of stiffness variability $\langle k^*_{task2_i} - k^*_{task1_i} \rangle$ with force (*test statistics for correlation* $r = 0.30$, $p < 0.05$).
The plots in Fig. 2.14 provide an overview to what extent subjects were able to decouple grip force and stiffness using cocontraction, while probably revealing only parts of it: Firstly, subjects in this study had problems to stably hold the lower force levels at high cocontraction, where effects of motor noise on hand shaking are considerably higher (this confirms the supposition that cocontraction is the wrong strategy to stably hold a force level). Similarly, Kearney and Hunter reported in a study [KH90] performed at the human ankle that subjects had difficulties achieving cocontractions involving high levels of muscle activations at zero net torque. Thus, subjects probably do not use their full ability to decouple force and stiffness for the lower force levels, while doing so for the higher ones. Maybe the strategy used in the experiments of restricting subjects to exactly hold a certain force level is not the optimal solution for the lower levels. A better strategy might be monitoring the steadiness of force as a perturbation criterion, while the experimenter supervises the force range in order to help subjects reaching the higher cocontraction levels for the lower forces. Nevertheless there is evidence suggesting that neural mechanisms of muscle inhibition and excitation exist which limit the ability to produce all possible sets of cocontractions, probably to avoid harming the muscular system [DLM87]. On the other site, Milner *et al.* reported in [MCLF95] that subjects could not voluntarily apply maximal

cocontraction (MVC), but could possibly increase it by days of training similar to [DMG+04]. Furthermore, *task 2* is performed up to forces of 55 % MVC, only. As reported within Section 2.2, this constraint avoids fast fatigue of corresponding muscles for subjects during this long-lasting experimental procedure, but does not allow draw conclusions about forces up to 100 % MVC.
In order to have similar cocontraction ranges at all force levels, in a former version of the experiments a combination of applied force and EMG was commanded similar to the work done in [SKK09, OG99, OFK+02]. The different EMG signals were merged into one lumped signal and subjects were asked to hold different combinations of force and summarized EMG; so instead of commanding a stiffness an EMG level was commanded, which should be related to cocontraction in some way. Due to the high density of muscles in the forearm lying in different layers and thus high crosstalk of multiple muscles, subjects learned to produce the EMG levels and simultaneously learned to reduce the metabolic costs for producing it. This results in subjects successfully solving the task without producing an increase in the measured grip stiffness. This finally led to the decision for a redesign of the experiments and to command grip stiffness *per se* rather than a combined EMG level.
Anyway, similar to the presented results, Akazawa *et al.* found in [AMS83] that the reflex responsiveness and stretch-evoked stiffness increase linearly with cocontraction as defined in their paper. Also, the slope of this increase is steeper the larger the tonic force is, corresponding to the presented result of an increasing stiffness modulation capability with higher force. However, please note that the authors of the study [AMS83] only compared the cocontraction levels of two tonic force levels achieved in the constant-load position control task and measured reflex-affected stiffness.

Finger Displacement

The measured kinematics show that over all measurements the index finger gets perturbed by about 2/3 and the thumb by about 1/3 of the whole displacement (see Table 2.10). This means that *the thumb is approximately twice as stiff as the index finger*. Assuming that the measured intrinsic stiffness and the force as well correspond to the number of attached cross-bridges [BFM13, p. 41f.], this would mean that *the thumb is also approximately twice as strong as the index finger*. This theory is backed by the findings of Olafsdottir *et al.* [OZL05], who showed MVC finger forces of thumb and index of $73 \pm 18\,\mathrm{N}$ and $33 \pm 6.6\,\mathrm{N}$, respectively. During their measurements all digits were activated simultaneously and the thumb opposed the other fingers.

Correlation of Force and Stiffness to $\sqrt{\text{EMG}}$

The difference in correlation between mm. flexor and mm. extensor activation to force and stiffness is for no experimental condition significant; both muscle groups have a positive correlation to force and stiffness. This is somewhat confusing, since one would expect a strong positive correlation for both to stiffness, but a significant difference in their correlation to force, with a higher correlation for the flexor muscles. Similarly, the arrows in the EMG intra- and inter-subject regressor plots in Fig. 2.14 do not show the expected behavior with flexor and extensor arrows pointing to quadrant I and II, respectively, as explained in Subsection 2.5.1. Most likely, the main reason for this result is that subjects were asked to keep their wrist position constant using visual feedback. It is known that during pure flexion of the pinch grip extrinsic extensor muscles activate as well in order to keep the wrist in its position, namely extensor carpi ulnaris and extensor carpi radialis longus / brevis. Thus, it is most likely that the electrodes EIP and ED measure in all experimental conditions an influence of crosstalk from extensor muscles purely stabilizing / extending the wrist as well, which would explain the positive correlation of the extensor muscles to the measured force.

Furthermore, there is a clear difference when comparing the tasks. The correlations significantly drop from *task 1* to *task 2* for the extrinsic muscles and for the correlation of the interossei $\sqrt{}$EMG to force. This provides evidence that the pure force task *task 1* requires all muscles to play in concert, meaning the muscles in the forearm and in the hand activate similarly and force and stiffness are coupled. Still, there is a significant difference for the variances of the correlation coefficients when comparing intrinsic and extrinsic muscles over subjects (Fig. 2.18). Nevertheless on average they correlate similarly. But as soon as cocontraction comes into play with *task 2*, all muscles starts acting completely different in order to decouple force and stiffness. Since the measured surface EMG signal involves the EMG pattern from other, deep, muscles—we can interpret that as a lower signal-to-noise-ratio (SNR) for the extrinsic muscles—the correlation of forearm muscles drops, while not for the intrinsic muscles in the hand. The hypothesis of a higher SNR for the intrinsic muscles is confirmed by the finding that the standard deviations of the correlation coefficients of $\sqrt{}$EMG to force or stiffness are significantly less for the intrinsic muscles in the hand than for the extrinsic muscles between subjects for all experimental conditions ($p < 0.05$; compare the error bars in Fig. 2.18).
One question is left to be answered: Why does the correlation to force significantly drop between tasks for the *intrinsic muscles* and not in their correlation to stiffness? One explanation might be that there is a linear relation to stiffness and a highly non-linear to force for the interossei. But this would argue against the results of *task 1* with similar correlation coefficients, to both, force and stiffness. Alternatively, can it be concluded from these differences between force and stiffness within *task 2*, that the interossei predominate the production of stiffness and the mechanism of cocontraction, caused by, e.g., different moment arms or pennation angles affecting the increase of force with stiffness, while the production of force is produced by all groups of muscles equally? Or is it just the case that the intrinsic muscles are simultaneously (high) activated with muscles that were not measured with EMG, but which contribute to the measured stiffness? So could it be concluded from a high *correlation* between stiffness and activation of the intrinsic muscles in the hand the *causality* that these muscles predominate the decoupling between force and stiffness? Most likely not. First of all it need to be acknowledged, that prestudies lead to the wrong conclusion of a predominant role of the index finger on the measured stiffness. Since it was found the thumb to be *just* twice as stiff, one cannot speak about a dominating role of the index finger with certainty. Based on this assumption it was decided to exclude relevant muscle activating the thumb. Thus, it cannot be clarified plausibly if it is causality (intrinsic muscles predominate the measured stiffness) or just correlation (intrinsic muscles are synergistically activated) from the conducted experiments. Moreover, interosseus muscles dominating finger stiffness stands in contrast to the argumentation of Milner and Dhaliwal [Mil02]. They revealed from an investigation of moment arms and physiological cross-sectional areas of the mm. first dorsal interosseus and lumbricalis that these muscles have a predominant role for controlling the force direction at the index finger, while the extrinsic muscles in the forearm act as stabilizers. Hence the extrinsic muscles should contribute much more to finger stiffness. Another study by Kozin *et al.* [KPCT99] focused on the influence of intrinsic hand muscles on grip strength. They found that low ulnar nerve lesion—the nerve which is responsible for dorsal interosseus activation (and other intrinsic hand muscles)—results in an average decrease in grip strength of 38 %. However, they made not comparable nerve lesions for extrinsic muscles and investigated force only. This difference between force and stiffness will be discussed more detailed below.

Regressing Stiffness and Force from $\sqrt{}$EMG

Based on results in [JR69, VR73], Hogan reported [Hog84] a linear dependency between muscle force and measured EMG activation until 30% of MVC and a muscle force proportional to the square root of the pooled firing rate. On the other side, Shil *et al.* [SKK09] proposed to use a

quadratic function between muscle tension an measured activation. Thus, it was tested whether applying a square or square root to the processed EMG data would improve the fit. The results show that the square root of EMG provides a significantly better correlation for all groups of muscles to both force and stiffness than plain EMG or squared EMG (*dependent one-tailed paired t-test on mean of intra-subject correlation coefficients;* $p < 0.05$). Therefore the findings of [Hog84] that stiffness and force correlate better to the square root of EMG can be confirmed, while it cannot be confirmed that taking the square as suggested in [SKK09] provides a better correlation between muscular activation and force or stiffness.

Furthermore, the interosseus muscles in the hand dominate the regression of stiffness from $\sqrt{\text{EMG}}$, while not the regression of force. For an adequate intra-subject regression of force from $\sqrt{\text{EMG}}$, the information of all muscles is necessary (see Fig. 2.20). The force–stiffness plots in Fig. 2.19 show how much of the independence between force and stiffness is preserved after prediction from $\sqrt{\text{EMG}}$. The amount of preserved independence differs between subjects. For example, the predicted force and predicted stiffness are closely coupled in subject S7, whereas they retain almost the full amount of independence in subject S6. For most subjects, the independence of force and stiffness are well preserved after the prediction from EMG. Moreover, the regression of stiffness is found to work for inter-subject regressions as well, while an inter-subject regression of force from $\sqrt{\text{EMG}}$ is not. Adding additional state information, cq. the measured grip force, does not significantly improve results.

To improve the results the use of non-linear regression models was investigated as well: Gaussian processes [RW06], linear regression with random Fourier features [RR07], and neural networks. None of these methods showed a significant improvement of model fitness over the linear approach, which is why they are neglected in this study. It is hypothesized that the small amount of data available (approx. 100 data points for 10 subjects) does not allow fully leveraging the power of more expressive models.

It has to be acknowledged that the method described in Subsection 2.5.1 probably allowing to reveal the force–stiffness field of possible cocontractions out of the EMG regressors works for the interossei only (see Fig. 2.14); the dominating (red) arrows of the interossei in the inter-subject regressor plot in Fig. 2.14 pointing to quadrant I show the expected behavior of interossei having flexor-like properties at the metacarpophalangeal joints (see Table 2.8). Furthermore, the intra-subject regressor plots show the expected behavior for a few of the flexor muscles, while for only one of the extensors out of 10 subjects (ED of S1). A possible reason is the high density of muscles in the forearm and the influence of extensor muscles purely stabilizing the wrist during pinch grip flexion.

Anyway, similar to the results of the correlation analysis, the results of the regression analysis provide evidence of a dominant role of the interossei for stiffness but not for force. While for the regression of stiffness the interossei are sufficient, they are wide off the mark for the regression of force. By looking at Fig. 2.15 one can see that there is a clear difference between the two tasks in their level of $\sqrt{\text{EMG}}$ at a certain force. Obviously, one needs to produce more muscular activation in the task requiring cocontraction for same forces and one would expect the same for stiffness (to achieve a higher force at a certain stiffness a higher muscular activation is required). But in contrast, the representation of $\sqrt{\text{EMG}}$ to stiffness (Fig. 2.16) is not as clear as one might expect (except for the FDP), which means that similar muscular activations are required to produce stiffness in both tasks. Evidently, there are several mechanism in the experimental procedure allowing to produce the same force, but only few mechanisms to produce a change in stiffness by cocontraction. In other words, it might be that the interossei dominate the change of stiffness caused by cocontraction, while for the production of force all muscles have a similar role. This would also explain why stiffness allows for linear inter-subject regression and force not, since the low SNR of the extrinsic muscles reduces the quality of the regression.

All in all, the intrinsic muscles in the hand are found to dominate the regression of stiffness and not of force, while the design of the experiments does not allow revealing whether the stiffness itself is dominated by these muscles. A good possibility to answer this question might be the use of functional electrical stimulation placed on respective extrinsic and intrinsic muscles as performed for the human hand [LKP+99] or for the intrinsic plantar foot muscles in [KCR+14], which was not the focus of the experiments performed in [GD13]. Nevertheless the result is promising since it also works for inter-subject regression, which means that $73 \pm 9.4\,\%$ of pinch grip stiffness variance effected by cocontraction can be explained just by measuring pinch grip force and $\sqrt{\text{EMG}}$ from the interossei without any prior knowledge about the subject, while the measurement of force does not contribute much to regress stiffness ($71 \pm 12\,\%$ without the information of force). This information allows continuously measuring pinch grip stiffness as it is influenced by cocontraction, i.e., for analyzing tasks of human motor control. Furthermore, this information might be useful for the teleoperation of human pinch grip stiffness for teleoperating an actively controlled, task-dependent impedance for robotic systems such as the DLR MIRO [HNJ+08] or the DLR HUG [HHK+11], without the necessity of calibrating stiffness to EMG in advance.

2.6 Discussion on Grip Stiffness

In this Chapter a novel, wearable, light-weight, and hand-held device was demonstrated. It is able to reveal properties of grip stiffness. Capable to induce two static positions well below the onset of any kind of neural feedback, it allows for the measurement of intrinsic mechanical properties only. In a first set of experiments the device was verified in a force task by measuring a linear relation between force and stiffness. In contrast to common sense, this linear relation was found to be less fixed as initially regarded. Rather, the task plays a dominant role. In another set of experiments it was shown that the difference can be mainly attributed to changes in the kinematic configuration, i.e. wrist and fingers, rather than to cocontraction. While offset and slope of the linear relation varied with to the task, its linear nature persisted. It was hypothesized that subjects optimized the wrist positions by maximizing the norm of $\boldsymbol{J}(\boldsymbol{q})^{-T}\boldsymbol{\Pi}(\boldsymbol{q})^{T}$ (see Section 1.3) in order to reduce the latency between commanded changes in muscle activations and actual changes of grip force applied at the fingertips, rather than optimizing the grip impedance *per se*. Finally, the influence of cocontraction to decouple stiffness from force and how to reveal it from the measurement of muscular activity was investigated. Literature is lacking on this issue and—to the author's knowledge—reported about cocontraction at the production of zero torque or force only. Initially, a rather low ability of cocontraction in comparison to change in kinematics to decouple stiffness from force was expected. Nevertheless, subjects were found to be able to decouple stiffness from its linear relationship to force on average by about 20%, while their ability of doing so increased with force. In contrast to expectations, the thumb was found to be twice as stiff in comparison to the index finger. This can be useful for designers of robotic hands and fingers. Moreover, it was found that taking the square root of muscular activity allows to explain more of the measured variances in force and stiffness in comparison to the linear case or taking the square. In difference to what was expected, the knowledge of force does not improve the regression of stiffness from muscular activity considerably. Additionally, the intrinsic muscles in the hand were found to dominate the regression of stiffness, but not the regression of force.

It should be acknowledged that the results of this Chapter are only valid for expanding objects. Thus, the measured force–stiffness characteristic is dominated by corresponding flexor muscles. Results to a contracting object might be different and therefore characterizing the reaction as a linear stiffness might not be appropriate. In [VD98] Van Doren measured grip stiffness by

measuring exerted forces of a contracting and expanding handle and used the subtraction of respective forces of two respective perturbations for calculating grip stiffness. But still if his definition of stiffness is different from the definition in this Thesis, and includes information of an contracting object, as well (and active response), Van Doren found a monotonic increase of reflexive stiffness with grip force.
Although the extent of performed studies on grip stiffness within this Thesis is huge, there are still open questions left. First of all, it would be interesting to know how the change of wrist flexion/extension and ulnar and radial flexion will influence the relation between force and stiffness. A strong influence of wrist movement on the measured linear relation was found. But still, an exact model of how it might influence this relation is lacking. Moreover, it is of interest, if the intrinsic muscles in the hand dominate the measured grip stiffness or just the regression of stiffness. However, the experimental design of Section 2.5 does not allow to reveal whether stiffness itself is dominated by these muscles.

In general, we can learn that, (a) independently from kinematics, the linear nature between force and stiffness of an areflexive single muscle can be measured in the end-effector space, i.e. at the fingertip. (b) The parameters of this linear relation vary according to the kinematics. (c) There is a strong ability of cocontraction to substantially decouple stiffness from force with an increasing ability for higher forces. These three findings for a one-DoF simplification of the human multi-joint system are expected to be valid independently from the observed end-effector space.

3 Arm Stiffness

Different techniques for measuring impedance of human limbs have been developed. The most accurate and dependable approaches are steady-state perturbations introduced by Mussa-Ivaldi *et al.* in 1985 [MIHB85] and which are used to measure stiffness only. Similarly to the method reported within Chapter 2, the limb is displaced by short positional perturbations and the reaction forces in two static positions are measured. Assuming that influences of velocity and acceleration are negligible, stiffness will be the main contribution to the measured response. However, since the dynamic performance of the manipulandum used is limited, the second static level was not reached before approximately 550 ms and the last data point was collected 1000 ms after the onset of the perturbation [MIHB85]. Hence, *reflexive* stiffness is measured.
This shows the main drawback of existing step-perturbation methods: since the stiffness estimates use time windows substantially longer than the stretch, spinal, and long-latency reflex loops, and even longer than the onset of voluntary responses—which occurs after 300 to 500 ms [Lat94]—the measurements are highly influenced by active control. As humans usually attempt to actively resist displacements, subjects are usually instructed to *not voluntarily intervene* after perturbations [MIHB85, OG99, OFK$^+$02, MMIB96, GK97, SMIB93]. As this approach leads to inconsistencies between the data and the stiffness model, this Chapter focuses on the design of manipulandi to perform fast, pre-reflex impedance measurements of the human arm—i.e. completing the perturbation movement and collecting the data *before* the effect of spinal reflexes can influence the measurements. It further describes the design and validation of a dedicated orthoglide robot able to reveal the range of controllable human arm stiffnesses.

3.1 Background of Arm Stiffness Measurement

Ignoring the shoulder girdle, the human arm consists of at least seven DoF, three shoulder joints, one elbow joint, one forearm rotation, and two wrist joints, actuated by sets of mono- and biarticular muscles. While mono-articular muscles activate one dedicated joint, biarticular muscles are spanning across two joints, e.g. the biceps and triceps between shoulder and elbow joint. In order to simplify calculation of forward and backward kinematics and dynamics, this Thesis focuses on planar human arm stiffness consisting of one elbow and one shoulder joint only (two DoF), as it is common in standard literature [Hog85b, MIHB85, dVSvdH$^+$03]. The arm is reduced to a six-muscle model for the activation of two joints. It consists of bones assumed to be rigid bodies, two biarticular muscles (biceps long, biarticular flexor; triceps long, biartic-

ular extensor) crossing elbow and shoulder, and four mono-articular muscles (pectoralis major, shoulder flexor; deltoid posterior, shoulder extensor; brachioradialis, elbow flexor; triceps lateral, elbow extensor) while assuming single points of origin and insertion [Hog85b] (see Fig. 3.1).

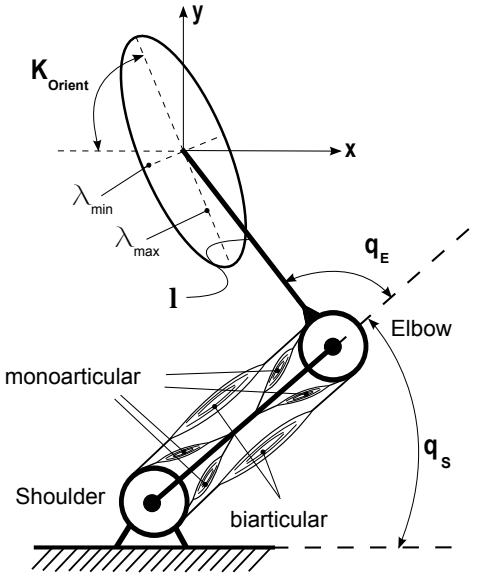

Figure 3.1: Simplified planar arm model (reproduced and adapted from [HWvdS14] ©2014 IEEE). — Consisting of the two joints shoulder and elbow driven by six actuators, four mono-articular and two biarticular muscles. The orientation K_{orient} of a Cartesian stiffness ellipse and its eigenvalues $\lambda_{\text{min/max}}$ are depicted.

This allows to reveal relevant insights into human arm mechanical properties and the role of mono-articular and biarticular muscles without the necessity of considering the full complex model consisting of all seven DoF. Moreover, it facilitates a direct mapping between Cartesian and joint space (two by two instead of six by seven DoF). In difference to the fingers, for the arm the influence of gravitational forces cannot be neglected. Thus, subject's arm will always be assisted using a strap hanging from the ceiling as a kind of gravity compensation in order to minimize influences of gravitational forces in Eq. (1.37).
Since stiffness is not directly measurable, a set of linear algebraic Eqs. will be defined

$$\Delta \boldsymbol{x} \hat{\boldsymbol{K}} = \Delta \boldsymbol{F}, \tag{3.1}$$

relating the observed input (displacement) and measured output (force). This can be transformed to a normal equation system

$$\left(\Delta \boldsymbol{x}^T \Delta \boldsymbol{x}\right) \hat{\boldsymbol{K}} = \Delta \boldsymbol{x}^T \Delta \boldsymbol{F}, \tag{3.2}$$

the solution of which yields the matrix $\hat{\boldsymbol{K}}$ containing the optimal parameter values. The matrix $\left(\Delta \boldsymbol{x}^T \Delta \boldsymbol{x}\right)$ is the so-called *Gramian matrix* of $\Delta \boldsymbol{x}$. It is the second derivative of the squared error function. It has some valuable characteristics, e.g. positive semi-definiteness. The algebraic solution of the normal equation system leads to the least-squares solution

$$\hat{\boldsymbol{K}} = \left(\Delta \boldsymbol{x}^T \Delta \boldsymbol{x}\right)^{-1} \Delta \boldsymbol{x}^T \Delta \boldsymbol{F} = \Delta \boldsymbol{x}^{+} \Delta \boldsymbol{F}, \tag{3.3}$$

with the Moore-Penrose pseudoinverse $\Delta \boldsymbol{x}^{+}$. This equation will be used in this Chapter for the identification of the Cartesian endpoint-stiffness matrix.

3.1.1 Metrics Representing endpoint-stiffness

It was established by Mussa-Ivaldi *et al.* in 1985 to represent the endpoint-stiffness matrix graphically as an ellipse with orthogonal axes of major and minor stiffness (see Fig. 3.1). They further introduced the metrics size, shape and orientation for comparing stiffness ellipses. They are calculated using singular value decomposition of the Cartesian stiffness matrix [MIHB85]. Similarly, the measured Cartesian stiffness matrices within this Chapter will be represented by these metrics. This allows comparing the results across subjects and studies. The size of the stiffness ellipse can be computed by

$$K_{\text{size}} = |\pi \cdot \lambda_{\max} \cdot \lambda_{\min}|\,, \tag{3.4}$$

and is a quantitative representation of the measured amount of stiffness. The larger the size, the stiffer the endpoint of the arm. The values $\lambda_{\min/\max}$ are the eigenvalues and denote the stiffness in the direction of the major and minor axes of the stiffness ellipse. The shape of the stiffness ellipse is computed by

$$K_{\text{shape}} = \left|\frac{\lambda_{\max}}{\lambda_{\min}}\right|, \tag{3.5}$$

and is a qualitative characterization of isotropy of the endpoint-stiffness [MIHB85]. K_{shape} of 1 (also 100 %) represents an ideal isotropic endpoint-stiffness, i.e. the endpoint-stiffness can be represented by a circle. It means that a force perturbing the endpoint in any direction would lead to a unique and proportional restoring force and a displacement in exactly the opposite direction. For the general case, K_{shape} is different to 1. The directions of displacement and restoring force are not collinear, except in the directions of major and minor stiffness. Please note, the definition of stiffness prohibits negative major and minor eigenvalues (positive definiteness; see Section 1.3 as well). However, since measurements can include, e.g. active responses, as well, eigenvalues are possibly negative. That's why K_{size} and K_{shape} are introduced as absolute values.
Similar to [MIHB85] the orientation of the stiffness ellipses can be calculated using the definition of the dot product in Euclidean space

$$K_{\text{orient}} = \arccos\left(\begin{pmatrix}-1\\0\end{pmatrix} \cdot v\right), \tag{3.6}$$

where v denotes the normalized eigenvector corresponding to $\lambda_{\max}$. K_{orient} is the angle between the negative x-axis and v [HWvdS14]. The orientation reveals the direction of maximum resistance and is defined according to standard literature [MIHB85].
Additionally, Z_{mean} will be used which is the square root of the relation between the determinants of symmetric $\mathbf{K_{sym}}$ and asymmetric $\mathbf{K_{asym}}$ components [Hog85b] of the measured stiffness matrix $\mathbf{K}$

$$\begin{gathered} Z_{\text{mean}} = \sqrt{\frac{\det(\mathbf{K_{asym}})}{\det(\mathbf{K_{sym}})}}, \text{with} \\ \mathbf{K_{asym}} = \begin{bmatrix} 0 & \frac{\mathbf{K_{xy}}-\mathbf{K_{yx}}}{2} \\ \frac{\mathbf{K_{yx}}-\mathbf{K_{xy}}}{2} & 0 \end{bmatrix}, \text{and} \qquad \mathbf{K_{sym}} = \begin{bmatrix} \mathbf{K_{xx}} & \frac{\mathbf{K_{xy}}+\mathbf{K_{yx}}}{2} \\ \frac{\mathbf{K_{xy}}+\mathbf{K_{yx}}}{2} & \mathbf{K_{yy}} \end{bmatrix}. \end{gathered} \tag{3.7}$$

Z_{mean} compares the influence of non-spring-like forces on measured stiffness matrices and is independent of the used coordinate frame (joint or Cartesian space). A Z_{mean} value of 0 % determines an ideal elastic behavior (perfectly symmetric stiffness matrix), while 100 % shows that the measured forces are not originating from a conservative (spring-like) force field. Note, that Z_{mean} can not be used to separate stiffness for reflexive and purely mechanical properties, since the neuromuscular system including reflexive response is predominantly spring-like [Hog85b]. But it allows to reveal information about the portion of inertia and damping which is wrongly interpreted as stiffness on the obtained results.

Finally, the stiffness matrix of a captive mechanical system needs to be positive definite, since the generated force field of a conservative mechanical system has to be energy conserving [Hog85b], which will be determined within this Chapter as well (*elasticity* of stiffness).

3.1.2 General Properties of Arm Endpoint-Stiffness

Planar human-arm endpoint-stiffness is directional, with a greater resistance in a certain direction in comparison to another. In the pioneering work of Mussa-Ivaldi *et al.* [MIHB85], the researchers found that the Cartesian stiffness ellipse highly depends on the joint configuration of elbow and shoulder. While it is thin and elongated with its major axis pointing towards the shoulder joint for the more distal positions, it becomes isotropic with a direction of the major axis aligned with the pointing direction of the forearm for proximal positions. Note that an ideal isotropy of that ellipse, meaning the large and small eigenvalue of the stiffness matrix are equal, can only be achieved in a joint range of 0 to 90° for the shoulder and 90 to 180° for the elbow [Hog85b], while humans are most-likely not able to produce isotropy voluntarily. Furthermore, the researchers of [MIHB85] showed that shape and orientation are comparable over time and subjects, while size differs. Another important finding of this work was that the neuromuscular system—including active and passive responses—can be regarded as predominantly spring-like. The researchers found that the curl of the force field (the asymmetric component of the stiffness matrix) produced by the neuro-muscular system is small in comparison to the symmetric component. The symmetric component represents the portion of the stiffness matrix which can be attributed to a potential function and is representing the spring-like behavior. As Hogan showed in [Hog85b], non-zero curl components can only be caused by heteronymous inter-muscular reflexes, e.g. causing the shoulder to be activated if the elbow is stretched, and can thus be attributed to non-spring-like behavior.

3.1.3 Voluntary Control of Endpoint-Stiffness

Contrary to what one might expect [IVC11], the ability to voluntarily control shape, size and orientation of the endpoint-stiffness ellipse is quite limited during posture maintenance [PKC01, PKC02, DMG$^+$04]. In simulation studies Hu *et al.* showed that humans should be able to vary endpoint-stiffness ellipse orientation in the range of 93° (no external forces, no gravity) and in the range of 41° with gravity [HMP12]. But, in general, researchers of [PKC02, DMG$^+$04, GO98] showed an ability to voluntarily change its orientation by only 30° during posture maintenance, with an almost twice as large ability for the clockwise direction [PKC02, DMG$^+$04] (i.e. $\approx$ 20°). Furthermore, the range in orientation decreases as endpoint force production increases; its magnitude and orientation is further constrained by the direction of produced endpoint forces [PKC02]. Hence, joint stiffness increases with joint torque due to muscle mechanics, while it is less related to joint position in comparison to passive joint stiffness[1] [BFM13].

Besides it was shown that the capability to alter the orientation of the endpoint-stiffness ellipse highly increases during movement [BOF$^+$01, PKC01] in comparison to postural tasks [PKC02]. Using divergent force fields with an orientation of instability of 0°, -45°, and 80° in reference to the positive x-axis, the researchers of [BOF$^+$01, FLM$^+$07] showed that the orientation of maximum stiffness matched the direction of instability when moving from one point to another. Note that, as discussed in Section 1.3, the definition of stiffness does not hold for measurements during movement and has to be regarded as *quasi-stiffness*.

[1] Note that joint viscosity and passive stiffness are comparably small in joint resting position, while they increase considerably when reaching joint limits [BFM13].

3.1.4 The Influence of Cocontraction

It has been suggested that the size of the stiffness ellipse and thus the overall stiffness could be varied by synchronous cocontraction of elbow and shoulder muscles [MIHB85]. Besides that, Gomi and Osu showed in 1998 [GO98] that shape and orientation can be affected by cocontraction during posture maintenance, as well: While an increase in elbow stiffness rotates the endpoint-stiffness ellipse clockwise, an increase in shoulder stiffness results in a counter-clockwise rotation [GO98, PKC02]. The single-joint muscles of shoulder and elbow can be activated independently, while the activation of cross-joint muscles is constrained by single-joint muscle activation [PKC02]. It is suggested that the cocontraction of single-joint elbow muscles results in cocontraction of cross-joint muscles [DMG$^+$04] and that there are at least two independent cocontraction commands to control planar arm stiffness [DMG$^+$04]; cross-joint stiffness correlating with elbow torque [GO98] argues in the same direction. Furthermore, the researchers of [GO98] found a posture-dependent sensitivity of endpoint-stiffness characteristics (shape and orientation) with a higher variability for the proximal positions in comparison to the distal ones, which is similar to Hogan's analysis of endpoint-stiffness isotropy for certain ranges [Hog85b] mentioned above. Moreover, Hogan showed that double-joint stiffness is important in altering endpoint-stiffness characteristics and postulated that biarticular muscles need to be at least twice as stiff as the single joint muscles to reach isotropy at the endpoint [Hog85b].

3.2 Manipulandum

Planar human arm motor studies are typically performed with a specific type of manipulandum: an asymmetric 5R parallel mechanism design [MIHB85, dVSvdH$^+$03, HKC$^+$92, HIW09, CSMA06]. Competing designs include a 5R symmetric parallel mechanism design [GK96, KRB13], a 2P cable-driven approach [CTG$^+$14], and a compact cam disc-based device with one active degree of freedom [MSSM12].

In difference to the Grip Perturbator developed within Chapter 2, which is a body-based device, the manipuladum that is described in this Section is a ground-based device, i.e. induces an *actio*-force into the arm and the *reactio*-force into the basement. Building such a robotic manipulandum that can measure intrinsic, pre-reflexive human arm properties inside the entire human arm workspace implies several requirements: (a) the moving mass of the manipulandum needs to be minimal; (b) the structure needs to be maximally stiff in order to measure the human and not the manipulandum; (c) the manipulandum must be stronger than the subject; (d) since position perturbations are small displacements with an amplitude around 10 mm, special care needs to be taken to reduce the mechanical clearance. Further requirements for the development are a workspace of approximately 0.5 m radius and the avoidance of insertion of torques around the axis of forearm pronation and supination.
In order to match these requirements, a design decision was taken to not use gears—thus primarily addressing requirements (b) and (d) above—and using direct-drive actuation based on linear motors instead. Along this approach, Wenger *et al.* [WGC07] investigated the motor arrangement of planar parallel kinematic mechanisms. It was shown that the orthogonal mechanism—introduced by the same authors in [CWA00] and there dubbed the *orthoglide mechanism*—is better, since it has an optimal quadratic workspace resulting in smaller lengths struts and lower dimensions, better stiffness isotropy, smaller mass in motion, and thus higher dynamic performance than a non-orthogonal arrangement [WGC07]. Inspired by this work, it was decided to build the manipulandum using the orthoglide kinematic arrangement.
Knowing that the human elbow joint has an eigen-frequency around 25 Hz [XHHB91], Böhm performed measurements of a perturbation profile with 10 mm in 10 ms similar to the profiles as

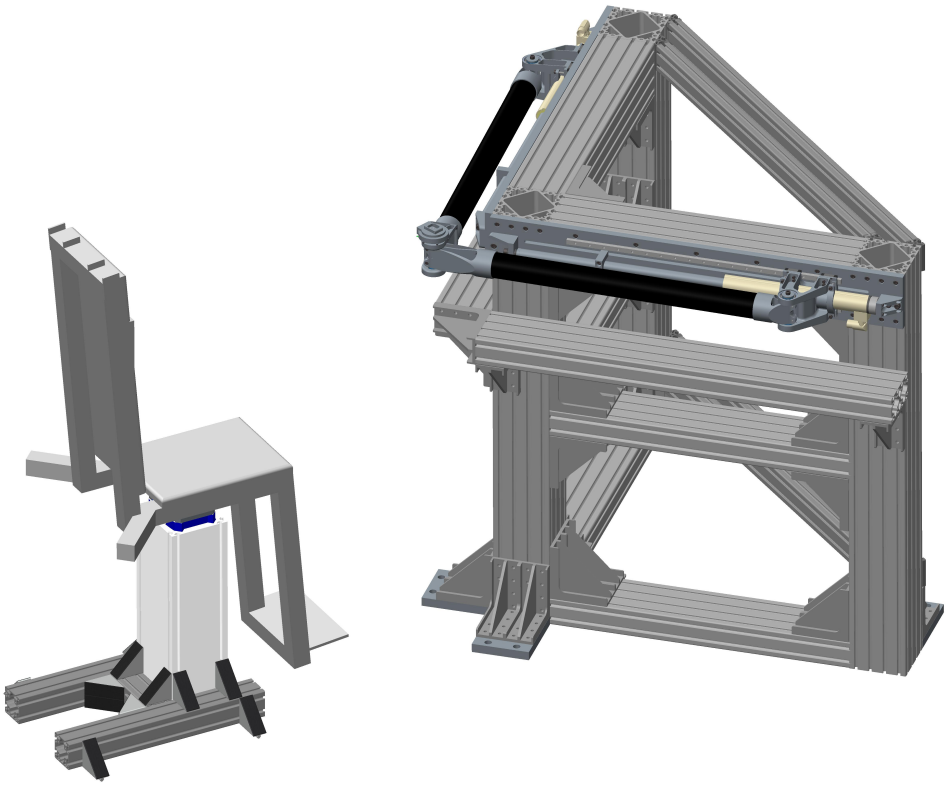

Figure 3.2: CAD drawing of the manipulandum (reproduced from [HGvdS15] ©2015 IEEE). — Two linear motors are orthogonally arranged, which is why the kinematic arrangement is called *orthoglide mechanism*. The sliders are fixed to the base instead of the motors in order to reduce the moving mass. Guiding functionality is provided by four linear guides beside each of the two motors. A force-torque sensor is attached to the end-effector in order to measure mechanical responses induced by position perturbation. In order to reduce high-frequency oscillations, a massive base made of standard aluminum ITEM profile is used.

they were used for the experiments on grip stiffness within Chapter 2—with a similar motor type, viz. PS01-48×240-C as it is used for the designed manipulandum. He found the relevant eigen-frequencies of the motor with different attached masses lying below 62.5 Hz [Böh13]. Therefore he decided to optimize the eigen-frequency of the structure to be higher than 125 Hz in order to reduce the influence of the manipulandum eigen-frequency on the human measurements. Using Pro/ENGINEER Mechanica, he simulated different profiles and materials for the structure. He found that only a round profile made of carbon fiber reinforced plastic (CFRP) for each arm is able to match the requirements of a low moving mass with an eigen-frequency above 125 Hz [Böh13]. His optimal choice was a CFRP tube of about 70 mm diameter and 800 mm length with a flexural stiffness and a flexural modulus of elasticity of $6.5{\cdot}10^{10}$ Nmm^2 and 230 GPa, respectively. Based on the initial design [Böh13], a manipulandum was designed with named requirements, whereof a 3D drawing is depicted in Fig. 3.2 [HGvdS15].

Since the weight of the motors (2.88 kg each) is smaller than that of the sliders (4.12 kg each), the sliders were fixed to the base instead of the motors. The linear motors P01-48×360 from NTI AG–LinMot provide no guiding functionality. Therefore additional ball bearing guides were used to guide the motors. In order to reduce the mechanical clearance at the end-effector, four parallel bearing guides were implemented beside each motor (two on each side, see Fig. 3.2) instead of one underneath/above the motor as proposed in [Böh13]. The base is massive, built out of standard aluminum ITEM profiles, and weighs approximately 250 kg. At the end-effector an ATI Mini45 SI-145-5 six-axis force–torque sensor was added, the orientation of which depends on the motor positions. The motors have a position repeatability of 0.05 mm.

Figure 3.3: Manipulandum in real (reproduced from [HGvdS15] ©2015 IEEE). — The subjects are attached via a plastic cuff to the end-effector. In order to ensure subject's safety, the connection is realized using a permanent magnetic clutch in order to allow subjects to decouple in each experimental situation.

Kinematic Analysis

According to [PCW06], the workspace of the manipulandum can be calculated by

$$L^2 = (p_x - \rho_x)^2 + {p_y}^2, \text{ and} \tag{3.8}$$
$$L^2 = {p_x}^2 + (p_y - \rho_y)^2, \tag{3.9}$$

where p_x and p_y are the position variables of the end-effector, L =1000 mm the length of the arms, and ρ_x and ρ_y the motor positions (please note the difference in the orientations between the coordinate systems of the manipulandum and of the subjects of about 135°; see Fig. 3.4). The inverse kinematics are simply given by

$$\rho_x = p_x \pm \sqrt{L^2 - {p_y}^2}, \text{ and} \tag{3.10}$$
$$\rho_y = p_y \pm \sqrt{L^2 - {p_x}^2}, \tag{3.11}$$

and the forward kinematics by

$$p_x = \frac{1}{2}\left(\rho_x \pm \rho_y \sqrt{\frac{4L^2}{{\rho_x}^2 + {\rho_y}^2} - 1}\right), \text{ and} \tag{3.12}$$
$$p_y = \frac{1}{2}\left(\rho_y \pm \rho_x \sqrt{\frac{4L^2}{{\rho_x}^2 + {\rho_y}^2} - 1}\right). \tag{3.13}$$

Similar to [KRB13] the differential kinematics can be derived by using the Jacobian $\mathbf{J}(\rho) = [\delta p_i / \delta \rho_j]$ (find the Jacobian in [PCW06]) and calculate the condition number over the manipulandum workspace (see Fig. 3.5(a)).

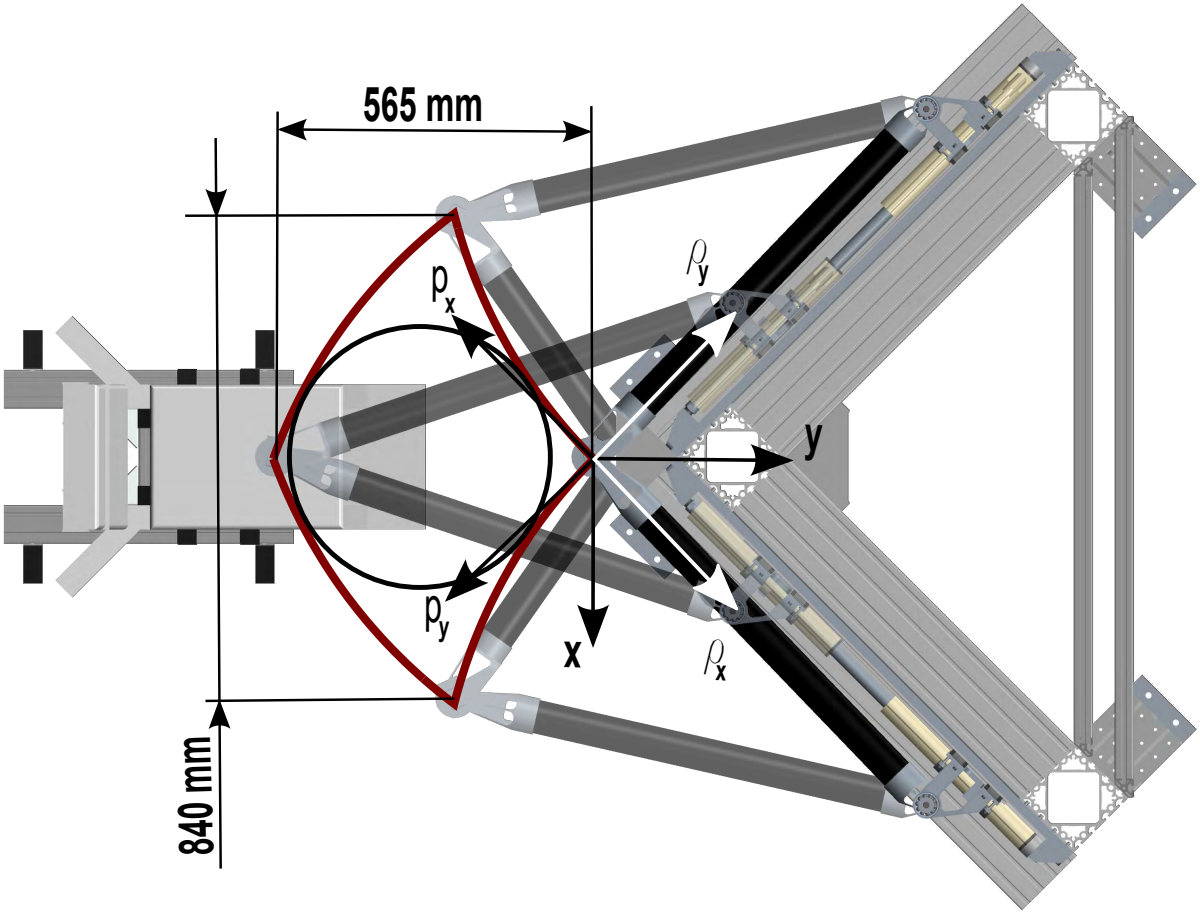

Figure 3.4: Workspace and coordinate frames (reproduced from [HGvdS15] ©2015 IEEE). — The reachable workspace and the coordinate frames of the motor $[\rho_x, \rho_y]$, of the manipulandum $[p_x, p_y]$, and the one used for the performed measurements $[x, y]$ is depicted.

The condition number $\text{cond}(\mathbf{J}) = \|\mathbf{J}\| \cdot \|\mathbf{J}^{-}1\| \in [1, \infty]$ is a quantitative measure of manipulandums dexterity, where $\|\mathbf{J}\|$ corresponds to the norm of the Jacobian. A condition number of 1 represents the ideal case, meaning that any input force or velocity in motor space results in equal distributed velocities and forces in end-effector space between both axis. Fig. 3.5(a) shows that for the chosen design condition numbers between 1 and 3.2 can be achieved. Additionally, the Jacobian is used to calculate the norm of maximum end-effector forces depending on the workspace by knowing that one motor is able to produce a maximum force of 1024 N (see Fig. 3.5(b)).

3.2.1 Safety Concept

In order to ensure subject safety, different safety mechanisms working in parallel were developed (see Fig. 3.6):

- First of all, the arrangement between manipulandum and chair is chosen such that the manipulandum is never able to reach the chest of the subject.
- Secondly, mechanically adjustable stops ensure that the workspace of the manipulandum is never larger than the workspace of the arm of the subject.
- Additionally, there is an emergency stop (ultimate limit switch) at each of the four mechanical stops. If the manipulandum reaches one of the mechanical stops, both motors

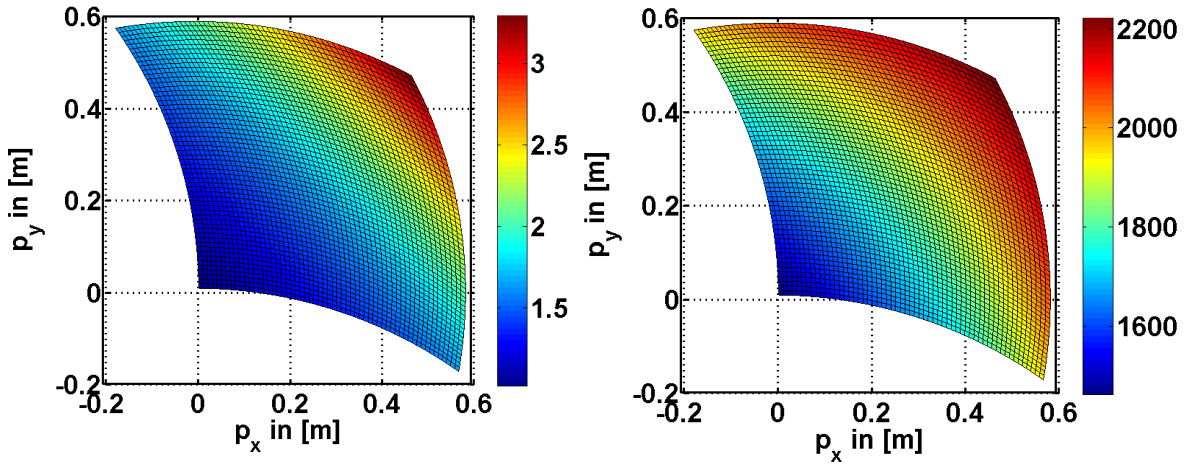

(a) Condition number

(b) Maximum forces

Figure 3.5: Condition number and maximum forces at the end-effector (reproduced from [HGvdS15] ©2015 IEEE). — (a) A condition number of the Jacobian of 1 is targeted, meaning an input in motor force or velocity will lead to an equal distributed velocity and force output in end-effector space. (b) The norm of the maximum forces which can be achieved at the end-effector (note that the directional data is discarded).

are switched off instantaneously. When switched off, the manipulandum is always easily backdrivable.

- There are two more emergency stops: one attached to the chair and which can be reached by the subject's left arm, and one for the experimenter. If either one is pressed, both motors are switched off instantaneously.
- The subject's arm is coupled to the manipulandum with a plastic cuff using a permanent magnetic safety clutch in order to allow the subject to decouple in each experimental situation.
- For activating the measurement setup, the subject must hold a dead man's switch with the right foot. If released, zero Ampere is instantaneously commanded to the motors.

3.3 First Experiments—Results of a Force Task

In this Section and similar to the procedure used for validating the Grip Perturbator within Section 2.2, the manipulandum will be validated in a force task knowing that intrinsic stiffness varies linearly with the applied force.

The measurement setup consists of a host running Linux, and a real-time target machine running QNX where a Matlab/Simulink model to control the device is running at 2 kHz. The sensors signals are amplified and measured with an analogue–digital converter. The LinMot E1200 motor control boxes are controlled using an Ethercat connection. Both motor control boxes and analogue–digital converter are directly connected to the real-time machine. The nominal range of the ATI force sensor in x and y is 145 N with a resolution of 1/16 N. The nominal range was chosen to allow a proper identification with a suitable sensor resolution of changes in forces—and thus optimizing the measurement of stiffness—rather than setting it up to measure maximally exertable arm forces.

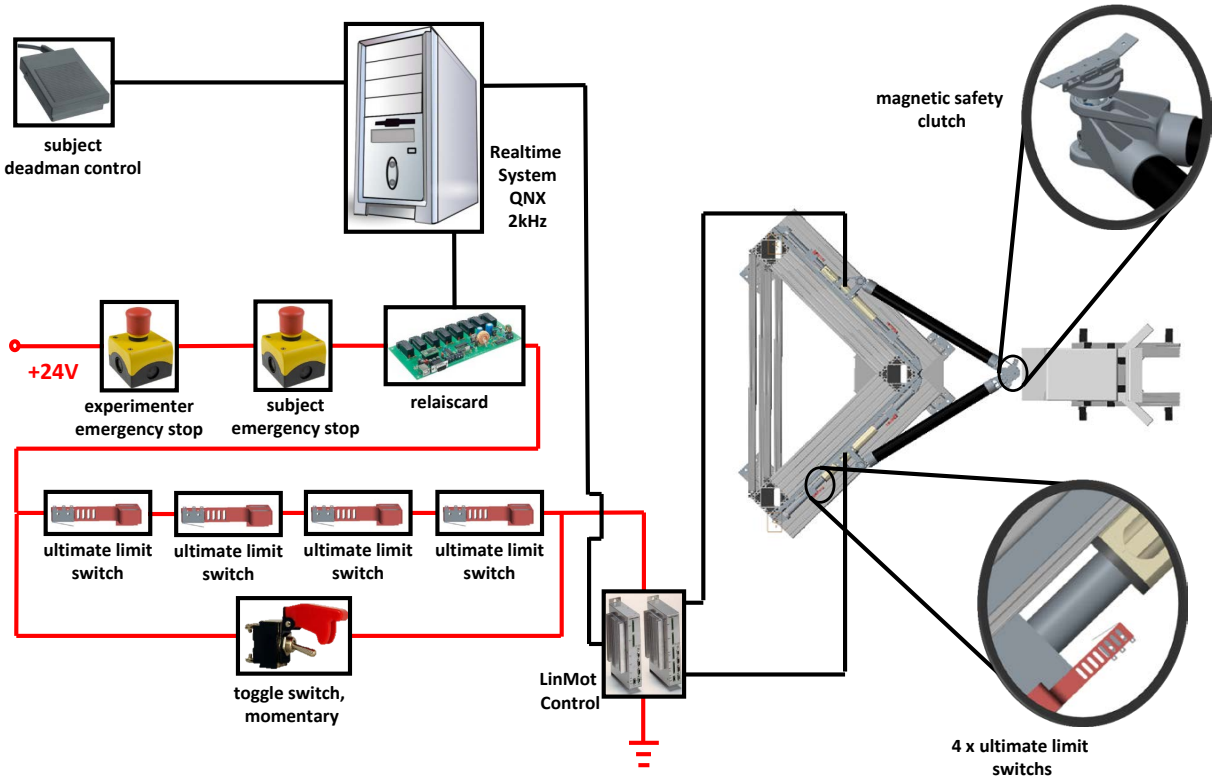

Figure 3.6: Safety concept (reproduced from [HGvdS15] ©2015 IEEE). — (a) Four adjustable mechanical stops limit the workspace to the workspace of the subjects; (b) at each of the four mechanical stops emergency stops (ultimate limit switches) are attached; (c) additionally, there is one experimenter and one subject emergency stop; (d) the coupling between subjects arm and manipulandum is realized using a permanent magnetic safety clutch; (e) during the experimental procedure, the subject dead man's switch need to be hold by the subject. The toggle switch is necessary for initializing the motors; if pressed, the ultimate limit switches are bridged.

Initially, an arm dummy was designed based on standard parameters from literature with arm segment lengths [dL96] of forearm and upper arm of 250 mm and 330 mm, respectively. The maximal subject mass was set to 100 kg and the segment masses were designed according to [VZ90] of forearm (including the hand) and upper arm to be 2.1 kg and 2.7 kg, respectively. In order to identify the influence of the quantity of inertia which is wrongly interpreted as subject arm stiffness, two sets of experiments were designed: (a) The arm dummy was attached to the end-effector and its shoulder was placed at a similar position where the shoulder of the subject will be and performed the experimental protocol below (naturally, no external forces where applied; see Fig. 3.7); (b) the same experiment was repeated without the arm dummy.

A total of 5 healthy right-handed male subjects, age 27–35 years, performed the experimental protocol designed to measure their arm stiffness during the application of distal forces measured in one position using the proposed manipulandum (the definition of the distal direction is chosen according to standard literature [MIHB85, dVSvdH$^+$03, OG99]). The experimental procedure is similar to the previous Sections 2.2, 2.3, and 2.5 which is called "force task". All subjects gave written consent to the experimental procedures. Subjects were seated on a special adjustable chair fixed to the base. The subject's chest was restrained with seat belts to limit movement to arms only. The end-effector is placed at a central position such that a line between shoulder and end-effector would be parallel to the distal direction, so as to reach elbow angles around 90°. The end-effector is connected to subjects' arm via a plastic cuff; the elbow is assisted by a belt in order to compensate for the weight of the arm. The workspace of the manipulandum and the

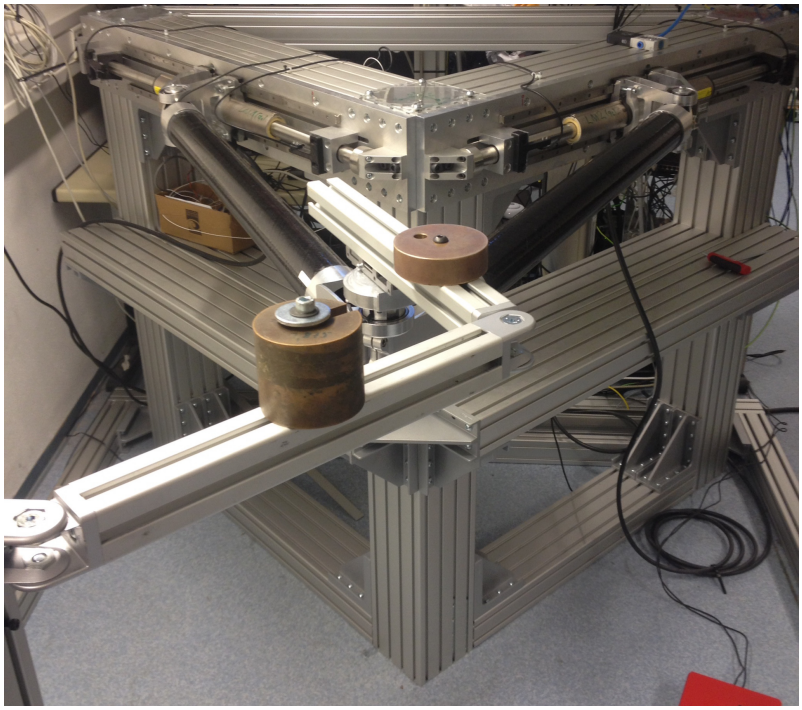

Figure 3.7: Arm dummy based on standard parameters from literature. — Masses are attached in order to meet fore- and upper arm parameters according to a subject mass of about 100 kg.

height of the chair is adapted to comfortably seat the subject. Initially, subjects were asked to apply maximum force in the distal direction (positive y-axis; see Fig. 3.4), while their MVC level in that direction was estimated. 3 of 5 subjects reached the force limit of the force sensor (145 N); in this case 160 N was chosen arbitrarily which lead to stable results without having subjects fatiguing too fast. Subsequently, subjects were shown visual feedback about the applied forces in a plane parallel to the actuator movement using a dot, and a circle representing a required amount of distal force with a tolerance of 2.0 %. Subjects were then asked to reach that distal force level with the aid of the presented circle, and keep it until the perturbation was felt. Since no influence is expected from active control and in contrast to the *do-not-voluntarily-intervene* paradigm, subjects were allowed to relax if perturbation was felt. The required NFLs were either at 20, 30, 40, 50, or 60 % of MVC and will be referred as NFL1 . . . 5. The perturbation consists of a 12 mm displacement (please note that the displacement was interpolated in end-effector coordinates rather than motor positions) of the hand in 8 different directions (0, 45, 90, 135, 180, 225, 270, and 315°; again, please note the difference in orientation between the coordinate systems of the manipulandum and of the subject of about 135°; see Fig. 3.4). Each combination of normalized distal force level and perturbation direction was repeated 5 times, leading to 200 trials in total per subject which were presented in a randomized order. After each perturbation the hand was moved back to the central position and subjects had to rest for approximately 10 seconds. In between tasks subjects were again asked to relax instead of using the *do-not-voluntarily-intervene* paradigm. Given a visual feedback this relaxation phase was used for automatically resetting the force sensor (similar to Section 2.3 perturbations lead to small drifts in the force signal). If subjects reported fatigue, they would be allowed to rest as much as needed. The whole experiment lasted about 90 minutes per subject; no subject reported discomfort.

3.3.1 Data Processing

Similar to Chapter 2, the force signals were first filtered using a 21-point moving average filter. The length of the time window before the perturbation T_1 was set to 50 ms, while the time window length T_2 after the perturbation was chosen to 100 ms; the last data point for the evaluation of stiffness, i.e. t_{trust}, was taken 200 ms after the onset of the perturbation (see Fig. 3.8; see Section 2.1 as well). These time window length were chosen by visual inspection of the respective position, velocity, and acceleration signals under the premiss of having almost no influence of damping and inertial properties. The differences in the mean values over these two time windows were evaluated for force and position and the Cartesian stiffness matrix was determined by L2 regression. Please note that for reasons of simplicity it was refrained from measuring arm joint angles, which is why Cartesian stiffness can be assessed only.

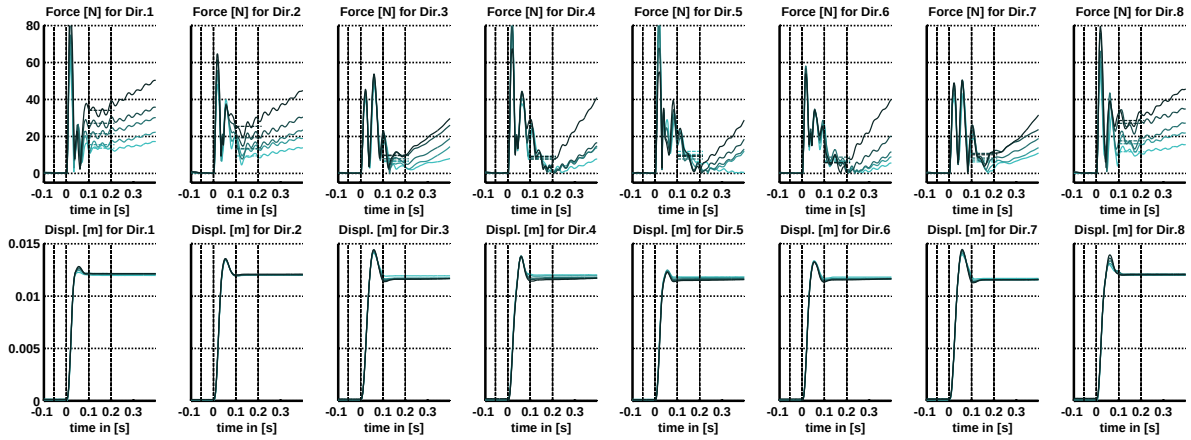

Figure 3.8: Exemplary force and displacement profiles (*rows*) of Subject S4 for each perturbation direction (*columns*) and force level (*colors*) (reproduced from [HGvdS15] ©2015 IEEE). — The mean force (upper row) and mean displacement profiles (lower row) shown corresponds to the norm of the perturbation along the axis of perturbation. Direction 1 corresponds to the distal pushing direction (positive y-axis; see Fig. 3.4) while the number of perturbation direction increases clockwise. The line colors indicate the NFL, while the darker colors refer to the higher NFL. Note, that the means over the time window before the perturbation were subtracted from each force profile. The start of the perturbation is indicated as t=0 s. The time window positions are depicted by 4 vertical dashed lines with the end of the first time window at t=0 s. Additionally, the mean force values taken over the second time window are shown as colored dashed horizontal lines.

3.3.2 Results

The experimental results are represented in Fig. 3.9 and Table 3.1. Fig. 3.9 shows the measured Cartesian stiffness matrices represented as ellipses. Additionally, the mean reaction forces and displacements are shown in Fig. 3.9 for each force level and perturbation direction. Table 3.1 summarizes the four metrics used to compare the measured stiffness matrices (see Section 3.1). While no significant correlation between K_{size} or Z_{mean} and the normalized force level was found, a significant correlation ($p \leq 0.001$) was found for both K_{orient} and K_{shape} to normalized force with $r = 0.66$ and $r = -0.63$, respectively (Pearson's r). All measured stiffness matrices were found to be positive definite. Additionally, using Z_{mean} it was found that the quantity of inertia and damping which is erroneously interpreted as stiffness for the manipulandum with and without attached arm dummy in comparison to all identified subject stiffness is around $4.9 \pm 0.79\,\%$ and $0.79 \pm 0.13\,\%$, respectively. Analogously, a mean influence of about $6.8 \pm 1.0\,\%$ over all force levels and subjects of non-springlike forces on the regressed stiffness with its maximum for the fifth force level of subject S1 was found.

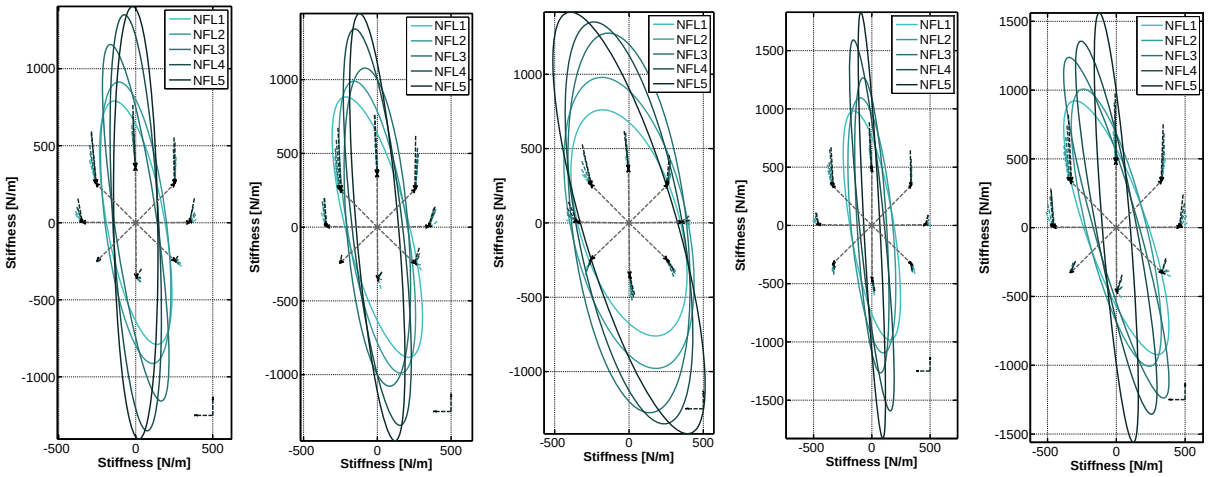

(a) Subject S1 (b) Subject S2 (c) Subject S3 (d) Subject S4 (e) Subject S5

Figure 3.9: Experimental results (reproduced from [HGvdS15] ©2015 IEEE). — The figures show the measured Cartesian stiffness matrices represented as ellipses for all subjects and force levels (*colors*). Additionally, the mean reaction forces and displacements are shown for each force level and perturbation direction. The depicted forces are scaled with the constant position displacements of 0.012 mm; exemplary, the two arrows in the lower right half of the figures corresponds to 10 N each. The line colors indicate the NFL, while the darker colors refer to the higher NFL.

3.4 Discussion on Arm Stiffness

In this Chapter, a new robotic manipulandum based on an orthoglide mechanism is introduced. The goal of this manipulandum is to identify intrinsic human arm parameters, by performing arm perturbation measurements before fast reflex effects influence stiffness. Though it was not possible to keep the end of the second time window for estimating stiffness below 50 ms—thus including the onset of measurable fast reflex responses in force—visual inspection of the perturbation profiles in Fig. 3.8 pleads for successful identification of stiffness before the onset of relevant active control. Furthermore, measurements using the manipulandum with and without an arm dummy shows that less than Z_{mean}=5 % of the identified stiffness matrix originates from wrongly interpreted inertia. All identified stiffness matrices were found to be positive definite and the influence of non-conservative components showed to have an influence of 6.8 ± 1.0 % on the performed measurements. [MIHB85] reported a Z_{mean} less than 21 %, corresponding to the less than 20 % found in this Chapter. Moreover, the orientation of the stiffness ellipse was found to increase while the ellipse shape decrease with the applied force. In other words, *the higher the applied forces, the thinner the measured ellipse, with its major axis turning towards the direction of pushing.* The orientation and shape changed on average about 5.7 ± 2.1° and 16.0 ± 3.2 %, respectively. Interestingly and contrary to initial expectations, no relevant trend for the size of the ellipses was found. Nevertheless, the length of major axis of the stiffness ellipse increases linearly with the applied force ($r = 0.93$, $p \leq 0.0001$), while there is no significant correlation for the small eigenvalue.

Furthermore, even for the first force level NFL1 the sizes of the measured stiffness ellipses are substantially larger than those reported in [MIHB85] measured in a posture maintaining task. Analyzing the differences, it has to be mentioned that in [MIHB85] position displacements of 5 and 8 mm were used in comparison to 12 mm used here. Moreover, the rising times for the perturbations differ considerably. Nevertheless, van Doren reported a decreasing stiffness with an increasing perturbation amplitude and an increasing stiffness with an increasing rising time [VD98], arguing in the opposite direction for both differences. Moreover, the subjects in the experiment were asked to *relax* after the perturbation, in contrast with the *do-not-voluntarily-intervene* paradigm, also arguing in the opposite direction. All in all, it is most likely that

Table 3.1: Experimental results (reproduced from [HGvdS15]).

Subject	$\mathbf{K}_{\text{size}}$	$\mathbf{K}_{\text{orient}}$	$\mathbf{K}_{\text{shape}}$	$\mathbf{Z}_{\text{mean}}$
S1-NFL1[1]	$47.3\,(\text{N/cm})^2$	73.5°	23.6%	10.2%
S1-NFL2[1]	$57.3\,(\text{N/cm})^2$	74.6°	22.0%	14.8%
S1-NFL3[1]	$50.8\,(\text{N/cm})^2$	78.6°	11.9%	8.1%
S1-NFL4[1]	$63.3\,(\text{N/cm})^2$	82.3°	11.1%	11.7%
S1-NFL5[1]	$63.1\,(\text{N/cm})^2$	82.0°	10.3%	19.7%
S2-NFL1[1]	$61.0\,(\text{N/cm})^2$	80.1°	23.6%	7.7%
S2-NFL2[1]	$63.9\,(\text{N/cm})^2$	81.1°	20.2%	1.0%
S2-NFL3[1]	$70.9\,(\text{N/cm})^2$	82.3°	19.3%	5.6%
S2-NFL4[1]	$72.5\,(\text{N/cm})^2$	82.9°	12.6%	1.2%
S2-NFL5[1]	$65.6\,(\text{N/cm})^2$	83.4°	9.9%	4.5%
S3-NFL1[1]	$83.1\,(\text{N/cm})^2$	75.8°	42.8%	2.2%
S3-NFL2[1]	$122\,(\text{N/cm})^2$	78.1°	39.0%	0.8%
S3-NFL3[1]	$155\,(\text{N/cm})^2$	81.5°	29.9%	2.4%
S3-NFL4[1]	$152\,(\text{N/cm})^2$	81.3°	25.7%	3.2%
S3-NFL5[1]	$146\,(\text{N/cm})^2$	79.0°	21.5%	9.5%
S4-NFL1[1]	$58.7\,(\text{N/cm})^2$	80.9°	18.9%	0.5%
S4-NFL2[1]	$61.8\,(\text{N/cm})^2$	81.6°	16.3%	6.5%
S4-NFL3[1]	$50.5\,(\text{N/cm})^2$	84.4°	10.0%	6.0%
S4-NFL4[1]	$53.8\,(\text{N/cm})^2$	84.8°	6.7%	1.7%
S4-NFL5[1]	$39.9\,(\text{N/cm})^2$	85.1°	3.8%	8.8%
S5-NFL1[1]	$68.7\,(\text{N/cm})^2$	76.6°	23.3%	9.7%
S5-NFL2[1]	$70.3\,(\text{N/cm})^2$	76.6°	20.8%	1.1%
S5-NFL3[1]	$65.4\,(\text{N/cm})^2$	82.1°	12.8%	19.4%
S5-NFL4[1]	$63.4\,(\text{N/cm})^2$	81.2°	10.6%	5.4%
S5-NFL5[1]	$49.9\,(\text{N/cm})^2$	83.2°	6.5%	7.7%

[1] The stiffness matrix is positive definite.

Representation of the measured stiffness matrices using K_{size}, K_{shape}, K_{orient}, and Z_{mean}.

the differences can be attributed to a larger mechanical response of more recruited motor units caused by the comparatively "earlier" identification of stiffness [NH76].
Notice that the force sensor was chosen so as to measure stiffness as accurately as possible. The sensor was selected with a limited force range for a precise identification of stiffness. Therefore, however, it is not possible to measure maximum voluntary contraction. Furthermore, stiffness was always measured at the same reference position, independent of the subject's arm kinematics. The selected central position corresponds to an elbow angle (between forearm and upper arm) above 90° and leads to more elongated ellipses rather than isotropic ones and a limited change in orientation.
In conclusion,, the device will help to understand how to choose limits for robotic stiffness and relations for a proper cam disc design in variable stiffness actuators (see Chapter 4). The perturbation profile needs further improvement, i.e. reducing the perturbation amplitude to 8 mm which is used in standard literature [MIHB85] in order to reduce the size of the second time window. For future applications, it is of interest to relate measured stiffness to electromyographic data in order to measure stiffness continuously without the use of disturbing perturbations. These relations can help to control the compliance of robotic systems in tele-operational approaches.

4

Intrinsic Stiffness Modulation for Humanoid Robots

Chapters 2 and 3 report a linear relation between force and stiffness for humans. In this Chapter the application of this linear relation will be transferred to a robotic joint principle called Bidirectional Antagonism with Variable Stiffness (BAVS), which can vary its *intrinsic* stiffness. The relation will be compared to the existing design in terms of analyzing the ability to decouple stiffness from force. Moreover, a two-joint planar VSA concept with and without biarticular coupling based on the BAVS will be presented and analyzed. The focus is to investigate the ability to adapt endpoint stiffness at zero net force. These two different types of VSAs will be compared and discussed in a simulation study in order to show what will be lost and what can be gained in a system with biarticular coupling. For this, a method will be proposed that allows to investigate the full ability of a mechanism to change stiffness, and used to compare the two types of VSA.

4.1 Principle of BAVS

All analyses within this Chapter have in common that they are based on a principle called Bidirectional Antagonism with Variable Stiffness (BAVS) [FHPH11], which is implemented in the forearm rotation and both wrist joints of the DLR Hand Arm System [GASB$^+$11]. It is based on a normal antagonistic mechanism, as found in nature, but allows both, agonist and antagonist, to push and pull at the drive side of the joint and assist each other. Therefore, the term *helping antagonism* is used often (a VIACTORS data sheet of the BAVS can be found in [Höp11]). BAVS is neither tendon-driven (possible drawback: tendon creeping) nor based on artificial pneumatic muscles (possible drawback: highly non-linear), and was introduced in [FHPH11]. Fig. 4.1 (top) depicts a simplified version of it. The motors can be turned around their motor axis instead of being fixed to a base frame. The two motors are coupled with the base by non-linear elastic elements.
The position of the joint can be changed by same-directional motor movement, while its stiffness is changed by an opposed motor movement. The realization as it is implemented in the DLR Hand Arm System is shown in Fig. 4.1 (bottom). The two non-linear elastic elements are realized using a combination of a linear spring and a cam disc with a non-linear relation between its rotation and the resulting spring deflection. In order to fix the motors to the base frame and to use their full power, a Harmonic Drive with a bedded circular spline, coupled to the non-linear elastic element is used (arrangement of the harmonic drive similar to a planetary gear). Please

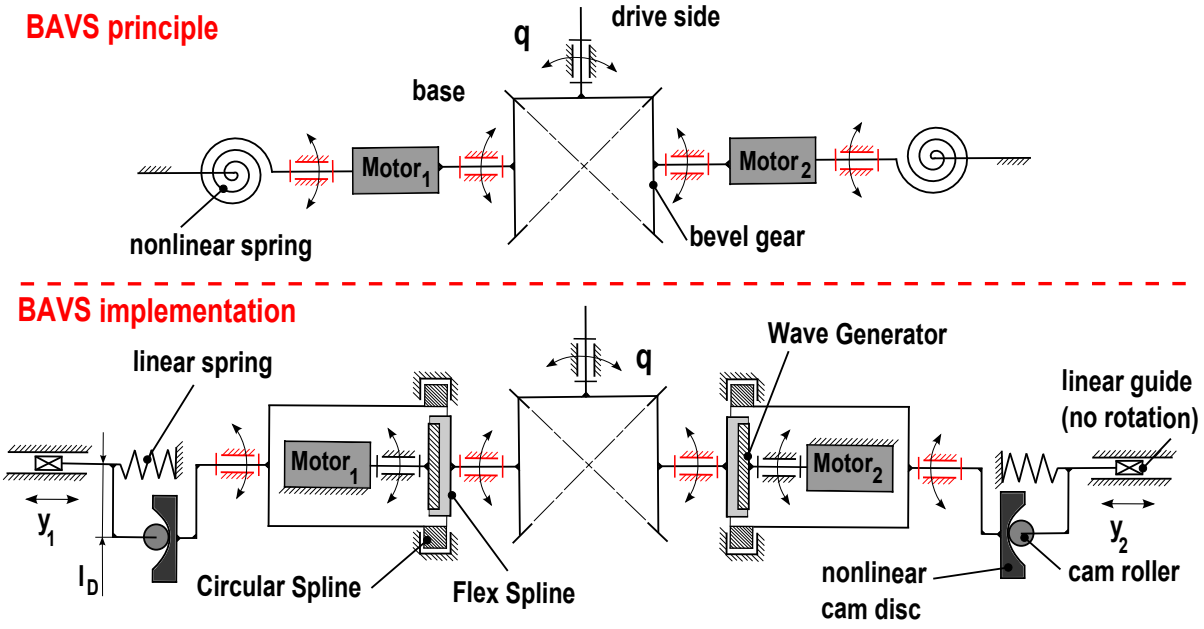

Figure 4.1: Principle of Bidirectional Antagonism with Variable Stiffness (reproduced from [HWvdS14] ©2014 IEEE). — The upper figure shows a simplified representation of BAVS, the lower figure the version of a double spring solution with symmetric cam discs. Note that for reasons of presentability the two cam discs are depicted orthogonal to the image plane.

note that the notation *normal mode* is used to describe the joint operation of joint torques below a maximum single motor torque τ_{stall}, and *helping mode* to describe joint torques in the range of $\tau_{\text{stall}} < \tau \leq 2 \cdot \tau_{\text{stall}}$ according to [FHPH11].

4.2 Cam Disc Design—Implementing the Force–Stiffness Characteristic

The most important mechanical characteristics of VSAs are their torque–velocity and torque–stiffness profiles [GWG+15]. While possible insights on the torque–velocity profile for the design of VSA can be revealed using Hill's Equation (1.1), there are no comparable references in literature for the torque–stiffness relation. Taking a look at state-of-the-art of VSAs (see Fig. 4.2), it becomes obvious that there is no common understanding of what their torque–stiffness characteristic should look like. Some of these curves are convex, some are concave. The MACCEPA, for example, joint is more or less unable to decouple torque and stiffness above 30 % of maximum joint torque. It turns out that the profiles result from the mechanical principle used rather than guiding the mechanism design by characteristic torque–stiffness criteria.
In Section 2.4, linearity between force and intrinsic stiffness in humans is reported. Moreover, Section 2.5 states that a human's ability to decouple force and stiffness increases with force, i.e. the human is able to decouple the two also for higher forces, opposed to the properties of several existing VSA mechanisms (see Fig. 4.2). Nevertheless, the possibility to decouple stiffness from force allows to match task requirements, i.e. according to its dynamics, and save considerable amounts of energy, since cocontraction efforts high metabolic costs. In this Section, the use of the linear relation as a design criterion is investigated and its implementation for VSAs on the example of the DLR BAVS mechanism is discussed. Furthermore, the resulting ability of the mechanism to decouple stiffness from torque (force, respectively) will be examined. As discussed in Section 2.2, the linear relation results in an exponential relation between force and displacement. Hence, it is called *the exponential approach* in this Section.

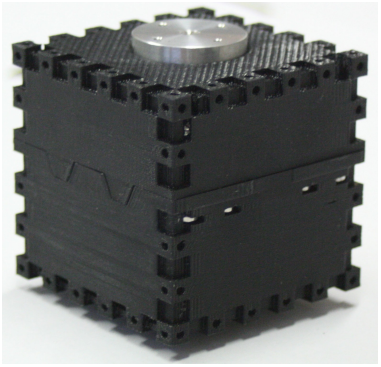

(a) VSA-cube (reprinted from [dP11]); [CGG+11].

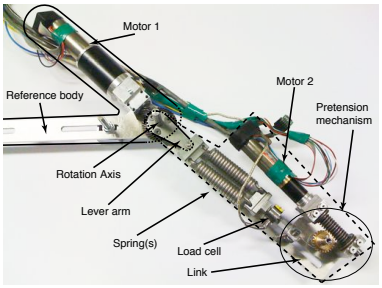

(b) MACCEPA joint (reprinted from [oB11]); [VHVVD+07].

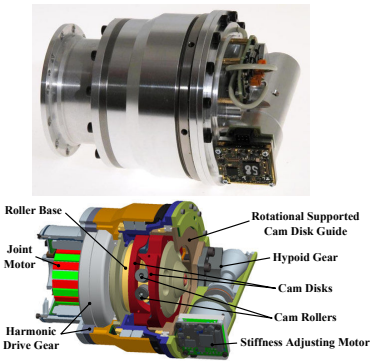

(c) DLR FSJ [Wol11] (reproduced from [WEH11] ©2011 IEEE).

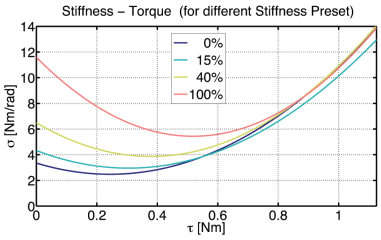

(d) VSA-cube: Torque–Stiffness profile (reprinted from [dP11]); [CGG+11].

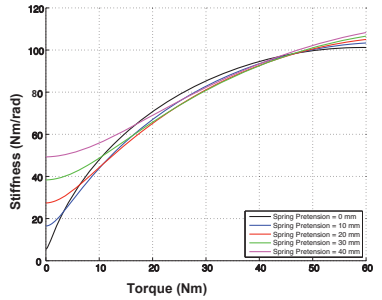

(e) MACEPPA: Torque–Stiffness profile (reprinted from [oB11]); [VHVVD+07].

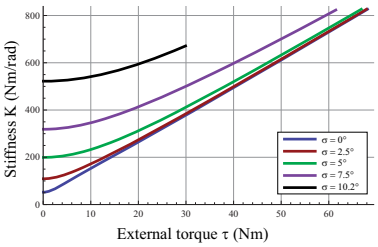

(f) DLR FSJ: Torque–Stiffness profile [Wol11] (reproduced from [WEH11] ©2011 IEEE).

Figure 4.2: Torque–Stiffness profiles of common state-of-the-art variable-stiffness actuators. — Each of the torque–stiffness profiles corresponds to the mechanism depicted on top. Noticeably, there is no common understanding of what these curves should look like.

The passive behavior, i.e. stiffness, of the BAVS joint is dominated by the non-linear spring, namely the cam disc shape and linear spring. Fig. 4.3 represents possible combinations which will be discussed in this Chapter. Fig. 4.4 depicts their implementations in the mechanical design of the DLR Hand Arm System.
Independent of these combinations, the stiffness r at the joint can be calculated by

$$r = \frac{\partial \tau}{\partial q}, \tag{4.1}$$

with τ being the joint torque and $q = [-q_{\max} \dots q_{\max}]$ its externally incurred deflection. The maximum possible deflection is set to $q_{\max} = 15.5°$ (chosen according to design specific conditions).

4.2.1 Single-Spring Solution with Symmetric Cam Disc Design—Exponential Approach

The single-spring solution with symmetric cam disc shape is depicted in Figs. 4.3(a) and 4.4(a). The movement of the two cam discs pretension the same spring. Hence it is called *single-spring solution*. According to [FHPH11] its joint torque τ can be computed by

$$\begin{aligned} \tau(\sigma, q) &= c_F \, l_D \, (y_1 + y_2) \, (y_1' + y_2') \,, \text{with} \\ y_1 &= f(\sigma + q) \,, \quad \text{and} \quad y_2 = f(\sigma - q) \,, \end{aligned} \tag{4.2}$$

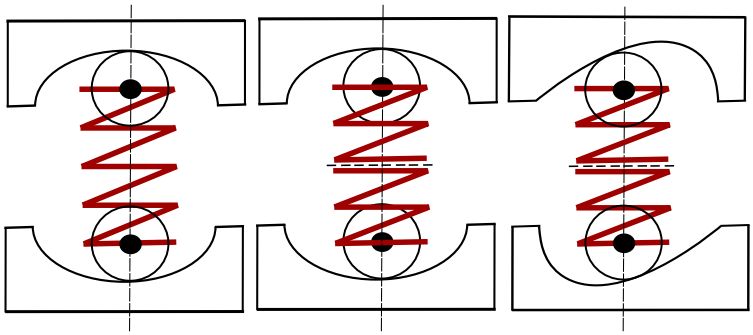

(a) Single-spring solution with symmetric cam disc shape.

(b) Double-spring solution with symmetric cam disc shape.

(c) Double-spring solution with asymmetric cam disc shape.

Figure 4.3: Possible combinations of linear springs and cam discs (adapted from [PFHG14] ©2015 IEEE).

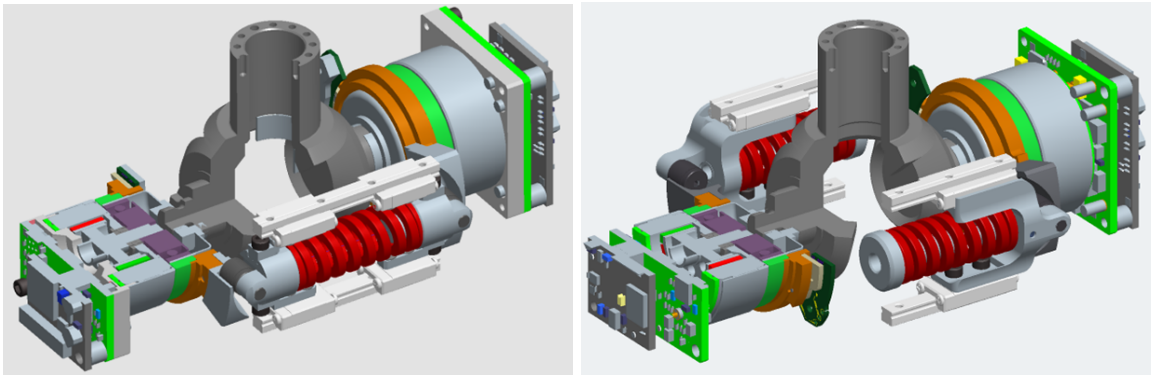

(a) Bidirectional Antagonism with Variable Stiffness as it was recently implemented in the forearm rotation of the DLR Hand Arm System with symmetric cam disc shape and single-spring solution.

(b) Bidirectional Antagonism with Variable Stiffness as it is currently implemented in the forearm rotation of the DLR Hand Arm System with asymmetric cam disc shape and double-spring solution.

Figure 4.4: Comparison of the old and new mechanical design of the forearm-rotation (reprinted from [HWvdS14] ©2014 IEEE). — (a) The old design had a single-spring solution with symmetric cam disc shape. (b) The new design uses a double-spring solution with asymmetric cam disc shape.

where $\sigma = [-q_{\max} \dots q_{\max}]$ is the pretension of the joint, $c_F = 22.1\,\mathrm{N/mm}$ the single-spring stiffness, $l_D = 21.65\,\mathrm{mm}$ the moment arm of the cam disc (both chosen according to design specific conditions), and $y_{1|2}$ and $y'_{1|2}$ the deflections of the spring-ends caused by the cam disc shapes and their slope.
The condition for linearity between torque and stiffness is

$$r(\tau) = c_1 \cdot \tau + c_2 = \frac{\partial \tau}{\partial q}, \tag{4.3}$$

where c_1 and c_2 are constants. Solving the differential equation leads to

$$\tau\,(\sigma, q) = \frac{c_2}{c_1} \cdot (\exp(c_1 \cdot |q|) - 1) \tag{4.4}$$

and thus an exponential relation between joint torque and its deflection under the condition (C1) of $\tau(0) = 0$ that the torque at no pretension should be zero.
Under the premise of condition (C2) $\tau(q_{\max}) = \tau_{\max}$, which is a limitation of torque to the

maximum motor torque at maximum pretension of the joint, it follows that

$$\tau\left(\sigma, q\right) = \tau_{\max}\left(\frac{\exp(c_1 \cdot |q|) - 1}{\exp(c_1 \cdot |q_{\max}|) - 1}\right), \text{ and} \tag{4.5}$$

$$r(\tau) = c_1 \cdot \tau_{\max}\left(\frac{\exp(c_1 \cdot |q|)}{\exp(c_1 \cdot |q_{\max}|) - 1}\right). \tag{4.6}$$

Using Eq. (4.2), modeling of the single-spring solution, and $x = q \cdot l_D$ leads to

$$y_{1|2}\left(\sigma, q\right) = \pm\sqrt{c_3 + \frac{\tau_{\max}}{c_F \cdot l_D} \cdot \frac{x - \frac{l_D}{c_1} \cdot \exp\left(\frac{c_1}{l_D} \cdot x\right)}{1 - \exp\left(\frac{c_1}{l_D} \cdot x_{\max}\right)}}, \tag{4.7}$$

where x is the length of the straight cam disc curve. Under the condition (C3) $y(0) = y_0$, implying that the linear spring should always have a minimum pretension $y_0 = 2\,\text{mm}$, it follows that

$$c_3 = {y_0}^2 + \frac{\tau_{\max}}{c_F \cdot c_1 \cdot \left(1 - \exp\left(\frac{c_1}{l_D} \cdot x_{\max}\right)\right)}. \tag{4.8}$$

This condition is of particular relevance, since it cancels mechanical clearance. Finally, a condition (C4) for c_1 has to be defined: minimum joint-stiffness at no pretension $r(0) = r_{\min}$[1]. However, for this last condition (C4) there is no symbolic solution available and a numeric only. Fortunately, the further condition $y'(0) = 0$ is an inherent design characteristic of the exponential approach.

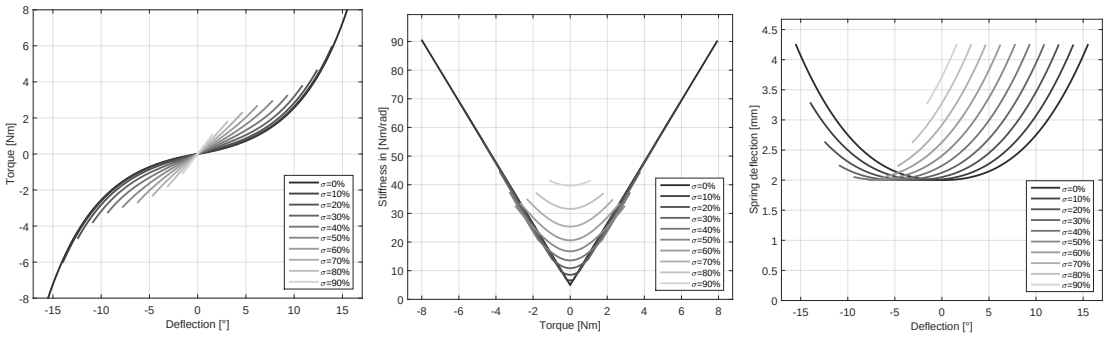

(a) Joint-torque depending on the joint-deflection.

(b) Joint-stiffness depending on the joint torque.

(c) Spring-deflection depending on the incurred joint-deflection.

Figure 4.5: Single-spring solution with symmetric cam disc design and an exponential relation between torque and displacement.

Fig. 4.5 shows a numerical solution for the single-spring solution with symmetric cam disc design and an exponential relation between torque and displacement. The graphs can be interpreted as follows: The step size between the curves is an increase of 10 % of the maximum pretension $\sigma_{\max}$. The highest pretension shown is 90 %. Keep in mind that for any torque higher than $\tau_{\text{stall}} = 4\,\text{Nm}$ one motor has to assist the other, which is the stall torque of the motors used. E.g., for σ =50 % both motors are preloaded with 2 Nm against each other. This means, at 50 % pretension any torque higher than 2 Nm can be reached only by using the helping mode.

[1]Please note that an alternative condition (C4) might be to limit the maximum deflection of the spring $y(q_{\max}) = y_{\max}$.

The conditions $r_{\min} = 5\,\mathrm{Nm/rad}$, $q_{\max} = \pm 15.5°$, and $\tau_{\max} = 8\,\mathrm{Nm}$ are clearly visible in the graphs. As it can be seen in Fig. 4.5(b), the joint-stiffness can be decoupled for low motor torques between $\pm 2\,\mathrm{Nm}$ only. This is in general not a desirable characteristic for variable-stiffness actuators. Moreover, the desired linear relation is achieved for pretensions below approximately 30 % only. For no pretension $\sigma = 0\,\%$ the curve is perfectly linear.

4.2.2 Double-Spring Solution with Symmetric Cam Disc Design—Exponential Approach

In order to overcome this drawback, a double-spring solution has been developed [FHPH11] (see Figs. 4.3(b) and 4.4(b)). According to [FHPH11] the joint torque τ of the double-spring solution can be computed by

$$\tau\left(\sigma, q\right) = c_F\, l_D\, \left(y_1 y_1' + y_2 y_2'\right). \tag{4.9}$$

Similarly to Eqs. (4.7) and (4.8), this leads to

$$y_{1|2}\left(\sigma, q\right) = \pm \sqrt{c_3 + \frac{2 \cdot \tau_{\max}}{c_F \cdot l_D} \cdot \frac{x - \frac{l_D}{c_1} \cdot \exp\left(\frac{c_1}{l_D} \cdot x\right)}{1 - \exp\left(\frac{c_1}{l_D} \cdot x_{\max}\right)}}, \text{ with} \tag{4.10}$$

$$c_3 = {y_0}^2 + \frac{2 \cdot \tau_{\max}}{c_F \cdot c_1 \cdot \left(1 - \exp\left(\frac{c_1}{l_D} \cdot x_{\max}\right)\right)}.$$

The resulting joint behavior is depicted in Fig. 4.6.

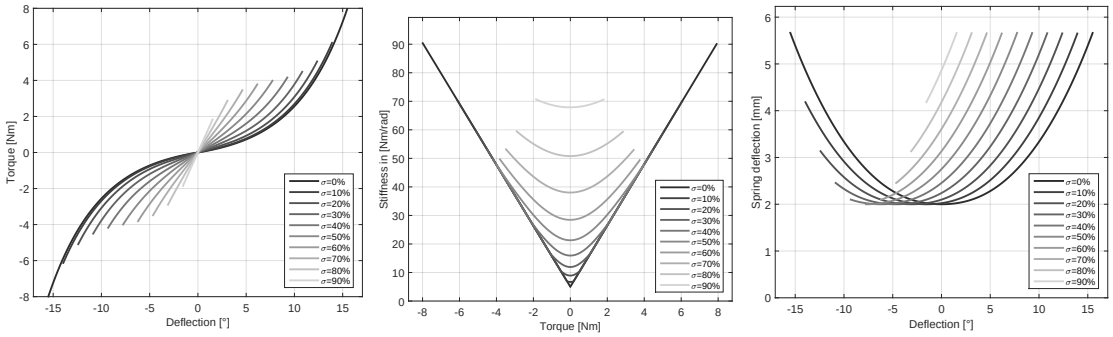

(a) Joint-torque depending on the joint-deflection.

(b) Joint-stiffness depending on the joint torque.

(c) Spring-deflection depending on the incurred joint-deflection.

Figure 4.6: Double-spring solution with symmetric cam disc design and an exponential relation between torque and displacement.

The improvement of the desired torque–stiffness characteristic is clearly visible. The ability of the mechanism to decouple stiffness from torque has been increased considerably. Moreover, this configuration is able to store twice the elastic energy in comparison to the single-spring solution. Nevertheless, there is no variability of the joint-stiffness in the helping mode, meaning for torques higher than the maximum torque of a single motor $\tau_{\mathrm{stall}} = 4\,\mathrm{Nm}$.

4.2.3 Double-Spring Solution with Asymmetric Cam Disc Design—Exponential Approach

In order to avoid discontinuities, the radius of the cam roller should be smaller than the radius of the cam disc. This leads to mechanical clearance-like behavior at no pretension and no

applied torque at the joint. In order to overcome this issue, an asymmetric cam disc design is implemented in a double-spring solution in the current forearm rotation of the DLR Hand Arm System (see Fig. 4.3(c)). This requires conditions (C1)–(C4) to be reached within $[q_{\max} - q_{\text{asym}} \cdots - q_{\max} + q_{\text{asym}}]$ on each of the two sides of the cam disc. q_{asym} is arbitrarily set to 5°. The double-spring solution with asymmetric cam disc shape is depicted in Figs. 4.3(c) and 4.4(b); moreover, its numerical solution is depicted in Fig. 4.7.

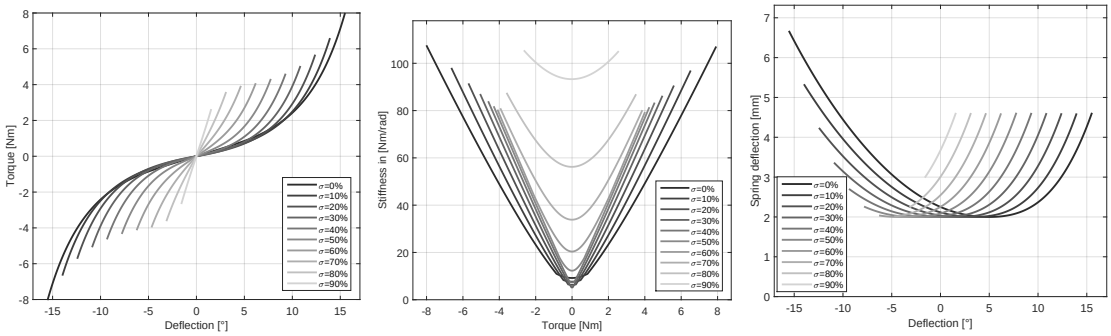

(a) Joint-torque depending on the joint-deflection.

(b) Joint-stiffness depending on the joint torque.

(c) Spring-deflection depending on the incurred joint-deflection.

Figure 4.7: Double-spring solution with asymmetric cam disc design and an exponential relation between torque and displacement.

The asymmetric shape with zero-crossing at $q_{\text{asym}} = 5°$ for $\sigma = 0\,\%$ is clearly visible in Fig. 4.7(c). Surprisingly, the asymmetric shape not only improves the joint behavior at zero pretension. It further improves the linear torque–stiffness relation also for higher pretensions (see Fig. 4.7(b)). Moreover, the designed characteristic is able to decouple stiffness from torque for the helping mode, as well. The drawback of the asymmetric design is its behavior at zero torque: the stiffness decreases with an increase of pretension until $\sigma = 50\,\%$, making it difficult to control the joint at zero torque.

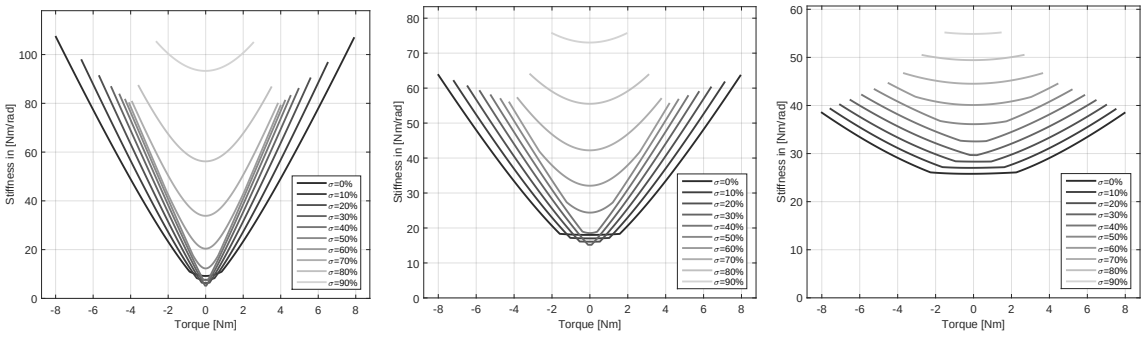

(a) $r_{\min} = 5\,\text{Nm/rad}$.

(b) $r_{\min} = 15\,\text{Nm/rad}$.

(c) $r_{\min} = 30\,\text{Nm/rad}$.

Figure 4.8: Double-spring solution with asymmetric cam disc design and an exponential relation between torque and displacement. — Influence of varying the condition (C4) $r(0) = r_{\min}$.

Fig. 4.8 exhibits that this drawback can be compensated by increasing $r_{\min}$. Yet, this results in (a) a reduced maximum stiffness of the joint, (b) a reduced maximum increase of stiffness (bandwidth), and (c) a flat torque–stiffness profile for the lower pretensions and torques. Surprisingly, the slopes of the linear relation match for different pretensions by increasing stiffness at zero torque $r_{\min}$ (see Fig. 4.8(c)).

For the purpose of easy controlling being able to explicitly differentiate the curve is essential. Further, the first and second derivative have to be continuous. Since no symbolic solution exists for the approach discussed, an approximation of the cam disc shape is depicted in Fig. 4.9 using a 5th order polynomial[2]:

$$y_{1|2}(\sigma, q) = 1.16e^{-4} \cdot x^5 + 9.0e^{-4} \cdot x^4 - 8.2e^{-4} \cdot x^3 + 6.7e^{-2} \cdot x^2 - 0.28 \cdot x + 2.27. \tag{4.11}$$

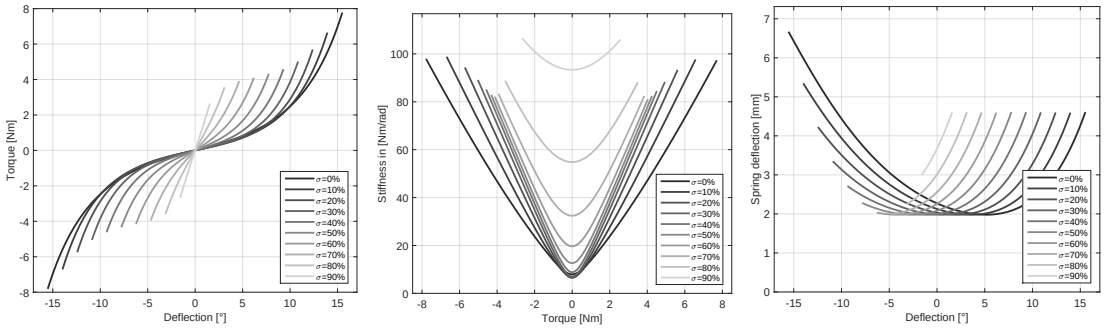

(a) Joint-torque depending on the joint-deflection.

(b) Joint-stiffness depending on the joint torque.

(c) Spring-deflection depending on the incurred joint-deflection.

Figure 4.9: Double-spring solution with approximated asymmetric cam disc design and an exponential relation between torque and displacement. — Approximation of the cam disc shape using a 5th order polynomial.

While the curvature is preserved quantitatively, the maximum joint-stiffness differs. Moreover, the concern of a decreasing stiffness with an increase of pretension at zero torque is reduced.

4.2.4 Double-Spring Solution with Asymmetric Cam Disc Design—Cubic Approach

Since an optimal design criterion for torque–stiffness characteristics of cam discs was unknown at the very beginning of the DLR Hand Arm System development, an asymmetric cam disc shape with a cubic relation between torque and displacement was chosen and is implemented in the forearm rotation [FHPH11][3]. The asymmetric cam disc shape with a cubic relation between torque and displacement is modeled by a quadratic cam disc shape

$$y_{1|2}(\sigma, q) = \begin{cases} R_1 - \sqrt{\left(R_1^2 - (x - x_{\text{asym}})^2\right)} + y_0 & : x \leq x_{\text{asym}}, \\ R_2 - \sqrt{\left(R_2^2 - (x - x_{\text{asym}})^2\right)} + y_0 & : x > x_{\text{asym}}, \end{cases} \tag{4.12}$$

where $R_{1|2}$ are different radii realizing condition (C2) on the two sides of the cam disc. The conditions $y'(0) = 0$ and $\tau(0) = 0$ are inherent characteristics of the cubic approach.
The resulting joint characteristics as implemented in the forearm rotation are depicted in Fig. 4.10.
In comparison to the exponential approach in Fig. 4.7(b), the cubic approach is able to reach higher maximum stiffness (cf. Fig. 4.10(b)). Moreover, the ability to decouple stiffness from

[2]Please note: while the curves of Fig. 4.9(c) are approximations of Eq. 4.10, Figs. 4.9(a) and 4.9(b) are derived from these approximated curves.

[3]Differently to this Thesis, the cubic approach was dubbed in [FHPH11] as *quadratic shape/design*, referring to the shape of the cam disc, and not to the relation between torque and displacement.

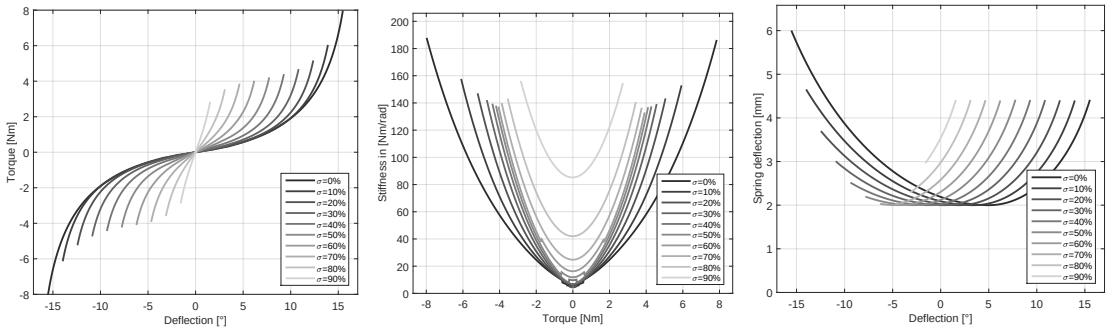

(a) Joint-torque depending on the joint-deflection.

(b) Joint-stiffness depending on the joint torque.

(c) Spring-deflection depending on the incurred joint-deflection.

Figure 4.10: Double-spring solution with an asymmetric cam disc shape and a cubic relation between torque and displacement.

torque is comparable to the exponential approach. However, discontinuities in the second derivative of the shape lead to steps in the torque–stiffness profile for the lower torques. Yet, it is questionable if these discontinuities are relevant for physical cam discs, since manufacturing of the discs is most-likely smoothen their shape. Hence these discontinuities lead to serious control problems and require the application of look-up-tables, a 5th order polynomial approximation of the cam disc shape

$$y_{1|2}(\sigma, q) = 7.6e^{-5} \cdot x^5 + 1.1e^{-3} \cdot x^4 - 5.5e^{-4} \cdot x^3 + 4.8e^{-2} \cdot x^2 - 0.20 \cdot x + 2.20 \tag{4.13}$$

should be implemented as depicted in Fig. 4.11.

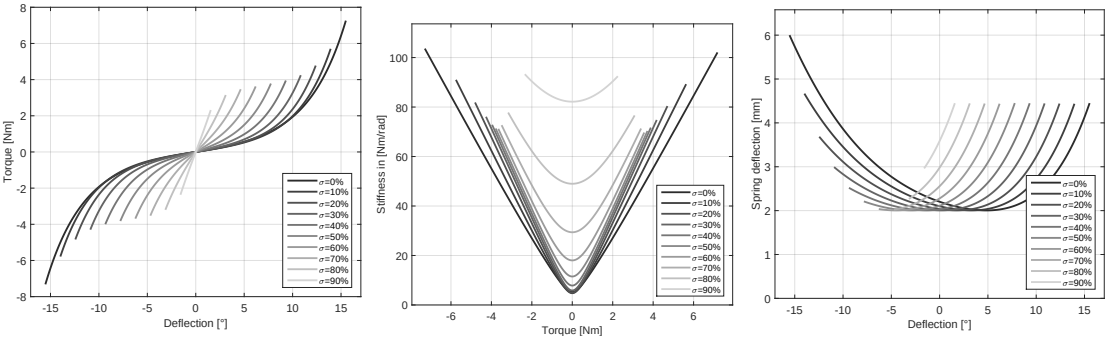

(a) Joint-torque depending on the joint-deflection.

(b) Joint-stiffness depending on the joint torque.

(c) Spring-deflection depending on the incurred joint-deflection.

Figure 4.11: Double-spring solution with approximated asymmetric cam disc shape and a cubic relation between torque and displacement. — Approximation of the cam disc shape using a 5th order polynomial.

4.3 Biarticular Variable Stiffness Actuator

VSAs are actively being researched because of their ability to absorb energy during highly dynamic impacts and their possibility to temporarily store elastic energy [MS95, ER99, BT04, MBD05, GvdS08, GASB+11, BPH+13]. Furthermore, humans modulate impedance in order to meet accuracy demands during goal-directed arm movements [SBD06]. However, all existing tendon-free VSAs are designed such that they are only able to change stiffness and position

of one joint (mono-articular actuators). In biology, however, one finds many multi-articulated skeletal muscles, crossing more than one joint and thus changing both stiffness and position of each joint when activated. A special case of these groups of muscles are biarticular muscles, with the prominent examples biceps and triceps brachii, coupling shoulder and elbow. The role of these muscles is as follows:

- *morphing endpoint stiffness*—In [Eng99, pp. 361–366] English *et al.* analyzed the influence of biarticular muscles based on a musculo-skeletal model of the human arm. They revealed that the loss of biarticular muscles leads to a more elongated stiffness ellipse (strong preferred displacement direction), a reduced maximum stiffness, a reduced possible orientation range and finally the result that stiffness produced by double-joint muscles cannot be replaced by using only single-joint stiffness.

- *stabilizing the limb*—McIntyre *et al.* discussed in [MMIB96] the role of destabilizing forces at the endpoint and their overall influence on joint torques. The amount of joint torque produced, e.g. in the elbow can affect the required stiffness at the shoulder. "*... With multi-joint muscles present, each muscle stiffness need be a function only of its own force output in order to maintain overall limb stability. The multi-articular muscles provide the necessary coupling between joints. This is an example of a mechanical design simplifying the control problem.*" The self-stabilizing characteristics of biarticular coupling were also shown by Iida *et al.* [IRS08], for both running and walking gaits.

- *independent control of force and position*—Kumamoto *et al.* showed [KOY94] that biarticular muscles allow for an independent control of endpoint force and position. Furthermore, they found that these muscles allow for an independent control of endpoint stiffness and output force direction.

- *open-loop control of position*—In [TGT75] Taub *et al.* showed that monkeys with deafferent limbs were able to reach visual targets with and without visual feedback of limb position. Consequently, Kumamoto *et al.* concluded [KOF00] that biarticular muscles allow for precise, smooth and rapid movement patterns of the endpoint without the use of any positional feedback. They concluded that "*... the arbitrary control of the output force direction, and elastic and viscous ellipses ... can move the endpoint precisely to any desired target point without use of a positional feedback signal, that is a possibility of an open loop control.*"

- *transferring energy*—biarticular muscles provide the capability to transport the mechanical output mainly produced by mono-articular muscles to joints where it can effectively contribute to the desired aim of movement [vIS89]. E.g., during running, instead of braking the knee using mono-articular muscles and dissipating the energy in form of heat, the biarticular muscles provide the possibility to optimally transfer the energy to the hip in order to maintain the forward motion.

In this Section it will be compared and discussed what will be lost and what can be gained in a system with biarticular coupling with respect to the possibility of alternating intrinsic stiffness.

4.3.1 Related Work

The use of biarticularity in robotic design is nothing new. Different implementations have been proposed: either by tendon-driven actuation with base-fixed motors [IRS08, KKO04, SKOH11, Bab12], by pneumatic artificial muscles [KOY94, NK10, RLvS12], by planetary gears [KOH10, OKH10, USH10], by pulleys [YHOH09], or by directly coupling a linear motor with the end-effector [NIN+12]. However, even if some of these actuators are able to change their

active (controlled) stiffness (e.g. impedance control [NIN+12] or stiffness control for disturbance rejection [OKH10, YHOH09]), not all of these actuators are designed to change their intrinsic stiffness [Bab12, KOH10, OKH10, USH10, YHOH09, NIN+12] even when actuated by six actuators for two joints [SKOH11].
One of the main objectives of many studies is to show what is gained with biarticular coupling with respect to endpoint force production [SKOH11, NK10, USH10, YHOH09, KOF02]. It was shown that with biarticular coupling the shape of the maximum output force distribution at the endpoint becomes more homogeneous and changes from quadrangular to hexagonal.
A view also concentrated on the ability to change intrinsic stiffness [KOY94, KOF00, KKO04, KOKH11]. In [KKO04] Kadota *et al.* built a tendon-based robotic platform with biarticular coupling called *HIPRO*. *HIPRO* consists of six actuators arranged in an antagonistic manner with non-linear elastic elements for a planar robotic system with two DoF. It was shown that the system can vary the position of the endpoint with negligible effects on the orientation of the Cartesian endpoint stiffness ellipse[4].
In [KOY94] and [KOF00], Kumamoto *et al.* investigated the capabilities of a robotic planar arm with two DoF actuated by six pneumatic artificial muscles. As mentioned before the authors showed that a biarticular coupling will positively contribute to the compliant properties and allows for independent control of either endpoint position and force or endpoint force direction and stiffness. Furthermore it was shown that this coupling will lead to smooth, fine, and precise movement patterns of the endpoint.
Another study which concentrates on stiffness ellipse control using VSA mechanisms with biarticular coupling was presented by Kashiwagi *et al.* [KOKH11]. They proposed a control method called *hybrid stiffness ellipse control* which merges mechanical and controlled stiffness of a tendon-based two-DoF planar robotic actuator with six muscle-like VSA and ideal exponential elastic elements. Biarticular coupling was provided in order to be able to change all elements of the mechanical joint stiffness matrix. With simulated perturbations they showed that their control method is always able to adapt to a desired control stiffness, while the initial response is dominated by the adjusted intrinsic mechanical stiffness.

4.3.2 Types

Mono-articular VSA System

The mono-articular VSA system that is analyzed within this Section is a planar robotic system with two DoF, elbow and shoulder joint, whose joints are based on the BAVS principle explained above. The system has no biarticular coupling. Unlike the implementation in the DLR Hand Arm System (see Fig. 4.4(b)), a double-spring solution with *symmetric* cam disc shape is chosen for both joints, thus simplifying the comparability for the planned analysis (see Fig. 4.4(a)). In this joint configuration the maximum stall torque of a single joint is $\pm 8\,\mathrm{Nm}$ and the maximum joint stiffness $127.6\,\mathrm{Nm/rad}$.

Biarticular VSA System

The proposed biarticular VSA system contains two mono-articular joints described above and a biarticular coupling (see red dashed regions in Fig. 4.12).
The two joints are coupled using two series of non-linear elastic elements and rotatory motors. The biarticular stiffness is changed by opposed movement of the biarticular coupling motors 3 and 4. In contrast to, e.g., the human legs, this configuration is able to adjust both joint positions and mono-articular as well as biarticular joint stiffnesses independently.

[4]Unfortunately, the paper is written in Japanese, and the author was not able to fully understand it.

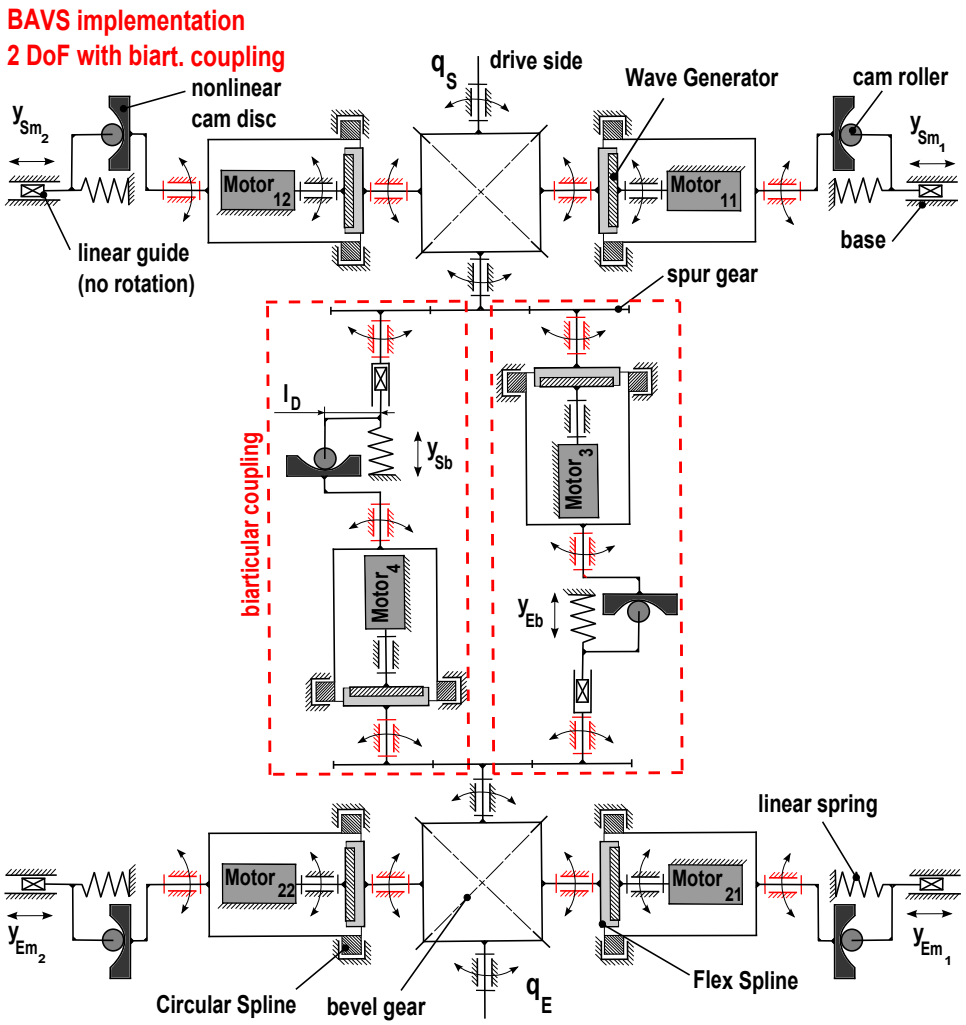

Figure 4.12: A biarticular VSA system with six actuators and two DoF (reproduced from [HWvdS14] ©2014 IEEE). —The two drive sides of the arm are at the bottom and top of each figure. Imagine the depicted base as the upper arm of an elbow-shoulder configuration.

This is realized through the cam disc–roller combination—contrary to the mono-articular BAVS—by rotating about the motor axis without changing their relative orientations. Thus, by identical movements of motors 3 and 4 the joint positions can be changed without changing the biarticular or mono-articular stiffnesses.
In order to equally compare the mono-articular and biarticular VSA systems in terms of stiffness adaptability, identical components—same motors, springs and cam discs—are used: the motor is fixed to the frame using a Harmonic Drive with a bedded circular spline; the non-linear elastic element is again realized by a combination of symmetric cam discs and linear springs. The symmetric cam disc shape used is indeed not the optimal configuration presented in [FHPH11] and Section 4.2. But if an asymmetric cam disc shape would be used, different behavior depending on ratios of pretension of biarticular and mono-articular actuators could emerge, which makes it hard to equitably compare both principles. E.g., it would be difficult to keep the joint position constant during cocontraction of the biarticular elastic elements.

4.3.3 Analysis and Results

In this Subsection the two systems will be modeled and compared with respect to adjustable static stiffness; no effects of damping and inertia will be considered. Even if the difference

between the two mechanisms would be more obvious in joint space because the biarticular VSA is also able to adjust off-diagonal joint stiffness terms, they will be compared in Cartesian space. This way of comparison is more intuitive due to its comparability to human measurements, e.g. [Hog85b] or as they are done within Chapter 3. The analysis of the different types is done by modeling a planar two-DoF arm systems with shoulder (S) and elbow (E) joints (see Fig. 3.1).

Model

The torque at the shoulder τ_S and elbow τ_E joint can be calculated by

$$\tau_{S|E} = \tau_{S|E_{\text{mon}}} + \tau_{\text{biart}}, \tag{4.14}$$

where $\tau_{S|E_{\text{mon}}}$ is the torque produced by the mono-articular and τ_{biart} the torque produced by the biarticular actuators at the shoulder and elbow joint. Similar to Eq. (4.9) of Section 4.2 the torque produced by one BAVS with a double spring solution can be calculated by

$$\begin{aligned} \tau_{S_{\text{mon}}}(\sigma_{m_S}, q_S) &= c_F\, l_D \left(y_{S_{m1}} y'_{S_{m1}} + y_{S_{m2}} y'_{S_{m2}}\right) \\ \tau_{E_{\text{mon}}}(\sigma_{m_E}, q_E) &= c_F\, l_D \left(y_{E_{m1}} y'_{E_{m1}} + y_{E_{m2}} y'_{E_{m2}}\right), \end{aligned} \tag{4.15}$$

where $\sigma_{m_{S|E}}$ are the pretension and $q_{S|E}$ the external deflections of the shoulder and elbow joint. y_m and y'_m are the deflections of the springs and the correspondent cam disc slope (see Fig. 4.12). The torque of the biarticular actuators can be derived by

$$\tau_{\text{biart}}(\sigma_b, q_S, q_E) = c_F\, l_D \left(y_{S_b} y'_{S_b} + y_{E_b} y'_{E_b}\right), \tag{4.16}$$

and depends on the biarticular pretension σ_b and the external joint deflections $q_{S|E}$.
Similar to Eq. (4.12), the symmetric cam disc with quadratic shape can be modelled by

$$y_{1|2}(\sigma \pm q) = R - \sqrt{R^2 - (l_D(\sigma \pm q))^2} + y_0, \tag{4.17}$$

where $R = 8.2\,\text{mm}$ is the radius of the symmetric cam disc, σ the pretension of the joint in $^\circ$ and $y_0 = 2\,\text{mm}$ the initial pretension of the spring. The maximum deflection of each cam disc is limited by $\pm 18^\circ$ being the maximum deflection of the joint around an equilibrium position.
In general, the joint stiffness matrix can be calculated by $R = \partial T / \partial Q \in \mathbb{R}^{n \times n}$, where T and Q are the joint torques and the external joint deflections; n the number of joints. Because the stiffness of each joint can be changed, R is a square matrix. For the systems considered here this matrix equals

$$\begin{aligned} R &= \begin{bmatrix} r_{SS} & r_{SE} \\ r_{ES} & r_{EE} \end{bmatrix} \\ &= \begin{bmatrix} r_{S_{\text{mon}}} + r_{\text{biart}} & r_{\text{biart}} \\ r_{\text{biart}} & r_{E_{\text{mon}}} + r_{\text{biart}} \end{bmatrix}. \end{aligned} \tag{4.18}$$

The first index of the scalar entries of (4.18) indicates the entry of T, the second the entry of Q for the partial differentiation (cf. [Hog85b]). Note that for the mono-articular VSA no joint coupling is provided and thus the joint stiffness has no off-diagonal terms $r_{SE} = r_{ES} = 0$. If stiffness is computed around an equilibrium position, a mapping between joint and Cartesian stiffness can be achieved by

$$R = J(Q)^T\, K\, J(Q), \tag{4.19}$$

where $J(Q)$ is the Jacobian, which is a 2×2 matrix for the hand-arm model [ASFS+04]. Both stiffness matrices R and K are symmetric because the two systems are modeled as conservative systems. Eq. (4.19) can be rewritten as

$$K = J(Q)^{-T}\, R\, J(Q)^{-1}. \tag{4.20}$$

Because $J(Q)$ is square for the considered model its inverse can be computed. The Jacobian is obtained by

$$J(Q) = \begin{bmatrix} -l_S s_S - l_E s_{SE} & -l_E s_{SE} \\ l_S c_S + l_E c_{SE} & l_E c_{SE} \end{bmatrix}$$
$$s_S = \sin q_S \quad s_{SE} = \sin(q_S + q_E) \tag{4.21}$$
$$c_S = \cos q_S \quad c_{SE} = \cos(q_S + q_E),$$

and contains the information about the geometrical relations between the joints. q_S and q_E are the angles describing the position of the shoulder and elbow, l_S and l_E are the link length of the upper and lower arm, respectively.

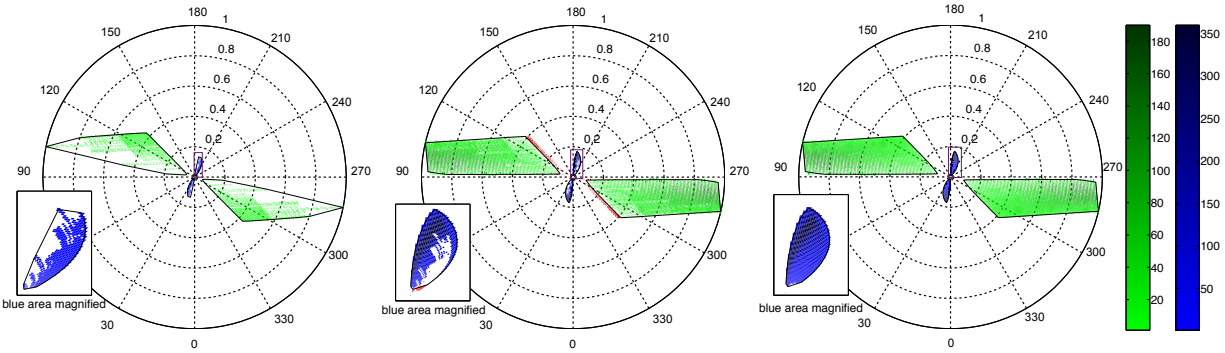

(a) mono-articular VSA (b) difference between mono-articular & biarticular VSA (c) biarticular VSA

Figure 4.13: Comparison of the Cartesian stiffness K that can be reached by the two systems and their difference (reproduced from [HWvdS14] ©2014 IEEE). — The eigenvalues of the (symmetric) Cartesian stiffness matrix and the orientation of the corresponding eigenvector are depicted. In Fig. 4.13(a) and 4.13(c) the larger eigenvalue $\lambda_{\max}$ is depicted in green, the small eigenvalue $\lambda_{\max}$ in blue in form of a distance to the center of the polar plot. The radius of the polar plot is normalized to range between 0 and 1 where a radius of 1 corresponds to the biggest $\lambda_{\max}$. The polar angle of each eigenvalue corresponds to the respective orientation. The darker a color of a segment the more often this eigenvalue was reached. Note that for aesthetic reasons the orientation of the eigenvectors was shifted by 180° (compare [ASFS+04]). The black line in each plot corresponds to the convex hull. The comparison in Fig. 4.13(b) shows in green and blue, which points can only be reached by the biarticular system, and in red which only the mono-articular system can reach. The mono-articular VSA can reach 0.2% of the 10^6 Cartesian stiffness combinations, whereas the biarticular VSA reaches 14.5%. The area of the convex hull enclosing the larger eigenvalue of the biarticular system is 1.6 times as large; the area of the convex hull enclosing the smaller eigenvalue twice as large as the mono-articular system.

Comparison of the Eigenvalues in Cartesian Space

It is obvious that the biarticular actuator can reach larger stiffness ranges than the mono-articular VSA, because the biarticular coupling increases off-diagonal as well as diagonal terms of the joint stiffness matrix R (see Eqs. (4.14)–(4.18)). In order to show what can be gained with respect to the biarticular coupling rather than showing how more actuators will increase the stiffness the compared Cartesian stiffness space will be limited to the maximum/ minimum range that the mono-articular actuator is able to reach ($4 \leq K_{xx} \leq 99\,\mathrm{N/m}$, $-99 \leq K_{xy/yx} \leq -4\,\mathrm{N/m}$ and $20 \leq K_{yy} \leq 498\,\mathrm{N/m}$). Thus the Cartesian stiffness matrix K is varied at the end-effector within the achievable range of Cartesian stiffness the mono-articular actuator is able to reach instead of varying stiffness in joint space. In order to keep the analysis simple, following restrictions are taken:

- The link lengths $l_S = l_E = l = 0.8\,\mathrm{m}$ are identical.
- As it can be seen from Eqs. (4.20) and (4.21), Cartesian stiffness K can be adjusted by changing the joint position and keeping joint stiffness R constant. Because the suggested

VSA systems are able to adjust their joint stiffness independent from joint position they will be compared in a central position with a shoulder angle fixed at 45° and an elbow angle of 90°.

- Changes in stiffness caused by cocontraction which can be preset by the VSA around an equilibrium position without any interaction with the environment will be allowed only. Changes in stiffness that will lead to a change in joint position or emerge from an external deflection of the joints will not be considered.
- Only cocontraction of respective antagonistic pairs will be allowed for the biarticular VSA. Thus, it will not be possible to contract a biarticular actuator against a mono-articular one and vice versa.

Cocontraction can be achieved by pretensioning the two mono-articular actuators σ_{m_S} and σ_{m_E} and for the biarticular VSA additionally by pretensioning the biarticular coupling σ_b. Because within this Section only stiffness around an equilibrium position without any external deflection is assumed, Eqs. (4.17), (4.15), and (4.16) depend on the mentioned pretensions.
The (symmetric) Cartesian stiffness matrix K was computed for 10^6 different configurations. These Cartesian stiffnesses were transformed to joint space and it was checked whether a corresponding set of combinations of mono-articular and biarticular cam disc pretensions within the maximum deflection of the cam discs could be found. The transformation of the set into joint space will typically lead to non-zero off-diagonal joint stiffness terms. Since the mono-articular VSA can only vary diagonal joint stiffness terms of R and a computation of R out of varying K will almost never lead to zero off-diagonal terms, they will be limited to a corresponding maximum pretension of 0.1° for the mono-articular VSA. This corresponds approximately to the accuracy within which the cam discs can be adjusted. If only exactly zero off-diagonal terms would be allowed for the mono-articular system, the capability of this system would be disproportionately high underestimated. Note that, in a real system as well, e.g. due to static friction, the computation of R out of a measured K of a system without biarticular coupling would most likely never lead to zero off-diagonal terms of R.
Following the representation in [ASFS+04], the distributions of Cartesian stiffnesses that can be reached by the two systems are depicted in Fig. 4.13. The mono-articular system is able to reach 0.2 %, the biarticular VSA 14.5 % of the 10^6 Cartesian stiffness combinations. Fig. 4.13(b) shows the difference between the compared systems. It shows that the biarticular coupling allows the system to reach many more eigenvalues of K than just the mono-articular system is capable of[5]. However, there are also sections which can only be reached by the mono-articular VSA. They will be examined more closely below.

Comparison of Shape and Orientation of Endpoint Stiffness

Hogan introduced in [Hog85b] a singular value decomposition of the endpoint stiffness matrix K to visualize the stiffness as an ellipse with its attributes size, shape and orientation as a way of graphical representation of the stiffness configuration at the endpoint and which were introduced in Section 3.1. The characteristics shape and orientation can be considered as criterion of quality while the size is a criterion of quantity. Since it is quite obvious that the biarticular VSA can generate higher stiffnesses with two more built-in springs, the focus in this Section is more on the quality rather than the quantity of stiffness that can be obtained by biarticular springs.
K_{shape} of 1 represents an ideal isotropic endpoint stiffness, i.e. the endpoint stiffness can be represented by a circle. It means that a force perturbing the endpoint in any direction would

[5]Note that, if the same representation would be used to depict the stiffness R in joint space, the mono-articular system will only be able to reach values along the horizontal and vertical axis, while the biarticular system will as well reach in-between stiffness combinations.

lead to an unique and proportional restoring force and displacement in exactly the opposite direction. Thus, it is reasonable to conclude that a K_{shape} of 1 is a desirable property and can be used as a metric for stability, e.g. for holding a position in unstable force fields or in a situation of an expected load with unknown impact direction [Mil02]. As Hogan discussed in [Hog85b] a mechanism without biarticular coupling will never be able to achieve ideal isotropy at the endpoint, and with biarticular coupling only in a limited space of an elbow angle larger than 90° and less than 180°. Using Eqs. (4.19) and (4.21) and the condition for isotropy at the endpoint [Hog85b]

$$K = \begin{bmatrix} -k & 0 \\ 0 & -k \end{bmatrix}, \tag{4.22}$$

it follows that the mechanism must hold the following condition in joint space:

$$R = \begin{bmatrix} r_{SS} & r_{SS}/2 \\ r_{SS}/2 & r_{SS}/(2 + 2\cos(q_E)) \end{bmatrix}, \tag{4.23}$$

to achieve isotropy at the end-effector. With Eq. (4.18) it follows that $r_{\text{biart}} = 2r_{S_{\text{mon}}}$ [Hog85b]. The condition shows that the joint stiffness of the biarticular coupling must be twice the stiffness of the mono-articular shoulder actuator to achieve isotropy at the endpoint. This condition is somewhat similar to the fact that the biarticular muscles in the human arm are much stronger compared to the mono-articular muscles. On the other hand, a large K_{shape} can be desirable in reaching movements with a perpendicular instable force field [FLM+07], where high stiffness is required in the direction of the unstable force field and low stiffness in the direction of the movement in order to stay on the track. All in all, it can be concluded that a wide range for K_{shape} with a minimum close to 1 is desirable.

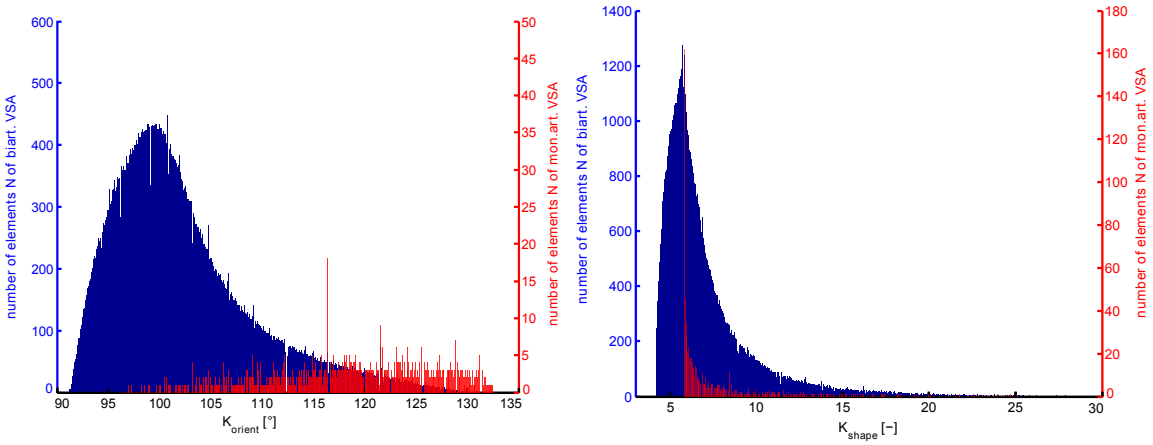

(a) Histogram of occurrence of K_{orient} for the reached K of the 10^6 Cartesian stiffness combinations.

(b) Histogram of occurrences of K_{shape} for the reached K of the 10^6 Cartesian stiffness combinations.

Figure 4.14: Histograms of occurrences of stiffness ellipse shape and orientation showing which how often which metric can be reached by either mechanism (reproduced from [HWvdS14] ©2014 IEEE).

In Fig. 4.14(b) the distribution of K_{shape} of the reachable Cartesian stiffness combinations for both actuator types is depicted in form of a histogram showing how often which K_{shape} can be reached by either mechanism. It shows that the minimum K_{shape} that can be reached by the mechanism with biarticular coupling is 4.2 and without 5.8. Additionally, the mechanism with biarticular coupling can reach values up to 29.0 while the mono-articular system has an upper limit of 25.1. The minimum K_{shape} of the mono-articular VSA is also its most often occurring K_{shape} and one of the most occurring values of the biarticular VSA and belong to Cartesian

stiffness combinations, where a large mono-articular shoulder joint stiffness r_{SS} and a small elbow joint stiffness r_{EE} is required. However, even if biarticular coupling is provided a K_{shape} of 1 cannot be reached. Further analysis showed that the minimum K_{shape} of the biarticular VSA remains the same even if the Cartesian space is not limited to the mono-articular stiffness. Nevertheless, in the proposed biarticular mechanism it is of interest to use the same springs for both, for the mono-articular actuators as well as for the biarticular, leading to a minimum K_{shape} unequal to 1.
Moreover, Fig. 4.14(a) shows the distribution of K_{orient} that could be reached by the two mechanisms (similar to Fig. 4.14(b)). It shows that the biarticular system covers a range of about 39.2° and the mono-articular system of about 36.2° of different K_{orient}. However, in contrast to K_{shape}, there are a few orientations up to 2.1° higher than the largest orientations of the biarticular VSA which appear either generally or more frequently be used by the mono-articular actuator. So why does the biarticular VSA, which has the same mono-articular properties, but additionally biarticular coupling, not reach these orientations? This is caused by the pretension y_0 of the biarticular springs, similar to the mono-articular springs. This pretension causes a positive shift in the stiffness r_{SS} and r_{EE} in a way that the difference between r_{SS} and r_{EE} decreases. As a result the orientation of the stiffness ellipse changes. Thus, if it is favored to reach also the higher orientations, the pretension of the biarticular springs had to be reduced, but it has to be considered that these larger orientations usually belong to a high K_{shape} (extremely elongated stiffness ellipse).

4.4 Discussion on Robots

In general, inherent characteristics of state-of-the-art VSAs—i.e. torque–velocity and torque–stiffness profiles—result from their mechanism technology. This Chapter proposes to use the linear relation between force and stiffness found in human as a criterion for synthesis of mechanism designs. Using the BAVS joint, it was demonstrated how the application of the linear relation will extend the capability for state-of-the-art VSAs to decouple stiffness from torque.
A cubic relation between torque and displacement is implemented in the forearm rotation of the DLR Hand Arm System causing control problems due to discontinuities in its derivatives of the shape. Control requires an easily differentiable equation. This Chapter introduces such equations for both, the exponential approach (see Fig. 4.9 and Eq. (4.11)), and for the cubic approach (see Fig. 4.11 and Eq. (4.13)). Visual inspection of both Figs. shows that the approximated exponential approach is slightly better at decoupling stiffness from torque. This holds not only at zero torque, but for the higher torques, as well, as found in humans (see Section 2.5). Moreover, the approximation of the exponential approach can reach higher torques. On the other side, the behavior at low torques and pretensions seems to be slightly better for the cubic approach, i.e. an increase of pretension will lead to an increase of stiffness.

Jafari analyzed the influence of the chosen relation between torque and displacement on the coupling between torque and stiffness for different types of VSAs, including a helping antagonism [Jaf14]. Comparing a quadratic, exponential, and cubic relation between torque and displacement he revealed that the exponential approach is most-likely the worst approach to chose, since it provides a maximal coupling between torque and stiffness, independently of the VSA principle. Using his defined measure α which ideally reflects the intensity of the coupling between torque and stiffness, Jafari claims that a quadratic relation between torque and displacement—resulting in stiffness depending on the square root of torque—is the optimal choice since it can totally decouple stiffness and external load for the analyzed antagonistic classes. For the exponential case, the author states *"... it would be difficult to consider the actuator as a VSA, since the unintentionally changes in the stiffness due to the external force occur in a far*

larger scale than can be controlled through the actuation unit . . . " [Jaf14].
It is most-likely that the results of Jafari correspond to the results of the straightforward single-spring solution with symmetric cam disc shape as depicted in Fig. 4.5. In this setup the helping antagonism is almost unable to decouple stiffness from torque for almost the full range of torque. As Jafari reported, his performed analysis only takes the mechanism principle into account, and does not consider its exact implementation. Similarly, Petit *et al.* (including the author of this Thesis) performed comparisons for *symmetric* cam disc designs, i.e. discussing the cubic and exponential approach [PFHG14]. From the performed analyses it was concluded that the linear torque–stiffness characteristic is unfavorable since variation of stiffness is also desired in the helping mode and a non-linear torque–stiffness relation has to be used.
Nature chose a linear relation between torque and stiffness for normal antagonistic principles, which can pull only. By simply copying this relation, a bad performance is found. This is not surprising, since a comparable *helping* antagonism is unknown in nature. Nevertheless, the results of Section 4.2 show that substantial improvement of the decoupling between torque and stiffness can be achieved by taking advantage of a double-spring solution with an asymmetric cam disc shape. In this configuration, the exponential approach is able to vary stiffness independently of torque even for higher forces within the helping mode, as well (see Fig. 4.7).
Independent of the named differences, in the author's opinion, the performed analyses of [Jaf14] take too narrow a view. If the exponential approach was the worst relation one could choose for antagonistic principles, why would nature choose it? And not a quadratic relation between force and displacement, which allows for a better decoupling as suggested by [Jaf14]? As mentioned in Subsection 1.2.3, Shadmehr revealed that *stiffness needs to increase at least linearly with force* in order to provide joint stability during cocontraction [SA92]. However, the condition *increasing at least linearly with force* contradicts a quadratic relation between force and displacement—in other words stiffness depending on the square root of force—as suggested in [Jaf14][6].

Moreover, a mechanism of a VSA with biarticular coupling was proposed within this Chapter. The biarticular mechanism is based on the BAVS principle, introduced in [FHPH11]. Thus, the biarticular mechanism is able to independently change endpoint stiffness and position. Furthermore, a change in mono-articular stiffness will not lead to a change in biarticular stiffness and vice versa, thus giving more control stability.
A simulation study investigated how systems with vs. without biarticular coupling can reach a range of Cartesian endpoint stiffnesses. A method to plot multiple sets of stiffness configurations as described in [ASFS$^+$04] was used to compare different planar VSA mechanisms. With respect to stiffness reachability, a biarticular coupling considerably extends the system capabilities by a 70-fold improvement in versatility and is therefore strongly favored over solely mono-articular ones.
The range of orientations and shapes of Cartesian endpoint stiffness ellipses that the proposed biarticular actuator can reach is slightly larger than that of a purely mono-articular system. Additionally, with 39.2° the range of orientations of the biarticular system is larger than that found in studies of humans with 30° [PKC02, GO98, DMG$^+$04]. Interestingly, the mono-articular mechanism reaches stiffness combinations that the biarticular VSA cannot reach; this can be attributed to the pretension of the biarticular springs.
It has to be acknowledged that more complex principles may enrich biarticular manipulator behavior. For instance, allowing to preload the biarticular actuator against a mono-articular one leads to non-symmetric cocontractions. Furthermore, if the system is designed with biarticular springs of twice the strength of the mono-articular ones, endpoint stiffness isotropy can be

[6] In order to avoid confusions: the *quadratic shape* refers to the shape of the cam disc and corresponds to a cubic relation between torque and displacement; the *quadratic relation* of Jafari [Jaf14] refers to a quadratic relation between torque and displacement.

achieved. This can be helpful for absorbing the energy of an expected load with unknown impact direction.
As already stated in the introduction of this Chapter, the BAVS design neither requires the use of pneumatic artificial muscles nor tendon-coupling, which can be advantageous if one aims at avoiding non-linearities due to tendon creeping, compressibility of air, and hysteresis effects of viscoelastic materials. Conversely, it cannot be claimed that the proposed approach is universally optimal; for instance, in comparison to tendon driven systems it increases inertia at the drive side of the joint.
Suitable applications for this actuator are humanoid robotics, in particular for constructing versatile arms and legs. But the approach is also useful for industrial robotics. As initially stated, the biarticular coupling will stabilize the locomotion system obtaining inherent mechanical stability, and thus simplifying the control problem. Furthermore, the possibility to transfer energy between joints can be used to reduce the amount of required energy during highly dynamic tasks. The increased stiffness range allows the system to assume bandwidth-dependent optimal stiffness. This is useful for, e.g. switching between running and walking gaits or in a pick-and-place task. On the other hand, the wide range of stiffnesses allows the system to be highly precise in a static positioning tasks, by being stiff in one direction and flexible in another.
Finally, it has to be noted that the biarticular coupling leads to mechanical complexity. The additional gears and motors introduce more backlash, tolerances, and friction issues. Implementing 6 motors for a planar 2-DoF movement seems like a mechanical overkill. Thus, in future work different underactuated versions of the proposed actuator and optimizing the stiffness ratios for mono-articular as well as for the biarticular actuators need to be addressed, e.g. with respect to ranges of Cartesian endpoint-stiffness-ellipse orientations and shapes and regarding its isotropy.

In general, we can learn that, (a) using the linear torque–stiffness relation found in humans seems to be a suitable criterion for the design of VSA mechanisms, and (b) that biarticular coupling can considerably improve stiffness versatility and should thus be considered for the design of robotic systems with multiple joints based on VSA technology.

5 Conclusion

Unnecessary mentioning it again—pure stiffness is linearly coupled to the applied force for the single areflexive TMC, observable in Cartesian space as well, i.e. at the wrist and fingers. Nevertheless, stiffness can be decoupled substantially from force under isometric conditions in different tasks or with the aid of cocontraction, which is presumably the most valuable and promising finding of this Thesis (Section 2.5). Applying the linear relation—an exponential relation between force and displacement—to an existing VSA technology, visual inspection shows a slightly increased performance in comparison to the existing approach (Section 4.2). However, existing literature states that *"... it would be difficult to consider the actuator as a VSA ..."*, which are based on an exponential relation between torque and displacement [Jaf14]. Albeit, the surprisingly good performance of subjects within Section 2.5—which naturally use an exponential approach—to decouple stiffness from force, and the results of applying the exponential approach to robotic VSA within Section 4.2 disagrees with this statement.

Another result of Section 2.5 is quite promising: by measuring the muscular activity of Mm. interossei it is possible to reveal relevant information about said stiffness of a pinch grip, while the measurement of grip force does no add much to regression. Nevertheless, the proof of an applicable method—including electrode placement, calibration, and commanding grip stiffness, e.g. to a robotic VSA hand—is still missing and needs to be verified in a separate set of experiments. The method allows to continuously teleoperate finger stiffness, *as it is decoupled from force*, to impedance controlled robotic hands, as well as hands based on VSA. The application and feedback of forces, e.g. during tasks of manipulation is highly relevant, since it is troublesome to manipulate with visual feedback only. However, state-of-the-art stiffness-teleoperation methods are based on commanding stiffness at zero net torque of the human arm only. For example, the work of Ajoudani *et al.* utilizes visual feedback from the task scene, but is unilateral in force [AGTB13, ATL+14]. This means that the arm position of the user is utilized to control the position of an impedance-controlled robot arm. Simultaneously, muscular activity of relevant muscles is measured to reveal information about users arm-stiffness and used to control the robot-impedance. Accordingly, users have no feedback about applied forces. Further, the calibration does not include information on how stiffness is decoupled by cocontraction at a certain force. Thus, as soon as force is applied by the arm—for purpose of feeding back forces from the task scene to the user—the change in the corresponding EMG will be interpreted as a change of stiffness only, making it impossible to give users a force feedback. Therefore, future

research will focus on the integration of the proposed method into the calibration process, (a) in order to accurately teleoperate stiffness, and (b) providing the possibility to feedback forces of the task scene. Similarly, the manipulandum presented in Section 3 for measuring arm stiffness will be used to investigate the relation between arm stiffness and muscular activation since a similar method for the arm would be highly valuable. This method has to be practicable, meaning that it allows for an easy placement of as few electrodes as possible and a negligible duration of required calibration.
Leidner *et al.* started categorizing *Compliant Manipulation Tasks* into a task taxonomy, e.g. by classifying tasks of contact/no contact, in-hand manipulation/external manipulation tasks, or tasks with and without deformation of the environment [LBD$^+$15]. By continuously measuring stiffness of hand and arm, it will be possible to measure a *task dependent stiffness* during activities of daily living, such as cutting an onion, cleaning with a sponge or connecting a plug [LBD$^+$15], and to add a meaningful range of hand and arm stiffness values to the derived taxonomy matrix.

The limitations of the performed measurements within Chapters 2 and 3 have to be mentioned, as well: The results of stiffness concern *static stiffness* measured during posture maintenance only. It is questionable, whether intrinsic stiffness measured during movement equals stiffness obtained during posture maintenance, since metrics of *dynamic stiffness* and *static stiffness* are compared, if not almost impossible to reveal. E.g. as indicated in Chapter 3 possibilities to alter stiffness highly increase during movement. But it remains unclear, whether this concerns intrinsic stiffness measured during movement, as well. Same is true for the calibration of measured stiffness to muscular activity, since it relies on static stiffness only. Thus, it is doubtful if the derived stiffness from the measurement of EMG still reflects the *real* stiffness of the hand and arm during highly-dynamic movements. This exhibits the troubles caused by using stiffness as a metric to describe human dynamics. The overall puzzle is lacking two essential pieces, possibly investigated in future: (a) it is of high interest whether the interossei dominate the measured grip stiffness, if it is possible to be revealed at all; (b) completing the analysis of Section 2.3, the influence of wrist flexion/extension and abduction/adduction on the measured force–stiffness relation and the corresponding muscular activity—in particular of Mm. interossei—is of interest.

Conclusively, industrial robots can be enriched by the implementation of VSA technology, not only due to their capability of limiting impact forces during collisions. Standard position controlled robotics dissipate considerable amounts of energy in form of heat by continuous acceleration and deceleration in reversal points. I.e., they are controlled such that their inherent mechanical properties are well identified and canceled out in control in order to accurately meet task dynamics and position, resulting in a high energetic effort. Addressing this purpose VSAs can provide the possibility to embody desired task behavior into the robotic structure [VSB11]. The mechanical properties can be exploited by pumping energy into the structure at optimal points and exciting the inherent mechanical resonance frequency of the system. This results in robotic systems performing *non-linear oscillations in cyclic movements* under minimal energetic costs [LPAS14]. By changing the intrinsic stiffness of the VSA and thus its resonance frequency, different types of oscillations can emerge. Finally, the implementation of the proposed biarticular VSA of Section 4.3 allows to considerably extend this task coordinate frame of desired compliant behavior, and allows for a broader variety of possible tasks which can be solved under minimal costs.

Bibliography

[AG80] G.C. Agarwal and G.L. Gottlieb. Effect of vibration of the ankle stretch reflex in man. *Electroencephalography and Clinical Neurophysiology*, 49(1-2):81–92, July 1980.

[AGTB13] A. Ajoudani, M. Gabiccini, N.G. Tsagarakis, and A. Bicchi. Human-like impedance and minimum effort control for natural and efficient manipulation. In *Robotics and Automation (ICRA), 2013 IEEE International Conference on*, pages 4499–4505, May 2013.

[AKP00] A.M. Acosta, R.F. Kirsch, and E.J. Perreault. A robotic manipulator for the characterization of two-dimensional dynamic stiffness using stochastic displacement perturbations. *Journal of Neuroscience Methods*, 102(2):177–186, 2000.

[AM84] J.H. Allum and K.-H. Mauritz. Compensation for intrinsic muscle stiffness by short-latency reflexes in human triceps surae muscles. *Journal of Neurophysiology*, 52(5):797–818, November 1984.

[AMS83] K. Akazawa, T.E. Milner, and R.B. Stein. Modulation of reflex EMG and stiffness in response to stretch of human finger muscle. *Journal of Neurophysiology*, 49(1):16–27, 1983.

[AMV82] J.H.J. Allum, K.-H. Mauritz, and H. Vögele. The mechanical effectiveness of short latency reflexes in human triceps surae muscles revealed by ischaemia and vibration. *Experimental Brain Research*, 48(1):153–156, 1982.

[Arn76] K.H. Arndt. Achillessehnenruptur und sport. *Leipzig: Johann Ambrosius Barth*, 1976.

[ASFS+04] A. Albu-Schäffer, M. Fischer, G. Schreiber, F. Schoeppe, and G. Hirzinger. Soft robotics: what Cartesian stiffness can obtain with passively compliant, uncoupled joints? In *Proceedings IEEE/RSJ International Conference on Intelligent Robots and Systems*, volume 4, pages 3295–3301, 2004.

[ASHO+07] A. Albu-Schäffer, S. Haddadin, C. Ott, A. Stemmer, T. Wimböck, and G. Hirzinger. The DLR lightweight robot: design and control concepts for robots in human environments. *Industrial Robot: an international journal*, 34(5):376–385, 2007.

[ATL+14] A. Ajoudani, N.G. Tsagarakis, J. Lee, M. Gabiccini, and A. Bicchi. Natural redundancy resolution in dual-arm manipulation using configuration dependent stiffness (CDS) control. In *Proceedings ICRA—International Conference on Robotics and Automation*, pages 3312–3316, 2014.

[Bab12] J. Babič. *Biarticular Actuation of Robotic Systems*, chapter 13, pages 251–270. InTech, February 2012.

[BFM13] E. Burdet, D.W. Franklin, and T.E. Milner. *Human Robotics: Neuromechanics and Motor Control*. MIT Press, 2013.

[BH99] P.W. Brand and A. Hollister. *Clinical Mechancis of the Hand*. Mosby, August 1999.

[BH08] B. Bäuml and G. Hirzinger. When hard realtime matters: Software for complex mechatronic systems. *Robotics and Autonomous Systems*, 56(1):5–13, 2008.

[BL00] I.E. Brown and G.E. Loeb. A reductionist approach to creating and using neuromusculoskeletal models. In *Biomechanics and neural control of posture and movement*, pages 148–163. Springer, 2000.

[BLMB04] T.S. Buchanan, D.G. Lloyd, K. Manal, and T.F. Besier. Neuromusculoskeletal modeling: estimation of muscle forces and joint moments and movements from measurements of neural command. *Journal of applied Biomechanics*, 20(4):367, 2004.

[BOF+00] E. Burdet, R. Osu, D.W. Franklin, T. Yoshioka, T.E. Milner, and M. Kawato. A method for measuring endpoint stiffness during multi-joint arm movements. *Journal of Biomechanics*, 33(12):1705–1709, December 2000.

[BOF+01] E. Burdet, R. Osu, D.W. Franklin, T.E. Milner, and M. Kawato. The central nervous system stabilizes unstable dynamics by learning optimal impedance. *Nature*, 414(6862):446–449, November 2001.

[Böh13] C. Böhm. Konzeptionierung und Auslegung eines planaren Manipulators zur reflexfreien Steifigkeitsmessung des menschlichen Arms. Diploma Thesis, DLR interner Bericht, University of Applied Sciences, Munich, April 2013.

[BPH+13] D.J. Braun, F. Petit, F. Huber, S. Haddadin, P. van der Smagt, A. Albu-Schäffer, and S. Vijayakumar. Robots driven by compliant actuators: Optimal control under actuation constraints. *IEEE Transactions on Robotics*, 99(5):1–17, 2013.

[BS14] R. Balasubramanian and V.J. Santos. *The human hand as an inspiration for robot hand development*. Springer, 2014.

[BT04] A. Bicchi and G. Tonietti. Fast and soft arm tactics: dealing with the safety-performance trade-off in robot arms design and control. *IEEE Robotics and Automation Mag.*, 11:22–33, 2004.

[CCG93] R.R. Carter, P.E. Crago, and P.H. Gorman. Nonlinear stretch reflex interaction during cocontraction. *Journal of Neurophysiology*, 69(3):943–952, 1993.

[CCK90] R.R. Carter, P.E. Crago, and M.W. Keith. Stiffness regulation by reflex action in the normal human hand. *Journal of Neurophysiology*, 64(1):105–118, 1990.

[CGG+11] M.G. Catalano, G. Grioli, M. Garabini, F. Bonomo, M. Mancinit, N. Tsagarakis, and A. Bicchi. VSA-cubebot: A modular variable stiffness platform for multiple degrees of freedom robots. In *Robotics and Automation (ICRA), 2011 IEEE International Conference on*, pages 5090–5095, May 2011.

[Cli07] K.S. Clippinger. *Dance Anatomy and Kinesiology*. Human Kinetics, 2007.

[Col13] OpenStax College. *Anatomy and Physiology*. OpenStax College `http://cnx.org/content/col11496/latest/`, June 2013.

[CSMA06] M. Casadio, V. Sanguineti, P.G. Morasso, and V. Arrichiello. Braccio di ferro: a new haptic workstation for neuromotor rehabilitation. *Technology and Health Care*, 14(3):123–142, 2006.

[CTG+14] D. Campolo, P. Tommasino, K. Gamage, J. Klein, C. Hughes, and L. Masia. H-Man: A planar, H-shape cabled differential robotic manipulandum for experiments on human motor control. *Journal of neuroscience methods*, 235:285–97, September 2014.

[Cut89] M.R. Cutkosky. On grasp choice, grasp models, and the design of hands for manufacturing tasks. *Robotics and Automation, IEEE Transactions on*, 5(3):269–279, June 1989.

[CWA00] D. Chablat, P. Wenger, and J. Angeles. Conception isotropique d'une morphologie parallèle: application à l'usinage, 3rd int. In *3th International Conference on Integrated Design and Manufacturing in Mechanical Engineering*, May 2000.

[CZ82] S.C. Cannon and G.I. Zahalak. The mechanical behavior of active human skeletal muscle in small oscillations. *Journal of Biomechanics*, 15(2):111–121, 1982.

[DH93] J. Duchateau and K. Hainaut. Behaviour of short and long latency reflexes in fatigued human muscles. *The Journal of Physiology*, 471(1):787–799, 1993.

[dL96] P. de Leva. Adjustments to Zatsiorsky-Seluyanov's segment inertia parameters. *Journal of Biomechanics*, 29(9):1223–1230, 1996.

[DLM87] C.J. De Luca and B. Mambrito. Voluntary control of motor units in human antagonist muscles: coactivation and reciprocal activation. *Journal of Neurophysiology*, 58(3):525–42, September 1987.

[DMG+04] M. Darainy, N. Malfait, P.L. Gribble, F. Towhidkhah, and D.J. Ostry. Learning to control arm stiffness under static conditions. *Journal of Neurophysiology*, 92(6):3344–3350, December 2004.

[dP11] Universita di Pisa. VSA-cube: Bidirectional agonistic - antagonistic; `http://www.viactors.org/{VSA}%20data%20sheets.htm` – VIACTORS VSA data sheet, 2011.

[DPSV91] P. Dyhre-Poulsen, E.B. Simonsen, and M. Voigt. Dynamic control of muscle stiffness and H-reflex modulation during hopping and jumping in man. *The Journal of Physiology*, 437(1):287–304, 1991.

[dV02] D. de Vaus. *Analyzing Social Science Data: 50 Key Problems in Data Analysis*. Sage Publications Inc., London, June 2002.

[dVSvdH+03] E. de Vlugt, A.C. Schouten, F.C.T. van der Helm, P.C. Teerhuis, and G.G. Brouwn. A force-controlled planar haptic device for movement control analysis of the human arm. *Journal of Neuroscience Methods*, 129(2):151–168, October 2003.

[dVvdHSB01] E. de Vlugt, F.C.T. van der Helm, A.C. Schouten, and G.G. Brouwn. Analysis of the reflexive feedback control loop during posture maintenance. *Biological cybernetics*, 84(2):133–141, February 2001.

[EB14] M.S. Erden and A. Billard. End-point impedance measurements at human hand during interactive manual welding with robot. In *Robotics and Automation (ICRA), 2014 IEEE International Conference on*, pages 126–133, May 2014.

[Eng99] C.E. English. *Stiffness behaviour in two degree of freedom mechanisms*. Ph.d. thesis, Carleton University, Ottawa, Ontario, December 1999.

[ER99] C.E. English and D. Russell. Implementation of variable joint stiffness through antagonistic actuation using rolamite springs. *Mechanism and Machine Theory*, 34(1):27–40, 1999.

[EWJ92] B.B. Edin, G. Westling, and R.S. Johannson. Independent control of human finger-tip forces at individual digits during precision lifting. *The Journal of Physiology*, 450:547–564, 1992.

[FCRG11] W. Friedl, M. Chalon, J. Reinecke, and M. Grebenstein. FAS—A flexible antagonistic spring element for a high performance over actuated hand. In *Intelligent Robots and Systems (IROS), 2011 IEEE/RSJ International Conference on*, pages 1366–1372, September 2011.

[FEK+91] H. Forssberg, A.C. Eliasson, H. Kinoshita, R.S. Johansson, and G. Westling. Development of human precision grip. I: Basic coordination of force. *Experimental Brain Research*, 85(2):451–457, 1991.

[FHPH11] W. Friedl, H. Höppner, F. Petit, and G. Hirzinger. Wrist and forearm rotation of the DLR hand arm system: Mechanical design, shape analysis and experimental validation. In *IEEE/RSJ International Conference on Intelligent Robots and Systems*, pages 1836–1842, 2011.

[FLM+07] D.W. Franklin, G. Liaw, T.E. Milner, R. Osu, E. Burdet, and M. Kawato. Endpoint stiffness of the arm is directionally tuned to instability in the environment. *The Journal of Neuroscience*, 27(29):7705–7716, 2007.

[Fri11] W. Friedl. A flexible antagonistic spring element (DLR FAS); `http://www.viactors.org/{VSA}%20data%20sheets.htm` – VIACTORS VSA data sheet, 2011.

[FT94] J.R. Flanagan and J.R. Tresilian. Grip-load force coupling: A general control strategy for transporting objects. *The Journal of Experimental Psychology: Human Perception and Performance*, 20:944–957, October 1994.

[FW93] J.R. Flanagan and A.M. Wing. Modulation of grip force with load force during point-to-point arm movements. *Experimental Brain Research*, 95:131–143, 1993. 10.1007/BF00229662.

[FW95] J. R. Flanagan and A. M. Wing. The stability of precision grip forces during cyclic arm movements with a hand-held load. *Experimental Brain Research*, 105:455–464, 1995.

[GASB+11] M. Grebenstein, A. Albu-Schäffer, T. Bahls, M. Chalon, O. Eiberger, W. Friedl, R. Gruber, S. Haddadin, U. Hagn, R. Haslinger, H. Höppner, S. Jörg, M. Nickl, A. Nothhelfer, F. Petit, J. Reill, N. Seitz, T. Wimböck, S. Wolf, T. Wüsthoff, and G. Hirzinger. The DLR hand arm system. In *IEEE International Conference on Robotics and Automation (ICRA)*, pages 3175–3182, May 2011.

[GD13] M. Große-Dunker. Untersuchung des Zusammenhangs von Fingerkinematik, Fingersteifigkeit und Muskelaktivität. Master Thesis, DLR interner Bericht, University of Applied Sciences, Munich, December 2013.

[GH24] H.S. Gasser and A.V. Hill. The dynamics of muscular contraction. *Proceedings of the Royal Society of London. Series B, containing papers of a biological character*, pages 398–437, 1924.

[GHJ66] A.M. Gordon, A.F. Huxley, and F.J. Julian. The variation in isometric tension with sarcomere length in vertebrate muscle fibres. *The Journal of physiology*, 184(1):170–192, 1966.

[GK96] H. Gomi and M. Kawato. Equilibrium-point control hypothesis examined by measured arm stiffness during multijoint movement. *Science (New York, N.Y.)*, 272(5258):117–20, April 1996.

[GK97] H. Gomi and M. Kawato. Human arm stiffness and equilibrium-point trajectory during multi-joint movement. *Biological cybernetics*, 76(3):163–171, 1997.

[GKHT97] H. Granzier, M. Kellermayer, M. Helmes, and K. Trombitas. Titin elasticity and mechanism of passive force development in rat cardiac myocytes probed by thin-filament extraction. *Biophysical Journal*, 73(4):2043–2053, 1997.

[Gla74] S.A. Glantz. A constitutive equation for the passive properties of muscle. *Journal of Biomechanics*, 7(2):137–145, 1974.

[GM79] P.R. Greene and T.A. McMahon. Reflex stiffness of man's anti-gravity muscles during kneebends while carrying extra weights. *Journal of Biomechanics*, 12(12):881–891, 1979.

[GMCM03] P.L. Gribble, L.I. Mullin, N. Cothros, and A. Mattar. Role of cocontraction in arm movement accuracy. *Journal of Neurophysiology*, 89(5):2396–2405, 2003.

[GO98] H. Gomi and R. Osu. Task-Dependent Viscoelasticity of Human Multijoint Arm and Its Spatial Characteristics for Interaction with Environments. *J. Neurosci.*, 18(21):8965–8978, November 1998.

[Gre14] M. Grebenstein. The Awiwi Hand: An Artificial Hand for the DLR Hand Arm System. In *Approaching Human Performance*, volume 98 of *Springer Tracts in Advanced Robotics*, pages 65–130. Springer International Publishing, 2014.

[GvdS08] M. Grebenstein and P. van der Smagt. Antagonism for a highly anthropomorphic hand-arm system. *Advanced Robotics*, 22(1):39–55, January 2008.

[GWG+15] G. Grioli, S. Wolf, M. Garabini, M. Catalano, and E. *et al.* Burdet. Variable stiffness actuators: The user's point of view. *The International Journal of Robotics Research*, 34(6):727–743, 2015.

[HA81] J.A. Hoffer and S. Andreassen. Regulation of soleus muscle stiffness in premammillary cats: intrinsic and reflex components. *Journal of Neurophysiology*, 45(2):267–285, 1981.

[Haj97] A.Z. Hajian. A characterization of the mechanical impedance of the human hands. *Ph.D., Harvard University*, September 1997.

[HASEH10] S. Haddadin, A. Albu-Schäfer, O. Eiberger, and G. Hirzinger. New insights concerning intrinsic joint elasticity for safety. In *Intelligent Robots and Systems (IROS), 2010 IEEE/RSJ International Conference on*, pages 2181–2187, October 2010.

[HASH07] S. Haddadin, A. Albu-Schäffer, and G Hirzinger. Safety evaluation of physical human-robot interaction via crash-testing. In *Robotics: Science and Systems*, volume 3, pages 217–224, 2007.

[HC02] C.J. Hasser and M.R. Cutkosky. System identification of the human hand grasping a haptic knob. In *HAPTICS '02: Proceedings of the 10th Symposium on Haptic Interfaces for Virtual Environment and Teleoperator Systems*, page 180, Washington, DC, USA, 2002. IEEE Computer Society.

[HFDKR00] H.J. Hermens, B. Freriks, C. Disselhorst-Klug, and G. Rau. Development of recommendations for s{EMG} sensors and sensor placement procedures. *Journal of Electromyography and Kinesiology*, 10(5):361–374, 2000.

[HGDSvdS16] H. Höppner, M. Große-Dunker, G. Stillfried, and P. van der Smagt. Key insights into hand biomechanics: On decoupling grip stiffness from force by cocontraction and stiffness-regression from electromyography. *submitted to Frontiers in Neurorobotics*, 2016.

[HGvdS15] H. Höppner, M. Grebenstein, and P. van der Smagt. Two-dimensional orthoglide mechanism for revealing intrinsic human arm mechanical properties. In *2015 IEEE/RSJ International Conference on Intelligent Robots and Systems, Hamburg*, pages 1178–1185, September 2015.

[HH97] A.Z. Hajian and R.D. Howe. Identification of the mechanical impedance at the human finger tip. *Journal of Biomechanical Engineering*, 119(1):109–114, 1997.

[HHK+11] T. Hulin, K. Hertkorn, P. Kremer, S. Schätzle, Jordi Artigas, M. Sagardia, F. Zacharias, and C. Preusche. The DLR bimanual haptic device with optimized workspace. In *Robotics and Automation (ICRA), 2011 IEEE International Conference on*, pages 3441–3442, May 2011.

[Hil38] A.V. Hill. The heat of shortening and the dynamic constants of muscle. *Proceedings of the Royal Society of London. Series B - Biological Sciences*, 126(843):136–195, 1938.

[HIW09] I.S. Howard, J.N. Ingram, and D.M. Wolpert. A modular planar robotic manipulandum with end-point torque control. *Journal of Neuroscience Methods*, 181(2):199–211, 2009.

[HK82] I.W. Hunter and R.E. Kearney. Dynamics of human ankle stiffness: Variation with mean ankle torque. *Journal of Biomechanics*, 15(10):747–752, 1982.

[HKC+92] N. Hogan, H.I. Krebs, J. Charnnarong, P. Srikrishna, and A. Sharon. MIT-MANUS: a workstation for manual therapy and training. In *Robot and Human Communication, 1992. Proceedings., IEEE International Workshop on*, pages 161–165, September 1992.

[HLe13] H. Höppner, Deutsches Zentrum für Luft, Raumfahrt e.V., and 51147. Roboter-Gelenksystem, August 2013. DE Patent 102012214094.

[HLU+11] H. Höppner, D. Lakatos, H. Urbanek, C. Castellini, and P. van der Smagt. The Grasp Perturbator: Calibrating human grasp stiffness during a graded force task. In *Proceedings of IEEE International Conference on Robotics and Automation (ICRA), 2011*, pages 3312–3316, 2011.

[HMP11] X. Hu, W.M. Murray, and E.J. Perreault. Muscle short-range stiffness can be used to estimate the endpoint stiffness of the human arm. *Journal of neurophysiology*, 105(4):1633–1641, 2011.

[HMP12] X. Hu, W.M. Murray, and E.J. Perreault. Biomechanical constraints on the feedforward regulation of endpoint stiffness. *Journal of Neurophysiology*, 108(8):2083–2091, 2012.

[HMvdS13] H. Höppner, J. McIntyre, and P. van der Smagt. Task dependency of grip stiffness—A study of human grip force and grip stiffness dependency during two different tasks with same grip forces. *PLoS ONE*, 8(12):e80889, December 2013.

[HNJ+08] U. Hagn, M. Nickl, S. Jörg, G. Passig, T. Bahls, A. Nothhelfer, F. Hacker, L. Le-Tien, A. Albu-Schäffer, and R. *et al.* Konietschke. The DLR MIRO: a versatile lightweight robot for surgical applications. *Industrial Robot: An International Journal*, 35(4):324–336, 2008.

[Hog84] N. Hogan. Adaptive control of mechanical impedance by coactivation of antagonist muscles. *Automatic Control, IEEE Transactions on*, 29(8):681–690, August 1984.

[Hog85a] N. Hogan. Impedance control: An approach to manipulation: Part II—implementation. *Journal of dynamic systems, measurement, and control*, 107(1):8–16, 1985.

[Hog85b] N. Hogan. The mechanics of multi-joint posture and movement control. *Biological Cybernetics*, 52(5):315–331, 1985.

[Höp11] H. Höppner. Bidirectional antagonism with variable stiffness (DLR BAVS); `http://www.viactors.org/{VSA}%20data%20sheets.htm` – VIACTORS VSA data sheet, 2011.

[HS71] A.F. Huxley and R.M. Simmons. Proposed mechanism of force generation in striated muscle. *Nature*, 233(5321):533–538, 1971.

[Hux57a] A.F. Huxley. Muscle structure and theories of contraction. *Progress in Biophysics & Biological Chemistry*, 7:255–318, 1957.

[Hux57b] H.E. Huxley. The double array of filaments in cross-striated muscle. *The Journal of Biophysical and Biochemical Cytology*, 3(5):631–648, 1957.

[Hux04] A.F. Huxley. A.F. huxley. In L.R. Squire, editor, *The History of Neuroscience in Autobiography*, volume 4 of *The History of Neuroscience in Autobiography*, pages 282–318. Academic Press, 2004.

[HWH+90] J.D. Harry, A.W. Ward, N.C. Heglund, D.L. Morgan, and T.A. McMahon. Cross-bridge cycling theories cannot explain high-speed lengthening behavior in frog muscle. *Biophysical Journal*, 57(2):201–208, 1990.

[HWvdS14] H. Höppner, W. Wiedmeyer, and P. van der Smagt. A new biarticular joint mechanism to extend stiffness ranges. In *Proceedings of IEEE International Conference on Robotics and Automation (ICRA), 2014*, pages 3403–3410, May 2014.

[IR04] K. Iqbal and A. Roy. Stabilizing PID controllers for a single-link biomechanical model with position, velocity, and force feedback. *Journal of biomechanical engineering*, 126(6):838–843, 2004.

[IRS08] F. Iida, J. Rummel, and A. Seyfarth. Bipedal walking and running with spring-like biarticular muscles. *Journal of Biomechanics*, 41(3):656–667, 2008.

[IVC11] J.M. Inouye and F.J. Valero-Cuevas. Regulation of human arm stiffness is heavily dependent on existence of muscle synergies. In *Proceedings of the 16th Annual Fred S. Grodins Graduate Research Symposium, Los Angeles, CA*, pages 2–3, 2011.

[Jaf14] A. Jafari. Coupling between the output force and stiffness in different variable stiffness actuators. *Actuators*, 3(3):270–284, 2014.

[Jin14] Z. Jin. *Computational modelling of biomechanics and biotribology in the musculoskeletal system: biomaterials and tissues*. Elsevier, 2014.

[JR69] G.C. Joyce and P.M.H. Rack. Isotonic lengthening and shortening movements of cat soleus muscle. *The Journal of Physiology*, 204(2):475–491, 1969.

[JRW69] G.C. Joyce, P.M.H. Rack, and D.R. Westbury. The mechanical properties of cat soleus muscle during controlled lengthening and shortening movements. *The Journal of Physiology*, 204(2):461–474, 1969.

[JW84] R.S. Johannson and G. Westling. Roles of glabrous skin receptors and sensorimotor memory in automatic control of precision grip when lifting rougher or more slippery objects. *Experimental Brain Research*, 56:550–554, 1984.

[KCJ97] I. Kao, M.R. Cutkosky, and R.S. Johansson. Robotic stiffness control and calibration as applied to human grasping tasks. *Robotics and Automation, IEEE Transactions on*, 13(4):557–566, August 1997.

[KCR+14] L.A. Kelly, A.G. Cresswell, S. Racinais, R. Whiteley, and G. Lichtwark. Intrinsic foot muscles have the capacity to control deformation of the longitudinal arch. *Journal of The Royal Society Interface*, 11(93), 2014.

[KH90] R.E. Kearney and I.W. Hunter. System identification of human joint dynamics. *Critical Reviews in Biomedical Engineering*, 18(1):55–87, 1990.

[KKIT96] H. Kinoshita, S. Kawai, K. Ikuta, and T. Teraoka. Individual finger forces acting on a grasped object during shaking actions. *Ergonomics*, 39(2):243–256, 1996.

[KKO04] Z. Fukai K. Kadota, K. Suzuki and T. Oda. Study on the basic robot platform model "HIPRO" using biarticular muscles functions—evaluation of biarticular muscles functions by the robot arm using VEA-(in japanese). In *The Japan Society for Precision Engineering, Committee of Biological Control System and Its Applied Technology, workshop*, pages 11–16, 2004.

[KOF00] M. Kumamoto, T. Oshima, and T. Fujikawa. Control properties of a two-joint link mechanism equipped with mono- and biarticular actuators. In *IEEE Int. Workshop on Robot and Human Interactive Communication*, pages 400–404, 2000.

[KOF02] M. Kumamoto, T. Oshima, and T. Fujikawa. Biarticular muscle as a principle keyword for biomimetic motor link system. In *Proc IEEE-EMB Conf. Microtechnologies in Medicine and Biology*, pages 346–351, 2002.

[KOH10] Y. Kimura, Sehoon Oh, and Y. Hori. Novel robot arm with bi-articular driving system using a planetary gear system and disturbance observer. In *IEEE International Workshop on Advanced Motion Control*, pages 296–301, March 2010.

[KOKH11] H. Kashiwagi, F. Okumura, S. Komada, and J. Hirai. Stiffness ellipse control of tendon mechanisms with nonlinear springs. In *Robotics and Biomimetics (ROBIO), 2011 IEEE International Conference on*, pages 1261–1266, December 2011.

[Kon05] P. Konrad. *EMG-Fibel: Eine praxisorientierte Einführung in die kinesiologische Elektromyographie*. Noraxon INC. USA, 1 edition, 2005.

[KOY94] M. Kumamoto, T. Oshima, and T. Yamamoto. Control properties induced by the existence of antagonistic pairs of biarticular muscles–mechanical engineering model analyses. *Human Movement Science*, 13(5):611–634, 1994.

[KPCT99] S.H. Kozin, S. Porter, P. Clark, and J.J. Thoder. The contribution of the intrinsic muscles to grip and pinch strength. *The Journal of Hand Surgery*, 24(1):64–72, 1999.

[KRB13] J. Klein, N. Roach, and E. Burdet. 3DOM: a 3 degree of freedom manipulandum to investigate redundant motor control. *IEEE transactions on haptics*, 7(2):229–39, 2013.

[KSP97] R.E. Kearney, R.B. Stein, and L. Parameswaran. Identification of intrinsic and reflex contributions to human ankle stiffness dynamics. *Biomedical Engineering, IEEE Transactions on*, 44(6):493–504, 1997.

[Lat94] M.L. Latash. Virtual trajectories and joint stiffness reconstructed with smooth perturbation technique under different instructions. *Journal of Biomechanics*, 27(6):732, 1994.

[LBD+15] D. Leidner, C. Borst, A. Dietrich, M. Beetz, and A. Albu-Schäffer. Classifying compliant manipulation tasks for automated planning in robotics. In *to be published at the 2015 IEEE/RSJ International Conference on Intelligent Robots and Systems, Hamburg*, September 2015.

[Lie02] R.L. Lieber. *Skeletal Muscle Structure, Function, and Plasticity*. Lippincott Williams & Wilkins, second edition, 2002.

[LKP+99] R.T. Lauer, K.L. Kilgore, P.H. Peckham, N. Bhadra, and M.W. Keith. The function of the finger intrinsic muscles in response to electrical stimulation. *Rehabilitation Engineering, IEEE Transactions on*, 7(1):19–26, March 1999.

[LPAS14] D. Lakatos, F. Petit, and A. Albu-Schäffer. Nonlinear oscillations for cyclic movements in human and robotic arms. *Robotics, IEEE Transactions on*, 30(4):865–879, August 2014.

[LZ93] M.L. Latash and V.M. Zatsiorsky. Joint stiffness: Myth or reality? *Human Movement Science*, 12(6):653–692, December 1993.

[Man84] J. Mandel. *The Statistical Analysis of Experimental Data*. Courier Dover Publications Inc., September 1984.

[MBD05] S. Migliore, E. Brown, and S. Deweerth. Biologically inspired joint stiffness control. In *Proceedings IEEE International Conference on Robotics and Automation*, pages 4519–4524, 2005.

[MCLF95] T.E. Milner, C. Cloutier, A.B. Leger, and D.W. Franklin. Inability to activate muscles maximally during cocontraction and the effect on joint stiffness. *Experimental Brain Research*, 107(2):293–305, 1995.

[ME13] A.S. Mikhailov and G. Ertl. *Engineering of Chemical Complexity*. World Scientific, 2013.

[MF98] T.E. Milner and D.W. Franklin. Characterization of multijoint finger stiffness: dependence on finger posture and force direction. *Biomedical Engineering, IEEE Transactions on*, 45(11):1363–1375, November 1998.

[MH07] E.N. Marieb and K. Höhn. *Human Anatomy & Physiology*. Pearson Education, 2007.

[MIHB85] F.A. Mussa-Ivaldi, N. Hogan, and E. Bizzi. Neural, mechanical, and geometric factors subserving arm posture in humans. *The Journal of Neuroscience*, 5(10):2732–2743, 1985.

[Mil02] T.E. Milner. Contribution of geometry and joint stiffness to mechanical stability of the human arm. *Experimental Brain Research*, 143(4):515–519, 2002.

[MMIB96] J. McIntyre, F. Mussa-Ivaldi, and E. Bizzi. The control of stable postures in the multijoint arm. *Experimental brain research*, 110(2):248–64, July 1996.

[MS95] T. Morita and S. Sugano. Design and development of a new robot joint using a mechanical impedance adjuster. In *IEEE Int. Conf. on Robotics and Autom.*, pages 2469–2475, 1995.

[MSSM12] L. Masia, V. Squeri, G. Sandini, and P. Morasso. Measuring end-point stiffness by means of a modular mechatronic system. In *Robotics and Automation (ICRA), 2012 IEEE International Conference on*, pages 2471–2478, May 2012.

[MUSD13] M.J.H. Millard, T.K. Uchida, A. Seth, and S.L. Delp. Flexing computational muscle: Modeling and simulation of musculotendon dynamics. *Journal of Biomechanical Engineering*, 135(2):11, 2013.

[Mut02] N.M. Muthayya. *Human Physiology*. Jaypee Brothers Medical Publishers Ltd., third edition, 2002.

[MYT+13] S. Maeo, Y. Yoshitake, Y. Takai, T. Fukunaga, and H. Kanehisa. Effect of short-term maximal voluntary co-contraction training on neuromuscular function. *International journal of sports medicine*, 35(02):125–134, 2013.

[Nel01] O. Nelles. *Nonlinear System Identification*. Springer Berlin Heidelberg New York, 2001.

[NH76] T.R. Nichols and J.C. Houk. Improvement in linearity and regulation of stiffness that results from actions of stretch reflex. *Journal of Neurophysiology*, 39(1):119–142, 1976.

[NIN+12] Y. Nakata, A. Ide, Y. Nakamura, K. Hirata, and H. Ishiguro. Hopping of a monopedal robot with a biarticular muscle driven by electromagnetic linear actuators. In *Proceedings IEEE International Conference on Robotics and Automation*, pages 3153–3160, May 2012.

[NK10] R. Niiyama and Y. Kuniyoshi. Design principle based on maximum output force profile for a musculoskeletal robot. *Industrial Robot: An Int. Journal*, 37(3):250–255, 2010.

[Nob22] The Nobel-prize in Physiology or Medicine 1922; `http://www.nobelprize.org/nobel_prizes/medicine/laureates/1922/`, 1922.

[Nob63] The Nobel-prize in Physiology or Medicine 1963; `http://www.nobelprize.org/nobel_prizes/medicine/laureates/1963/`, 1963.

[oB11] Free University of Brussels. VUB mechanically adjustable and controllable compliance equilibrium position actuator (MACCEPA); `http://www.viactors.org/{VSA}%20data%20sheets.htm` – VIACTORS VSA data sheet, 2011.

[OFK+02] R. Osu, D.W. Franklin, H. Kato, H. Gomi, K. Domen, T. Yoshioka, and M. Kawato. Short- and long-term changes in joint co-contraction associated with motor learning as revealed from surface EMG. *Journal of neurophysiology*, 88(2):991–1004, 2002.

[OG99] R. Osu and H. Gomi. Multijoint muscle regulation mechanisms examined by measured human arm stiffness and EMG signals. *Journal of Neurophysiology*, 81(4):1458–1468, 1999.

[OHN+92] S.W. O'Driscoll, E. Horii, R. Ness, T.D. Cahalan, R.R. Richards, and K.-N. An. The relationship between wrist position, grasp size, and grip strength. *The Journal of Hand Surgery*, 17(1):169–177, 1992.

[OKH10] S. Oh, Y. Kimura, and Y. Hori. Reaction force control of robot manipulator based on biarticular muscle viscoelasticity control. In *IEEE/ASME International Conference on Advanced Intelligent Mechatronics*, pages 1105–1110, July 2010.

[OZL05] H. Olafsdottir, V.M. Zatsiorsky, and M.L. Latash. Is the thumb a fifth finger? a study of digit interaction during force production tasks. *Experimental Brain Research*, 160(2):203–213, 2005.

[PCK00] E.J. Perreault, P.E. Crago, and R.F. Kirsch. Estimation of intrinsic and reflex contributions to muscle dynamics: a modeling study. *Biomedical Engineering, IEEE Transactions on*, 47(11):1413–1421, November 2000.

[PCW06] A. Pashkevich, D. Chablat, and P. Wenger. Kinematics and workspace analysis of a three-axis parallel manipulator: The orthoglide. *Robotica*, 24(1):39–49, Januar 2006.

[Pet14] F.P. Petit. *Analysis and Control of Variable Stiffness Robots*. PhD thesis, Diss., Eidgenössische Technische Hochschule ETH Zürich, Nr. 22134, 2014.

[PFHG14] F. Petit, W. Friedl, H. Höppner, and M. Grebenstein. Analysis and synthesis of the bidirectional antagonistic variable stiffness mechanism. *Mechatronics, IEEE/ASME Transactions on*, PP(99):1–12, 2014.

[PKC01] E.J. Perreault, R.F. Kirsch, and P.E. Crago. Effects of voluntary force generation on the elastic components of endpoint stiffness. *Experimental Brain Research*, 141(3):312–323, 2001.

[PKC02] E.J. Perreault, R.F. Kirsch, and P.E. Crago. Voluntary control of static endpoint stiffness during force regulation tasks. *Journal of Neurophysiology*, 87(6):2808–2816, 2002.

[Pro86] M.B. Propp. A model of muscle contraction based upon component studies. *Lect. Math. Life Sci*, 16:61–119, 1986.

[RH01] D. Rancourt and N. Hogan. Dynamics of pushing. *J Mot Behav*, 33(4):351–362, December 2001.

[RLvS12] K. Radkhah, T. Lens, and O. von Stryk. Detailed dynamics modeling of BioBiped's monoarticular and biarticular tendon-driven actuation system. In *IEEE/RSJ International Conference on Intelligent Robots and Systems (IROS)*, pages 4243–4250, October 2012.

[RMH99] D.E. Rassier, B.R. MacIntosh, and W. Herzog. Length dependence of active force production in skeletal muscle. *Journal of Applied Physiology*, 86(5):1445–1457, 1999.

[RR07] A. Rahimi and B. Recht. Random features for large-scale kernel machines. In *Advances in neural information processing systems*, pages 1177–1184, 2007.

[RW06] C.E. Rasmussen and C.K.I. Williams. *Gaussian Processes for Machine Learning*. Adaptative computation and machine learning series. University Press Group Limited, 2006.

[SA92] R. Shadmehr and M. Arbib. A mathematical analysis of the force-stiffness characteristics of muscles in control of a single joint system. *Biological cybernetics*, 66(6):463–477, 1992.

[SBD05] L.P.J. Selen, P.J. Beek, and J.H. van Dieën. Can co-activation reduce kinematic variability? A simulation study. *Biological Cybernetics*, 93(5):373–381, 2005.

[SBD06] L.P.J. Selen, P.J. Beek, and J.H. van Dieën. Impedance is modulated to meet accuracy demands during goal-directed arm movements. *Experimental Brain Research*, 172(1):129–138, 2006.

[SH89] T. Sinkjær and R. Hayashi. Regulation of wrist stiffness by the stretch reflex. *Journal of Biomechanics*, 22(11-12):1133–1140, 1989.

[SHL+11] P. van der Smagt, H. Höppner, Deutsches Zentrum für Luft, Raumfahrt e.V., and 51147. Verfahren und Messsystem zur Messung der Steifigkeit von Körperteilen, October 2011. DE Patent 102010014895.

[SHSvdS14] G. Stillfried, U. Hillenbrand, M. Settles, and P. van der Smagt. MRI-based skeletal hand movement model. In R. Balasubramanian and V.J. Santos, editors, *The Human Hand as an Inspiration for Robot Hand Development*, volume 95 of *Springer Tracts in Advanced Robotics*, pages 49–75. Springer-Verlag, 2014.

[SKK09] D. Shin, J. Kim, and Y. Koike. A myokinetic arm model for estimating joint torque and stiffness from EMG signals during maintained posture. *Journal of Neurophysiology*, 101(1):387–401, 2009.

[SKOH11] V. Salvucci, Y. Kimura, Sehoon Oh, and Y. Hori. BiWi: Biarticularly actuated and wire driven robot arm. In *Proceedings IEEE Intl. Conf. Mechatronics*, pages 827–832, April 2011.

[SMIB93] R. Shadmehr, F.A. Mussa-Ivaldi, and E. Bizzi. Postural force fields of the human arm and their role in generating multijoint movements. *The Journal of neuroscience*, 13(1):45–62, 1993.

[SSS05] M. Schünke, E. Schulte, and U. Schumacher. *Prometheus - Allgemeine Anatomie und Bewegungssystem*. Prometheus LernAtlas der Anatomie. Thieme, 2005.

[STAH88] T. Sinkjær, E. Toft, S. Andreassen, and B. C. Hornemann. Muscle stiffness in human ankle dorsiflexors: intrinsic and reflex components. *Journal of Neurophysiology*, 60(3):1110–1121, 1988.

[Str98] S. Stroeve. Neuromuscular control model of the arm including feedback and feedforward components. *Acta psychologica*, 100(1):117–131, 1998.

[Str99] S. Stroeve. Impedance characteristics of a neuromusculoskeletal model of the human arm i. posture control. *Biological cybernetics*, 81(5-6):475–494, 1999.

[TGT75] E. Taub, I.A. Goldberg, and P. Taub. Deafferentation in monkeys: Pointing at a target without visual feedback. *Experimental Neurology*, 46(1):178–186, 1975.

[THT05] L. Tskhovrebova, A. Houmeida, and J. Trinick. Can the passive elasticity of muscle be explained directly from the mechanics of individual titin molecules? *Journal of Muscle Research & Cell Motility*, 26(6-8):285–289, 2005.

[TL86] I.M. Tarkka and T.A. Larsen. Short and long latency reflex responses elicited by electrical and mechanical stimulation in human hand muscle. *Acta Physiologica Scandinavica*, 128(1):71–76, 1986.

[USH10] A. Umemura, Y. Saito, and T. Haneyoshi. The rigidity of the bi-articular robotic arm with a planetary gear. In *IEEE International Workshop on Advanced Motion Control*, pages 490–495, March 2010.

[VASB+13] B. Vanderborght, A. Albu-Schäffer, A. Bicchi, E. Burdet, D.G. Caldwell, R. Carloni, M. Catalano, O. Eiberger, W. Friedl, G. Ganesh, M. Garabini, M. Grebenstein, G. Grioli, S. Haddadin, H. Höppner, A. Jafari, M. Laffranchi, D. Lefeber, F. Petit, S. Stramigioli, N. Tsagarakis, M. Van Damme, R. Van Ham, L.C. Visser, and S. Wolf. Variable impedance actuators: A review. *Robotics and Autonomous Systems*, 61(12):1601–1614, 2013.

[VD98] C.L. Van Doren. Grasp stiffness as a function of grasp force and finger span. *Motor Control*, 2(4):352–378, 1998.

[vdHSdVB02] F.C.T. van der Helm, A.C. Schouten, E. de Vlugt, and G.G. Brouwn. Identification of intrinsic and reflexive components of human arm dynamics during postural control. *Journal of Neuroscience Methods*, 119(1):1–14, September 2002.

[VHVVD+07] R. Van Ham, B. Vanderborght, M. Van Damme, B. Verrelst, and D. Lefeber. Maccepa, the mechanically adjustable compliance and controllable equilibrium position actuator: Design and implementation in a biped robot. *Robotics and Autonomous Systems*, 55(10):761–768, 2007.

[vIS89] G.-J. van Ingen Schenau. From rotation to translation: Constraints on multi-joint movements and the unique action of biarticular muscles. *Human Movement Science*, 8(4):301–337, 1989.

[VR73] J. Vrendenbregt and G. Rau. Surface electromyography in relation to force, muscle length and endurance. *Desmedt, J.E. (Editor): New Developments in EMG and Clinical Neurophysiology*, 1:607–622, 1973.

[VSB11] L.C. Visser, S. Stramigioli, and A. Bicchi. Embodying desired behavior in variable stiffness actuators. In *Proceedings of the 18th IFAC World Congress, 2011*, pages 9733–9738, Milan, Italy, August 2011. IFAC, IFAC.

[VZ90] L. Chugunova V. Zatsiorsky, V. Seluyanov. In vivo body segment inertial parameters determination using a gamma-scanner method. *Biomechanics of Human Movement: Applications in Rehabilitation, Sports and Ergonomics*, pages 186–202, 1990.

[WBCt15] S. Wolf, T. Bahls, M. Chalon, and *et al.* Soft robotics with variable stiffness actuators: Tough robots for soft human robot interaction. In A. Verl, A. Albu-Schäffer, O. Brock, and A. Raatz, editors, *Soft Robotics*. Springer Berlin Heidelberg, 2015.

[WEH11] S. Wolf, O. Eiberger, and G. Hirzinger. The DLR FSJ: Energy based design of a variable stiffness joint. In *IEEE International Conference on Robotics and Automation (ICRA)*, pages 5082–5089, May 2011.

[WGC07] P. Wenger, C. Gosselin, and D. Chablat. A comparative study of parallel kinematic architectures for machining applications. *CoRR*, abs/0707.3665, 2007.

[WH08] S. Wolf and G. Hirzinger. A new variable stiffness design: Matching requirements of the next robot generation. In *Robotics and Automation, 2008. ICRA 2008. IEEE International Conference on*, pages 1741–1746. IEEE, 2008.

[Wil11] W.O. Williams. Huxley's model of muscle contraction with compliance. *Journal of elasticity*, 105(1-2):365–380, 2011.

[Win90] J.M. Winters. Hill-based muscle models: a systems engineering perspective. *Multiple muscle systems*, 1990.

[Wol11] S. Wolf. DLR floating spring joint (FSJ); `http://www.viactors.org/{VSA}%20data%20sheets.htm` – VIACTORS VSA data sheet, 2011.

[WS87] J.M. Winters and L. Stark. Muscle models: what is gained and what is lost by varying model complexity. *Biological cybernetics*, 55(6):403–420, 1987.

[WTW+11] O. White, J. Thonnard, A.M. Wing, R.M. Bracewell, J. Diedrichsen, and P. Lefèvre. Grip force regulates hand impedance to optimize object stability in high impact loads. *Journal of Neuroscience*, 189, 2011.

[XHHB91] Yangming Xu, I.W. Hunter, J.M. Hollerbach, and D.J. Bennett. An airjet actuator system for identification of the human arm joint mechanical properties. *Biomedical Engineering, IEEE Transactions on*, 38(11):1111–1122, November 1991.

[YHOH09] K. Yoshida, N. Hata, S. Oh, and Y. Hori. Extended manipulability measure and application for robot arm equipped with bi-articular driving mechanism. In *35th Annual Conference of IEEE Industrial Electronics*, pages 3083–3088, November 2009.

[YI03] T. Yoshikawa and Y. Ichinoo. Impedance identification of human fingers using virtual task environment. *Proceedings of the 2003 IEEE/RSJ*, 3:3094–3099, 2003.

[Yun13] Youngmok Yun. Hill type muscle model with MATLAB code; http://youngmok.com/category/theory/biomechanics/, 2013.

[Zah00] G.I. Zahalak. The two-state cross bridge model as a link between molecular and macroscopic muscle mechanics. *Skeletal muscle mechanics: from mechanisms to function. New York: John Wiley and sons*, pages 95–124, 2000.

[Zaj89] F.E. Zajac. Muscle and tendon: properties, models, scaling, and application to biomechanics and motor control. *Critical reviews in biomedical engineering*, 17(4):359–411, 1989.

[ZGL05] V. M. Zatsiorsky, F. Gao, and M. L. Latash. Motor control goes beyond physics: differential effects of gravity and inertia on finger forces during manipulation of hand-held objects. *Experimental Brain Research*, 162(3):300–308, April 2005.

[ZGL06] V.M. Zatsiorsky, F. Gao, and M.L. Latash. Prehension stability: experiments with expanding and contracting handle. *Journal of Neurophysiology*, 95(4):2513–29, 2006.